An investigation of roles for SIRT1 and dietary polyphenols in modulating the ageing process through DNA methylation

Laura Jane Ions

Thesis submitted for the degree of Doctor of Philosophy

Institute for Cell and Molecular Biosciences,

Newcastle University, UK

September 2011

Declaration

I certify that this thesis is my own work, except where stated, and has not been previously submitted for a degree or any other qualification at this or any other university.

Laura J Ions
September 2011

Thank you to Professor Dianne Ford and Dr Luisa Wakeling whose support, guidance and enthusiasm have been invaluable over the last four years.

Abstract

Dietary restriction (DR) can increase lifespan across evolutionarily distinct species, from yeast to rodents. The NAD^+-dependent (class III) histone deacetylase SIRT1 in mammals, and its ortholog in other species, may play a major role in this response, but may affect 'healthspan' (number of years of good health), rather than lifespan *per se*. Ageing is accompanied by changes in genome methylation, which may be causal in the ageing process. Since histones are one of the many substrates that are deacetylated by SIRT1, we hypothesised that epigenetic effects of SIRT1 activity – and specifically effects on DNA methylation, which is associated closely with histone acetylation – mediate some of the beneficial effects of DR that contribute to increased healthspan. We also propose that dietary polyphenols may act at the cellular level in a similar way.

To test this hypothesis, we first investigated effects of altering SIRT1 expression, by overexpression of a transgene or siRNA-mediated knockdown, on global DNA methylation (methylation of the LINE-1 element) in the human intestinal cell line, Caco-2. We also measured effects on global DNA methylation of dietary isoflavones and resveratrol, under control conditions as well as conditions of SIRT1 overexpression. Measured effects on global DNA methylation revealed possible complex interactions between SIRT1 and these dietary polyphenols but were dependent on the assay used to measure methylation at the LINE-1 element (COBRA or pyrosequencing), so were not considered to be robust observations.

We investigated factors that may affect SIRT1 expression – specifically we examined *SIRT1* promoter activity in response to polyphenols, effects of promoter methylation and effects of age. Treatment of Caco-2 cells with dietary polyphenols had no effect on the *SIRT1* promoter in a promoter-reporter construct. In contrast, methylation of the *SIRT1* promoter reduced reporter gene expression in this model. Age did not appear to change the levels of SIRT1 protein expressed in mouse intestinal tissue when comparing young and older mice.

An *in silico* analysis was carried out to investigate if overlaps between groups of genes compiled from published and publically-available data found to i) associate with SIRT1, ii) show altered expression in response to DR, and iii) show altered methylation with ageing were greater than expected by chance, which would support the hypothesis, and provided targets to investigate possible site-specific effects of SIRT1 on DNA methylation. Ten genes were found to fit into the 'three way' overlap, which was statistically greater than expected by chance. Pyrosequencing assays could be optimised for only 8 of these 10 genes, so we focused further investigations on this sub-set. Significant effects of SIRT1 overexpression and/or knockdown on methylation were observed on at least one CpG site in the

promoters of six of these genes (*CDC7, EIF5, IRX3, KLF3, PTPRG, TBX3*) and expression at the mRNA level of all of the eight genes (also *PCYT1A* and *SLC39A4*) was affected significantly.

To gain a more comprehensive view of the extent to which DNA methylation at specific loci may be affected by SIRT1 expression levels microarray-based analysis of the methylation pattern across the genome in Caco-2 cells was carried out under conditions where SIRT1 was overexpressed or where expression was reduced by siRNA. In parallel, we measured the response to expressing SIRT1 at different levels at the level of the transcriptome. Overlaps that were statistically greater than expected by chance between these data and the lists of genes compiled from published and publically-available data used for the *in silico* analysis were found to exist between the complied list of genes reported to respond to dietary restriction and the set of genes we found to show altered expression in response to changing the level of SIRT1 expression and the set of genes we found to be differentially-methylated in response to reducing the level of SIRT1 expression. This observation is in broad support of our overarching hypothesis.

The findings of this study indicate that effects of SIRT1 on methylation of specific genes may correspond with altered expression under conditions of dietary restriction. The data reveal a large number of gene targets for which causal links between these modifications roles in modulating the ageing process could be investigated.

.

Abbreviations

A	Adenine
A_{260}	Absorbance reading at 260nm
Acetyl-CoA	Acetyl-coenzyme A
AceCS2	Acetyl-coenzyme A Synthetase 2
ADP	Adenosine diphosphate
AROS	Active regulator of SIRT1
ASP	Adenosine 5' phosphosulfate
ATCC	American Tissue Culture Collection
ATP	Adenosine triphosphate
Bax	Bcl2-associated
bp	Base pair
BSA	Bovine serum albumin
C	Carbon
C	Cytosine
Caco-2	Colonic adenocarcinoma
cAMP	Cyclic adenosine monophosphate
CCD	Charged coupled device
CDC7	Cell division cycle 7
CDK	Cyclin dependent kinase
cDNA	copy DNA
C/EBPα	CCAAT/enhancer binding protein alpha
ChREBP	Carbohydrate response element binding protein
COBRA	Combined bisulfite restriction analysis
CPRG	Chlorophenol red-β-D-galactopyranoside
CPS-1	Carbamoyl phosphate synthetase 1
CR	Calorie restriction
CREB	cAMP response element binding protein
CTα	CTP:phosphocholine cytidylyltransferase alpha
CtBP	C-terminal binding protein
CTP	cytidine 5’-triphosphate
D	Aspartic acid
DBC-1	Deleted in breast cancer 1
DMSO	Dimethyl sulfoxide
DNA	Deoxyribonucleic acid
DNMT1	DNA methyltransferase 1

dNTP	Deoxynucleotide triphosphate
DR	Dietary restriction
E	Glutamic acid
EDTA	Ethylenediaminetetraacetic acid
EIF5	Eukaryotic translation initiation factor 5
ERC	Extrachromosomal circles
FOXO	Forkhead box type O
G	Guanine
GAP	GTPase accelerating protein
GDH	Glutamate dehydrogenase
GDI	GDP dissociation inhibitor
GDP	Guanosine diphosphate
GSTP-1	Glutathione S-transferase 1
GTP	Guanosine triphosphate
H	Histone
HAT	Histone acetyltransferase
HIC-1	Hypermethylated in cancer 1
HDAC	Histone deacetyltransferase
HeLa	Henrietta Lacks
IF	Intermittent fasting
IGF-1	Insulin-like growth factor 1
IgG	Immunoglobulin G
IIS	Insulin/IGF-1 signalling
INHAT	Inhibitor of histone acetyltransferases
InR	Insulin receptor
IRX3	Iroquois related homeobox 3
JNK	c-Jun N-terminal kinase
K	Lysine
kb	Kilo bases
KLF3	Krüppel-like factor 3
LB	Luria Bertoni
LDLR	Low density lipoprotein receptor
LINE-1	Long interspersed nucleotide element 1
LUMA	Lumometric methylation assay
MCK	Muscle creatine kinase
MCM2-7	Minichromosome maintenance 2-7
MeCP2	Methyl CpG binding protein 2

MeDIP	Methylated DNA immunoprecipitation
MGMT	O6-methylguanine DNA methyltransferase
miR	Micro RNAs
MMLV RT	Moloney murine leukaemia virus reverse transcriptase
mRNA	Messenger ribonucleic acid
MYH10	Myosin, heavy chain 10
NaDC3	Na+-dependent dicarboxylate cotransporter
NAD(H)	Nicotinamide adenine dinucleotide (hydrogen)
NM II	Non muscle myosin II
NMHC II	NM II heavy chain isoform
NMNAT-1	Nicotinamide mononucleotide adenylyltransferase 1
p	Phosphate
p	Probability
PBS	Phosphate buffered saline
PCR	Polymerase chain reaction
PCYT1A	Phosphate cytidylyltransferase 1 choline alpha isoform
PGC-1α	PPAR-gamma coactivator 1 alpha
PI3K	Phosphoinositide 3 kinase
PIC	Pre-initiation complex
PPAR γ	Peroxisome proliferator-activated receptor gamma
PPi	Pyrophosphate
PTPRG	Protein tyrosine phosphate receptor type G
PVDF	Polyvinylidene difluride
RARβ	Retinoic acid receptor beta
r.f.	Representation factor
RISC	RNA-induced silencing complex
RNA	Ribonucleic acid
RNAi	Ribonucleic acid interference
ROS	Reactive oxygen species
RPTC	Renal proximal tubular cells
RT-PCR	Reverse transcriptase-polymerase chain reaction
RT-qPCR	Reverse transcriptase-quantitative polymerase chain reaction
S	Serine
SDS-PAGE	Sodium dodecyl sulphate-polyacrylamide gel electrophoresis
SEM	Standard error of the mean
SIR	Silent information regulator
siRNA	Short interfering ribonucleic acid

SLC30A5	Solute carrier 30, member 5
SLC39A4	Solute carrier 39, member 4
SMRT	Silencing mediator of retinoid and thyroid hormone receptor
STAC	Sirtuin activating compound
T	Thymine
TBX3	T-box3 transcription factor
TDR	Transcriptional repressor domain
TEMED	N,N,N',N'-Tetramethylethylenediamine
tk	Thymidine kinase
TOR	Target of rapamycin
TSA	Trichostatin A
UCP2	Uncoupling protein 2
UV	Ultra violet
WAT	White adipose tissue

Contents

List of Figures

List of Tables

1 Introduction

This research project addresses an overarching hypothesis concerning a proposed mechanism through which some of the effects of dietary restriction (DR), which increases lifespan, are mediated. The sirtuin Sir2 in yeast, and its homologue SIRT1 in mammals, appear pivotal in extending lifespan in response to DR. SIRT1 deacetylates many cellular substrates, including histone proteins. We propose that histone deacetylation by SIRT1 affects DNA methylation, because these two tiers of epigenetic modifications are linked. DNA methylation patterns alter with ageing and these changes may be causal in the ageing process. Thus, we propose that SIRT1-mediated histone deacetylation underlies some of the beneficial effects of DR on ageing/lifespan through maintenance of DNA methylation. We also propose that specific dietary factors may bring about similar epigenetic consequences and so mimic beneficial effects of DR. The following sections will introduce in detail the elements of this hypothesis – DR, sirtuins and epigenetic modifications (particularly in the context of ageing) – then consider evidence that diet, and in particular specific dietary components, can affect epigenetic modifications.

1.1 Dietary restriction

Dietary restriction extends lifespan in evolutionarily-distinct species including *Saccharomyces cerevisiae*, *Caenorhabditis elegans*, *Drosophila melanogaster* and mammals. DR is a reduction in dietary intake without compromising the nutrition of the organism. In this introductory section the term DR is used to cover dietary restriction (which is often used as the interchangeable or overarching definition of the reduction of total nutrient intake and/or specific nutrient intake) and calorie restriction (CR - defined as the reduction of energy intake). This section will discuss the phenotypic effects of DR in higher and lower eukaryotes. The proposed mechanisms by which DR affects lifespan are discussed in Section 1.1.3.

1.1.1 DR in lower eukaryotes

The single celled budding yeast *S. cerevisiae* provides a simple model with which to study the effects of DR on both chronological and replicative lifespan. DR in yeast, and the associated increase in chronological or replicative lifespan, is frequently achieved through either dilution of the glucose concentration within the yeast medium from 2 % to 0.5 %, which has produced a 75 % increase in lifespan (Kaeberlein et al., 2005b; Lin et al., 2000) or starvation, where yeast cells are switched from standard yeast medium to water, producing a reported 300 % increase in lifespan (Wei et al., 2008). Lifespan extension through DR in the multi-cellular worm *C. elegans* has been elicited through multiple interventions, including mutations in the *Eat* genes, which prevent correct pharyngeal pumping (Lakowski and Hekimi, 1998), manipulation of the bacterial food source through decreased bactopeptone (Hosono et al., 1989), bacterial dilution (Chen et al., 2009) or synthetic alternatives to bacteria (Houthoofd et al., 2002) in the media. Such interventions have increased lifespan by up to 85

%. Many decades of study into *D. melanogaster*, including the comprehensive mapping of conserved genes to higher eukaryotes and the presence of two distinct genders, make it a well-established and complex bilaterally symmetric metazoan model. DR in flies is most commonly achieved through a reduction in yeast (Kapahi et al., 2004) or a dilution of media (Giannakou et al., 2008), yielding reported increases of up to 66 % in lifespan.

1.1.2 DR in higher eukaryotes

Studies of DR in the mammalian models provided by rodents and primates allow for physiological comparisons with humans, which augment the genetic and nutritional comparisons provided by lower eukaryotes. In rodents, restriction of energy intake by 25–50 % compared with *ad libitum* levels has been observed consistently to increase lifespan by up to 50 % (Weindruch et al., 1986; Weindruch and Walford, 1982; Yu et al., 1982; Ross, 1961). Since the 1930s a plethora of DR studies using rodents have suggested that this overall increase in lifespan is due, at least in part, to the modulation of multiple factors that decrease the prevalence of age-associated diseases such as diabetes, osteoporosis, cardiovascular disease, kidney disease, respiratory diseases and cancer (Masoro, 2002).

Studies in long-lived mammals, such as non-human primates, are still at a relatively early stage to obtain data on the effects of DR on lifespan; however, data from ongoing studies in rhesus monkeys (*Macaca mulatta*) have mirrored the metabolic and physiological changes demonstrated in rodents in response to DR. These observations include reduction in body mass and total body fat (Colman et al., 1999), reduced core body temperature (Lane et al., 1996) and resting energy expenditure (Blanc et al., 2003), as well as observations that may implicate a beneficial effect on age-related diseases such as cardiovascular disease and diabetes, which include reduced blood pressure, reduced plasma glucose and insulin concentrations, increased insulin sensitivity (Gresl et al., 2001; Lane et al., 1999), decreased levels of inflammatory mediators (Kim et al., 1997) and a reduction in oxidative damage in skeletal muscle (Zainal et al., 2000). The most recent report into the effects of long term DR in rhesus monkeys observes that after 2 decades monkeys subjected to 30 % DR showed a reduction in age-associated muscle wasting, maintained control of glucose homeostasis, had a reduction in neoplasia and cardiovascular disease and a preservation of grey matter associated with a decrease in age-related brain atrophy compared with controls. Although data allowing either the maximum or average lifespan of the rhesus monkeys to be established has yet to been obtained in this study, current survival of those monkeys on DR at the time of reporting stood at 80 %, compared with 50 % survival of the controls. Conclusions on effects of DR on overall lifespan in primates are therefore yet to emerge (Colman et al., 2009).

In humans, DR studies are based on cohorts of willing volunteers who are practicing self-regulated DR or where DR has occurred due to external events creating a nutrient rich but calorie poor diet. Members of CR Society International have provided researchers with a model to study the effects of

between 15-30 % DR (from the recommended adult calorie intake of 2500 for men and 2000 for women) on the physiological outcomes of reduced dietary intake in humans. A comparison of individuals who had been practicing dietary restriction for at least 6 years compared to age- and sex-matched controls on a typical Western diet showed a reduction in percentage body fat, reduced cholesterol, fasting insulin and glucose, a reduction in inflammatory markers (Fontana et al., 2004) and beneficial effects on cardiovascular function (including a reduction in blood pressure and myocardial fibrosis) in subjects undertaking DR (Meyer et al., 2006). The Comprehensive Assessment of Long-term Effects of Reducing Intake of Energy (CALERIE) study investigated the effects of DR alone (25 %) or in combination with exercise (12.5 % DR and 12.5 % increased exercise) over 6 months. Both interventions caused a reduction in blood pressure and cholesterol associated with reduced cardiovascular disease (Lefevre et al., 2009). A study with similar levels of DR over 3 months also showed positive effects on memory function in individuals over 50 years of age (Witte et al., 2009).

The Okinawa Centenarian Study is one of the most cited centenarian studies, due to the large number of individuals reaching ages exceeding 100 years relative to the overall population (Willcox et al., 2008a). The Okinawan population stands out from other centenarian studies as, although this generation is known to have been subjected to poverty-induced food shortages, the composition of the local Japanese diet uniquely mimics the qualities of DR. This low calorie diet has been implicated in the delay or absence of age-related diseases such as cardiovascular disease, stroke and cancer in those over 100 in the Okinawa population (Willcox et al., 2008b). Other centenarian studies, including longitudinal studies, have been running globally for many years comparing various measures with contrasting groups including survival of groups with natural diets aligned to some elements of DR or other lifestyle factors or exposures. Of particular note with regard to the potential role of diet on lifespan is the correlation of the Mediterranean diet and moderate exercise with the large Italian centenarian population (Tafaro et al., 2009).

In 1991, an experiment to explore the interactions between humans and the environment in an enclosed space, known as Biosphere 2, was established. The poor yield of crop and high demand of physical labour demanded of the crew led to a state of 20 % dietary restriction and 15-20 % weight loss and resulted over two years in reduced blood pressure, fasting glucose, cholesterol and insulin levels, thus mimicking effects observed in DR rodents or rhesus monkeys (Walford et al., 2002).

1.1.3 Mechanisms through which DR may extend healthy lifespan

Several biological pathways have been proposed through which DR may extend healthy lifespan. Many of these mechanisms involve processes involved in nutrient-sensing and positive data have been reported in many instances suggesting that multiple pathways play a role in the response to DR. Key observations made in this regard are noted below.

The insulin signalling pathway is crucial in regulating glucose metabolism. Mutations in the insulin/insulin-like growth factor signalling (IIS) pathway have been shown to extend lifespan in model organisms. Mutations in the insulin-like receptor Daf2 (Kenyon et al., 1993) and Age-1, the downstream target of Daf2 (Johnson, 1990), have extended life in worms. Similarly in flies the deletion of the insulin receptor substrate chico (Clancy et al., 2001) or the insulin receptor (InR) itself (Tatar et al., 2001) have increased lifespan by up to 48 % and 85 % respectively. However, flies lacking expression of the downstream IIS pathway target Foxo (forkhead box type o), which have reduced lifespan, still showed an increase in lifespan when subjected to DR (Giannakou et al., 2008), suggesting that other pathways – additional to the IIS pathway – are also required for the effects of DR on lifespan. In mice, heterozygous knockout (Holzenberger et al., 2003) and adipose-specific homozygous knockout (Blüher et al., 2003) of the insulin-like growth receptor IGF-1 increased the lifespan of mice compared with controls, as did knockout of the insulin receptor substrate (Taguchi et al., 2007). In humans, variations in the FOXO genes have been implicated in several age-related diseases and lifespan. For example, the FOXO1 haplotype 3 'TCA' was associated with increased levels of glycosylated haemoglobin (HbA1c), a marker of diabetes risk, and myocardial infarction. This haplotype predisposed carriers to an increase in mortality. Similarly, the FOXO3 haplotype 2 'GAGC' was associated with an increased risk of stroke and therefore also an increase in mortality (Kuningas et al., 2007).

Restriction of amino acids and mutations in the amino acid-sensing target of rapamycin (TOR) signalling pathway have both shown a conserved increase in lifespan in yeast (Powers et al., 2006). Deletion of nutrient-responsive kinases Tor and Sch9, which regulate the stress response serine/threonine kinase Rim15, led to an increase in yeast replicative lifespan (Kaeberlein et al., 2005b). An increase in chronological lifespan was also observed in response to inhibition of Tor and Sch9. Rim15 was additionally found to be activated in another nutrient-sensing pathway – Ras/cAMP/PKA – through deletion combinations with the Ras gene (Wei et al., 2008). Deletion of all three stress resistance transcription factors downstream of Rim15 regulation – Gis-1 in the TOR pathway and Msn2/4 in the Ras pathway – reversed the lifespan-extension effects of DR, suggesting that these factors are intermediates in the response of Rim15 to DR (Wei et al., 2008). In worms, a deletion of the Tor kinase (Vellai et al., 2003) and downstream target Hif-1 (Chen et al., 2009) and in flies, a reduction in the amounts of amino acids through casein restriction (Min and Tatar, 2006), overexpression of TOR inhibitors Tsc1 and Tsc2 and deletion of components of the TOR pathway TOR and S6K (the fly and mammalian homologue of Sch9) (Kapahi et al., 2004) have been shown to extend lifespan. A diet deficient in the amino acid methionine (Miller et al., 2005) has also been reported to extend lifespan in mice. AKT activation by phosphoinositide 3 kinase (PI3K – the fly and mammalian homologue of Age-1) in the IIS pathway to inhibit TSC1 and TSC2 in the TOR pathway (Inoki et al., 2002) and negative feedback of the TOR downstream target S6K in the TOR pathway by

phosphorylation of insulin receptor substrate 1 (IRS-1) in the IIS pathway (Shah and Hunter, 2006) connects these two pathways.

Yeast models have indicated that the silent information regulator protein, Sir2, has an important role in lifespan extension in DR. The exact mechanism through which Sir2 has a role in increasing lifespan (chronological or replicative) is unclear; however, upon addition or deletion of a copy of the *SIR2* gene in yeast, lifespan was extended or shortened, respectively (Kaeberlein, 1999). Addition or deletion of the Sir2 homologue in worms increased or decreased lifespan respectively and functions upstream of Daf-16, the fly homologue of the FOXO transcription factor (Wang and Tissenbaum, 2006; Tissenbaum and Guarente, 2001), and deletion of Sir2 in flies prevented increased lifespan with DR (Rogina and Helfand, 2004). These observations have led to the investigation of the role of SIRT1, the mammalian homologue of Sir2, in the longevity response to DR in mammals. There is some evidence, though inconsistent, that DR increases SIRT1 expression in several rodent tissues (Barger et al., 2008; Kanfi et al., 2008; Nisoli et al., 2005; Brunet et al., 2004), suggesting that SIRT1 is regulated by dietary intake. In SIRT1 transgenic mouse models, overexpression of SIRT1 in several tissues led to reduced body weight, reduced fasting levels of insulin, glucose and cholesterol and improved glucose homeostasis, mimicking effects seen in DR mice (Bordone et al., 2007), and SIRT1 knockout mice subject to DR showed a reduction in physical activity compared with wild type DR mice, suggesting the increase in physical activity observed in DR mice requires the SIRT1 gene (Chen et al., 2005a). In addition, DR has also been observed to increase SIRT1 mRNA levels in the skeletal muscle of human subjects (Civitarese et al., 2007). In human and mouse cell lines, SIRT1 was found to associate with TSC2, an upstream inhibitor of the TOR pathway, to negatively regulate TOR signalling (Ghosh et al., 2010) and in human cell lines SIRT1 was found to interact with, and represses, the FOXO transcription factors, reducing the rate of apoptosis but increasing resistance to stress (Brunet et al., 2004; Motta et al., 2004). These findings interconnect the response of SIRT1 to DR with the above mentioned TOR and IIS pathways.

With the introduction of microarray technology, allowing the assay of thousands of genes and their expression in a single experiment, it has been possible to examine gene expression changes induced by DR in multiple tissues, predominately in mice. Vast amounts of data have now been generated, listing genes whose expression changes upon DR; these datasets confirm studies relying on physiological and metabolic observations, highlighting up-regulation of groups of genes involved in fatty acid metabolism, cellular transport and gluconeogenesis and down-regulation of gene groups involved in lipid biosynthesis, cell proliferation and protein building and development (Selman et al., 2006), emphasising the switch in gene expression from energy expenditure to energy conservation that is associated with DR.

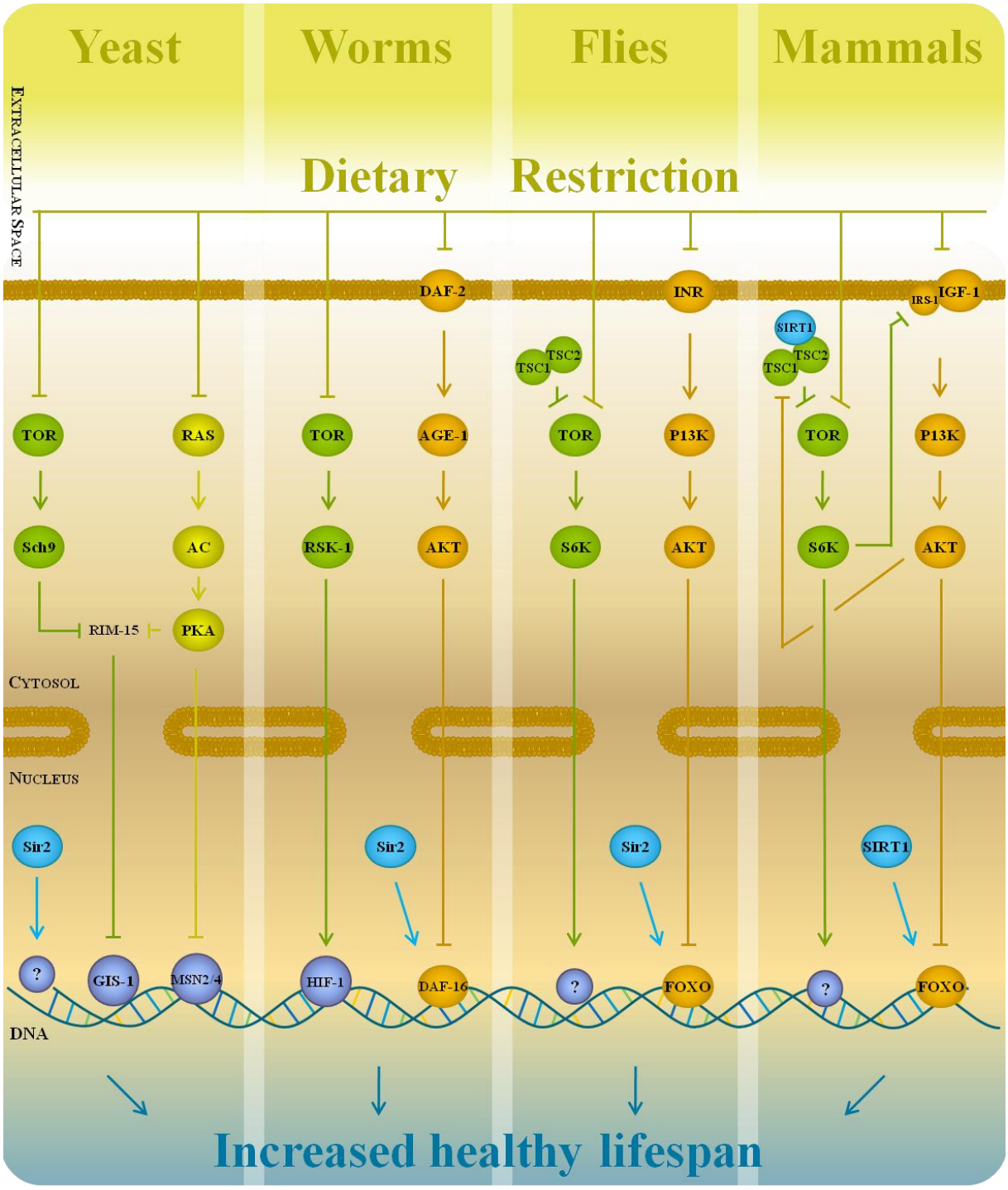
Yeast
Worms
Flies
Mammals
Dietary Restriction
Extracellular Space
DAF-2
INR
IRS-1
IGF-1
SIRT1
TSC1
TSC2
TOR
RAS
TOR
AGE-1
TOR
P13K
TOR
P13K
Sch9
AC
RSK-1
AKT
S6K
AKT
S6K
AKT
RIM-15
PKA
Cytosol
Nucleus
Sir2
Sir2
Sir2
SIRT1
?
GIS-1
MSN2/4
HIF-1
DAF-16
?
FOXO
?
FOXO
DNA
Increased healthy lifespan

Figure 1.1. Conserved pathways associated with longevity in different species. *The conserved TOR signalling pathway (green), IIS pathway (orange), and actions of the silent information regulator (blue), all of which have been shown to increase healthy lifespan upon manipulation, are shown in yeast, worms, flies and mammals where applicable. SIRT1/Sir2 is represented in an upregulated state in response to DR. The Ras/cAMP/PKA pathway (yellow) another nutrient-sensing pathway which interacts with downstream components of the TOR signalling pathway in yeast, is also shown. Inhibition of TOR signalling during conditions of DR leads to the inhibition or activation of transcription factors required for mediation of the increase in healthy lifespan. Inhibition of the IIS pathway during conditions of DR prevents the inhibition of the Daf-16/FOXO transcription factor to mediate effects on longevity. Sir2/SIRT1 is activated under conditions of DR; only those interactions relevant to the TOR or IIS pathways are shown. Many other downstream targets of SIRT1 are likely to play a role in the longevity response to DR. The proteins that reside on the same plane in the same colour (green, orange or blue) in the species-specific pathways are homologues of one another. Those proteins in purple are transcription factor targets of the upstream nutrient-sensing pathways. Downstream inhibition or activation of a component is represented by an arrow or flat line respectively. For simplicity, and excluding SIRT1/Sir2, mammalian nomenclature has been used. Adapted from (Fontana et al., 2010).*

1.1.4 DR involving restriction of selected nutrients

Effects on lifespan of forms of DR involving limiting availability/intake of only selected nutrients have also been investigated.

In flies, lowering levels of dietary casein, the primary source of amino acids, caused an extension in lifespan and reduction in fecundity similar to that observed in DR (Min and Tatar, 2006). Addition of the amino acid methionine back into the diet was sufficient to reverse the effects on fecundity without reducing lifespan (Grandison et al., 2009). A lifelong low level of methionine in rats without any change in body weight-corrected energy intake caused a 30 % increase in lifespan (Orentreich et al., 1993). A further study went on to test whether the effects of methionine restriction were conserved amongst rodents by administering a low methionine-deficient diet to mice. Reduction in the levels of dietary methionine again caused an increase in lifespan as well as reducing glucose and insulin levels and increasing stress resistance, traits also associated with DR and healthy ageing (Miller et al., 2005). In the particular context of our hypothesis, it may be reasonable to speculate that some of the effects of a methionine-deficient diet are through the reduced levels available for synthesis of S-adenosylmethionine, the methyl donor substrate required in methylation of DNA, the maintenance of which is required for correct gene expression.

The effect on lifespan of the ratio of carbohydrate to protein in the diet, in the form of yeast and sucrose respectively, has also been explored in flies. A higher ratio of carbohydrates to protein increased lifespan (Lee et al., 2008), suggesting that, in some instances, the balance of macronutrients rather than overall energy content, can bring about lifespan extension in response to DR in flies (Mair et al., 2005). Lifespan extension in response to DR in flies was abrogated when water was available *ad libitum*, further suggesting that regulation of the response to DR in flies is different from that of mammals; studies in the latter have typically allowed *ad libitum* access to water (Ja et al., 2009). Protein restriction alone extended lifespan in rats (Yu et al., 1985) and also reduced oxidative damage (Youngman et al., 1992).

1.1.5 Periodic DR

Long term dietary restriction studies have been complemented by studies using severe, but intermittent, fasting (IF), for example where food is available *ad libitum* every other day. Extensive study of IF in mice has led to recorded effects that parallel those of DR, such as an increase in glucose metabolism, cerebrovascular (Anson et al., 2003) and cardiovascular (Ahmet et al., 2005) protection and an increase in resistance to cancer (Descamps et al., 2005), despite overall energy intake being matched with non-IF controls. To our knowledge, rigorous studies in humans have not been carried out to investigate effects of intermittent fasting. Another aspect of food intake periodicity that may have effects on lifespan is the time during the daily cycle at which meals are taken. Time of day when

food is available has been shown to affect the expression of circadian genes involved in the mammalian circadian clock, which responds to levels of light to regulate metabolic pathways (Froy et al., 2009). The dysregulation of circadian genes has been associated with premature ageing and reduced lifespan (Penev et al., 1998).

Studies on specific nutrient deficiencies suggest that although the overall response to DR – possibly even the multiple mechanisms by which it increases lifespan – are similar, the conditions under which divergent species trigger these downstream responses differ.

1.2 Sirtuins, focusing on SIRT1

Histone deacetylases (HDAC) are a family of enzymes that catalyse the deacetylation of histone substrates through removal of the acetyl group from the ε-N-acetyl lysine histone tail. The HDAC family consists of three classes. Class III HDACs include the sirtuin subfamily, which are, unlike classes I and II, nicotinamide adenine dinucleotide (NAD^+)- dependent lysine deacetylases. The first identification of a sirtuin gene, the *S. cerevisiae* gene silent information regulator 2 (Sir2) (Klar, 1979), was followed by the discovery of a host of homologues from many other organisms, including mammals.

The catalytic core domain is conserved through all five classes of sirtuins, which have been identified through phylogenetic analysis (summarised in *Figure 1.2*). Class I is composed of three subclasses, all of which contain only eukaryotic sirtuins. The mammalian sirtuin SIRT1 and the yeast homologue Sir2 are in Class Ia. Class Ib contains the mammalian SIRT2 and SIRT3 and Class Ic groups eukaryotic sirtuins from yeast and fungi. Class II bands bacterial sirtuins as well as eukaryotic sirtuins including mammalian SIRT4. Class III includes archaeal, eubacteria and eukaryotic sirtuins, including mammalian Sirt5. Class IV, similar to Class I, only bands eukaryotic sirtuins, including mammalian SIRT6 and SIRT7, which reside in subclasses a and b respectively. Finally all unclassified sirtuins are banded along with gram positive eubacteria Sir2 homologues in Class U (Frye, 2000).

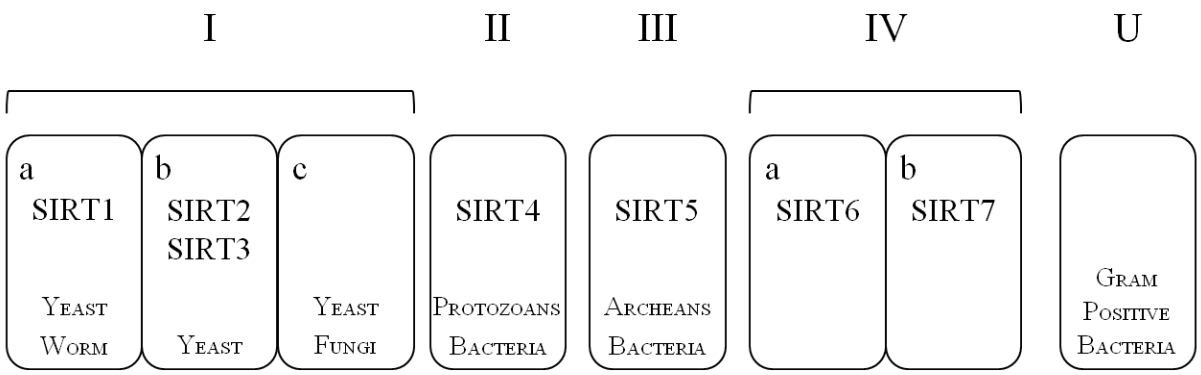

Figure 1.2. Sirtuin classification. *Five families of sirtuins I-IV and U. Human sirtuins are specified individually in the relevant class in bold upper case lettering. Sirtuins from other organisms are not specified, but the families in which they occur are indicated. Adapted from (Michan and Sinclair, 2007).*

The mammalian homologues SIRT1-7, which are represented throughout the five sirtuin subclasses, all share a conserved 275 amino acid catalytic core domain that acts as a NAD^+-dependent lysine deacetylase and cleaves the glycosidic bond of NAD^+ that lies between the nicotinamide and ADP-ribose groups. This core domain is flanked at the N- and/or C-termini by sequences unique to the individual sirtuin (Grubisha, 2005; Frye, 1999). NAD^+ is involved in many essential roles in cellular metabolism, and the reliance of the sirtuin family on NAD^+ indicates that they too may be involved in metabolic processes, as suggested by the proposed role of SIRT1 in DR. There is currently no crystal structure of SIRT1 available, but a 3D comparative model of amino acids 244-498 based on the backbone of human sirtuin SIRT2 has revealed information about ligand interactions in the active site. The use of a number of indoles to observe docking at the SIRT1 active site elucidated a complex H-bond network and its importance in SIRT1 substrate binding. Additionally, a binding model for a SIRT1 inhibitor - 1000-fold more potent than nicotinamide - has been proposed (Huhtiniemi et al., 2006).

SIRT1 has remained the main focus of studies after homologues exhibited lifespan extension properties in many species; however other members of the sirtuin family have been shown to be involved in processes that can be linked with healthy ageing.

SIRT2 is localised to the microtubules in the cytoplasm, where it deacetylates α-tubulin (North et al., 2003) and through this action plays a role inhibition of oligodendroglial differentiation, perhaps preventing overdifferentiation in the central nervous system (Li et al., 2007). SIRT2 has been shown to shuttle to the nucleus to deacetylate H4K16 (Vaquero et al., 2006). Levels of SIRT2 are increased during mitosis controlling exit from the cell cycle (Dryden et al., 2003). Adipocyte differentiation is regulated by SIRT2-dependent deacetylation of FOXO1, preventing export of the peroxisome

proliferator-activated receptor gamma (PPARγ) repressor from the nucleus and therefore regulating glucose metabolism and storage of fatty acids (Jing et al., 2007).

The mitochondrial sirtuins SIRT3 (Schwer et al., 2006), SIRT4 (Haigis et al., 2006) and SIRT5 (Nakagawa et al., 2009) contain a specific N-terminal sequence that targets the sirtuins for translocation into the mitochondria matrix. SIRT3 increases acetyl-coenzyme A (acetyl-CoA) synthesis, a substrate in the energy-producing citric acid cycle in the mitochondria, by deacetylation and subsequent activation of lysine 642 of acetyl-CoA synthetase 2 (AceCS2) (Schwer et al., 2006). The expression of AceCS2 is also induced with fasting; deacetylation by SIRT3 activates oxidation of long chain fatty acids into acetyl-CoA and fasting of SIRT3 knockout mice resulted in an accumulation of intermediate products in the liver (Hirschey et al., 2010). SIRT4 is an ADP-ribosyltransferase that uses NAD^+ in ADP-ribosylation and inhibits the mitochondrial glutamate dehydrogenase (GDH), which in turn prevents insulin secretion in pancreatic β cells (Haigis et al., 2006). siRNA mediated knockdown of SIRT4 in mouse hepatocytes caused an increase in fatty acid oxidation regulated through a increase in SIRT1 levels (Nasrin et al., 2010).

The urea cycle prevents failure of the liver through metabolism of toxic ammonia build up, which can occur during fasting. Carbamoyl phosphate synthetase 1 (CPS-1) is required to catalyse the first and rate limiting step of the urea cycle. SIRT5 activates CPS-1 through deacetylation. Knockout of SIRT5 in mice caused a decrease in CPS-1 activity (Nakagawa et al., 2009) and SIRT5 overexpression increased CPS-1 activity, measured by blood ammonia levels. SIRT5 mRNA was upregulated during fasting in the heart and liver of the transgenic mice (Ogura et al., 2010).

SIRT6 knockout mice die at 4 weeks from symptoms that mimic many aspects of premature ageing, including increased blood glucose (Xiao et al., 2010), lowered immune system activity, and loss of subcutaneous fat (Mostoslavsky et al., 2006). Further investigation revealed that the premature cellular senescence and genomic instability seen in SIRT6 deficiency is the result of telomere dysfunction due to the lack of H3K9 deacetylation of telomeric chromatin (Michishita et al., 2008). Deletion of SIRT6 in mouse liver increased fatty liver formation caused by upregulation of triglyceride synthesis and glycolysis, adding weight to the view that SIRT6 plays a critical role in metabolism. This study also showed that SIRT1 positively regulated SIRT6, both of which are upregulated during nutrient deprivation, through interaction with the transcription factors FOXO3a and NRF-1 at the SIRT6 promoter (Kim et al., 2010).

SIRT7 has been shown to localise to the nucleolus and interact with RNA polymerase I through immunofluorescence assays and co-immunoprecipitation respectively. SIRT7 positively regulates RNA polymerase I-mediated transcription of ribosomal DNA, which encodes the ribosomal subunits

required for protein translation (Ford et al., 2006). It is not clear if SIRT7 has a role in lifespan and/or ageing. SIRT7 knockout mice displayed a premature ageing phenotype characterised by reduced lifespan indicative of a role for SIRT7 in preserving a normal ageing trajectory. In apparent discordance with such a role, however, overexpression of SIRT7 in mouse embryonic fibroblasts inhibited cell growth and proliferation (Vakhrusheva et al., 2008).

1.2.1 Substrates for SIRT1 deacetylation

A large number of cellular substrates undergo SIRT1-mediated deacetylation (*Figure 1.3*) and have a potential role in ageing, identifying multiple pathways through which DR may affect longevity via SIRT1 activation. Notable examples of SIRT1 substrates include: p53, which may mediate cell survival through reducing cellular senescence (Langley et al., 2002); PPAR-γ coactivator 1 alpha (PGC-1α), an important regulator of mitochondrial biogenesis (Wu et al., 1999) that may contribute to healthy ageing through the maintenance of the mitochondria and thereby energy production and related oxidative stress (Lopez-Lluch et al., 2008); the FOXO transcription factors (Brunet et al., 2004; Motta et al., 2004), which regulate a variety of genes involved in glucose metabolism, apoptosis, cell cycle arrest, reactive oxygen species (ROS) detoxification and DNA repair; Ku70, which is required in double strand break repair and telomere maintenance and complexes with the proapoptotic factor Bcl2-assocated X (Bax) to prevent localisation of Bax to the mitochondria to induce programmed cell death (Cohen et al., 2004); the histone subunits H1, H3 and H4, which have been implicated in initiation of heterochromatin formation (Vaquero et al., 2004). In addition, SIRT1 regulates insulin secretion through a deacetylation-independent mechanism that may also have effects on lifespan. SIRT1 brings about its effect on insulin secretion by binding to and repressing the promoter of the mitochondrial uncoupling protein 2 gene (UCP2) to enhance glucose-stimulated insulin release (Bordone et al., 2006).

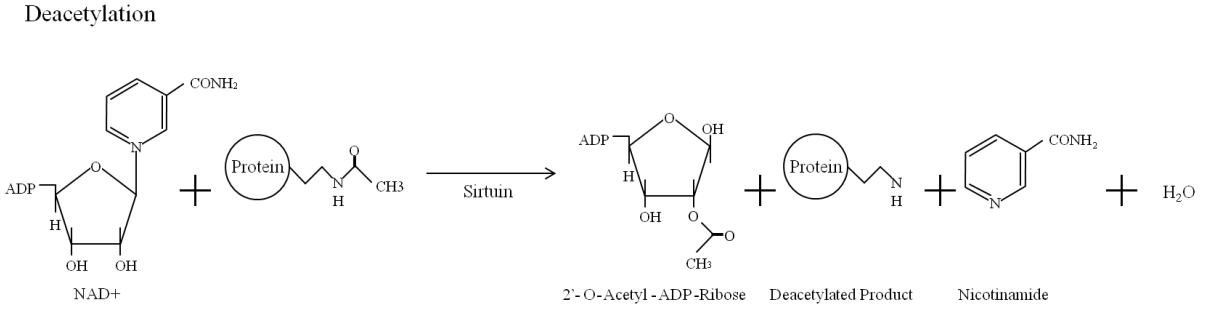

Figure 1.3. Deacetylation by sirtuins enzymatic action. *Deacetylation occurs through cleavage of the glycosidic bond between the nicotinamide and ADP-ribose groups of NAD^+ to produce 2'-O-Acetyl-ADP ribose, nicotinamide and the deacetylated product.*

1.2.2 Regulation of SIRT1

As a deacetylase of multiple proteins SIRT1 has a crucial role in endogenous and stress response regulation within the cell. Since increases in expression of SIRT1 (or its homologues in lower eukaryotes) are linked with increased lifespan/healthspan it is of relevance to consider age-dependent or ageing-related effects on its expression. In mammals, levels of SIRT1 mRNA expression in the hypothalamus are higher in young compared to old mice (Lafontaine-Lacasse et al., 2010). Additionally, levels of SIRT1 mRNA and protein expression were shown to decrease as cells progressed into a senescent state, and in lung, heart and fat tissues of old compared with young mice. Increased SIRT1 deacetylase activity was associated with resistance to senescence. The very many cellular processes in which SIRT1 plays a regulatory role invokes a need for tight regulation of SIRT1 expression and activity. This need is perhaps reflected by the many identified mechanism through which SIRT1 is regulated, allowing levels of expression and activity to be sensitive to many different perturbations in cellular status.

1.2.2.1 Transcriptional regulation of the SIRT1 gene

Several transcription factors have been shown to modulate transcription of *SIRT1* under conditions of oxidative stress and interactions with the translated SIRT1 protein suggest feedback loops in which normal homeostasis of SIRT1 expression and therefore cellular responses to stress are controlled, primarily through p53-regulated growth arrest and apoptosis. The transcriptional suppressor Hypermethylated in cancer 1 (HIC-1), together with p53, suppresses age-related cancer formation. HIC1 forms a complex with SIRT1, which then binds to the promoter of, and suppresses the transcription of, *SIRT1* under conditions of oxidative stress. The suppression of SIRT1 prevents deacetylation and subsequent deactivation of p53-dependent apoptotic responses, inhibiting SIRT1-mediated stress resistance (Chen et al., 2005b). The nuclear transcription factor EVI-1 is required for embryogenesis and has been identified as aberrantly expressed in some leukaemias due to a chromosomal rearrangement; SIRT1 levels have also been shown to be increased in chronic myeloid leukaemia cases positive for EVI-1. Binding of EVI-1 to the promoter region of *SIRT1* causes transcriptional upregulation of the gene. Deacetylation of EVI-1 by SIRT1 protein then allows ubiquitin-mediated proteosomal degradation in a negative feedback loop. The mechanism behind the imbalance of SIRT1 in EVI-1 positive diseases is unclear (Pradhan et al., 2011). E2F-1 activates the transcription of genes within the apoptosis pathway and control of the cell cycle. In a mechanism independent of p53, E2F-1 targets the *SIRT1* promoter under conditions of oxidative stress and upregulates *SIRT1* gene expression, again invoking a negative feedback loop in which SIRT1 inhibits the action of E2F-1 regulating stress resistance (Wang et al., 2006).

Nutrient availability is also a strong regulator of *SIRT1* transcription. The increased SIRT1 mRNA levels due to nutrient deprivation were abrogated when FOXO3a was knocked down in a human cell

line model (Nemoto et al., 2004). Similar increases in *SIRT1* mRNA have also been observed with the interaction of FOXO1 at the *SIRT1* promoter (Xiong et al., 2010). As well as the aforementioned response of HIC-1 to oxidative stress, SIRT1 transcription is induced under conditions of nutrient deprivation where levels of the HIC-1 co-repressor C-terminal binding protein (CtBP) are diminished (Zhang et al., 2007). Under conditions of nutrient deprivation, the cyclic adenosine monophosphate (cAMP) response element binding protein (CREB), responsible for glucose production, is activated and has been shown to upregulate *SIRT1* expression via binding to the promoter region. This action is reversed through suppression at the *SIRT1* promoter by the carbohydrate response element binding protein (ChREBP) responsible for promoting energy storage with increased nutrient availability (Noriega et al., 2011). After initiation of adipogenesis the CCAAT/enhancer binding protein (C/EBPα) increases the levels of SIRT1 expression to inhibit further differentiation in homeostatic control of the adipose tissue (Jin et al., 2010).

Peroxisome proliferator-activated receptor gamma (PPARγ), which induces cellular senescence via cell cycle arrest, negatively regulates SIRT1 under normal physiological conditions, allowing PPARγ to promote ageing (Han et al., 2010).

1.2.2.2 Posttranscriptional regulation of SIRT1 mRNA

HuR, an RNA binding protein that associates with the 3' UTR of the SIRT1 mRNA in a stabilising manner, increases protein expression. Chk2, a cell cycle check point kinase phosphorylates HuR under conditions of oxidative stress, resulting in the degradation of the SIRT1 mRNA (Abdelmohsen et al., 2007).

RNA interference (RNAi) involves the loss of gene function by the processing of double stranded RNA dioligonulceotides by an enzyme known as dicer into smaller ~21 nucleotide length microRNAs (miRNAs). The miRNA antisense strand is then loaded into the RNA-induced silencing complex (RISC) allowing recognition and cleavage of the target mRNA sequence by the complex. The cleaved mRNA sequencing is then targeted for degradation and ultimately leads to the prevention of protein expression. An miRNA can have more than one target mRNA sequence and similarly an mRNA sequence can be targeted by more than one miRNA. A cursory literature search indicates the extent to which miRNAs (denoted with miR accessions) have been observed to influence SIRT1 regulation to date. MiRNAs account for, but are by no means limited to: SIRT1 downregulation in endothelial cells leading to cellular senescence (miR-217; (Menghini et al., 2009) and in endothelial progenitor cells leading to inhibition of angiogenesis (miR-34a; (Zhao et al., 2010); SIRT1 downregulation and associated apoptosis protection in cardiomyocytes (miR-195; (Zhu et al., 2011) and downregulation of the high embryonic mouse stem cell SIRT1 levels after differentiation (miR-9; miR-135a; miR-199b; miR-204; miR-181a and b; (Saunders et al., 2010). Conversely, epigenetic silencing of miRNAs has

been associated with upregulation of SIRT1 in the transformation of mammary epithelial cells in breast cancer (miR-200a; (Eades et al., 2011),

.

The presence of UAGG motifs characteristic of exon skipping within exon 8 of the SIRT1 mRNA led to identification of a splice variant of the full length SIRT1. Under irradiation stress the levels of the SIRT1-ΔExon8 mRNA were increased compared with the full length SIRT1 mRNA. The SIRT1-ΔExon8 protein exhibited altered deacetylase activity due to partial deletion of the catalytic domain by splicing. These observations suggest alternative splicing as another possible mechanism by which the functional potential of SIRT1 can be increased (Lynch et al., 2010).

1.2.2.3 Posttranslational regulation of the SIRT1 protein

Posttranslational modifications of the SIRT1 protein include sumoylation and phosphorylation. Sumoylation of the SIRT1 protein at K734 within the Ψ-K-X-D/E consensus sequence by small ubiquitin-related modifiers (SUMOs) activates SIRT1 under normal physiological conditions, increasing stress resistance through deacetylation and thus inhibition of proapoptotic substrates. The desumoylase SENP1 inactivates SIRT1 during acute DNA damage allowing entry of the cell into the apoptotic pathway (Yang et al., 2007). Multiple phosphorylation sites have been identified at threonine and serine residues within the SIRT1 protein sequence that could potentially activate the deacetylase activity (Sasaki et al., 2008). Phosphorylation of the SIRT1 protein by CK2 has been reported at S154, S649, S651 and S683 (Kang et al., 2009; Zschoernig and Mahlknecht, 2009). Phosphorylation by CK2 resulted in SIRT1 activation and increased substrate binding in response to DNA damage induced by genotoxic stress, for example inhibiting p53-mediated apoptosis (Kang et al., 2009). The dual-specificity tyrosine phosphorylation-regulated kinases DYRK1A and DYRK3 regulate body growth and normal brain development and cell proliferation and apoptosis respectively. Both tyrosine kinases have been shown to phosphorylate SIRT1 at T522 under conditions of genotoxic stress (Guo et al., 2010). Finally, JNK1 and JNK2, members of the c-Jun N-terminal kinase (JNK) family, which induce signalling cascades in response to cellular stress, also phosphorylate SIRT1. JNK1 phosphorylates SIRT1 at S47 and T530 promoting resistance to cellular stress (Nasrin et al., 2009). JNK2 phosphorylates SIRT1 at S27 and stabilises the protein (Gao et al., 2011; Ford et al., 2008). Interestingly, after many interactions with JNK1, phosphorylation leads to ubiquitination and degradation of the SIRT1 protein, in line with observations that JNK1 activation is upregulated in obesity while SIRT1 is inhibited (Gao et al., 2011).

Subcellular localisation is another mechanism through which SIRT1 is regulated, providing a means of control over whether substrates for deacetylation encounter the enzyme. Initially thought to only exist in the nucleus (Michishita et al., 2005), SIRT1 was identified in the first instance as an enzyme able to deacetylate histones. As other substrates for deacetylation by SIRT1 began to emerge, so did the evidence for cytosolic localisation, where SIRT1 has been found to stimulate apoptosis (Jin et al.,

2007). The location of SIRT1 was also found to be dependent on the tissue and cell type, and possibly regulated through the PI3K pathway (Tanno et al., 2007). Active PI3K sequesters SIRT1 in the cytoplasm, possibly allowing deacetylation and therefore deactivation of the PI3K inhibitor and SIRT1 target PTEN (Byles et al., 2010), which has been linked with the aberrant cell growth observed when PI3K is constitutively active.

The search for proteins that regulate SIRT1 deacetylase activity through complex formation led to the discovery of active regulator of SIRT1 (AROS) and deleted in breast cancer-1 (DBC-1), which activate and reduce SIRT1 deacetylase activity respectively. The AROS protein interacts directly with amino acids 114 – 217 in the SIRT1 protein to enhance deacetylation activity as measured by SIRT1-dependent p53 suppression (Kim et al., 2007). It remains to be seen whether AROS is also implicated in the deacetylation of other SIRT1 substrates. DBC-1 binds at amino acids 243-268, a region in the catalytic core of the SIRT1 protein, to confer reduced deacetylase activity, observed as an increase in p53 activity and cell death (Kim et al., 2008; Zhao et al., 2008).

The dependence of SIRT1 on the availability of the NAD^+ cofactor means that changes in the cellular concentration of NAD^+ can have profound effects on downstream SIRT1-mediated responses. The high-affinity Na^+-dependent dicarboxylate cotransporter (NaDC3) is required for the transport of Krebs' cycle intermediates so affects the NAD^+/NADH ratio within the cell. Overexpression of NaDC3, increasing Krebs' cycle intermediates and decreasing NAD^+, caused downregulation of (NAD^+-dependent) SIRT1 activity and associated cellular senescence in embryonic lung fibroblasts (Liu et al., 2010). Similarly, in transgenic mice with increased nicotinamide mononucleotide adenylyltransferase 1 (NMNAT-1) activity and therefore increased NAD^+ biosynthesis a SIRT1-mediated increase in axonal protection was observed (Araki et al., 2004).

1.2.2.4 Regulation of SIRT1 by lifestyle factors

Intensive exercise was found to increase the levels of SIRT1 protein within rat (Suwa et al., 2008) and human (Guerra et al., 2010) skeletal muscle though the mechanism by which this is mediated remains unclear. Notable with respect to regulation of SIRT1 by dietary factors is the controversial evidence that the plant polyphenol resveratrol is a SIRT1 activator. This topic is discussed in detail in Section 1.4. Vitamin B_3, of which the NAD^+ precursors nicotinamide and nicotinic acid are both forms, has also been proposed as a potential regulator of SIRT1 activity, but has yet to be investigated thoroughly.

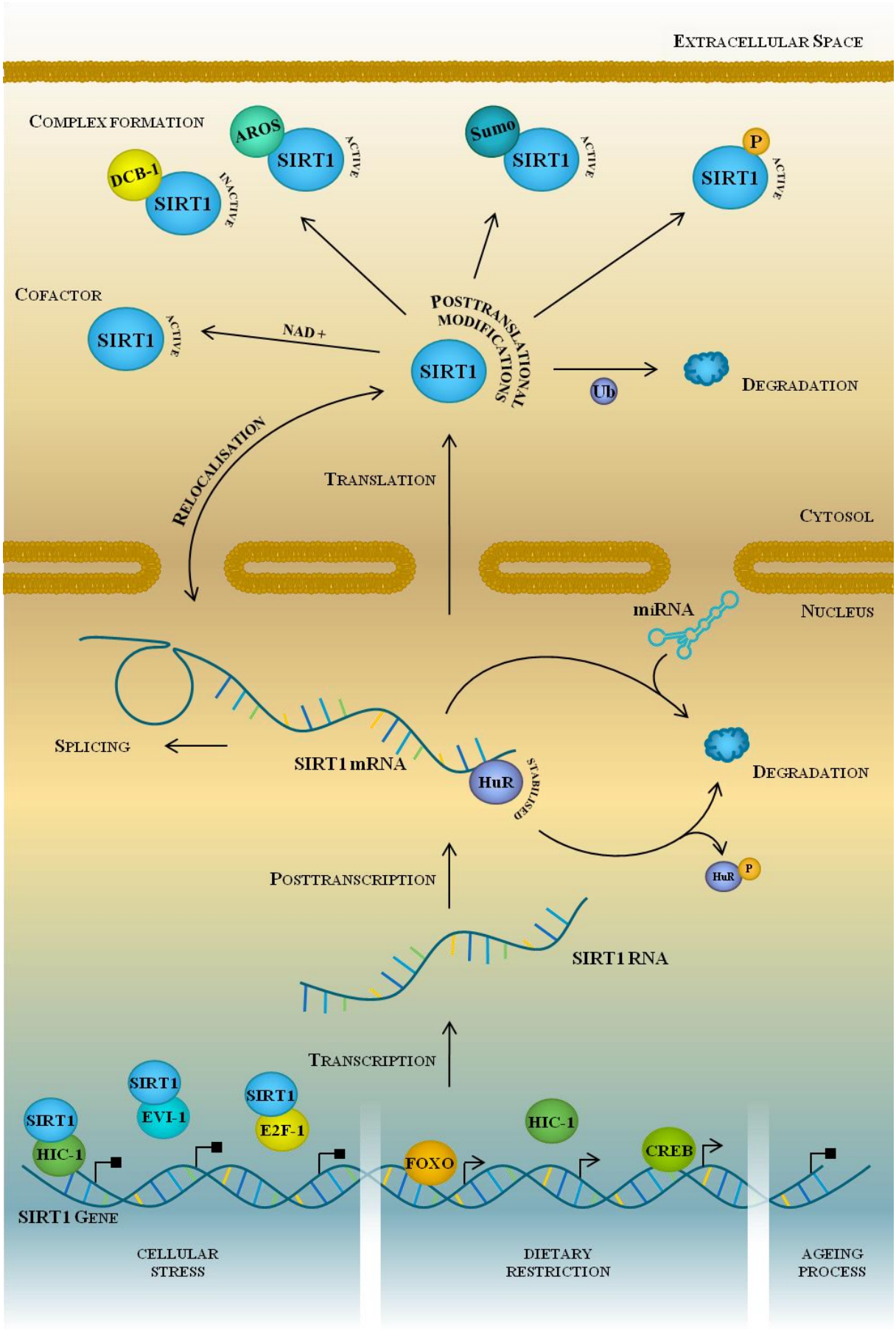
EXTRACELLULAR SPACE
COMPLEX FORMATION
AROS
SIRT1
ACTIVE
DCB-1
SIRT1
INACTIVE
Sumo
SIRT1
ACTIVE
P
SIRT1
ACTIVE
COFACTOR
SIRT1
ACTIVE
NAD+
POSTTRANSLATIONAL MODIFICATIONS
SIRT1
Ub
DEGRADATION
RELOCALISATION
TRANSLATION
CYTOSOL
miRNA
NUCLEUS
SPLICING
SIRT1 mRNA
HuR
STABILISED
DEGRADATION
HuR
P
POSTTRANSCRIPTION
SIRT1 RNA
TRANSCRIPTION
SIRT1
EVI-1
SIRT1
E2F-1
SIRT1
HIC-1
FOXO
HIC-1
CREB
SIRT1 GENE
CELLULAR STRESS
DIETARY RESTRICTION
AGEING PROCESS

Figure 1.4. Regulation of SIRT1, from gene to protein. *At the level of transcription, up- or downregulation of the SIRT1 gene is represented by an arrow or a closed square respectively. The stage in transcription under cellular stress at which the SIRT1 protein, through a negative feedback loop, suppresses further SIRT1 gene transcription is shown. HIC-1 is a repressor of SIRT1 transcription and binds as a complex with SIRT1. EVI-1 and E2F-1 are activators of SIRT1 transcription and form a complex with SIRT1, as shown, which no longer can bind to the SIRT1 promoter. At the level of translation, the activation state of the SIRT1 protein is indicated around the protein in response to the post-translational event shown. miRNA – microRNA; Sumo – sumoylation; P – phosphorylation; Ub – ubiquitiation.*

1.2.3 Current debate concerning a role for SIRT1 in lifespan extension

The many relevant processes and pathways that include substrates that are deacetylated by SIRT1, coupled with the factors found to regulate SIRT1, can be linked in multiple ways to provide plausible mechanisms through which SIRT1 may increase lifespan. Moreover, as already noted, there is a body of evidence based on transgenic models of Sir2 overexpression or ablation in model organisms that link the protein directly with increased lifespan. More recent evidence based on similar genetic approaches in model organisms however, challenge the view that SIRT1 plays a fundamental role in determining lifespan. In particular, longevity in two long lived worm lines with overexpression of Sir2 was abrogated on backcrossing to wild-type, without reduction in Sir2 expression, and Sir2 knockdown by siRNA had no effect on lifespan (Burnett et al; Nature, 2011; in press).

1.3 Epigenetic modifications

Post-translational modifications of histone proteins by acetylation, methylation and phosphorylation, alongside methylation of the DNA at cytosine residues in CpG dinucleotide sites, form the major components of epigenetic marking that create changes in gene expression without affecting the underlying DNA sequence.

1.3.1 Histone acetylation

Histone acetylation is the covalent addition of an acetyl group to the ε-N of lysine in the histone tail catalysed by histone acetyltransferase (HAT) enzymes (Vidali et al., 1968). The removal of this acetyl group is by the histone deacetylase (HDAC) group of enzymes, which includes the sirtuin family (*Figure 1.2*). The HAT and HDAC enzymes together modulate histone acetylation status throughout the genome (Grozinger and Schreiber, 2002; Roth et al., 2001). Acetylation of the positively charged lysine residues on the histone tails by HAT neutralises the histone charge. This modification, in turn, repels the negatively charged DNA wrapped around the histone core making it more transcriptionally accessible, further enhanced by the creation of specific binding sites for transcription factors. Removal of the acetyl groups through histone deacetylation reinstates the positive charge of the lysine residues inducing a conformational change of the chromatin around the histones, which becomes condensed, highly compacted and transcriptionally-repressed. Therefore, the SIRT1 histone deacetylase may potentially influence epigenetic status, and hence gene expression, through its histone deacetylase activity. This view is substantiated through studies on the epigenetic effects of SIRT1. Evidence includes the observation that under conditions of SIRT1 knockdown in human embryonic kidney cells there was hyperacetylation of histones and in conditions of SIRT1 overexpression there was reduced histone acetylation of an exogenous target (Vaquero et al., 2007). SIRT1 knockdown or inhibition led to reactivation of aberrantly silenced, hypermethylated tumour suppressor genes associated with an increase in histone acetylation in the corresponding gene promoter region (Pruitt et al., 2006).

1.3.2 DNA methylation

DNA methylation involves DNA methyltransferase catalysing the covalent addition of a methyl group from S-adenosylmethionine to the 5' carbon of the nucleotide cytosine forming 5-methylcytosine. Upon donating the methyl group S-adenosylmethionine converts to S-adenosylhomocysteine (*Figure 1.5*).

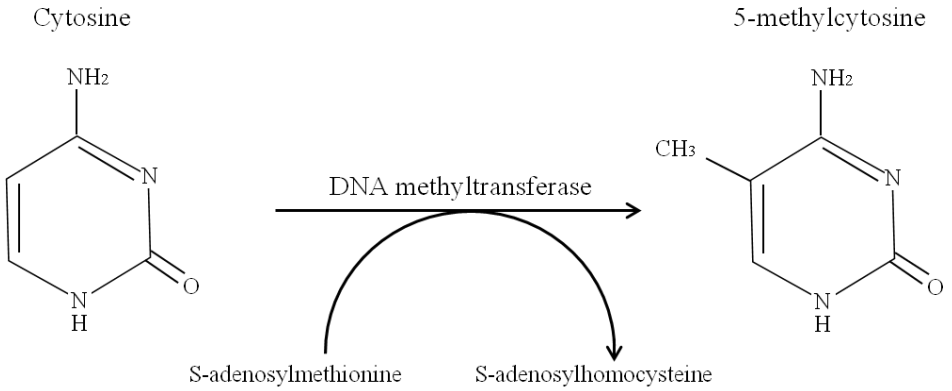

Figure 1.5. Methylation of the nucleotide cytosine. *The methyl group is donated by S-adenosylmethionine, catalysed by DNA methyltransferase, to the 5' carbon of cytosine forming 5-methylcytosine.*

DNA methylation is associated with transcriptional suppression. Methylated cytosines occur in CpG dinucleotide pairs; around 70 % of CpG sites across the genome are methylated. The remaining unmethylated CpG sites are found predominately in CpG islands - areas of the genome that are GC rich (Bird et al., 1985). Many mammalian gene promoters include a CpG island, which may include binding sites for transcription factors (Saxonov et al., 2006). A relatively new concept to emerge from the study of CpG distribution throughout the genome is the description of CpG shores, defined as regulatory regions within 2000 bp of CpG islands, whose methylation status correlates with the expression of the associated gene (Irizarry et al., 2009).

The presence of epigenetic modifications explains how genetically identical somatic cells can take up diverse functional roles and make up phenotypically distinct tissue types within the body. The current dogma is that DNA hypomethylation results in gene expression and hypermethylation results in gene suppression, although emerging data now challenge the ubiquity of this idea. Upon methylation of CpG sites the methyl CpG binding protein 2 (MeCP2), which contains a methylcytosine binding domain and a transcriptional repressor domain, binds to DNA and recruits histone deacetylases and mSin3A, a transcriptional repressor, in a repressive multiprotein complex (*Figure 1.6*) (Nan et al., 1997). Genome-wide studies have allowed for the investigation and observation of tissue-specific DNA methylation patterns at CpG islands in the promoter regions of genes (Illingworth et al., 2008; Rakyan et al., 2008; Schilling and Rehli, 2007; Bock et al., 2006). Of particular note is the discovery

of the involvement of epigenetics in inter-individual variation (Schneider et al., 2010; Bock et al., 2008; Flanagan et al., 2006) and the role played by epigenetics in the ageing process (Kwabi-Addo et al., 2007; Fraga et al., 2005).

1.3.3 The link between DNA methylation and histone acetylation

Evidence that DNA methylation can initiate changes in histone acetylation is robust and includes the observation that the MeCP2 transcriptional repressor domain in mouse fibroblasts once bound to methylated DNA recruits histone deacetylases (HDACs), mediating repression of chromatin (Nan et al., 1998), and that *Xenopus laevis* oocytes injected with methylated and unmethylated plasmid constructs revealed chromatin assembly on the methylated DNA followed by MeCP2 binding and recruitment of HDACs (Jones et al., 1998). Similarly, transfection of mouse fibroblasts with an unmethylated thymidine kinase gene construct or an equivalent methylated construct, followed by immunoprecipitation of the acetylated fraction, revealed the acetylated fraction to be associated predominantly with the unmethylated construct (Eden et al., 2003). All of these studies highlight the importance of DNA methylation and of the MeCP2 complex to induce changes in histone acetylation and, therefore, gene expression.

In contrast, evidence supporting the view that histone acetylation status can influence DNA methylation status is less well represented within the literature. It is proposed that histone acetylation confers protection of the adjacent DNA preventing methylation. Insulator elements are known to exist within chromatin, defining the boundaries between heterochromatic and euchromatic regions of the genome through inhibiting DNA methylation machinery and encouraging acetylation of histones H3 and H4, allowing the binding of transcription factors (Mutskov et al., 2002). Additional evidence for histone acetylation dictating DNA methylation comes from the use of histone deacetylase inhibitors; n-butyrate caused global DNA demethylation in mouse splenocytes (Szyf et al., 1985); the histone deacetylase inhibitor trichostatin A (TSA) caused selective DNA demethylation in *Neurospora* (Selker, 1998) and in the human embryonic kidney cell line HEK293 (Ou et al., 2007). Treatment with TSA also resulted in marked demethylation of transiently-transfected reporter constructs in HEK293 cells (Cervoni and Szyf, 2001). A successive study observed that overexpression of the oncoprotein Set/TAF-1β, an inhibitor of histone acetylation, in HEK293 cells resulted in hypermethylation of reporter constructs (Cervoni et al., 2002). Similar consequences for DNA methylation were observed with the histone deacetylase inhibitor valproate in mouse brain (Dong et al., 2007) and HEK293 cells (Milutinovic et al., 2007). These interactions between DNA methylation and histone acetylation are summarised diagrammatically in Figure 1.6.

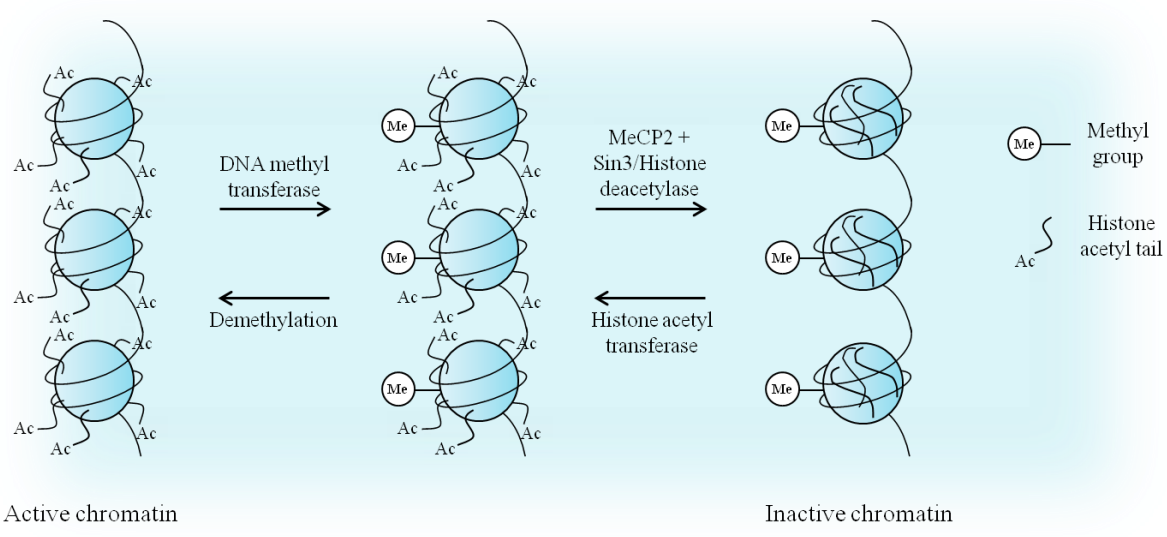

Figure 1.6. The interrelationship between DNA methylation and histone acetylation. *DNA methylation leads to the assembly of a multiprotein co-repressor complex in which MeCP2 binds to methylated DNA and recruits proteins including the transcription repressor mSin3A and histone deacetylases, bringing about changes to histone acetylation status. Some evidence suggests these change can be reversed through histone acetyltransferase activity and DNA demethylation.*

1.3.4 DNA methylation and ageing

Changes in DNA methylation are associated with the ageing process (Wilson and Jones, 1983) and may have effects on gene expression, chromosomal instability and telomere integrity (Gonzalo et al., 2006; Eden et al., 2003; Richardson, 2003). Inter-individual variation in DNA methylation has been implicated in the divergence of disease susceptibility; monozygotic twin studies have shown an increasing discordance in the level and distribution of DNA methylation with age (Fraga et al., 2005). Demethylation with ageing has been observed in many tissues across many species (Wilson et al., 1987; Vanyushin et al., 1973), however these early studies measured total methylcytosine content. More recently-developed technologies, in particular those utilising downstream array hybridisation or that measure site-specific methylation within a sequence of interest, have given a greater insight into the role that DNA methylation plays in the ageing process. A study using methylation-sensitive restriction digestion followed by array hybridisation showed considerable difference in the methylation profile between young and old measured in the mouse small intestine (Maegawa et al., 2010). Similar divergence with age in methylation patterns has also been observed in multiple human tissues, where it was observed that the direction of change in methylation with age at a specific loci was dependent upon whether the locus resides in a CpG island (Christensen et al., 2009). Previous investigations of site-specific methylation changes with age, have also shown hypermethylation with age at CpG islands associated with genes implicated in prostate cancer (Kwabi-Addo et al., 2007) and

conversely loci within CpG rich regions associated with pancreatic cancer have show hypomethylation with the onset of the age-associated disease (Sato et al., 2003).

With the introduction of whole-genome array technologies the classic view that the genome is hypomethylated with ageing, though still apparent at the global level when measuring repetitive elements such as Alu (Bollati et al., 2009), has been replaced with an ever growing body of evidence suggesting a complex pattern of methylation status within individual tissue types that is dysregulated during aging (Maegawa et al., 2010; Rakyan et al., 2010; Teschendorff et al., 2010; Christensen et al., 2009; Kwabi-Addo et al., 2007).

1.4 Nutrient-mediated modulation of epigenetic mechanisms

Substantial inter-individual variation in age-related DNA methylation may be due to different environmental and lifestyle factors (Issa, 2002). Comparison of the DNA methylation profiles of pairs of monozygotic twins revealed that differences between twin pairs were greater in older individuals and that twins who had led different lifestyles and/or lived apart showed greater divergence in DNA methylation patterns that twins subject to similar environmental factors, indicating a role of environment, and possibly diet, in influencing DNA methylation (Fraga et al., 2005). Numerous studies, both *in vitro* and *in vivo*, have shown effects of specific dietary components on DNA methylation. These factors include folate, a precursor in the synthesis of S-adenosylmethionine, the universal methyl donor involved in methylation (Balaghi and Wagner, 1993), selenium (Davis et al., 2000), and polyphenolic compounds found in plants, such as genistein (Day et al., 2002) and (-)-epigallocatechin-3-gallate. Epigallocatechin-3-gallate, a polyphenolic compound found in green tea, competes for the catalytic domain of DNA methyltransferase I, inhibiting the methylation of cytosine (Fang et al., 2003). A screen of ~20,000 molecules for activators of the SIRT1 histone deacetylase identified the plant polyphenol resveratrol (Howitz et al., 2003) which, may therefore, through the action of SIRT1 deacetylation affect DNA methylation.

1.4.1 Potential sirtuin-activating polyphenolic compounds

Dietary compounds naturally derived from various plant sources include polyphenols that potentially activate SIRT1. The compounds include resveratrol, noted above for its ability to activate SIRT1, and the isoflavones genistein and daidzein (*Figure 1.7*).

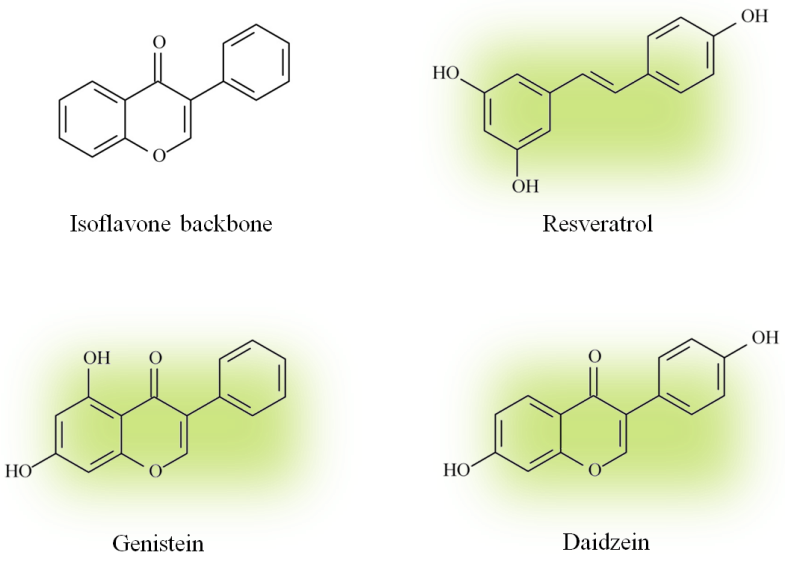

Figure 1.7. Chemical structures of selected polyphenols.

1.4.1.1 Resveratrol

Resveratrol (3, 5, 4'-trihydroxystilbene) is a polyphenolic compound that acts as a phytoalexin produced in plants as a response to bacterial and fungal infection. Resveratrol is in the stilbene subgroup of the polyphenol family and can be found in a range of fruits and nuts, particularly in the skins of red grapes. Resveratrol has been shown to cause an increase in SIRT1 affinity for the NAD^+ substrate and the acetylated substrate through allosteric affects and so increases SIRT1 activity (Howitz et al., 2003). In lower eukaryotes, resveratrol has been shown to increase lifespan in a Sir2-dependent manner (Wood et al., 2004; Howitz et al., 2003). The literature includes discordance over whether or not Sir2 in lower eukaryotes plays a role in determining lifespan and in particular if resveratrol can have effects to extend lifespan through activation of Sir2 (Bass et al., 2007; Gruber et al., 2007; Kaeberlein et al., 2005a; Viswanathan et al., 2005; Bauer et al., 2004; Jarolim et al., 2004). The main source of controversy surrounding activation of SIRT1 by resveratrol is an *in vitro* fluorescence activity assay used to measure SIRT1 deacetylase activity (Howitz et al., 2003), with several groups reporting independently that activation of SIRT1 by resveratrol is only observed when SIRT1 is attached to a fluorescent moiety (Pacholec et al., 2010; Beher et al., 2009; Borra et al., 2005; Kaeberlein et al., 2005a). Irrespective of whether measures of the effects of resveratrol on SIRT1 deacetylase have been flawed, a body of evidence indicates that resveratrol may influence lifespan and/or healthspan through actions involving SIRT1. At the transcriptional level resveratrol has been shown to change levels of SIRT1 mRNA (Csiszar et al., 2009), upregulate transcription factors in a SIRT1-dependent manner (Gracia-Sancho et al., 2010) and mediate SIRT1-regulated adipogenesis (Picard et al., 2004). Mammalian studies into the potential of dietary resveratrol to mimic some of the

beneficial effects of DR in ageing and lifespan-extension include studies of the role of dietary resveratrol in protecting against some of the biochemical and physiological effects of a high fat diet in mice. Effects of resveratrol included a reversal in increased glucose, insulin and IGF-1 levels and a reversal in increased liver size (Baur et al., 2006). In a second study, dietary resveratrol increased mitochondrial biogenesis, consistent with a reduction in the acetylation levels of the main regulator of mitochondrial production, PGC-1α. This effect was not observed in $SIRT1^{-/-}$ mouse embryonic fibroblasts, suggesting that SIRT1 may play a role in mediating this action (Lagouge et al., 2006). Evidence that resveratrol can mimic some changes associated with DR were obtained through comparison of gene expression profiles between mice fed resveratrol or mice subjected to DR. Both treatments showed a high level of similarity in their effect on gene expression and these changes opposed age-related changes in gene expression (Barger et al., 2008). This observation was corroborated in an independent study (Pearson et al., 2008). However, the resveratrol-fed mice did not show an increase of SIRT1 in brain or liver (Barger et al., 2008) and the lifespan extension properties of resveratrol have yet to be seen in lean mice (Pearson et al., 2008).

1.4.1.2 Isoflavones

The polyphenols genistein (4', 5, 7-trihydroxyisoflavone) and daidzein (4', 7-dihydroxyisoflavone) reside in the isoflavone subgroup of the flavonoids and share a degree of structural similarity to resveratrol (*Figure 1.7*). Genistein and daidzein are both found in abundance in soyabeans and have been associated with beneficial effects against age-related diseases that include osteoporosis, various cancers and cardiovascular disease. The isoflavones have been observed to have both negative and positive effects on DNA methylation. These observations include the reversal of DNA hypermethylation of the $p16^{INK4a}$, retinoic acid receptor beta (RARβ) and O6-methylguanine DNA methyltransferase (MGMT) loci in esophageal squamous carcinoma cells treated with genistein and the reversal of hypermethylation and induced mRNA expression of RARβ upon treatment of prostate cancer cell lines with genistein. Daidzein treatment of esophageal squamous cell carcinoma cells showed similar effects on expression of the RARβ mRNA (Fang et al., 2005). The glutathione S-transferase gene, GSTP-1 is hypermethylated in prostate cancer; glutathione S-transferase catalyses the detoxification of oxidative stress byproducts. Treatment of human prostate cancer cell lines with genistein and daidzein induced demethylation of the GSTP-1 promoter region, and was proposed to contribute to the lower incidence of prostate cancer within Asian populations whose diet is rich in soy polyphenols (Vardi et al., 2010).

Conversely, differential hybridisation to a DNA microarray of methylated and unmethylated mouse DNA identified CpG islands that were hypermethylated in response to a genistein-supplemented diet (Day et al., 2002). Studies using the agouti variable yellow mouse model, which shows a shift in coat colour from yellow to pseudo-agouti in response to methylation of DNA upstream of the Agouti gene, revealed increased DNA methylation in response to genistein supplementation (Dolinoy et al., 2006).

Isoflavones have mechanisms of action independent of effects on DNA methylation. Of particular relevance in the context of our hypothesis, genistein and daidzein were found to increase mitochondrial biogenesis in renal proximal tubular cells, in concert with deacetylation and activation of the SIRT1 substrate and regulator of mitochondrial biogenesis PGC-1α. It remains unclear if these effects were mediated through SIRT1 activation, since only daidzein activated recombinant SIRT1 *in vitro* (Rasbach and Schnellmann, 2008).

The indication that the soyabean isoflavones may, as with resveratrol, mediate cellular effects through SIRT1 identifies these dietary agents as potential mimetics of some aspects of the longevity response to DR.

1.5 Techniques employed for analysis of the epigenetic mechanism DNA methylation

A variety of methods are currently employed to measure DNA methylation status. Many methods utilise the sequence recognition properties of restriction enzymes to distinguish between products that have, or have not, been deaminated by bisulfite modification, or restriction enzymes whose cleavage is hindered by the presence of a methyl group in combination with an isoschizomer that is not. These techniques can be refined to measure both global and site-specific DNA methylation. DNA methylation detection methods also include the use of chromatin immunoprecipitation with antibodies that recognise 5-methylcytosine or proteins that bind to methylated DNA. These methods are now regularly followed by hybridisation of the products to a microarray chip. High-throughput next generation sequencing, of either bisulfite-modified or immunoprecipitated DNA, is fast becoming the state-of-the-art approach to measuring DNA methylation across genomes. The techniques employed in this thesis are detailed below.

1.5.1 Bisulfite Modification

Bisulfite modification is used in conjunction with a downstream application to distinguish between methylated and unmethylated cytosines at the level of a single nucleotide. Genomic DNA is bisulfite modified, which involves deamination of unmethylated cytosines to uracil through removal of an amino group (*Figure 1.8A*). This sodium bisulfite treatment effectively fixes the DNA methylation pattern within the sample, as the methyl group protects methylated cytosines from deamination, in contrast to the unprotected cytosines which when converted to a uracil base are read by DNA polymerase in a subsequent PCR reaction as thymine (Clark et al., 1994) (*Figure 1.8B*).

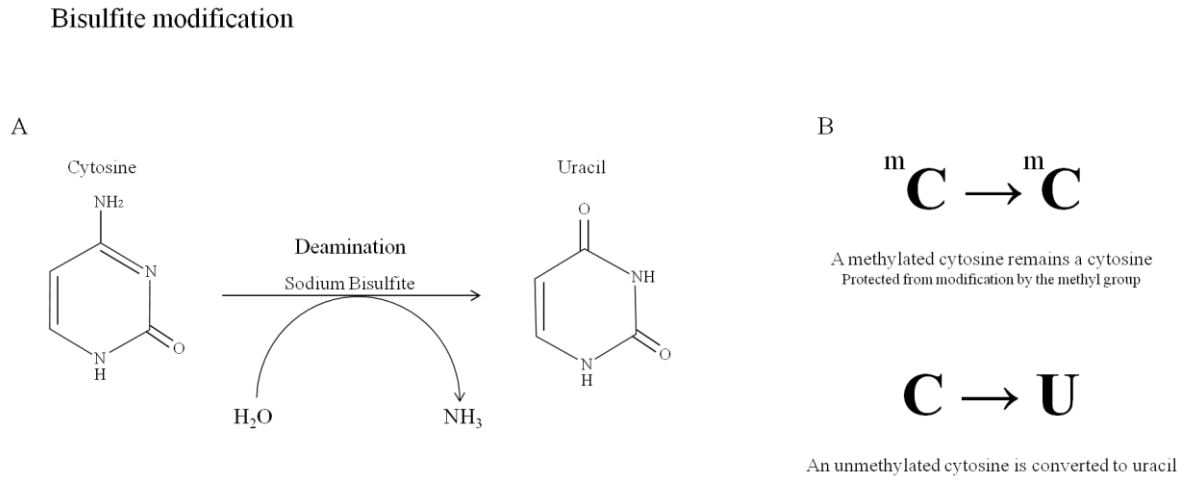

Figure 1.8. Deamination through bisulfite modification. *A – Sodium bisulfite catalyses the hydrolytic removal of an amino group from cytosine to form uracil. B – Methylated cytosines are protected from deamination.*

1.5.2 Combined Bisulfite Restriction Analysis (COBRA)

Bisulfite modification of DNA followed by PCR amplification leads to the loss or retention of existing methylation-dependent restriction sites, dependent on the methylation status of the cytosine residing in the restriction site upon deamination. Combined Bisulfite Restriction Analysis (COBRA) (Xiong and Laird, 1997) is a method that exploits the change in restriction sites dependent on methylation status through digestion with a restriction enzyme whose recognition sequence contains a cytosine as part of a CpG site.

To estimate global DNA methylation the COBRA technique is applied to a repetitive element within the genome. The LINE-1 (long interspersed nucleotide element 1) retrotransposons contribute to around 21 % of the human genome sequence through the ability to self replicate and reintegrate into the genome, making it an ideal surrogate marker of global DNA methylation (Babushok and Kazazian, 2007). DNA samples are first bisulfite modified, fixing the DNA methylation pattern. COBRA LINE-1 (Yang et al., 2004) then involves amplification of the bisulfite modified DNA to the LINE-1 retrotransposon by PCR using specific LINE-1 primers. The PCR product is digested with the restriction enzyme *HinfI*. The *HinfI* restriction sequence is 5' -G/ANTC- 3', so after bisulfite modification the enzyme will cleave only PCR product generated from a methylation sequence where the cytosine has been protected against deamination. Within the LINE-1 retrotransposon sequence there are two such *HinfI* restriction sites. The methylation at these two CpG sites in a DNA sample is expressed as the ratio of uncut to cut PCR product as determined by densitometric quantification of SYBR green-stained agarose gels (*Figure 1.9*).

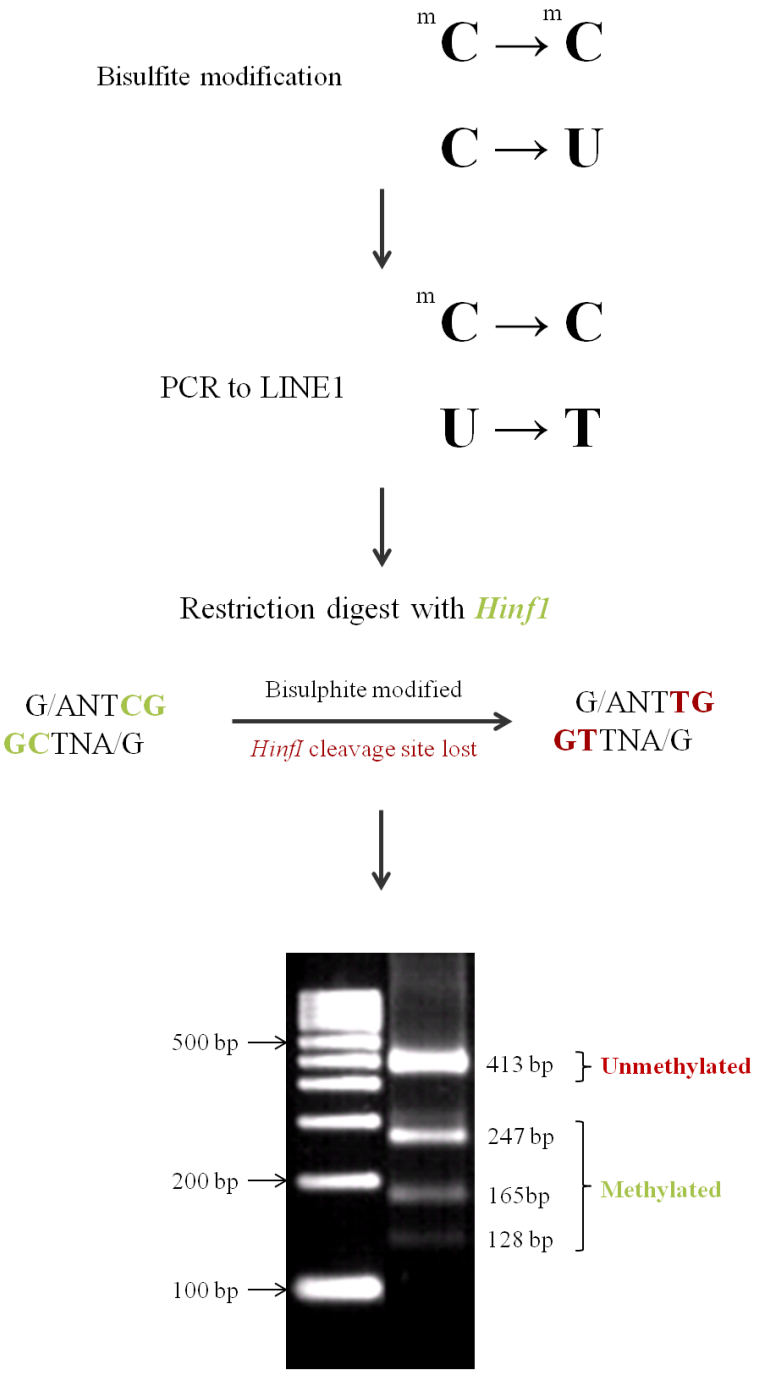

Figure 1.9. Schematic representation of COBRA. *Genomic DNA is bisulfite modified to 'fix' the DNA methylation pattern. Bisulfite modified DNA is then PCR amplified to the LINE-1 sequence and the PCR products are digested with the restriction enzyme HinfI. Deamination reaction with by sodium bisulfite of unmethylated (and therefore unprotected) CpG sites results in the loss of the HinfI recognition sequence, preventing digestion by the enzyme. This procedure produces two sets of fragments – uncut, representing unmethylated DNA and cut, representing methylated DNA – the ratio of which can be used to express the methylation status within the original sample of the CpG sites within the recognition sequence.*

1.5.3 Pyrosequencing

1.5.3.1 Principle of pyrosequencing

Pyrosequencing is a method of sequencing DNA and analysing methylation status through the release and quantification of pyrophosphate by a nucleotide incorporation event. One of the four deoxynucleotide triphosphates (dNTPs) is added to the reaction and incorporated by DNA polymerase if complementary to the template sequence. As the correct base is incorporated pyrophosphate (PPi) is released. PPi and adenosine 5' phosphosulfate (ASP) are converted to adenosine triphosphate (ATP) by sulfurylase which drives luciferase to convert luciferin to oxyluciferin. This conversion generates light which is detected by a charged coupled device (CCD) camera and produces a signal peak on the pyrogram. Apyrase degrades unincorporated dNTPs and excess ATP. Upon completion of degradation another of the four dNTPs is added. As each dNTP is added the sequence of the complementary strand is elucidated.

1.5.3.2 Performing the pyrosequencing assay

To prepare a sample for pyrosequencing, genomic DNA is first bisulfite modified to fix the methylation pattern. The bisulfite modified DNA is subjected to two rounds of PCR amplification. Primers are designed to a target sequence, focusing on a region containing CpG sites whose DNA methylation status is of interest. The first PCR is to a larger region around the target sequence using bisulfite-modified genomic DNA as a template and degenerate primers – 50 % C and 50 % T – at the site of a CpG location, to avoid bias selection of the methylated or unmethylated sequence. The second round of PCR performed is a nested PCR to a smaller region within the target sequence, focusing in on the specific CpG sites to be measured. PCR reactions contain HotStarTaq Master Mix, sense primer, biotinylated antisense primer and the first PCR reaction to act as a DNA template. Biotinylated antisense primer is used at a lower concentration within the reaction to prevent excess biotin and reduce primer dimerisation. The size of the PCR product is confirmed by agarose gel electrophoresis and used in the pyrosequencing reaction as described above. The primers and sequencing primer used in the second PCR are designed using the PyroMark Assay Design Software 2.0 (Qiagen). Percentage DNA methylation is then measured at the target CpG sites within the sequence of interest.

The ratio of converted cytosine (thymine) to unconverted cytosine within each CpG site (C/T) is used to determine the percentage DNA methylation at each CpG site. An inbuilt control, a cytosine not followed by a guanine, acts to assess the efficiency of the bisulfite modification step, as the cytosine should not be methylated and so upon bisulfite treatment be fully converted to a thymine following PCR.

1.5.3.3 Confirmation of linear amplification

For each target sequence analysed by pyrosequencing the linear amplification of methylated and unmethylated sequences is confirmed using a standard curve. Unmethylated DNA template is generated through PCR amplification of the target sequence from genomic DNA. Unmethylated PCR product is methylated *in vitro* using CpG *SssI* methylase. Methylated and unmethylated products are bisulfite modified to fix the DNA methylation pattern and combined to give appropriate methylation percentages to generate the standard curve (0, 5, 10, 25, 50, 75, 90, 95, 100 % methylated). A non linear relationship between standard concentration and percentage DNA methylation indicates biased amplification of methylated or unmethylated DNA and requires assays to be redesigned to achieve a more reliable result.

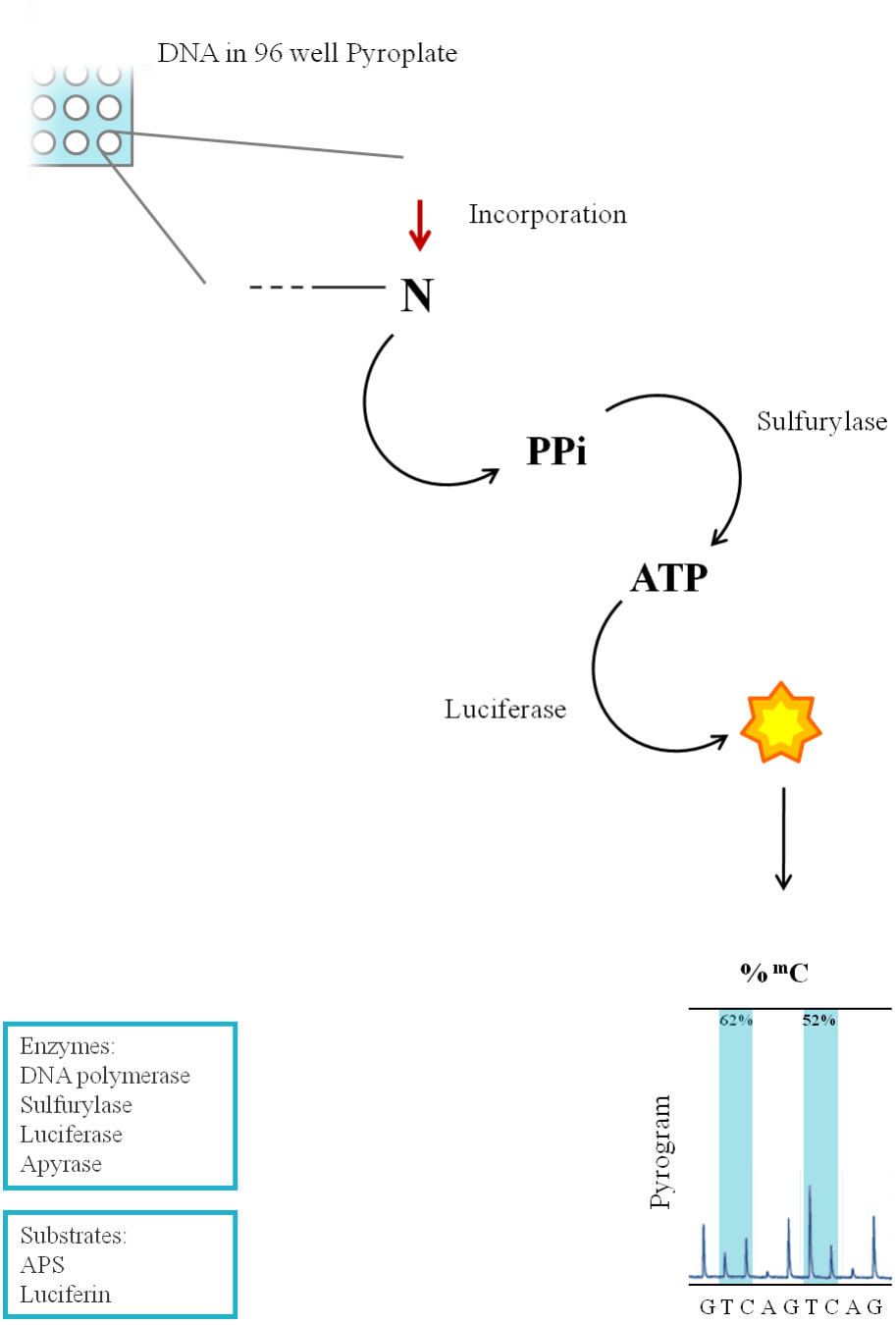

Figure 1.10. Schematic representation of the pyrosequencing reaction. *Upon incorporation of a dNTP by DNA polymerase PPi is released. PPi and APS are converted to ATP by sulfurylase. ATP then drives the luciferase-mediated conversion of luciferin to oxyluciferin (light), which is recorded as a signal peak on the pyrogram. dNTP/'N' – deoxynucleotide triphosphates; PPi – pyrophosphate; APS – adenosine 5' phosphosulfate; ATP – adenosine triphosphate;* ^{m}C *– 5'-methyl cytosine.*

1.5.4 LUminometric Methylation Assay (LUMA) using Pyrosequencing

The LUminometric Methylation Assay (LUMA) (Karimi et al., 2006) uses methylation-specific cleavage by restriction enzymes to determine the methylation status of a cytosine by bioluminometric polymerase extension of the resulting overhang. The LUMA assay involves digestion of genomic DNA with either *EcoRI* and *MspI* restriction enzymes or *EcoRI* and *HpaII* restriction enzymes. *MspI* and *HpaII* are isoschizomers which are CpG methylation insensitive and CpG methylation sensitive, respectively, and upon DNA cleavage leave 5'-CG overhangs. The *EcoRI* enzyme leaves 5'-AATT overhangs and provides an inbuilt control for DNA concentration. The products of the two separate DNA digestions are then quantified using the pyrosequencer by extending the 5' overhangs. The percentage methylation of the DNA sample is determined by the *MspI*/*HpaII* ratio; a ratio of 1.0 would represent 100 % methylation whereas an *MspI*/*HpaII* ratio approaching zero would represent unmethylated DNA (*Figure 1.11*).

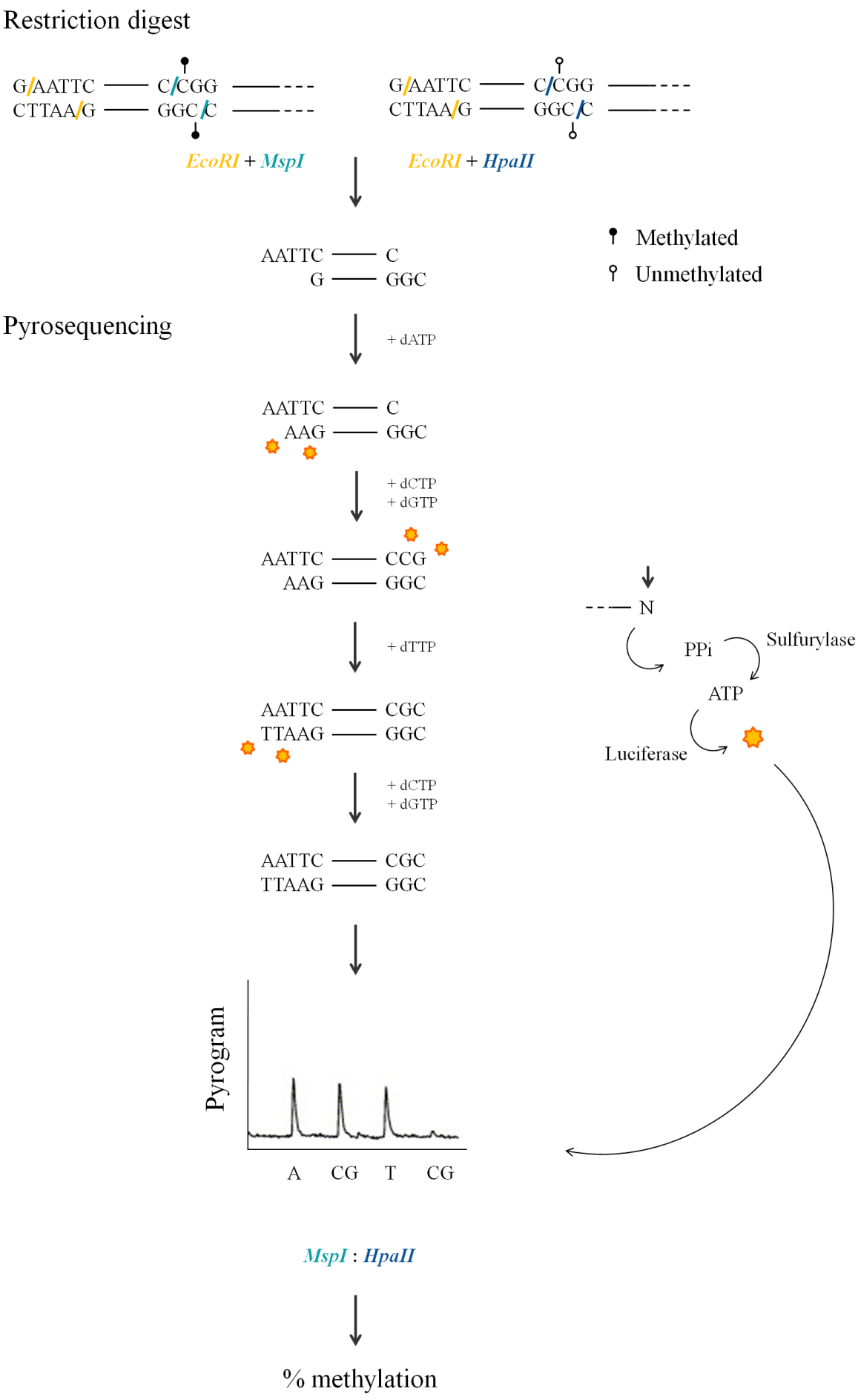
Restriction digest
G/AATTC
C/CGG
CTTAA/G
GGC/C
EcoRI + MspI
EcoRI + HpaII
Methylated
Unmethylated
Pyrosequencing
AATTC
C
G
GGC
+ dATP
AAG
+ dCTP
+ dGTP
CCG
+ dTTP
CGC
TTAAG
N
PPi
Sulfurylase
ATP
Luciferase
Pyrogram
A
CG
T
CG
MspI : HpaII
% methylation

Figure 1.11. Schematic representation of LUMA assay. *Genomic DNA is digested with a combination of either EcoRI and MspI or EcoRI and HpaII restriction enzymes. Pyrosequencing (Section 1.5.2) is employed to measure the extent of cleavage. EcoRI cleavage is represented by peaks produced upon incorporation of A and T (1st and 3rd peaks on the pyrogram). MspI or HpaII cleavage, in the respective reactions, is represented by the peak produced upon incorporation of C and G (2nd peak on the pyrogram). The ratio of these peaks is then used to calculate the percentage DNA methylation within the sample. The final incorporation event of C and G is an internal control to ensure that the previous extension was completed and so therefore any peak generated should be close to zero (4th peak on the pyrogram). Adapted from (Karimi et al., 2006).*

1.5.5 Methylated DNA Immunoprecipitation (MeDIP)

Methylated DNA Immunoprecipitation (MeDIP) (Weber et al., 2005) is an affinity-based method that utilises an antibody to 5-methylcytidine to produce an enriched product to detect methylation status across the genome. MeDIP involves sonication of genomic DNA via an ultrasonic homogeniser to fragment the DNA into 200 – 1000 bp lengths for immunoprecipitation. The fragmented DNA is incubated with a primary anti-5-methylcytidine antibody which binds methylated cytosines within the sample DNA sequence. The complex of antibody and methylated DNA is purified by the addition of secondary IgG coated superparamagnetic polystyrene beads and capture on a magnetic rack. This methylated-enriched fraction can then be co-hybridised to an array chip with a complementary input sample or subjected to high throughput sequencing and alignment to a reference genome (*Figure 1.12*).

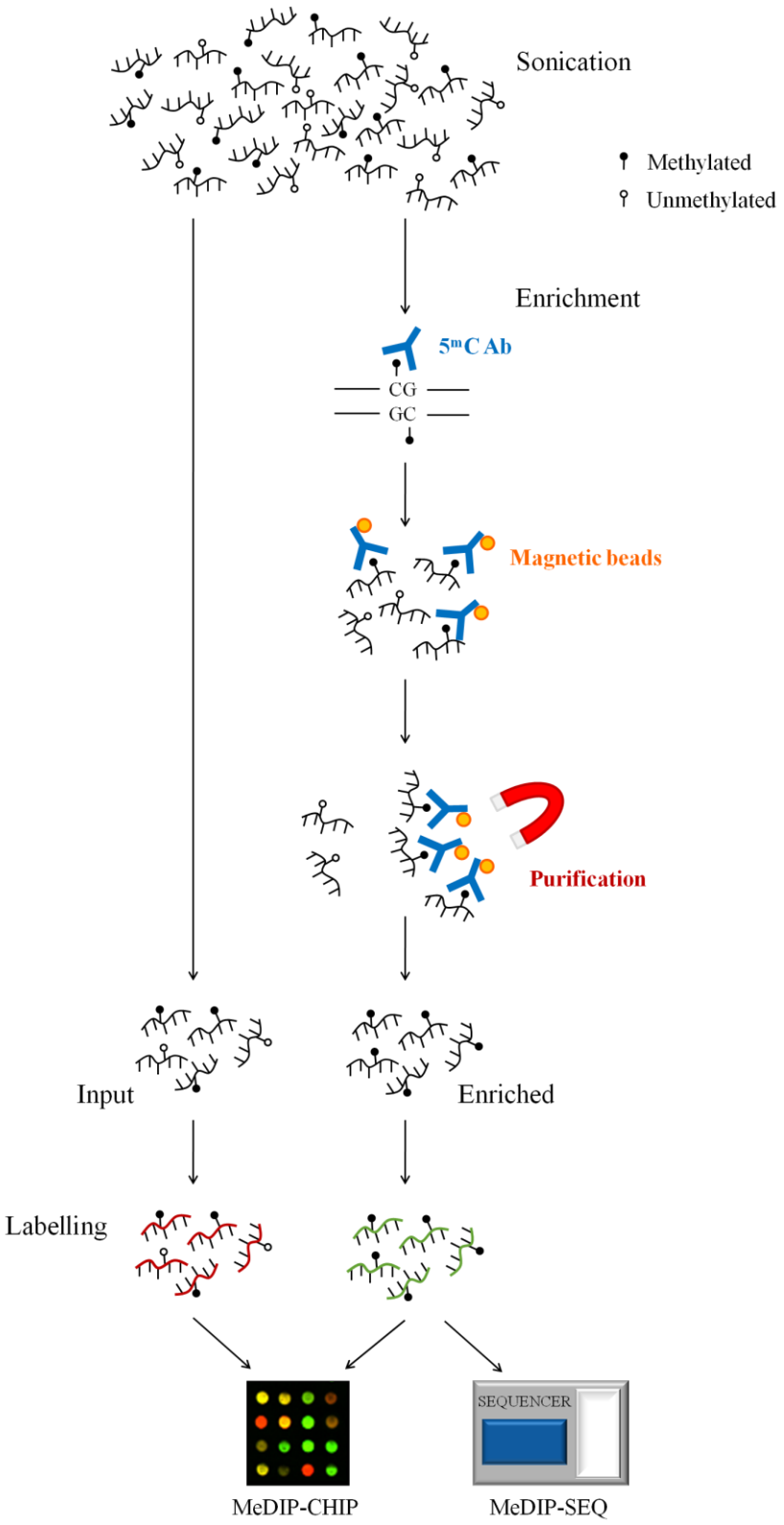

Figure 1.12. Schematic representation of methylated DNA immunoprecipitation followed by chip array hybridisation (MeDIP-CHIP) or high throughput sequencing (MeDIP-SEQ). *Genomic DNA is fragmented by sonication. A methylation-enriched fraction is generated through immunoprecipitation of methylated DNA using a 5mC Ab. This enriched fraction is then either co-hybridised to an array chip with an input sample (MeDIP-CHIP) or subjected to high throughput sequencing and alignment to a reference genome (MeDIP-SEQ). 5mC Ab – anti-5-methylcytidine antibody; magnetic beads – IgG coated superparamagnetic polystyrene beads.*

1.6 An investigation of roles for SIRT1 and dietary polyphenols in modulating the ageing process through DNA methylation

Our hypothesis is that effects on DNA methylation may contribute to the effects of DR to increase healthy lifespan through histone acetylation mediated by SIRT1, and these effects may be mimicked by plant derived polyphenolic compounds (*Figure 1.13*).

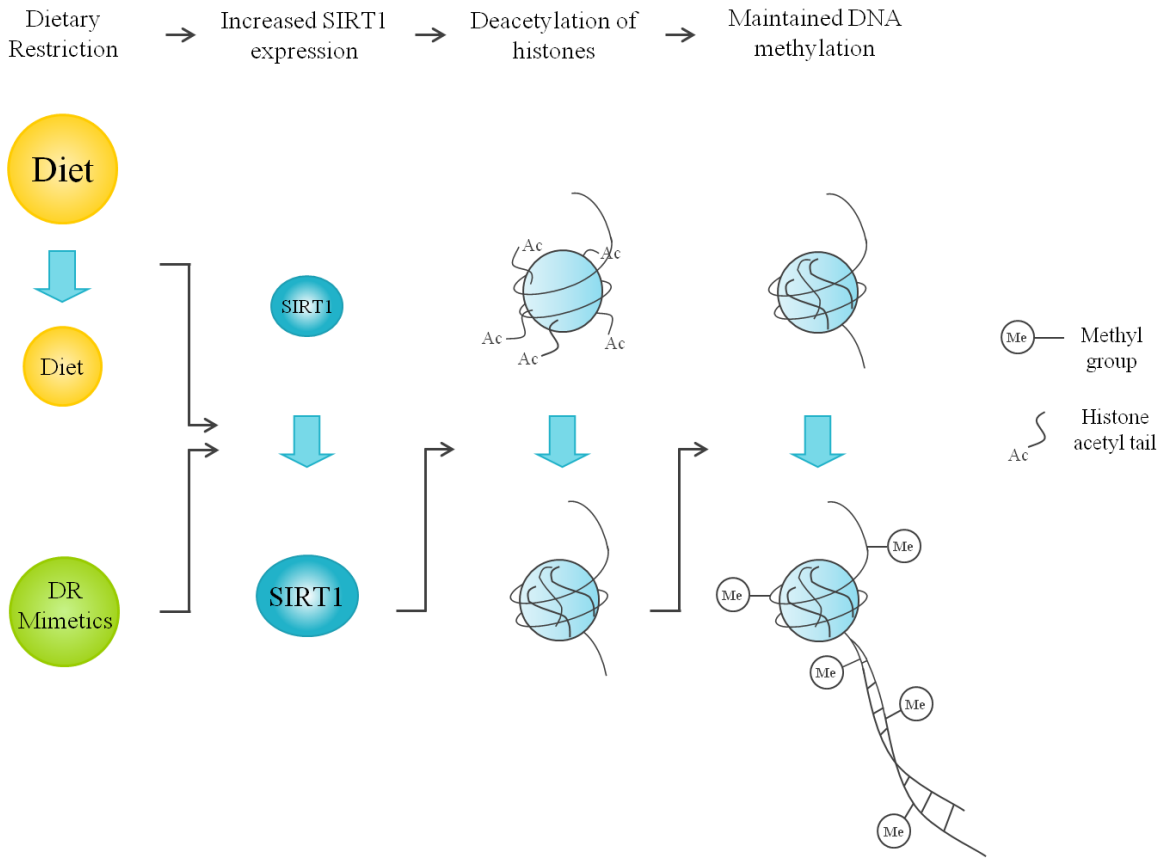

Figure 1.13. Diagrammatic representation of the hypothesis. *We propose that SIRT1-mediated histone deacetylation underlies some of the beneficial effects of dietary restriction (DR) on ageing/lifespan/healthspan through maintenance of DNA methylation. We also propose that specific dietary factors may bring about similar epigenetic consequences and so mimic beneficial effects of DR.*

1.7 Aims and objectives

This project aimed to investigate a role for SIRT1 and dietary polyphenols in healthy ageing by manipulating the expression levels or activity of SIRT1 in cultured human cells, including in combination with dietary polyphenols, to investigate if such interventions result in effects on DNA methylation, and to identify and investigate new targets whose regulation through SIRT1 may contribute to the mechanism of ageing proposed by the hypothesis. The specific objectives were:

i. to identify appropriate human cell lines for the investigation, taking into consideration levels of endogenous DNA methylation, ideally to identify cell lines with minimal and maximal levels of global DNA methylation to increase assay sensitivity with respect to detecting both increases and reductions in DNA methylation;

ii. to manipulate SIRT1 in a cell line model (human intestinal Caco-2 cells) through changes in activity (pharmaceutically) and expression (by overexpression of a transgene or siRNA mediated knockdown), and to determine the effect on global and site-specific DNA methylation;

iii. to investigate in the Caco-2 cell line model factors that may affect SIRT1 expression with regard to the central themes of the hypothesis: mimetics of dietary restriction, DNA methylation and age;

iv. to utilise an *in silico* approach to explore overlaps between groups of genes that associate with SIRT1, show altered expression in response to DR, and show altered methylation with ageing to support their relationship proposed by our hypothesis and identify further targets for *in vitro* investigation;

v. to investigate directly if methylation and/or expression of genes highlighted in the *in silico* analysis was affected by altering the expression of SIRT1 in the Caco-2 cell line model;

vi. to investigate on a genome-wide scale the effect on methylation and gene expression of altering SIRT1 expression and to explore overlaps between genes affected in these ways and genes that respond to DR and/or undergo age-related changes in methylation.

2 Materials and Methods

All chemical compounds were from Sigma Aldrich, UK unless otherwise stated and all water was molecular biology grade.

2.1 Culture of *Escherichia coli* cells

2.1.1 Growth

E. coli strains were grown overnight at 37 °C on Luria Bertoni (LB) agar plates (1 % NaCl, 1 % peptone, 0.5 % yeast extract, 15 g/L agar) containing 100 µg/ml ampicillin unless otherwise stated. Colonies were selected, grown overnight at 37 °C in 5 ml of LB containing 100 µg/ml ampicillin and, where applicable, screened for the corrected plasmid (Section 2.2.2). Where a larger yield of bacteria was required for plasmid preparation 1 ml of overnight culture was inoculated into 100 ml of LB containing the appropriate antibiotic; usually 100 µg/ml ampicillin and incubated at 37 °C in an orbital shaker until an optical density of 0.4 – 0.6 at 600 nm was reached, and plasmid DNA was prepared as described in Section 2.2.2.

2.1.2 Generation of competent cells

Competent OneShot TOP10 *E. coli* cells were purchased from Invitrogen for use in transformation.

2.1.3 Transformation of *E. coli* with plasmid DNA

Transformation of OneShot TOP10 *E. coli* (Invitrogen) with 3 µl plasmid DNA was performed on ice for 30 minutes, followed by heat shock at 42 °C and addition of 250 µl of SOC medium (2 % tryptone, 0.5 % yeast extract, 10 mM NaCl, 2.4 mM $MgCl_2$, 10 mM $MgSO_4$, 20 mM glucose) then cells were incubated shaking at 37 °C for 1 hour. Colonies were grown as described in Section 2.1.1.

2.1.4 Preparation of *E. coli* cell stocks

E. coli strains were cultured to an optical density of 0.4 – 0.6 at 600 nm as described in Section 2.1.1. Bacterial culture and 50 % glycerol were mixed in equal volumes, aliquoted into 1.5 ml microtube tubes, snap frozen in liquid nitrogen and stored at -80 °C.

2.2 Generation and manipulation of DNA plasmid constructs

DNA plasmid constructs were obtained from commercially available sources or generated as required within the laboratory. All plasmid are listed in Table 2.1. Plasmid maps are provided in Appendix A.

2.2.1 Sub-cloning of DNA into plasmid vectors

DNA products were cloned directly into pTOPO vectors (Invitrogen). Four microlitres of DNA product were incubated with 4 µl of vector, 1 µl 10x ligation buffer (Invitrogen) and 1 µl of ligase (Invitrogen) overnight at 16 °C. Three microlitres of the ligation reaction were then transformed with competent OneShot TOP10 *E. coli* as described in Section 2.1.3.

2.2.2 Preparation of plasmid DNA

Plasmid DNA from commercially available or laboratory generated clones was prepared using QuickLyse MiniPrep kit or EndoFree® MaxiPrep kit (Qiagen) yielding up to 20 and 50 – 250 µg respectively. All procedures were carried out according to the manufacturer's instructions.

2.2.3 Generation of unmethylated DNA plasmid constructs

Unmethylated DNA plasmid constructs were generated as outlined below. Plasmids were propagated through a specific *E. coli* strain (K12 ER2925; New England Biolabs) that is dcm^- and dam^- negative therefore is unable to replicate methylation patterns.

2.2.3.1 Generation of competent K12 ER2925 cells

Competent *E. coli* K12 ER2925 cells were generated from a non-competent K12 ER2925 strain (New England Biolabs). The non-competent strain was grown as described in Section 2.1.1 with the replacement of ampicillin for 34 µg/ml chloramphenicol. Cells were pelleted by centrifugation at 7,000 g for 15 minutes at 4 °C and the pellet was resuspended in 20 ml ice cold 100mM $MgCl_2$. Cells were pelleted again by centrifugation at 7,000 g for 15 minutes at 4 °C and the pellet was resuspended in 4 ml of ice cold 100 mM $CaCl_2$ and left on ice for 2 hours. Competent cells were stored at -80 °C as glycerol stocks prepared as described in Section 2.1.4.

2.2.3.2 Transformation of competent K12 ER2925 cells

Competent K12 ER2925 cells were transformed as described in Section 2.1.3 using 250 µl of competent cells and 34 µg/ml chloramphenicol for selection of transformed cells.

2.2.4 *In vitro* methylation of DNA

Methylated DNA was generated by *in vitro* methylation with CpG *SssI* methylase (4000 U/ml) (New England Biolabs). Reactions typically contained 4 µl CpG *SssI* methylase, 1X NE Buffer 2 (New England Biolabs), 160 µM S-adenosylmethionine (SAM) (New England Biolabs) and 2 µg DNA, in a final volume of 25 µl. Reactions were incubated overnight at 37 °C. An additional 1 µl SAM (1:8 dilution of 200X stock) was added after 3 hours incubation. Mock methylation reactions were identical to *in vitro* methylation reactions except the CpG *SssI* methylase was omitted.

2.2.4.1 Phenol:chloroform purification of DNA

Methylated DNA or PCR products required for downstream applications were purified by phenol:chloroform precipitation. The sample to be purified was made up to a total volume of 200 µl with water. An equal volume of phenol:chloroform pH8 was added before centrifugation at 13,000 g for 15 minutes at 4 ºC. The upper fraction was transfer to a new 1.5 ml microtube and lower fractions discarded. One tenth of the initial volume of 3 M sodium acetate and double the initial volume of ice cold 100 % ethanol were added to the upper fraction and stored at -20 ºC overnight. The mixture was centrifuged at 13,000 g for 15 minutes at 4 ºC and supernatant discarded. The pellet was resuspended in 10 µl of water and quantified (Section 2.4.4).

2.2.5 DNA sequencing

All laboratory-generated plasmids were sequenced by MWG Biotech.

2.3 Culture of mammalian cells

2.3.1 Growth and maintenance

Caco-2, (human epithelial colorectal adenocarcinoma), HeLa (human epithelial cervical adenocarcinoma), HepG2 (human liver hepatocellular carcinoma) and MDA (human epithelial breast adenocarcinoma) cells were cultured routinely in Dulbecco's modified Eagle's medium (GIBCO, Invitrogen) containing 10 % (v/v) fetal calf serum, 1 % non-essential amino acids, 60 µg/ml gentamycin in 75 cm^3 tissue culture flasks at 37 °C in an atmosphere of 5 % CO_2 in air.

MCF-7 (human epithelial breast adenocarcinoma) cells were routinely cultured in minimum Eagle's medium (GIBCO, Invitrogen) containing 10 % (v/v) fetal calf serum, 1 % sodium pyruvate, 1 % non-essential amino acids, 60 µg/ml gentamycin in 75 cm^3 tissue culture flasks at 37 °C in an atmosphere of 5 % CO_2 in air.

SW480 (human epithelial colorectal adenocarcinoma) cells were routinely cultured in Leibovitz's L15 (GIBCO, Invitrogen) containing 10 % (v/v) fetal calf serum, 1 % non-essential amino acids, 60 µg/ml gentamycin in 75 cm^3 tissue culture flasks at 37 °C in an atmosphere of 0 % CO_2 in air.

SH-SY5Y (human epithelial brain neuroblastoma) cells were routinely cultured in a 1:1 ratio of Dulbecco's modified Eagle's medium and F-12 Nutrient Mixture (Ham) (GIBCO, Invitrogen) containing 10 % (v/v) fetal calf serum, 1 % non-essential amino acids, 60 µg/ml gentamycin in 75 cm^3 tissue culture flasks at 37 °C in an atmosphere of 5 % CO_2 in air.

All cells were subcultured once they had reached 80 % confluence by removing the medium, washing the confluent monolayer with 15 ml sterile PBS (pH 7.4), then adding 2 ml trypsin (10 X Solution Trypsin-EDTA; Sigma). The cells were incubated at 37 °C for 5 minutes and once passaged were resuspended in 10 ml of medium. The cells were centrifuged for 5 minutes at 1500 rpm and the supernatant of fluid was removed. Cells were resuspended in 10 ml of medium and 1 ml of this was transferred to a new 75 cm^3 flask. Fifteen millilitres of medium were added and the cells were grown at 37 °C. All cell culture medium compositions are listed in Appendix B.

2.3.2 siRNA transfection of mammalian cells

For siRNA transfection reactions, once confluent, cells were subcultured onto six well plates at a seeding density of 3.5 x 10^5 cells per well and after 24 hours growth were transfected with validated stealth RNAi™ siRNA (Invitrogen) using the Lipofectamine™ RNAiMAX transfection reagent according to the manufacturer's instructions (Invitrogen). For each well, 500 µl transfection mixtures were prepared containing 100 pmol of siRNA in serum and antibiotic-free medium and 4 µl of Lipofectamine™ RNAiMAX. The mixture was added in a dropwise manner. All siRNAs are listed in Table 2.2A.

2.3.3 Transient transfection of mammalian cells

For transfection reactions, once confluent, cells were subcultured onto six well plates at a seeding density of 3.5 x 10^5 cells per well and after 24 hours' growth were transfected with endotoxin-free plasmid DNA (Qiagen) using the GeneJammer® Transfection Reagent, according to the manufacturer's instructions (Stratagene). For each well, 100 µl transfection mixtures were prepared containing 2 µg of DNA in serum and antibiotic-free medium and 5 µl of GeneJammer® Transfection Reagent. The mixture was added in a dropwise manner.

2.3.4 Co-transfection of mammalian cells

Co-transfection of mammalian cells was conducted as described in Section 2.3.2 with the exception of only 1 µg of each DNA plasmid being used.

2.3.5 Treatment of cells with polyphenols and other chemicals

Filter-sterilised stock concentrations of the polyphenols genistein (LC Laboratories), daidzein (LC Laboratories), and resveratrol and SIRT1 inhibitor sirtinol (10 mM) were prepared in DMSO (dimethyl sulfoxide) and tert-butyl hydrogen peroxide (100 mM) was dissolved in ethanol. Twenty four hours after transfection, cells were treated with genistein, daidzein, resveratrol, sirtinol, tert-butyl hydrogen peroxide or a control of DMSO or ethanol, as appropriate and at the same ratio as present in cells reviving treatments (usually 0.1 % v/v). Polyphenol treatments were complimented by the use of phenol free medium (Appendix B) to ensure effects were due to polyphenols and not the medium component.

2.3.6 Preparation of mammalian cell stocks

Mammalian cell stocks were prepared by trypsinisation as described in Section 2.3.1 and resuspended to a density of 3 x 10^6 cells/ml in 8 ml of complete medium specific to cell type, an additional 10 % fetal calf serum and 10 % DMSO. Cell suspensions were aliquoted into 1.8 ml cryovials and frozen slowly in isopropanol at -80 ºC. After 24 hours cryovials were transferred to liquid nitrogen storage.

2.4 DNA/RNA extraction

2.4.1 Simultaneous DNA/RNA lysate preparation

Cells were harvested 72 hours after transfection. Cells in each well were washed with 1 ml 1 x PBS which was then removed and replaced with 350 µl lysis buffer RLT (Qiagen). Cells were lysed by repeated (10x) homogenisation with a needle and syringe. The cell lysate was stored at -80 ºC for further analysis. Genomic DNA and total RNA were extracted from Caco-2 cells using the AllPrep DNA/RNA Mini Kit (Qiagen) following the manufacturer's protocol. Where only genomic DNA was required the QIAamp® DNA Mini Kit (Qiagen) was used following the manufacturer's protocol.

2.4.2 RNA lysate preparation using TRIzol® reagent

Cells were harvested 24 - 72 hours after transfection with siRNA or endotoxin-free plasmid DNA. Cells in each well were washed with 1 ml 1 x PBS which was then removed and replaced with 0.5 ml of TRIzol® Reagent (Invitrogen). Total RNA was extracted from Caco-2 cells using the TRIzol® Reagent protocol (Invitrogen).

2.4.3 RNA lysate preparation for microarray or qRT-PCR analysis

Cells were harvested 72 hours after transfection with siRNA or endotoxin-free plasmid DNA. RNA lysates were prepared as described in Section 2.4.2, lysates were then further purified using the PureLink™ RNA Mini Kit (Invitrogen) following the manufacturer's protocol.

2.4.4 Determination of DNA/RNA concentration

DNA and RNA concentrations were analysed using the Nanodrop 1000 spectrophotometer (Thermo Scientific, UK). DNA with an $A_{260}/A_{280} \geq 1.8$ and an $A_{260}/A_{230} \geq 1.8$ and RNA with an $A_{260}/A_{280} \geq 2.0$ and an $A_{260}/A_{230} \geq 1.8$ was considered suitable for downstream applications.

2.4.5 Determination of RNA integrity

RNA integrity was analysed using the Agilent 2100 bioanalyser (Agilent Technologies). A RIN (RNA Integrity Number) above the threshold of 7 was required for downstream applications.

2.5 Routine techniques for amplification, manipulation and analysis of DNA

2.5.1 End Point Polymerase chain reaction

2.5.1.1 Standard PCR

For amplification of DNA each PCR reaction contained 1 µl DNA, 0.5 µl BIOTAQ™ DNA polymerase (Bioline), 2 µl 10x NH_4 Buffer (Bioline), 1.2 µl 50 mM $MgCl_2$ (Bioline), 0.3 µl 100 mM dNTPs (Bioline), 0.5 µM sense and antisense primers (MWG Biotech) and water to a final volume of 20 µl. Cycling parameters for BIOTAQ™ DNA polymerase (Bioline) using a Thermohybaid PX2™ was as follows:

	95˚C	5 minutes initial denaturation
35 cycles	95˚C	30 seconds denaturation
	*45 - 65˚C	30 seconds annealing
	72˚C	1 minutes elongation
	72˚C	5 minutes
	4˚C hold	

* At temperature given in Table 2.2B for specific primer pairs

PCR primers (MWG Biotech) were designed to be 18-24 bases in length, to optimally have 50 % GC content and to preferably terminate at both ends in a G or a C. All primers used are listed in Table 2.2B.

2.5.1.2 High specificity hot-start PCR

For PCR products to be analysed on the Pyrosequencer (Qiagen), HotStarTaq Master Mix (Qiagen) was used to ensure higher PCR specificity and reduced non-specific amplification, and required a 15 minute, 95 °C activation step. Each PCR reaction contained 4 µl DNA, 25 µl HotStarTaq Master Mix, 0.25 µM sense and antisense primers (0.20 µM if biotinylated) (MWG Biotech) and water to a final volume of 50 µl. Cycling parameters for HotStarTaq MasterMix using a Thermohybaid PX2™ was as follows:

	95˚C	15 minutes initial denaturation
*35-50 cycles	95˚C	15 seconds denaturation
	*50-55˚C	*30 seconds – 1 minute annealing
	72˚C	*15 seconds – 2 minutes elongation
	72˚C	5 minutes
	4˚C hold	

* At temperature and duration given in Table 2.2B and C for specific primer pairs

PCR primers (MWG Biotech) for the amplification of bisulfite modified DNA were designed as described in Section 2.5.1.1 using the PyroMark Assay Design Software (Qiagen) to ensure compatibility with the pyrosequencing assay. Antisense pyrosequencing primers were designed with a 5' biotin label. For assay specific cycling parameters see Table 2.2C.

2.5.2 Restriction digest

Typically, DNA was incubated at 37 ºC for 2 hours with 2 µl of 10x restriction enzyme buffer (see individual Sections for enzyme specific buffer and manufacturer), 0.2 µl of 10 µg/ml BSA and 0.5 µl (5 U) of the restriction endonuclease/s (see individual Sections for manufacturer) and water to a final volume of 20 µl.

2.5.3 Agarose gel electrophoresis

PCR products and restriction digested DNA were analysed on a 1 % gel prepared by boiling 0.5 g Agarose and 50 ml of 1 x TBE buffer diluted from a stock of 10 x TBE buffer (Tris base 108 g, Boric Acid 55 g, EDTA 9.3 g, 1 L MQH_2O pH 8.3) then 2 µl of 10 mg/ml ethidium bromide were added. Eight microlitres of PCR product were mixed with 2 µl loading dye (50 mM Tris-HCl pH 8, 5 mM EDTA, 20 % glycerol and 0.1 % Bromophenol Blue) and the sample was loaded onto the gel. A 1000 bp ladder, (Hyperladder IV; Bioline) or 10000 bp ladder (Hyperladder I; Bioline) were used as size markers. The gel was run at 70 V for 30 minutes and DNA bands were visualised under UV light using a gel documentation system (Uvitec (model BTS-26M), UK).

2.5.4 SYBR® Green Agarose Gel Electrophoresis

Bisulfite modified, *Hinf*I digested, PCR products were analysed on a 3 % gel prepared by boiling 4.5 g agarose and 150 ml of 1 x TBE buffer diluted from a stock of 10 x TBE buffer (Tris base 108 g, Boric Acid 55 g, EDTA 9.3 g, 1 L MQH_2O pH 8.3). Twelve microlitres of PCR product were mixed with 2 µl loading dye (50 mM Tris-HCl pH 8, 5 mM EDTA, 20 % glycerol and 0.1 % bromophenol blue) and the sample was loaded onto the gel. A 1000 bp ladder, (Hyperladder IV; Bioline) was used as a size marker. The gel was run at 120 V for 1 hour 30 minutes after which the gel was incubated shaking at 4 ºC in 20 µl of 10 000 x concentrated SYBR® green stain in DMSO (Invitrogen) diluted in 200 ml of TBE. DNA bands were visualised under UV light using a gel documentation system (UVItec (model BTS-26M), UK). DNA band intensities were measured using densitometry software (UVItec (UVIBand software), UK) on the gel documentation system (UVItec (model BTS-26M), UK).

2.6 DNA methylation analysis

2.6.1 Bisulfite conversion of DNA

DNA was bisulfite modified using the EZ DNA Methylation-Gold™ Kit (Zymo Research Corp.) to convert unmethylated cytosines to uracils following the manufacturer's protocol.

2.6.2 Measurement of DNA methylation using the COBRA Assay

DNA was bisulfite modified as described in Section 2.6.1. The bisulfite modified products were then PCR amplified using high specificity HotStarTaq DNA polymerase (Qiagen) (Section 2.5.1.2) with primers specific to the LINE-1 retrotransposon (see *Table 2.2B*) and 10 µl of this PCR product was incubated at 37 ºC for 2 hours with 2 µl of 10x RE buffer (Fermentas) and 1 µl (5 U) of *Hinf*I (Fermentas) and water to a final volume of 20 µl. Digested PCR products were analyses using SYBR® Green Agarose Gel Electrophoresis (Section 2.5.4).

2.6.2.1 Data analysis of COBRA Assay

DNA methylation was calculated arbitrarily as the ratio of uncut to cut PCR product as determined by densitometric quantification of SYBR green-stained agarose gels. Results are shown as means ± standard error of the mean (SEM) for all experiments. Statistical analysis was performed using the statistical software package InStat (GraphPad), statistical tests used are stated in the figure legends. Data was taken to differ significantly at a p value of 0.05 or less.

2.6.3 Measurement of DNA methylation using Qiagen PyroMark MD System

2.6.3.1 Primer and assay design

Pyrosequencing assays and primers were designed using PyroMark Assay Design Software 2.0 (Qiagen). Biotin (5')-labelled PCR products were designed to be around 200 nucleotides in length and contain no CpG sites within the primer sequences. Sequencing primers were designed to anneal upstream of the initial CpG site to be quantified.

2.6.3.2 Pyrosequencing using Qiagen PyroMark MD system

Ten microlitres of biotinylated PCR product (Section 2.5.1.2) was purified and the biotinylated strand was separated use as a template in the pyrosequencing reaction by incubation with 80 µl binding master mix containing 2 µl streptavidin-coated sepharose beads (GE Healthcare), 38 µl binding buffer (Qiagen) and 40 µl H_2O on a shaker for 10 minutes. The sequencing primer was diluted to 0.3 µmol/L in annealing buffer (Qiagen) and 12 µl was added to each well of a Pyromark MD 96 well plate (Qiagen). The vacuum tool on the PyroMark Vacuum Prep Workstation (Qiagen) was primed in MQ H_2O for 30 seconds and then applied to the biotinylated PCR product/binding master mix. A series of 5 second washes (70 % ethanol, denaturing buffer (0.2 mol/L NaOH solution) and wash buffer (Qiagen), respectively) removed contaminants. The vacuum was removed and the purified single-

stranded PCR products, with primers annealed, were then added to the Pyromark MS 96 well plate containing sequencing primer by immersion of the probes, and the beads were shaken off. The 96 well plate was then incubated at 80 ºC for two minutes, cooled to room temperature and transferred to the PyroMark MD™ system (Qiagen). The principle of pyrosequencing is outlined in Section 1.5.3.

2.6.3.3 Standard Curves

Standard curves were generated for all sequencing primers to confirm linear amplification of methylated and unmethylated DNA controls. Unmethylated template DNA through the removal of methyl groups by PCR amplification using primers as specified (see *Table 2.2C*). Nine microlitres of unmethylated control PCR product was methylated *in vitro* as described in Section 2.2.4. Nine microlitres of methylated or 25 µl unmethylated was then bisulfite modified as described in Section 2.6.1 and reactions were combined to give appropriate methylated percentages (0, 5, 10, 25, 50, 75, 90, 95, 100 % methylated) in a total volume of 10 µl. PCR reactions for each sequencing primer were carried out in duplicate for each methylation percentage and a standard curve was generated. Non linear amplification indicated biased amplification of methylated or unmethylated DNA and assays deemed unreliable were redesigned. Typical methylation standard curves for each gene analysed are shown in Appendix C.

2.6.3.4 Data analysis

Data were analysed using PyroMark CpG software 1.0.11 (Qiagen). The ratio of converted cytosine (thymine) to unconverted cytosine within each CpG site (C/T) was used to determine the percentage DNA methylation at each CpG site. An inbuilt control, a cytosine not followed by a guanine, acts to assess the efficiency of the bisulfite modification step, as the cytosine should not be methylated and so upon bisulfite treatment be fully converted to a thymine following PCR. Output from the analysis using the PyroMark software indicated if reaction met the required quality threshold.

2.6.4 Measurement of DNA methylation using the CDC7 assay

Two micrograms of genomic DNA were bisulfite modified. The bisulfite modified DNA was subject to two rounds of PCR amplification. Primers were designed to the CDC7 sequence, focusing on a region containing CpG sites that could be analysed for DNA methylation. The first PCR was to a 912 bp region of the CDC7 sequence and performed using HotStar Taq Master Mix, 0.25 µM sense and antisense primers (CDC7#1F and CDC7#1R) and 2 µl bisulfite-modified genomic DNA made up to a final volume of 50 µl with water. The second round of PCR performed was a nested PCR to a smaller 301 bp region within the CDC7 sequence focusing in on eight specific CpG sites. PCR reactions contain HotStar Taq Master Mix, 0.25 µM sense primer (CDC7#2R), 0.20 µM biotinylated antisense primer (CDC7#2F) and 4 µl PCR#1 DNA template made up to a final volume of 50 µl with water. Primer annealing sites in the CDC7 sequence are displayed in Figure 6.1 and primer sequences and annealing temperatures are outlined in Table 2.2C. PCR product size was confirmed by agarose gel

electrophoresis and 5 µl used for pyrosequencing as described in Section 2.6.3. The CDC7 primers and sequencing primer (CDC7Seq) used in the second PCR were designed using the PyroMark Assay Design Software 2.0 (Qiagen).

2.6.5 Measurement of DNA methylation using the EIF5 assay

Two micrograms of genomic DNA were bisulfite modified. The bisulfite modified DNA was subject to two rounds of PCR amplification. Primers were designed to the EIF5 sequence, focusing on a region containing CpG sites that could be analysed for DNA methylation. The first PCR was to a 949 bp region of the EIF5 sequence and performed using HotStar Taq Master Mix, 0.25 µM sense and antisense primers (EIF5#1F and EIF5#1R) and 2 µl bisulfite-modified genomic DNA made up to a final volume of 50 µl with water. The second round of PCR performed was a nested PCR to a smaller 302 bp region within the EIF5 sequence focusing in on eight specific CpG sites. PCR reactions contain HotStar Taq Master Mix, 0.25 µM sense primer (EIF5#2R), 0.20 µM biotinylated antisense primer (EIF5#2F) and 4 µl PCR#1 DNA template made up to a final volume of 50 µl with water. Primer annealing sites in the EIF5 sequence are displayed in Figure 6.3 and primer sequences and annealing temperatures are outlined in Table 2.2C. PCR product size was confirmed by agarose gel electrophoresis and 5 µl used for pyrosequencing as described in Section 2.6.3. The EIF5 primers and sequencing primer (EIF5Seq) used in the second PCR were designed using the PyroMark Assay Design Software 2.0 (Qiagen).

2.6.6 Measurement of DNA methylation using the IRX3 assay

Two micrograms of genomic DNA were bisulfite modified. The bisulfite modified DNA was subject to two rounds of PCR amplification. Primers were designed to the IRX3 sequence, focusing on a region containing CpG sites that could be analysed for DNA methylation. The first PCR was to a 993 bp region of the IRX3 sequence and performed using HotStar Taq Master Mix, 0.25 µM sense and antisense primers (IRX3#1F and IRX3#1R) and 2 µl bisulfite-modified genomic DNA made up to a final volume of 50 µl with water. The second round of PCR performed was a nested PCR to a smaller 437 bp region within the IRX3 sequence focusing in on three specific CpG sites. PCR reactions contain HotStar Taq Master Mix, 0.25 µM sense primer (IRX3#2R), 0.20 µM biotinylated antisense primer (IRX3#2F) and 4 µl PCR#1 DNA template made up to a final volume of 50 µl with water. Primer annealing sites in the IRX3 sequence are displayed in Figure 6.5 and primer sequences and annealing temperatures are outlined in Table 2.2C. PCR product size was confirmed by agarose gel electrophoresis and 5 µl used for pyrosequencing as described in Section 2.6.3. The IRX3 primers and sequencing primer (IRX3Seq) used in the second PCR were designed using the PyroMark Assay Design Software 2.0 (Qiagen).

2.6.7 Measurement of DNA methylation using the KLF3 assay

Two micrograms of genomic DNA were bisulfite modified. The bisulfite modified DNA was subject to two rounds of PCR amplification. Primers were designed to the KLF3 sequence, focusing on a region containing CpG sites that could be analysed for DNA methylation. The first PCR was to a 904 bp region of the KLF3 sequence and performed using HotStar Taq Master Mix, 0.25 μM sense and antisense primers (KLF3#1F and KLF3#1R) and 2 μl bisulfite-modified genomic DNA made up to a final volume of 50 μl with water. The second round of PCR performed was a nested PCR to a smaller 309 bp region within the KLF3 sequence focusing in on six specific CpG sites. PCR reactions contain HotStar Taq Master Mix, 0.25 μM sense primer (KLF3#2R), 0.20 μM biotinylated antisense primer (KLF3#2F) and 4 μl PCR#1 DNA template made up to a final volume of 50 μl with water. Primer annealing sites in the KLF3 sequence are displayed in Figure 6.7 and primer sequences and annealing temperatures are outlined in Table 2.2C. PCR product size was confirmed by agarose gel electrophoresis and 5 μl used for pyrosequencing as described in Section 2.6.3. The KLF3 primers and sequencing primer (KLF3Seq) used in the second PCR were designed using the PyroMark Assay Design Software 2.0 (Qiagen).

2.6.8 Measurement of DNA methylation using the LINE-1 assay

Two micrograms of genomic DNA were bisulfite modified. The bisulfite modified DNA was subject to two rounds of PCR amplification. Primers were designed to the LINE-1 retrotransposon sequence, focusing on a region containing CpG sites that could be analysed for DNA methylation. The first PCR was to a 529 bp region of the LINE-1 sequence and performed using HotStar Taq Master Mix, 0.25 μM sense and antisense primers (LINE1#1F and LINE1#1R) and 2 μl bisulfite-modified genomic DNA made up to a final volume of 50 μl with water. The second round of PCR performed was a nested PCR to a smaller 146 bp region within the LINE-1 sequence focusing in on three specific CpG sites. PCR reactions contain HotStar Taq Master Mix, 0.25 μM sense primer (LINE1#2R), 0.20 μM biotinylated antisense primer (LINE1#2F) and 4 μl PCR#1 DNA template made up to a final volume of 50 μl with water. Primer annealing sites in the LINE-1 retrotransposon sequence are displayed in Figure 3.1 and primer sequences and annealing temperatures are outlined in Table 2.2C. PCR product size was confirmed by agarose gel electrophoresis and 5 μl used for pyrosequencing as described in Section 2.6.3. The LINE-1 primers and sequencing primer (LINE1Seq) used in the second PCR were designed using the PyroMark Assay Design Software 2.0 (Qiagen).

2.6.9 Measurement of DNA methylation using the LUMA assay

DNA (200 ng) from cells was digested using a combination of *EcoRI* plus *MspI* or *EcoRI* plus *HpaII* (New England Biolabs). Restriction digests were set up in a 96 well format and incubated at 37 ºC for 4 hours with 2 μl of Tango buffer (New England Biolabs) and 2.5 U of *EcoRI* or *MspI* or 5 U of *HpaII* in a final volume of 20 μl. Reactions were then transferred to a 96 well pyrosequencing plate and 20 μl of Annealing Buffer (Qiagen) added to each reaction. Pyrosequencing reactions were performed in the

PyroMark MD™ system (Qiagen). The nucleotide dispensation order was programmed as: ACTCGA. Methylation was then quantified using the PyroMark CpG software 1.0.11 (Qiagen) to analyse the peak heights at each nucleotide dispensation. The *MspI*/*EcoRI* and *HpaII*/*EcoRI* ratios were calculated by the ratio of 'C' peak'/A' peak in the two respective digestions. The *MspI* /*HpaII* ratio was then calculated as (*MspI*/*EcoRI*)/(*HpaII*/*EcoRI*). The principle of LUMA is outlined in Section 1.5.4.

2.6.10 Measurement of DNA methylation using the PCYT1A assay

Two micrograms of genomic DNA were bisulfite modified. The bisulfite modified DNA was subject to two rounds of PCR amplification. Primers were designed to the PCYT1A sequence, focusing on a region containing CpG sites that could be analysed for DNA methylation. The first PCR was to a 939 bp region of the PCYT1A sequence and performed using HotStar Taq Master Mix, 0.25 μM sense and antisense primers (PCYT1A#1F and PCYT1A#1R) and 2 μl bisulfite-modified genomic DNA made up to a final volume of 50 μl with water. The second round of PCR performed was a nested PCR to a smaller 433 bp region within the PCYT1A sequence focusing in on two specific CpG sites. PCR reactions contain HotStar Taq Master Mix, 0.25 μM sense primer (PCYT1A #2R), 0.20 μM biotinylated antisense primer (PCYT1A#2F) and 4 μl PCR#1 DNA template made up to a final volume of 50 μl with water. Primer annealing sites in the PCYT1A sequence are displayed in Figure 6.9 and primer sequences and annealing temperatures are outlined in Table 2.2C. PCR product size was confirmed by agarose gel electrophoresis and 5 μl used for pyrosequencing as described in Section 2.6.3. The PCYT1A primers and sequencing primer (PCYT1ASeq) used in the second PCR were designed using the PyroMark Assay Design Software 2.0 (Qiagen).

2.6.11 Measurement of DNA methylation using the PTPRG assay

Two micrograms of genomic DNA were bisulfite modified. The bisulfite modified DNA was subject to two rounds of PCR amplification. Primers were designed to the PTPRG sequence, focusing on a region containing CpG sites that could be analysed for DNA methylation. The first PCR was to a 917 bp region of the PTPRG sequence and performed using HotStar Taq Master Mix, 0.25 μM sense and antisense primers (PTPRG#1F and PTPRG#1R) and 2 μl bisulfite-modified genomic DNA made up to a final volume of 50 μl with water. The second round of PCR performed was a nested PCR to a smaller 501 bp region within the PTPRG sequence focusing in on nine specific CpG sites. PCR reactions contain HotStar Taq Master Mix, 0.25 μM sense primer (PTPRG#2R), 0.20 μM biotinylated antisense primer (PTPRG#2F) and 4 μl PCR#1 DNA template made up to a final volume of 50 μl with water. Primer annealing sites in the PTPRG sequence are displayed in Figure 6.11 and primer sequences and annealing temperatures are outlined in Table 2.2C. PCR product size was confirmed by agarose gel electrophoresis and 5 μl used for pyrosequencing as described in Section 2.6.3. The PTPRG primers and sequencing primer (PTPRGSeq) used in the second PCR were designed using the PyroMark Assay Design Software 2.0 (Qiagen).

2.6.12 Measurement of DNA methylation using the SLC39A4 assay

Two micrograms of genomic DNA were bisulfite modified. The bisulfite modified DNA was subject to two rounds of PCR amplification. Primers were designed to the SLC39A4 sequence, focusing on a region containing CpG sites that could be analysed for DNA methylation. The first PCR was to a 900 bp region of the SLC39A4 sequence and performed using HotStar Taq Master Mix, 0.25 μM sense and antisense primers (SLC39A4#1F and SLC39A4#1R) and 2 μl bisulfite-modified genomic DNA made up to a final volume of 50 μl with water. The second round of PCR performed was a nested PCR to a smaller 282 bp region within the SLC39A4 sequence focusing in on three specific CpG sites. PCR reactions contain HotStar Taq Master Mix, 0.25 μM sense primer (SLC39A4#2R), 0.20 μM biotinylated antisense primer (SLC39A4#2F), 3 μl 50 mM $MgCl_2$ (Bioline) and 4 μl PCR#1 DNA template made up to a final volume of 50 μl with water. Primer annealing sites in the SLC39A4 sequence are displayed in Figure 6.13 and primer sequences and annealing temperatures are outlined in Table 2.2C. PCR product size was confirmed by agarose gel electrophoresis and 5 μl used for pyrosequencing as described in Section 2.6.3. The SLC39A4 primers and sequencing primer (SLC39A4Seq) used in the second PCR were designed using the PyroMark Assay Design Software 2.0 (Qiagen).

2.6.13 Measurement of DNA methylation using the TBX3 assay

Two micrograms of genomic DNA were bisulfite modified. The bisulfite modified DNA was subject to two rounds of PCR amplification. Primers were designed to the TBX3 sequence, focusing on a region containing CpG sites that could be analysed for DNA methylation. The first PCR was to a 912 bp region of the TBX3 sequence and performed using HotStar Taq Master Mix, 0.25 μM sense and antisense primers (TBX3#1F and TBX3#1R) and 2 μl bisulfite-modified genomic DNA made up to a final volume of 50 μl with water. The second round of PCR performed was a nested PCR to a smaller 240 bp region within the TBX3 sequence focusing in on three specific CpG sites. PCR reactions contain HotStar Taq Master Mix, 0.25 μM sense primer (TBX3#2R), 0.20 μM biotinylated antisense primer (TBX3#2F) and 4 μl PCR#1 DNA template made up to a final volume of 50 μl with water. Primer annealing sites in the TBX3 sequence are displayed in Figure 6.15 and primer sequences and annealing temperatures are outlined in Table 2.2C. PCR product size was confirmed by agarose gel electrophoresis and 5 μl used for pyrosequencing as described in Section 2.6.3. The TBX3 primers and sequencing primer (TBX3Seq) used in the second PCR were designed using the PyroMark Assay Design Software 2.0 (Qiagen).

2.6.14 Measurement of DNA methylation profile of human genome by Methylated DNA Immunoprecipitation (MeDIP) analysis

2.6.14.1 Preparation of genomic DNA

Genomic DNA was extracted from Caco-2 cells as described in Section 2.4.1.

2.6.14.2 Sonication of genomic DNA

Genomic DNA was fragmented into 200 – 1000 bp lengths by sonication using an ultrasonic homogeniser (4710 Series; Cole Palmer). Fragmented DNA was then purified using the DNA Clean and Concentrator 25 kit (Zymo Research) following the manufacturer's protocol eluting in 50 µl of water and quantified (Section 2.4.4).

2.6.14.3 Preparation of internal controls

Unmethylated (negative) and methylated (positive) internal controls were generated to spike genomic DNA samples to calculate enrichment within the methylated fraction after immunoprecipitation. Two different fragments of ~500 bp in length were PCR amplified from Lambda phage dam dcm- genomic DNA (Fermentas) using high specificity HotStarTaq DNA polymerase (Qiagen) (Section 2.5.1.2; for primers see *Table 2.2B*) producing unmethylated PCR products. PCR products were purified as described in Section 2.2.4.1. Up to 5 µg of one unmethylated PCR product was then methylated *in vitro* as described in Section 2.2.4 and 2.2.4.1 to produce a purified methylated control. Purified unmethylated and methylated controls were diluted to a concentration of 10ng/µl with water and stored in aliquots at -20 ºC. The methylation status of the unmethylated and methylated controls was assessed by restriction digest of DNA (200 ng) with 2.5 U of the methylation sensitive restriction enzyme *AciI* (Fermentas) as described in Section 2.5.2.

2.6.14.4 Immunoprecipitation of methylated DNA (MeDIP)

Purified fragmented DNA (4.4 µg) (Section 2.6.14.2) was diluted to 487 µl with water, 4 µl (40 ng) of negative and positive internal control (Section 2.6.14.3) were added to each sample. The spiked fragmented DNA was denatured at 95 °C for 10 minutes on a heated shaker at 1000 rpm and immediately cooled on ice for a further 10 minutes. Forty five microlitres of spiked fragmented DNA was transferred to a separate microtube to act as an input and stored at 4 °C. Fifty one microlitres of 10x Immunoprecipitation Buffer (100 mM Na-Phosphate pH 7.0, 1.4 M NaCl, 0.5 % Triton X-100) and 12 µl 5-methylcytidine (5mC) antibody (Eurogentec) was added to the remainder of the spiked fragmented DNA and the sample was incubated at 4 °C for 2 hours on a rotating wheel.

During the 2 hour incubation sheep anti-mouse IgG Dynabeads (Invitrogen) were prepared, the Dynabeads were vortexed briefly before transferring 48 µl of beads per sample into a microtube. The Dynabeads were captured with a magnetic rack (Invitrogen) for 1 minute and the preservative solution was discarded. The Dynabeads were then washed twice with 800 µl of 1x Immunoprecipitation Buffer for 5 minutes shaking at 500 rpm and captured with the magnetic rack for 1 minute and the was solution was discarded. The Dynabeads were then resuspended in 48 µl of 1x Immunoprecipitation Buffer per DNA sample.

Forty eight microlitres of the Dynabeads suspension was added to each DNA/antibody sample and incubated at 4 °C for 2 hours on a rotating wheel. The Dynabeads/DNA were captured with a magnetic rack for 1 minute and the solution discard. The Dynabeads/DNA were then washed three times in 700 µl of 1x Immunoprecipitation buffer for 10 minutes shaking at 1000 rpm, captured with a magnetic rack for 1 minute and the solution discard. The Dynabeads/DNA were then resuspended in 250 µl of 1x Proteinase K Digestion Buffer (50 nM Tris pH8.0, 10 mM EDTA, 0.5 % SDS). Seven microlitres of Proteinase K (10 mg/ml stock; Roche) was added per sample to cleave the DNA/5mC antibody from the Dynabeads through incubation at 50 °C for 2 hours on heated shaker at 1000 rpm to prevent bead sedimentation. The Dynabeads were captured with a magnetic rack for 1 minute and the solution containing the DNA and 5mC antibody was transferred to a new microtube. The DNA sample enriched with the methylated fraction (hereafter referred to as MeDIP DNA was then purified using the DNA Clean and Concentrator 5 kit (Zymo Research) following the manufacturer's protocol, eluting in 15 µl of water, and quantified as single-stranded DNA (Section 2.4.4). Samples were diluted to 2 ng/µl with water.

2.6.14.5 Whole genome amplification of input and MeDIP DNA products

Eleven microlitres of Input or MeDIP DNA (2 ng/µl) was whole genome amplified using the GenomePlex® Complete Whole Genome Amplification kit following the manufacturer's protocol. Whole genome amplified products were then purified using the GenElute™ PCR Clean-Up kit following the manufacturer's protocol, eluting in 50 µl of water, and quantified (Section 2.4.4). Three hundred nanograms of each whole genome amplification product was analysed by agarose gel electrophoresis (Section 2.5.3) to check that DNA was still within the 200 – 1000 bp range. Five micrograms of each input and MeDIP whole genome-amplified DNA sample (250 ng/µl) was transferred to a new microtube for array hybridisation. The remainder of each whole genome-amplified DNA sample was diluted to 25 ng/µl with water for enrichment analysis by qPCR.

2.6.14.6 Enrichment analysis by qPCR

Reactions using primers to negative and positive controls (see *Table 2.2D*) were set up as described in Section 2.7.2.4 for each input and MeDIP DNA sample. Enrichment for each sample was calculated using the C_T values generated for each sample and applying the following equation:

$$2 \wedge [\text{MeDIP } (C_T \text{ Positive} - C_T \text{ Negative}) - \text{Input } (C_T \text{ Positive} - C_T \text{ Negative})]$$

2.6.14.7 Methylome profiling

The methylation profile of DNA samples was investigated using the DNA Methylation Service provided by NimbleGen Roche (Reykjavik, Iceland). After preparation and confirmation of quality (Sections 2.6.15.1 – 2.6.15.6), DNA samples were sent for array analysis by NimbleGen Roche. Input and MeDIP DNA samples were labelled using the NimbleGen Dual-Colour DNA Labelling Kit with

Cy3 and Cy5 respectively. The labelled samples were then co-hybridised to the Human 3x720K CpG Island Plus RefSeq Promoter Array using the NimbleGen Hybridisation System. The hybridised arrays were then washed with the NimbleGen Wash Buffer Kit, dried with the NimbleGen Microarray Drier and signal peak intensities for each probe measured with the NimbleGen MS 200 Microarray Scanner.

2.6.14.8 Data analysis by microarray

Data was provided as signal intensity data for each probe and calculate p-values which indicated if DNA fragments hybridising to the probe on the array were enriched for the methylated fraction (Cy5 signal > Cy3 signal). These data were used to detect peaks through manual inspection in Excel (Microsoft), accepting positive enrichment being where at least 2 probes met a >2 p-value minimum cut off.

2.7 RNA analysis

2.7.1 Measurement of mRNA expression analysed by reverse transcriptase PCR

2.7.1.1 Preparation of RNA

RNA was extracted from Caco-2 cells as described in 2.4.2.

2.7.1.2 DNase treatment of RNA

RNA (4.5 µg) was added to a mixture of 4.5 U DNase (Roche) and 2 µl 10X DNase buffer (Roche) with RNase free water to a final volume of 20 µl. The reaction was incubated at 37 °C for 30 minutes after which 4 µl of stop solution (EDTA, 20 mM, pH 8.0) was added. A further incubation of the sample at 65 °C for 10 minutes was carried out then the RNA was placed on ice if required for use immediately or stored at -80°C.

2.7.1.3 Reverse transcription of RNA

RNA from Caco-2 cells (5µl) was reverse transcribed to cDNA using Superscript™ III RNase H- Reverse Transcriptase (Invitrogen). RNA was added to 0.4 µl of 0.5 mM dNTPs (Bioline), 50 ng random primers (Promega) and RNase free water to a final volume of 13 µl. The reaction was heated at 65 ºC for 5 minutes. One microlitre of RNase Inhibitor (40 U/µl) (Promega), 1 µl Superscript™ III RT (200 U/µl), 4 µl 15x First Strand Buffer (250 mM Tris-HCl pH 8.3, 375 mM KCl, 15 mM $MgCl_2$) and 0.1 µl 0.1 M DTT were mixed into the reaction by pipetting. The reaction was then heated to 25 ºC for 5 minutes, 50 ºC for 45 minutes, and then 70 ºC for 15 minutes using a Thermohybaid PX2™ thermal cycler. Absence of DNA contamination of the RNA sample or reagents was confirmed with a negative control, where the reaction was repeated with the exclusion of the Superscript™ III RT.

2.7.1.4 PCR amplification of reverse transcribed cDNA

PCR of reverse transcribed cDNA was as described in Section 2.5.1.1.

2.7.2 Measurement of mRNA expression analysed by qRT-PCR

2.7.2.1 Preparation of RNA

RNA was extracted from Caco-2 cells as described in 2.4.2.

2.7.2.2 DNase treatment of RNA

RNA was DNase treated as described in Section 2.7.1.2

2.7.2.3 Reverse transcription of RNA

RNA was reverse transcribed to cDNA as described in Section 2.7.1.3

2.7.2.4 qPCR using the Roche LightCycler® 480

PCR reactions were set up in LightCycler® 96 well plates and contained 1 µl cDNA (diluted 1 in 4 with water), 10 µl LightCycler® 480 SYBR Green I Master (Roche), 0.5 µM sense and antisense primers (MWG Biotech; *Table 2.2D*) and water to a final volume of 20 µl. Cycling parameters were as follows:

	95˚C	5 minutes initial denaturation
45 cycles	95˚C	10 seconds denaturation
	*52 - 60˚C	10 seconds annealing
	72˚C	15 seconds elongation

* At temperature given in Table 2.2D for specific primer pairs.

Fluorescence was detected for each PCR cycle and the threshold crossing points (C_T values) determined. A melt curve peak analysis was performed at the end of all reactions to ensure amplification of a single product. Each sample was measured in duplicate. Typical amplification curves for each gene analysed are shown in Appendix D.

2.7.2.5 Standard Curves

Standard curves were generated for all target and reference genes to confirm linear amplification of PCR products. Undiluted cDNA extracted from untreated Caco-2 cells was used to create an 8 point 2-fold dilution series. Dilution concentrations were plotted against C_T values to generate a standard curve. Each dilution standard was measured in duplicate. A standard curve was run for each qRT-PCR analysis. Typical standard curves for each gene analysed are shown in Appendix D.

2.7.2.6 Data analysis

Expression of all target and reference genes was calculated for each sample using the gene specific standard curve generated during each run and reading off the C_T values. Each target cDNA

concentration was then normalised to the average value of the reference gene from the sample cDNA preparation.

2.7.3 Measurement of mRNA expression analysis by hybridisation to DNA microarray

2.7.3.1 Preparation of RNA

RNA was extracted from Caco-2 cells as described in Section 2.4.3, and quality and integrity was checked as described in Sections 2.4.4 and 2.4.5 respectively.

2.7.3.2 Gene expression profiling

Gene expression profiling of RNA samples was investigated using the Illumina Gene Expression Service provided by Service XS (Leiden, The Netherlands). RNA samples were reverse transcribed to produce a cDNA template that was then amplified by *in vitro* transcription, incorporating biotin-labelled nucleotides. This labelled RNA sample was then hybridised to the HumanHT-12 v4 Expression BeadChip (Illumina), the signal developed with Streptavidin-Cy3 and the BeadChip scanned. After scanning the Illumina Whole-genome Gene Expression For BeadStation system extracted gene expression data from the scan images and the intensity value for each probe was calculated.

2.7.3.3 Data analysis

Raw data generated from the microarray was imported into GeneSpring GX 11 (Agilent) for visualisation. Hierarchical clustering was used to assess the similarity of biological replicates. Probes were considered further if the detection p-value was >0.6 in all samples in a replicate group. RankProducts (Breitling et al., 2004) analysis was used to determine differential expression between groups using the RankProd (Hong et al., 2006) package from BioConductor (Gentleman et al., 2004) to report probes with a p.f.p of <0.05 over 100 permutations of the class labels with a resulting fold change of >1.5.

2.8 Protein analysis

2.8.1 Western blotting

2.8.1.1 Tissue preparation

Tissue samples were ground with a pestle and mortar in the presence of liquid nitrogen and added to 500 µl of protein buffer (100 mM NaCl, 10 mM Tris HCl, 1 mM EDTA, 1 % NP-40 and 1 protease inhibitor tablet per 10 ml of protein buffer). Tissues were further lysed by repeated (10x) homogenisation with a needle and syringe. The tissue lysate was centrifuged at 13,000 g for 15 minutes at 4 ºC and the supernatant fluid was transferred to a new 1.5 ml microtube tube and stored at -80 ºC for further analysis.

2.8.1.2 Whole cell lysate preparation

Cells were harvested 96 hours after transfection. Cells in each well were washed with 1 ml of 1 x PBS, which was then removed and replaced with 1 ml ice cold 1 x PBS plus 1 protease inhibitor tablet (Roche) per 10 ml of PBS. Cells were collected using a cell scraper (Greiner) and transferred to a new 1.5 ml microtube tube. Cells were then centrifuged at 13,000 g for 15 minutes at 4 ºC. Supernatant fluid was discarded and the pellet was stored at -80 ºC for further analysis. For further analysis the pellet was resuspended in 50 µl of suspension buffer (100 mM NaCl, 10 mM Tris HCl, 1 mM EDTA and 1 protease inhibitor tablet per 10 ml of suspension buffer).

2.8.1.3 Histone lysate preparation

Cells were harvested 96 hours after transfection. Two millilitres of cold lysis buffer (10 mM Tris, 50 mM sodium bisulfite, 1 % Triton X-100, 10 mM $MgCl_2$ 8.6 % sucrose and 1 protease inhibitor tablet per 10 ml of cold lysis buffer) were added to cells in each well. Cells were collected using a cell scraper and transferred to a new 20 ml tube. Cells were then centrifuged at 1900 rpm (700 g) for 15 minutes. The pellet formed was then washed with 1 ml of cold lysis buffer and centrifuged at 1900 rpm (700 g) for a further 15 minutes. The supernatant fluid was discarded and the cell pellet was stored at -20 ºC for further analysis.

Histone proteins were extracted from pellets of lysed Caco-2 cells. Each pellet was resuspended in 100 µl of water and then 100 µl of 0.4M H_2SO_4 was then added in a dropwise manner. The resuspended pellet was then incubated over night at 4 ºC. The resuspended pellet was then transferred to a 1.5 ml microtube tube and centrifuged at 10,000 g for 15 minutes. The supernatant was transferred to a new 1.5 ml microtube tube and 1 ml of acetone (Sigma, UK) was added before being incubated over night at -20 ºC. Following this step, the acetone was removed and the sample was air dried for 5 minutes. Ten microlitres of 2M NaOH and 10 µl of water were added to the sample.

2.8.1.4 Determination of protein concentration

A Bradford assay was carried out to determine the histone protein concentration of each intestinal epithelial cell lysate. Standards of 0, 20, 40, 60, 80 and 100 µM were made in triplicate using a 100 µg/ml bovine serum albumin standard solution and 50 µl of each were pipetted into a 96 well plate (SLS Ltd, UK). Intestinal epithelial cell lysates were diluted 1 in 50 for analysis and 50 µl was used in the assay. Biorad dye reagent concentrate (Biorad, UK) was diluted 1 in 5 from the stock with MQH_2O and 200 µl was added to the 96 well plate on top of the standards and samples and the absorbance was measured at 595 nm on a plate reader (ThermoLab Systems Multiscan Acent).

2.8.1.5 Electrophoresis of protein

Protein samples were separated by SDS-PAGE. A 12.5 % separating gel was made up with 2.19 ml 40 % Acrylamide/Bis Acrylamide Stock solution (37.5:1), 2.8 ml 2.5x separating gel buffer (1.875M Tris

base pH8.9 0.25 % SDS), 1.94 ml H_2O. Six microlitres of N,N,N',N'-Tetramethylethylenediamine (TEMED) diluted in water and 0.1 % (w/v) ammonium persulphate (from a 10 % stock solution) was added to polymerase the gel. A 5 % stacking gel containing the comb was placed on top of the separating gel. This gel was made up with 12.4 % (v/v) of 40 % Acrylamide/Bis Acrylamide (37.5:1), 20 % (v/v) stacking gel buffer (0.3M Trisphosphate, 0.5 % SDS, pH6.7). Two and a half microlitres of N,N,N',N'-Tetramethylethylenediamine (TEMED) diluted in water and 0.1 % (w/v) ammonium persulphate was added to set the gel. The gel was run in protein electrophoresis buffer (0.1 M Tris base, 0.384M glycine and 0.1 % SDS). Coloured protein ladders (high range markers (Sigma)) were run in parallel with the protein samples to determine the size of proteins detected. The ladder and samples were run in a vertical gel electrophoresis chamber (Atto, GRI, UK) at 120V until the blue dye reached the bottom of the gel.

2.8.1.6 Blotting and detection of protein

The proteins were transferred from the gel to a polyvinylidene difluride (PVDF) membrane (Roche, UK), by a semi-dry transfer method. The membrane was hydrated before transfer by incubating in 100 % methanol (Fisher Scientific) for 30 seconds followed by 2 minutes in deionised water, and finally placed in transfer buffer (2.5 mM Tris base, 150 mM glycine, 10 % (w/v) methanol, pH 8.3 without adjustment) until use. Three layers of Grade 3 mm Whatman® chromatography paper were soaked in transfer buffer and placed on the bottom electrode of the transfer apparatus (Atto, GRI, UK). Any air bubbles present between the layers of paper were removed before the membrane was laid on top of them. The SDS-PAGE gel was placed on top of the membrane followed by three more sheets of Whatman® paper soaked in transfer buffer, followed by the removal of any air bubbles. The top electrode was positioned and transfer was carried out at 15V for 1 hour.

After transfer of protein, the membrane was blocked to prevent non-specific binding of the antibodies to the membrane. The membrane was blocked with 5 % (w/v) dried milk powder (Marvel) in PBS containing 0.05 % (v/v) Tween 20, with over night shaking at 4 ºC. Primary antibodies (*Table 2.3*) were diluted in 5 % (w/v) dried milk powder in PBS containing 0.05 % (v/v) Tween 20 and were incubated with shaking for 1 hour. Bound unspecific primary antibody was removed by washing the membrane in PBS containing 0.05 % (v/v) Tween 20. The membrane was washed for 4 x 10 minute washes. After the washes the secondary antibodies (*Table 2.3*) were diluted in 5 % (w/v) dried milk powder in PBS and 0.5 % (v/v) Tween 20, and incubated with the membrane for 1 hour with shaking. Bound unspecific secondary antibody was removed by washing the membrane in PBS containing 0.05 % (v/v) Tween 20 for 5 x 10 minute washes.

The membrane was visualised using the Enhanced Chemiluminescence PLUS kit (Amersham Bioscience). This was followed by exposure of the membrane in a dark room with Kodak Biomax XAR film in a Hypercassette™ (Amersham Bioscience) for between 10 seconds and 5 minutes

(depending on the density of the signal). The films were developed in Kodak GBX developer followed by Kodak GBX fixer (Sigma).

2.8.1.7 Staining of protein

To assess loading efficiency of proteins when a house keeping antibody could not be used, SDS-PAGE gels were stained with a colloidal blue staining kit (Invitrogen) according to the manufacturer's instructions. Gels were incubated with shaking in 100 ml colloidal blue stain overnight. The following day the gel was incubated in 200 ml of deionised water until the background became clear.

2.8.1.8 Band quantification by densitometry

Protein band intensities were measured using densitometry software (UVItec (UVIBand software), UK) on a gel documentation system (UVItec (model BTS-26M), UK).

2.8.2 Reporter gene assay

The beta-galactosidase activity assay was used to measure the ability of a gene promoter region to drive the expression of the lacZ gene encoding beta-galactosidase.

2.8.2.1 Total cell lysate preparation

Cells were harvested 96 hours after transfection. Cells in each well were washed with 1 ml 1 x PBS which was then removed and replaced with 100 µl of lysis buffer (0.25 M Tris pH7.4, 0.25 % (v/v) NP-40, 2.5 mM EDTA). Cells were frozen at -20 ºC for a minimum of 30 minutes and then thawed at room temperature. Cells were collected using a cell scraper and transferred to a 1.5 ml microtube tube. Cell lysate was then centrifuged at 12,000 g for 5 minutes at 4 ºC. The supernatant fluid was transferred to a new 1.5 ml microtube tube. Pelleted cell debris was discarded.

2.8.2.2 Determination of protein concentration

Protein concentration was determined by Bradford assay as described in Section 2.8.1.4.

2.8.2.3 Beta-galactosidase reporter assay

The beta-galactosidase reporter assay is based on the conversion of chlorophenol red-β-D-galactopyranoside (CPRG) to galactose and chlorophenol red in the presence of beta-galactosidase enzyme expression and is seen as a colour change from yellow to red. One hundred and thirty microlitres of 1.2 ng/ml CPRG (in a buffer containing 100 mM NaCl, 25 mM MOPS & 10 mM MgCl2 pH7.5) was added to a 96 well plate containing 20 µl of cell lysate (Section 2.8.2.1) to give a final volume of 150 µl. The reactions were timed upon incubated at 37 ºC until a colour change was observed. The reactions were stopped with the addition of 50 µl of 0.5 M Na_2CO_3. Absorbance was measured at 560 nm on a plate reader (Thermo LabsSystems Multiskan Acent).

2.8.2.4 Data analysis

Beta-galactosidase activity was calculated as nmoles of chlorophenol red formed per minute per mg of total protein. Results are shown as means ± standard error of the mean (SEM) for all experiments. Statistical analysis was performed using the statistical software package InStat (GraphPad), statistical tests used are stated in the figure legends. Data were taken to differ significantly at a p value of 0.05 or less.

2.8.3 Fluor de Lys™ fluorescent activity assay

The Fluor de Lys™ fluorescent activity assay was used to measure the ability of endogenous SIRT1 to deacetylate the Fluor de Lys-SIRT1 substrate, comprising of the p53 sequence Arg-His-Lys. The procedure was carried out in accordance with the manufacturer's instructions; with modifications/details as below

2.8.3.1 Whole cell lysate preparation

Whole cell lysate was prepared as described in Section 2.8.2.1.

2.8.3.2 Determination of protein concentration

Protein concentration was determined by Bradford assay as described in Section 2.8.1.4.

2.8.3.3 Sirt1 fluorescent activity assay

The SIRT1 fluorescent activity assay (BIOMOL® International) is based on the deacetylation and sensitisation of the Fluor de Lys-SIRT1 substrate upon incubation of cell lysate containing endogenous SIRT1 together with the co-substrate NAD^+. Upon treatment with the Fluor de Lys Developer II, a detectable fluorophore is produced. Twenty five microlitres of cell lysate was added to a 96 well plate containing 25 µl of 2x substrate solution (3 mM NAD^+, 100 uM Fluor de Lys-SIRT1) and incubated at 37 ºC for 30 minutes after which 50 µl of stop solution (1 x Fluor de Lys Developer II, 2 mM Nicotinamide) was added to each reaction. Fluorescence emission was measured at 460 nm with an excitation wavelength of 355 nm, at 10 second intervals using the FLUOStar OPTIMA (BMG Labtechnologies) until readings plateaued.

2.8.3.4 Data analysis

SIRT1 activity was calculated as fluorophore fluorescence generated per minute per mg of total protein.

2.9 *In silico* bioinformatic analysis

2.9.1 Gene identifier conversion

To compare lists all gene identifiers were converted to the equivalent Ensembl identifier using the Ensembl Biomart Gene Conversion Tool at www.ensembl.org/biomart.

2.9.2 Gene overlaps

Gene lists converted into Ensembl identifiers were compared and duplicates identified using the Advanced Filter > Unique Records option in Excel (Microsoft).

2.9.2.1 Data analysis of gene overlaps

The representation factor for gene overlaps indicates whether the number of genes common between lists is more or less than expected from independent groups and was calculated by applying the following equation:

$$X / [(n \times D) / N]$$

Where X was the number of genes common between groups, n was the number of genes in one list, D the number of genes in the other list and N the total number of genes. A representation factor of >1 indicated more overlap than would be expected in two independent groups.

The cumulative hypergeometric probability indicates the probability that an n-trial hypergeometric experiment (number of genes on one list) results in greater than or equal to X overlaps, when the total gene lists consist of N items, D of which are the number of genes on the other list. Cumulative hypogeometric probability was calculated by applying the following equation:

$$h (\geq X; N, n, D) = [{}_{D}C_{X}] [{}_{N-D}C_{n-X}] / [{}_{N}C_{n}]$$

Where X was the number of genes common between groups, n was the number of genes in one list, D the number of genes in the other list, N the total number of genes and ${}_{D}C_{X}$ is the number of combinations of D things, taken X at a time. Cumulative hypogeometric probability was calculated using the StatTrek hypogeometric calculator at http://stattrek.com.

2.9.3 Identification of CpG islands within gene promoter sequences

The presence of a CpG island, typically located within the promoter region, in a target gene was investigated using an algorithm to analyse the promoter sequence of the gene for typical CpG Island features.

2.9.3.1 Determination of gene promoter sequence using Genomatix Gene2Promoter

Gene promoter sequences were retrieved in FASTA format using the Gene2Promoter Software (Genomatix, Germany). All proposed promoter sequences were checked against the genomic transcript to ensure the promoter lay upstream of the start of transcription of the specific gene and in the correct orientation.

2.9.3.2 CpG Island prediction using CpG Island Explorer

Gene promoter sequences generated as described in Section 2.9.3.1 were analysed for the presence of CpG Islands using the CpGIE2.0 software based on (Wang and Leung, 2004) and parameters set to 50 % GC content, 0.60 CpG observed/expected ratio and 200 bp minimum length.

2.10 Plasmids, Oligos and Antibodies

Table 2.1. Plasmids

Plasmid	Source	Insert
pCMV6-Neo	Origene	Random Sequence
pCMV6-ENTRYSIRT1	Origene	Human SIRT1 ORF
pBlue-TOPO	Invitrogen	

Table 2.2. Oligos

A

siRNA	Sequence 5'-3'
SIRT1 siRNA #1	GCAACAGCAUCUUGCCUGAUUUGUA
SIRT1 siRNA #2	UCAUAGAGCCAUGAAGUAUGACAAA

B

End Point Primer Name	Sequence 5'-3'	Length (bp)	Annealing °C
SIRT1F	GGCAAAGGAGCAGATTAGTAGG	22	55
SIRT1R	CATCAGGCTCATCTTCTAAGCC	22	55
RTPCR18sF	AGGAATTGACGGAAGGGCACCAC	23	55
RTPCR18sR	GTGCAGCCCCGGACATCTAAGG	22	55
LINE1COBRAF	TTGAGTTGTGGTGGGTTTTATTTAG	25	
LINE1COBRAR	TCATCTCACTAAAAAATACCAAACA	25	
SLC30A5PromoterF	GGCCATGAAGTTTCGCACGTG	21	55
SLC30A5PromoterR	CGGCTCCGGCTCACTAGCACACAC	24	55
pBlueTOPOR	CATTTGCTGTCCACCAGTCATGC	23	55
SIRT1PromoterF	GGAAGGGCTTTCCACTAAGC	20	55
SIRT1PromoterR	CTTCCAACTGCCTCTCTGG	19	55
GAPDHPromoterF	GAGCCTCGAGGAGAAGTTCC	20	60
GAPDHPromoterR	AAGAAGATGCGGCTGACTGT	20	60
λM#1F	AGCAACCAACAAGAAAACACT	21	60
λM#1R	TCATCCTCGGCAAACTCTTT	21	60
λUM#1F	GTGAGGTGAATGTGGTGAAGT	22	60
λUM#1R	TCGCAGAGATAAAACACGCT	20	60

C

Pyrosequencing Primer Name	Sequence 5'-3'	Length (bp)	Annealing °C	Annealing Time	Elongation Time	Cycle #
CDC7F#1	CACTATGCTTCCCCCACACT	20	54	30 sec	2 min	35
CDC7R#1	ACAAACCGTCGGAAACTCAC	20	54			
CDC7YF#1	TATTATGTTTTTTTTATATT	20	48	1 min	1 min	50
CDC7YR#1	AACAAACCYTCYAAAACTCA	20	48			
CDC7F#2	Bio-AGGGATGTGTTAGTATTTGAGATT	24	54			
CDC7R#2	TCTCCAAAAAATCCCCACCTA	21	54			
CDC7Seq	CCCTACCCAACACTTC	16	n/a	n/a	n/a	n/a
EIF5F#1	TGCCCACTAGGAGAAAGGTG	20	54	30 sec	2 min	35
EIF5R#1	CGGACTCACCTCTGGAATGT	20	54			
EIF5YF#1	TGTTTATTAGGAGAAAGGTG	20	48	1 min	1 min	50
EIF5YR#1	CCYAACTCACCTCTAAAATAT	21	48			
EIF5F#2	Bio-GAGGGAGGGGATTAATTATTATTT	24	58			
EIF5R#2	CCTCACTACCCATTAACTAAAAA	23	58			
EIF5Seq	ACTAAAAACCTACCACAACT	20	n/a	n/a	n/a	n/a
IRX3F#1	CGTCCCCTTTGTCCTGTAGA	20	54	30 sec	2 min	35
IRX3R#1	AACGTGTCTGCCTTTGTGTG	20	54			
IRX3YF#1	YGTTTTTTTTGTTTTGTAGA	20	40	1 min	1 min	50
IRX3YR#1	AACYTATCTACCTTTATA	18	40			
IRX3F#2	Bio-AATGGGGAAGAAGGGAGTGA	20	54			
IRX3R#2	ACTATAACCCCCCTATCTACCCC	23	54			
IRX3Seq	CCCCTATCTACCCCCT	16	n/a	n/a	n/a	n/a
KLF3F#1	AGAAAGAGCGCGCCTACAG	19	54	30 sec	2 min	35
KLF3R#1	GCTCCTGGCACCAACTCC	18	54			
KLF3YF#1	AGAAAGAGYGYGTTTATAG	19	48	1 min	1 min	50
KLF3YR#1	ACTCCTAACACCAACTCC	18	48			
KLF3F#2	GGGAATAATGAGTGTTTGTTAGGT	24	54			
KLF3R#2	Bio-CCAACTCCCAACAATCACATAAC	23	54			
KLF3Seq	AAGTGGGTGGGGATT	15	n/a	n/a	n/a	n/a

Continued…

LINE1#1F	AGAAATGTAGAAATTATT	18	55	30 sec	2 min	35
LINE1#1R	GAGGTTATTGTTGTTTTTT	19	55			
LINE1YF#1	AGAAGACYGGTGATTTCT	18	55			
LINE1YR#1	GAGGTTACTGCTGTCTTTT	19	55			
LINE1#2F	Bio-TTTTGAGTTAGGTGTGGGATATA	23	50	1 min	1 min	50
LINE1#2R	AAAATCAAAAAATTCCCTTTC	21	50			
LINE1Seq	GGGTGGGAGTGAT	13	n/a	n/a	n/a	n/a
PCYT1AF#1	GAGGGACAGAGGTCAAGGTG	20	54	30 sec	2 min	35
PCYT1AR#1	ACATCACTCACCCACACGAA	20	54			
PCYT1AYF#1	GAGGGATAGAGGTTAAGGTG	20	48			
PCYT1AYR#1	ACATCACTCACCCACACYAA	20	48			
PCYT1AF#2	Bio-TTTTATGGATTTTATTGGGTTTAA	24	51	1 min	1 min	50
PCYT1AR#2	CCCCCCAAAAACTTTATTTCA	21	51			
PCYT1ASeq	ATTATCATTTTCATTAAT	18	n/a	n/a	n/a	n/a
PTPRGF#1	CTCCAGAGAAGCTGCGAGTT	20	54	30 sec	2 min	35
PTPRGR#1	GGAAACGGAGGAAAACACAA	20	54			
PTPRGYF#1	TTTTAGAGAAGTTGYGAGTT	20	40			
PTPRGYR#1	AAAAACYAAAAAAAACACAA	20	40			
PTPRGF#2	Bio-TTGTAAATGTTAGGGTAGTGAAGT	24	54	1 min	1 min	50
PTPRGR#2	ACCATACCTCCATACAAAAAATA	23	54			
PTPRGSeq	AGATTTTTTTTTAGTAGTTA	20	n/a	n/a	n/a	n/a
SLC39A4F#1	GGTGCCTGTAATCCCAGCTA	20	54	30 sec	2 min	35
SLC39A4R#1	GATCCCACACCTCACAAACC	20	54			
SLC39A4YF#1	GGTGTTTGTAATTTTAGTTA	20	48			
SLC39A4YR#1	AATCCCACACCTCACAAACC	20	48			
SLC39A4F#2	Bio-TGATTTTTGTTTGGGGATAGGTT	27	54	1 min	1 min	50
SLC39A4R#2	ACCCCAATCCCAACTCCAATAA	22	54			
SLC39A4Seq	CTCAACTAAAAAAAAACAAT	20	n/a	n/a	n/a	n/a

Continued…

TBX3F#1	TCGCGTGACACAGCTAAGTT	20	54	30 sec	2 min	35
TBX3R#1	TTGAATTGGTGCCTGCCTAT	20	54			
TBX3YF#1	TYGYGTGATATAGTTAAGTT	20	48			
TBX3YR#1	TTAAATTAATACCTACCTAT	20	48			
TBX3F#2	Bio-GTAAGGGATTTTTGTTTTTAGTTT	24	51	1 min	1 min	50
TBX3R#2	CCCCTCTCTTTAAAACATCACTAA	24	51			
TBX3Seq	AAATTTACCCCCTTCC	16	n/a	n/a	n/a	n/a

D

qPCR Primer Name	Sequence 5'-3'	Length (bp)	Annealing °C
BACTINF	TGTTACAGGAAGTCCCTTGCCATC	24	60
BACTINR	CTCCCCTGTGTGGACTTGGG	20	60
CDC7F	TTTGGCCACAGCACAGTTAC	20	52
CDC7R	CAAAAACGACTCATGCTCCA	20	52
EIF5F	TCCAACGTATCCCACCAAAT	20	52
EIF5R	GCTTCTTTGGATTGACATGC	20	52
H19F	GAGCCGCACCAGATCTTCAG	20	60
H19R	TTGGTGGAACACACTGTGATCA	22	60
IRX3F	CGCGCAGTATGAGCTGAAG	19	52
IRX3R	CTGGTGCTCTCCCTGGTG	18	52
KLF3F	CAGCCTCTCATGGTCTCCTT	20	52
KLF3R	GGGGTGACATTTCTTCAGGA	20	52
L1.2F	CTGAGTCAAAGAAAGGGGTGA	22	60
L1.2R	GGATATAGTCTCGTGGTGCG	21	60
PCYT1AF	ACTCCTTGTGAGCGACCTGT	20	52
PCYT1AR	CACCGTGAAGCCTTTGAAGT	20	52
PTPRGF	ACCCGTACTGGGCCTACTCT	20	52
PTPRGR	GCGACTGTTTTCCCTGTGTT	20	52
SIRT1F	GGCAAAGGAGCAGATTAGTAGG	22	55
SIRT1R	CATCAGGTCATCTTCTAAGCC	21	55
SLC39A4F	CAAGACGGCCTGCGTAGATA	20	52
SLC39A4R	TGCTGCTGGAACACAAAGTC	20	52
TBX3F	ACTGGGGAACAGTGGATGTC	20	52
TBX3R	GAATTCAGTTTCGGGGAACA	20	52
UBE2BF	CTCAGGGGTGGATTGTTGAC	20	60
UBE2BR	TGTGGATTCAAAGACCACGA	21	60
WNT11F	TGACCTCAAGACCCGATACC	20	52
WNT11R	GCTTCCGTTGGATGTCTTGT	20	52
λM#2F	TACAGAAAGACGGACGAAGG	20	60
λM#2R	TGGTGGGCGTTTTCATACAT	21	60
λUM#2F	TTCGTGATATTCCGTCGCTG	21	60
λUM#2R	AGTTTTTTGCCGCTTTACCG	21	60

Table 2.3. Antibodies

1° Antibody	Source	Dilution
Rabbit Anti-Human SIRT1	AbCam	1 in 200
Rabbit Anti-AlphaTubulin	AbCam	1 in 5000
Mouse Anti-Mouse SIRT1	AbCam	1 in 1000

2° Antibody	Source	Dilution
Goat Anti-Rabbit IgG - Peroxidase	Sigma	1 in 5000
Goat Anti-Mouse IgG - Peroxidase	Sigma	1 in 10000

3 Effect of SIRT1 manipulation and dietary polyphenols on global DNA methylation in Caco-2 cells

3.1 Outline

The beneficial effects of dietary restriction (DR) to delay the ageing process and increase lifespan in model systems are well established but the underlying mechanisms are unclear. The yeast NAD^+-dependent deacetylase, Sir2, was the first of the sirtuin family to be implicated in DR and lifespan extension. Research into mammalian sirtuins has expanded due to their potential as targets for anti-ageing interventions or therapies. There are many cellular substrates of the mammalian homologue SIRT1, whose deacetylation activity may contribute to, or be responsible for, the apparent ability of sirtuins to increase lifespan. We propose that these effects may be exerted either directly or indirectly through changes in DNA methylation patterns via the deacetylation activity of SIRT1 on histone proteins. DNA methylation is potentially causal in the ageing process as age-associated changes in the DNA methylation state of the genome can result in genome instability, inappropriate gene expression or silencing so it is within reason to suggest correct maintenance of DNA methylation plays a role in the effects of lifespan extension seen with DR. A number of naturally occurring polyphenolic compounds, obtained though the diet from various plant sources, may activate SIRT1 mimicking DR and its beneficial effects. Experiments in lower eukaryotes have demonstrated that resveratrol, a polyphenol naturally found in a variety of fruits and nuts, increased lifespan in a Sir2-dependent manner (Baur et al., 2006; Lagouge et al., 2006). The ability of resveratrol to delay some aspects of ageing raises the question as to whether other polyphenolic compounds have similar properties and act through similar mechanisms.

Global DNA methylation levels in the Caco-2 cell line were measured by COBRA and the pyrosequencing assays LUMA and LINE-1 to investigate if changes in SIRT1 expression or exposure to dietary polyphenols had any effect at this level. The Caco-2 cell line was selected from a variety of cell lines on the basis of measurements of baseline levels of global DNA methylation. The SIRT1 inhibitor Sirtinol had no affect on DNA methylation when measured by COBRA or the LUMA pyrosequencing assay. SIRT1 manipulation by transfection was then achieved with either a transgene to overexpress SIRT1 or SIRT1-targetting siRNAs. Effects of these treatments on SIRT1 expression was confirmed at the mRNA level by RT-PCR or RT-qPCR and at the protein level by western blot. Dietary polyphenols were then tested alone and in combination with SIRT1 manipulation to determine if they affected global DNA methylation and if any such effects were mediated through SIRT1.

3.2 Selection of appropriate cell lines for the investigation of DNA methylation

A range of human cell lines derived from a variety of tissues were screened to find those with the minimum and maximum levels of endogenous DNA methylation, with the aim of maximising any observed effects of the experimental treatments on both hyper- and hypo-methylation of DNA. Cell lines for measurements of endogenous DNA methylation were chosen based on availability in the laboratory and included Caco-2, HeLa, HEPG2, MCF-7, MDA-MB321, SH-SY5Y, and SW480. These cell lines were grown in 75 cm^2 flasks and, on reaching confluency, were lysed and DNA was extracted as described in Section 2.3. Methylation status of the extracted DNA from each cell line was analysed by two different methods.

The first method involved assaying DNA methylation at the LINE-1 retrotransposon by pyrosequencing as described in Section 1.5.3 and 2.6.3. Percentage DNA methylation was measured at the three consecutive CpG sites within the LINE-1 element, occurring at 252 bp, 256 bp and 270 bp into the LINE-1 sequence (*Figure 3.1* and Section 2.6.8). Briefly, the LINE-1 pyrosequencing assay consisted of a two stage PCR reaction. The first PCR generated a 595 bp product, and contained 25 µl HotStar Taq MasterMix (Qiagen), 0.25 µM sense and antisense primers (LINE1YF#1 and LINE1YR#1) using 4 µl of bisulfite modified genomic DNA (Section 2.6.1) as a template. Primer sequences and annealing temperatures are outlined in Table 2.2C. This reaction was followed by a second, nested PCR, generating a 146 bp product, and contained 25 µl HotStar Taq MasterMix (Qiagen), 0.25 µM sense primer and 0.20 µM antisense biotinylated primer (LINE1F#2 and LINE1R#2) using 4 µl of the first PCR reaction as a template. Primer sequences and annealing temperatures are outlined in Table 2.2C. Pyrosequencing using the LINE-1 sequencing primer was carried out in duplicate for each sample (*Figure 3.2A*).

Standard curves were generated to confirm linear amplification of methylated and unmethylated LINE-1 sequences. Unmethylated LINE-1 DNA template was generated through the removal of methyl groups by PCR amplification of a 529 bp region (LINE1F#1 and LINE1R#1) of the LINE-1 sequence from genomic DNA as described above. Primer sequences and annealing temperatures are outlined in Table 2.2C. Nine microlitres of unmethylated LINE-1 PCR product was methylated *in vitro* as described in Section 2.2.4. Nine microlitres of methylated or 25 µl unmethylated LINE-1 PCR product was then bisulfite modified as described in Section 2.6.1. Nested PCR using primers to produce a smaller product focusing in on the specific CpG sites for analysis was then performed as described above. Primer sequences and annealing temperatures are outlined in Table 2.2C. Reactions were combined to give appropriate percentages of methylated DNA (0, 5, 10, 25, 50, 75, 90, 95, and 100 %) in a total volume of 10 µl. Pyrosequencing using the LINE-1 sequencing primer was carried out in duplicate. Methylation standard curves for LINE-1 can be found in Appendix C.

LINE-1 Sequence

Accession number: X58075

```
+1    gggggaggag ccaagatggc cgaataggaa cagctccggt ctacagctcc
50    cagcgtgagc gacgcagaag acgggtgatt tctgcatttc catctgaggt
100   accgggttca tctcactagg gagtgccaga cagtgggcgc aggccactgt
150   gtgcgcgcac cgtgcgcgag ccgaagcagg gcgaggcatt gcctcacctg
200   ggaagcgcaa ggggtcaggg agttcccttt ccgagtcaaa gaaaggggtg
250   acggacgcac ctggaaaatc gggtcactcc cacccgaata ttgcgctttt
300   cagaccggct taagaaacgg cgcaccacga gactatatcc cacacctggc
350   tcagaggtc ctacgcccac ggaatctcgc tgattgctag cacagcagtc
400   tgagatcaaa ctgcaaggcg gcaacgaggc tgggggaggg gcgcccgcca
450   ttgcccaggc ttgcttaggt aaacaaagca gccgggaagc tcgaactggg
500   tggagcccac cacagctcaa ggaggcctac ctgcctctgt aggctccacc
550   tctgggggca gggcacagac aaacaaaaag acagcagtaa cctctgcaga
600   cttaagtgtc cctgtctgac agctttgaag agagcagtgg ttctcccagc
650   acgcagctgg agatctgaga acgggcagac tgcctcctca agtgggtccc
700   tgacccctga cccccgagca gcctaactgg gaggcacccc ccagcagggc
750   acactgacac ctcacacggc agggtattcc aacagacctg cagctgaggg
800   tcctgtctgt tagaaggaaa actaacaacc agaaaggaca tctacacgaa
850   aacccatctg tacatcacca tcatcaaaga ccaaaagtag ataaaaccac
900   aaagatgggg aaaaaacaga acagaaaaac tggaaactct aaaacgcaga
950   ggccctctcc tcctccaaag gaacgcagtt cctcaccagc aacagaacaa
1000  agctggatgg agaatgattt tgacgagctg agagaagaag gcttcagacg
1050  atcaaattac tctgagctac aggaggacat tcaaaccaaa ggcaaagaag
1100  ttgaaaactt tgaaaaaaat ttagaagaat gtataactag aataacc
```

Figure 3.1. The LINE-1 sequence and related primers. *The LINE-1 sequence taken from NCBI (accession number: X58075) is shown. Primers were designed for PCR to a region in the LINE-1 sequence (LINE1YF#1 - light blue and LINE1YR#1 - dark blue) and a nested PCR (LINE1F#2 - light green and LINE1R#2 - dark green) to focus in on four specific CpG sites (pink) within the LINE-1 sequence. A sequencing primer was designed for use in the pyrosequencing reaction (LINE1Seq - orange). Primers and annealing temperatures are given in Table 2.2C.*

The second method for assessing the methylation status of the extracted DNA used LUMA, as described in Section 1.5.4 and 2.6.9. Two hundred nanograms of genomic DNA were digested with either *EcoRI* and *MspI* restriction enzymes or *EcoRI* and *HpaII* restriction enzymes. The percentage methylation of the DNA sample was determined by the *MspI*/*HpaII* ratio.

Results of the LINE-1 and LUMA assays did not correlate (*Figure 3.2C*), but this observation is not necessarily surprising since the two assays interrogate different CpG sites across the genome and it is completely feasible that methylation at these sites differs. Based on the observation that the range of methylation values for the different cell lines was smaller when methylation was measured using the LUMA assay, it may be argued that measurement of methylation at the LINE-1 element is a more sensitive measure of global DNA methylation.

No significant difference in DNA methylation in the cell lines tested was observed (*Figure 3.2*), thus the human intestinal Caco-2 cell line was selected as the model for this study, based on the fact that there was extensive experience in the laboratory in the culture, transfection and manipulation of this cell line. A second reason was that a model of the intestinal response to DR would allow for testing the effects of potential dietary mimetics of DR – specifically the polyphenol resveratrol, along with the isoflavones genistein and daidzein – using the (readily available) parent compounds, to which the intestinal mucosa would be exposed as a result of dietary intake; effects of such compounds on other tissues would have to take account of effects of metabolites (often unavailable commercially), rather than the parent compound.

The Caco-2 human epithelial colorectal adenocarcinoma cell line was derived from a carcinoma within the large intestine of a 72 year old Caucasian male (Fogh et al., 1977). The parental Caco-2 cell line from the American Tissue Culture Collection (ATCC) has a heterogeneous quality that may have led to divergence in published results based on this model as well as the emergence of homogenous subpopulations of clonal cell lines with specific differentiation characteristics. Key factors in maintaining a culture true to the parental cell line include passage number, seeding density and medium composition. Various functional traits of the Caco-2 cell line are affected after 35 or more passages in culture such as multi-layering (Briske-Anderson et al., 1997), metabolic (Nakumura et al., 2003) and transport activities (Bravo et al., 2004). Maintaining a consistent seeding density and time of passage to achieve a comparative confluency, and therefore stage of differentiation, over each experiment time course avoids variable differentiation-related traits. Additionally, composition of the cell culture medium should be taken into consideration (Papaconstantinou et al., 2000). It is therefore crucial to ensure a uniform approach to the culture of the Caco-2 parental cell line to generate reproducible results.

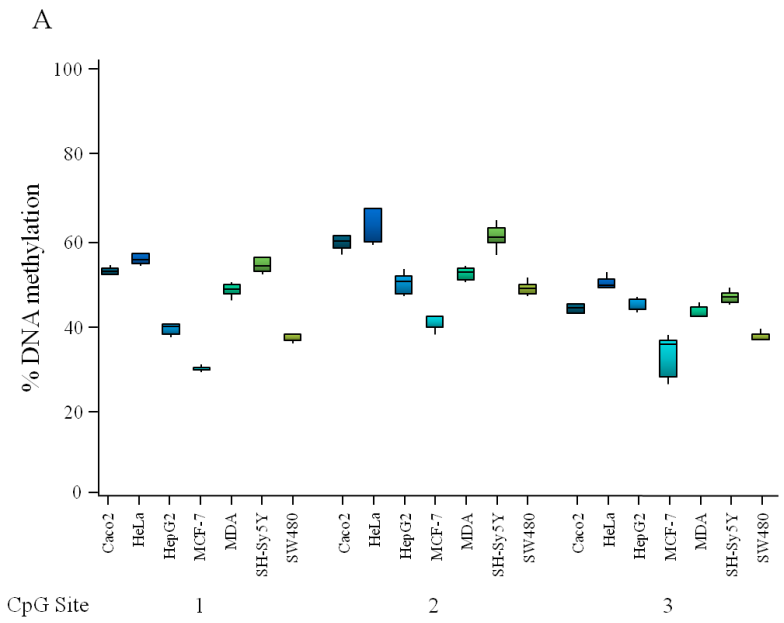
A
100
80
60
40
20
0
% DNA methylation
Caco2
HeLa
HepG2
MCF-7
MDA
SH-Sy5Y
SW480
CpG Site
1
2
3

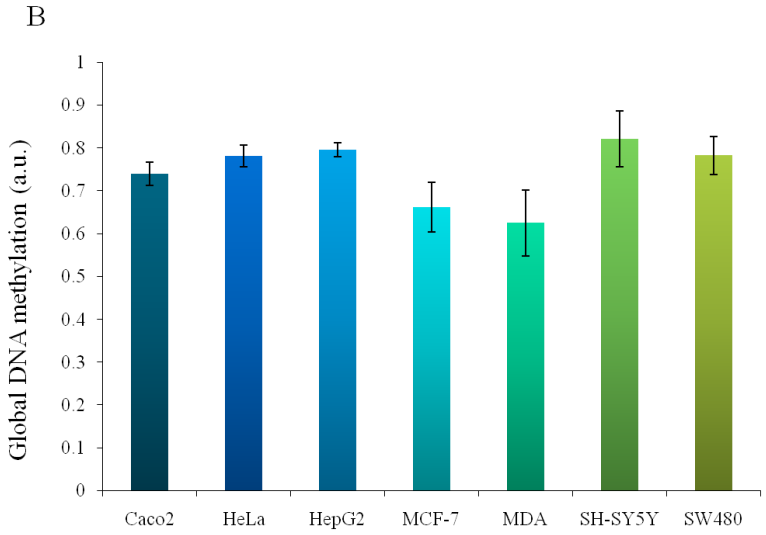
B
1
0.9
0.8
0.7
0.6
0.5
0.4
0.3
0.2
0.1
0
Global DNA methylation (a.u.)
Caco2
HeLa
HepG2
MCF-7
MDA
SH-SY5Y
SW480

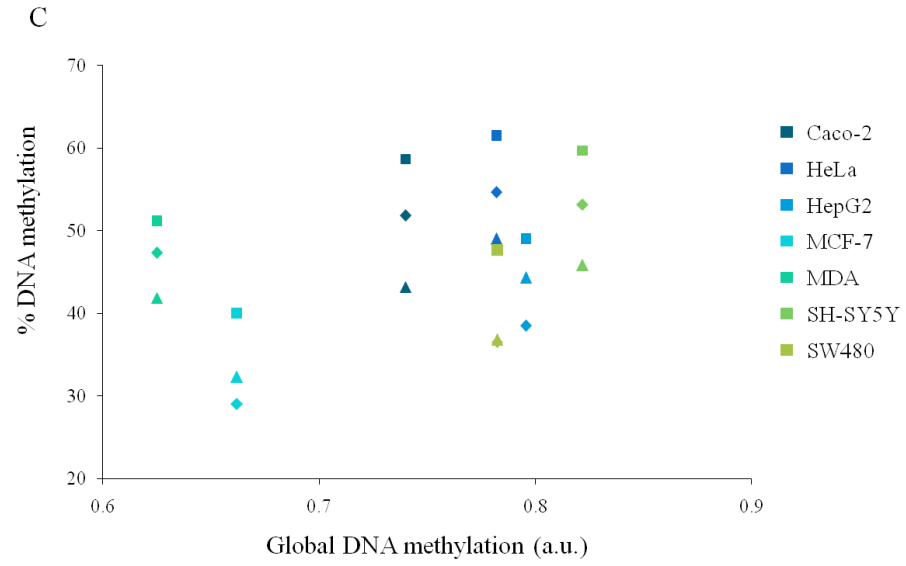
C
70
60
50
40
30
20
% DNA methylation
0.6
0.7
0.8
0.9
Global DNA methylation (a.u.)
Caco-2
HeLa
HepG2
MCF-7
MDA
SH-SY5Y
SW480

Figure 3.2. Comparison of LINE-1 (A) and LUMA (B) assay results for measurement of endogenous levels of DNA methylation in Caco-2, SW480, HeLa, SH-SY5Y, HepG2, MCF-7 and MDA cell lines. *A – The LINE-1 assay measured percentage DNA methylation at three CpG sites within the LINE-1 retrotransposon element and showed no statistically significant difference between endogenous DNA methylation at CpG sites in the range of cell lines tested ($p > 0.05$ by one way ANOVA followed by Bonferroni's multiple comparisons test). B – The LUMA assay used methylation sensitive and insensitive isoschizomers to produce a global ratio of methylated to unmethylated DNA and showed no statistical differences between the DNA methylation levels in the range of cell lines tested ($p > 0.05$ by one way ANOVA followed by Bonferroni's multiple comparisons test); $n = 2$. C – Relationship between LINE-1 CpG site % DNA methylation (y axis) and LUMA global DNA methylation (x axis). The colour representing each cell line is indicated in the key, CpG sites 1, 2 and 3 are represented as a diamond (♦), triangle (▲) and square (■) respectively. No correlation was found by Spearman rank correlation (sr) between the three CpG sites in the LINE-1 assay and the data from the LUMA assay; LUMA and CpG1 $sr = 0.2500$, $p = 0.59$, LUMA and CpG2 $sr = 0.2500$, $p = 0.59$, LUMA and CpG3 $sr = 0.5357$, $p = 0.2357$. There was strong correlation between all three CpG sites within the cell lines; CpG1 and CpG2 $sr = 1.000$, $p = 0.0004$, CpG2 and CpG3 $sr = 0.8929$, $p = 0.0123$, CpG1 and CpG3 $sr = 0.8929$, $p = 0.0123$. All data are mean ± SEM for $n = 9$.*

3.3 Effects on genomic DNA methylation of treating Caco-2 cells with the SIRT1 inhibitor Sirtinol

Sirtinol was identified as an inhibitor of the yeast Sir2p NAD^+-dependent deacetylase activity through a high-throughput cell-based screen of compounds (Grozinger et al., 2001) and later used to inhibit SIRT1 activity in the plant cell model *Arabidopsis thaliana* and a variety of human cell lines. Moieties on the aromatic ring of Sirtinol (*Figure 3.3A*) are proposed to interact with hydrophobic residues in the SIRT1 binding site that interacts with the adenosine base in the NAD^+ substrate (Trapp et al., 2006), a feature that prevents off-target inhibition of Class I and II HDACs (Bedalov et al., 2001; Grozinger et al., 2001). Concentrations of 10 - 100 μM Sirtinol have been used in SIRT1 inhibition experiments with the half maximal inhibitory concentration (IC_{50}) for Sir2/SIRT1 in yeast and human being 40 – 70 μM. At 10 μM Sirtinol inhibition of SIRT1 in white blood cells led to an increase in MMP9 levels, a matrix metalloproteinase involved in degradation of the extracellular matrix in age-related diseases (Nakamaru et al., 2009). At a 10-fold greater concentration (100 μM), Sirtinol was shown to induce senescence-like growth arrest in breast and lung cancer cell lines, as measured by senescence-associated β-galactosidase and increased plasminogen activator inhibitor 1 expression. This observation suggests that at high concentrations Sirtinol acts in a similar way to chemotherapeutic agents to arrest the growth of cancerous cells (Ota et al., 2005).

Caco-2 cells seeded 24 hours previously at 3.5 x 10^5 cells/well in a six well plate (area = 9.6 cm^2/well) were treated with 10, 40, 70 or 100 μM Sirtinol (in 0.1 % v/v DMSO) or a control of 0.1 % v/v DMSO as described in Section 2.3.5. The concentrations of Sirtinol used were to reflect the minimum and maximum amounts used in published work as well as cover the IC_{50} range. After an additional 48 hours cells were lysed and DNA was extracted as described in Section 2.4.1. DNA from cells treated with Sirtinol was assessed by two different methods for levels of DNA methylation at two CpG sites in the LINE-1 retrotransposon within two *HinfI* restriction enzyme sites, using the gel-based Combined Bisulfite Restriction Analysis (COBRA) as described in Sections 1.5.2 and 2.6.2 and at four CpG sites by pyrosequencing as described in Sections 1.5.3 and 2.6.8.

COBRA involved amplification of bisulfite modified DNA to the LINE-1 retrotransposon by PCR with primers specific to the LINE-1 retrotransposon (LINE1COBRAF and LINE1COBRAR – See *Table 2.1B*). Ten microlitres of the PCR product was digested with *HinfI*. Within the LINE-1 retrotransposon sequence there are two *HinfI* restriction sites both containing a CpG site. The methylation at these two CpG sites in a DNA sample was expressed as the ratio of uncut to cut PCR product as determined by densitometric quantification of SYBR green-stained agarose gels.

Based on measurement by pyrosequencing, LINE-1 methylation was expressed as the percentage of unmethylated cytosines converted to thymines as a result of bisulfite modification. To compare results

obtained using the two techniques more accurately the assay was modified and extended to assess a fourth CpG site. This site occurred 232 bp into the LINE-1 sequence and was within the second HinfI restriction site.

No significant difference in DNA methylation in response to Sirtinol treatment was detected when measured by COBRA (*Figure 3.3B*) or the LINE-1 pyrosequencing assay (*Figure 3.3C*). This observation may indicate either that Sirtinol did not effectively inhibit SIRT1 activity under the experimental conditions (it was not possible to measure SIRT1 activity directly – see Section 4.5) or that SIRT1 inhibition had no effect on methylation of DNA at the LINE-1 retrotransposon.

An alternative approach to inhibit protein function is through short interference RNA (siRNA) knockdown, the targeted cleavage and degradation of an mRNA by a specific siRNA preventing the translation into a protein. Using siRNA to achieve total mRNA and therefore protein knockdown provides a tool for SIRT1 manipulation whose efficacy can be measured (by RT-qPCR and western blotting) and may be a more effective way to assess the effects of reduced levels of SIRT1 on DNA methylation levels within a cell population.

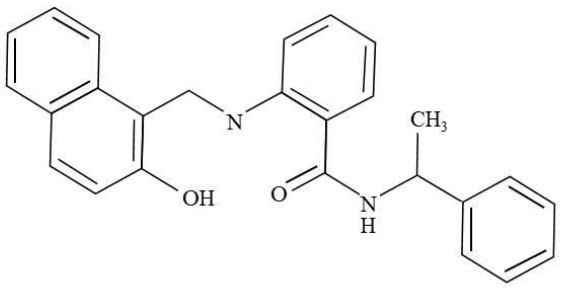
N
CH3
OH
O
N
H

A

B

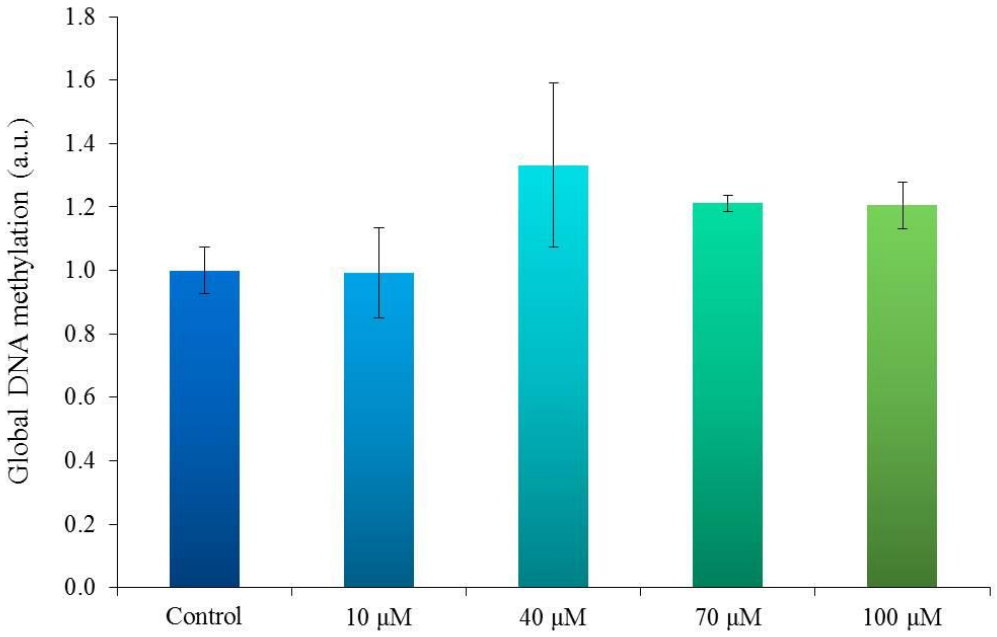
Global DNA methylation (a.u.)
1.8
1.6
1.4
1.2
1.0
0.8
0.6
0.4
0.2
0.0
Control
10 µM
40 µM
70 µM
100 µM

C

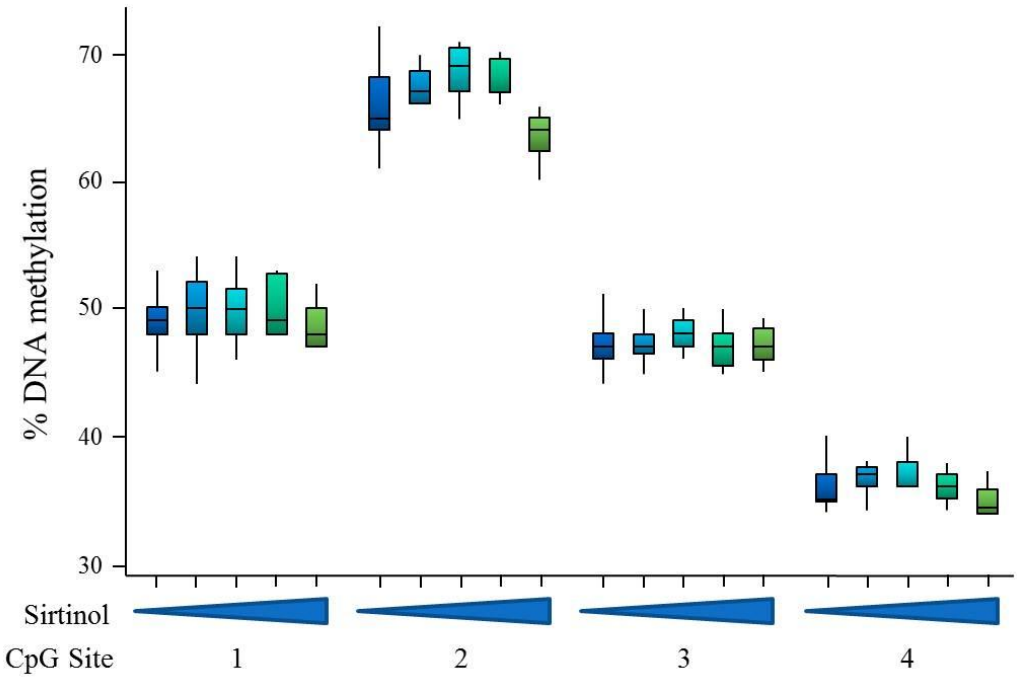
% DNA methylation
70
60
50
40
30
Sirtinol
CpG Site
1
2
3
4

***Figure 3.3*. Effect on genomic DNA methylation in Caco-2 cells of Sirtinol, the SIRT1 deacetylase activity inhibitor.** *A – Chemical structure of Sirtinol. B – COBRA showed no statistical differences between DNA methylation levels in Caco-2 cells treated with Sirtinol over a range of concentrations when compared with the control ($p > 0.05$ by one way ANOVA followed by Bonferroni's multiple comparisons test). C – The LINE-1 pyrosequencing assay showed no statistical differences between DNA methylation levels in Caco-2 cells treated with Sirtinol over a range of concentrations (10, 40, 70 and 100 μM – light blue to green respectively) when compared with the control (dark blue) ($p > 0.05$ by one way ANOVA followed by Bonferroni's multiple comparisons test). All data are mean ± SEM for n = 3 – 12.*

3.4 Effects on genomic DNA methylation of manipulated SIRT1 expression levels

Level of SIRT1 increased in the brain, kidney, visceral fat pads and liver of DR mice (Cohen et al., 2004). To achieve comparable levels of SIRT1 overexpression to that observed in response to DR Caco-2 cells were manipulated with the use of a SIRT1 overexpression construct, and the approach was complemented with use of SIRT1-targeting siRNAs to investigate if changes in expression of SIRT1 in human cells can influence DNA methylation, consistent with such a mechanism contributing to SIRT1-mediated effects of DR to increase lifespan.

3.4.1 Effects on genomic DNA methylation of knockdown of SIRT1 expression levels

The mechanism by which synthetic microRNAs known as short interference RNAs (siRNA) act upon a target mRNA sequence for degradation has recently become an effective tool to knockdown gene function within mammalian cells. RNA interference (RNAi) involves the loss of gene function by the processing of dsRNA dioligonulceotides by an enzyme known as dicer into smaller ~21 nucleotide length siRNAs. The siRNA antisense strand is then loaded into the RNA-induced silencing complex (RISC) allowing recognition and cleavage of the target mRNA sequence by the complex. The cleaved mRNA sequence is then targeted for degradation and ultimately leads to the prevention of protein expression. Synthetic molecules can be engineered to represent siRNA processed by dicer; with a better understanding of the RNAi pathway synthetic siRNAs have improved specificity and stability for use in cell culture as well as a reduction in off-target effects and innate immune responses. To achieve SIRT1 knockdown in the Caco-2 cell line, two non-overlapping validated Stealth RNAi™ siRNAs targeting SIRT1 mRNA were purchased from Invitrogen. Knockdown was assessed at 24, 48 and 72 hours after transfection to ascertain the most effective incubation time.

Caco-2 cells seeded 24 hours previously at 3.5 x 10^5 cells/well in a six well plate (area = 9.6 cm^2/well) were transfected transiently with 100 pmol SIRT1-targeting siRNA or with 100 pmol of a Stealth RNAi™ siRNA negative control of similar GC content (Section 2.3.2). After 24, 48 and 72 hours cells were lysed and RNA and total cell lysate were extracted from parallel experiments. RNA was used to assess SIRT1 knockdown at the mRNA level by RT-PCR as described in Section 2.7.1. Total RNA was extracted from Caco-2 cells using the Qiagen AllPrep DNA/RNA Mini Kit (Section 2.4.1). Four and a half micrograms of DNase-treated RNA (Section 2.7.1.2) was reverse transcribed using Superscript™ III RNase H- Reverse Transcriptase (Invitrogen) (Section 2.7.1.3). Reverse transcribed cDNA was then amplified by PCR (Section 2.5.1.1) using primers specific to a 128 bp region of the *SIRT1* gene (SIRT1F and SIRT1R) or to a 328 bp region of the reference gene *RN18S1* (18s rRNA) which acted as a control (18sF and 18sR). Primer sequences and annealing temperatures are specified in Table 2.2B. A decreased intensity of the SIRT1-specific band from cells transfected with the SIRT1 expression construct compared with the band generated from the control cells indicated that SIRT1

mRNA knockdown had been achieved. Optimum SIRT1 mRNA knockdown was achieved at 72 hours after siRNA transfection into Caco-2 cells (*Figure 3.4A*).

SIRT1 knockdown at the mRNA level 72 hours after transfection was also assessed by RT-qPCR (*Figure 3.4B*) as described in Section 2.7.2. RNA was extracted, DNase treated and reverse transcribed as described above. Reverse transcribed cDNA was then PCR amplified (Section 2.5.1.1) using the aforementioned primers specific to a 239 bp region of the *SIRT1* gene. Data were normalised to the reference gene *ACTB* (β ACTIN) using primers that amplified a 90 bp region. Primer sequences and annealing temperatures are outlined in Table 2.2D.

Reverse transcription-qPCR analysis of SIRT1 and β ACTIN was performed using the Roche LightCycler® 480 (Section 2.7.2.4). Standard curves were generated for SIRT1 and β ACTIN to confirm linear amplification of PCR products and were run in parallel with the experimental samples. To generate standard curves undiluted cDNA extracted from untreated Caco-2 cells and reverse transcribed was used to create an 8 point 2-fold dilution series (Section 2.7.2.5). Each dilution within this series was then used in qPCR amplification for each gene, and each reaction was performed in duplicate. Amplification and standard curves for SIRT1 and β ACTIN can be found in Appendix D. Relative levels of SIRT1 transcript in the Caco-2 cells transfected with either of the two siRNAs show a statistically significant reduction (68 % and 70 % respectively; $p < 0.001$) in SIRT1 mRNA compared with the control siRNA (*Figure 3.4B*), confirming observations made by the gel-based RT-PCR analysis.

Total cell lysate was used to assess SIRT1 knockdown at the protein level by western blot as described in Section 2.8. Total cell lysate was extracted (Section 2.8.2.2) and protein concentration determined by Bradford assay (Section 2.8.1.4). Ten micrograms of total cell lysate was separated by SDS-PAGE (Section 2.8.1.5) and blotted onto a polyvinylidene difluride (PVDF) membrane (Section 2.8.1.6), which was then probed with antibodies to SIRT1 and the loading control protein alpha tubulin. SIRT1 protein knockdown was confirmed by a decrease in binding of the SIRT1 antibody in cells transfected transiently with the SIRT1-targeting siRNA in comparison to cells transfected transiently with the Stealth RNAi™ siRNA negative control (*Figure 3.4C*). This transfection model was continued as a means to knockdown SIRT1 within Caco-2 cells in further experiments.

Global methylation status of the extracted DNA from Caco-2 cells transfected with either the SIRT1-targeting siRNA or with the Stealth RNAi™ siRNA negative control was assessed by LINE-1 COBRA and the LINE-1 pyrosequencing assay as described in Sections 1.5.2 and 2.6.2 and 1.5.3 and 2.6.8 respectively. SIRT1 knockdown alone had no apparent effect on LINE-1 methylation measured using either technique ($p > 0.05$) (*Figure 3.5A* and *Figure 3.5B*).

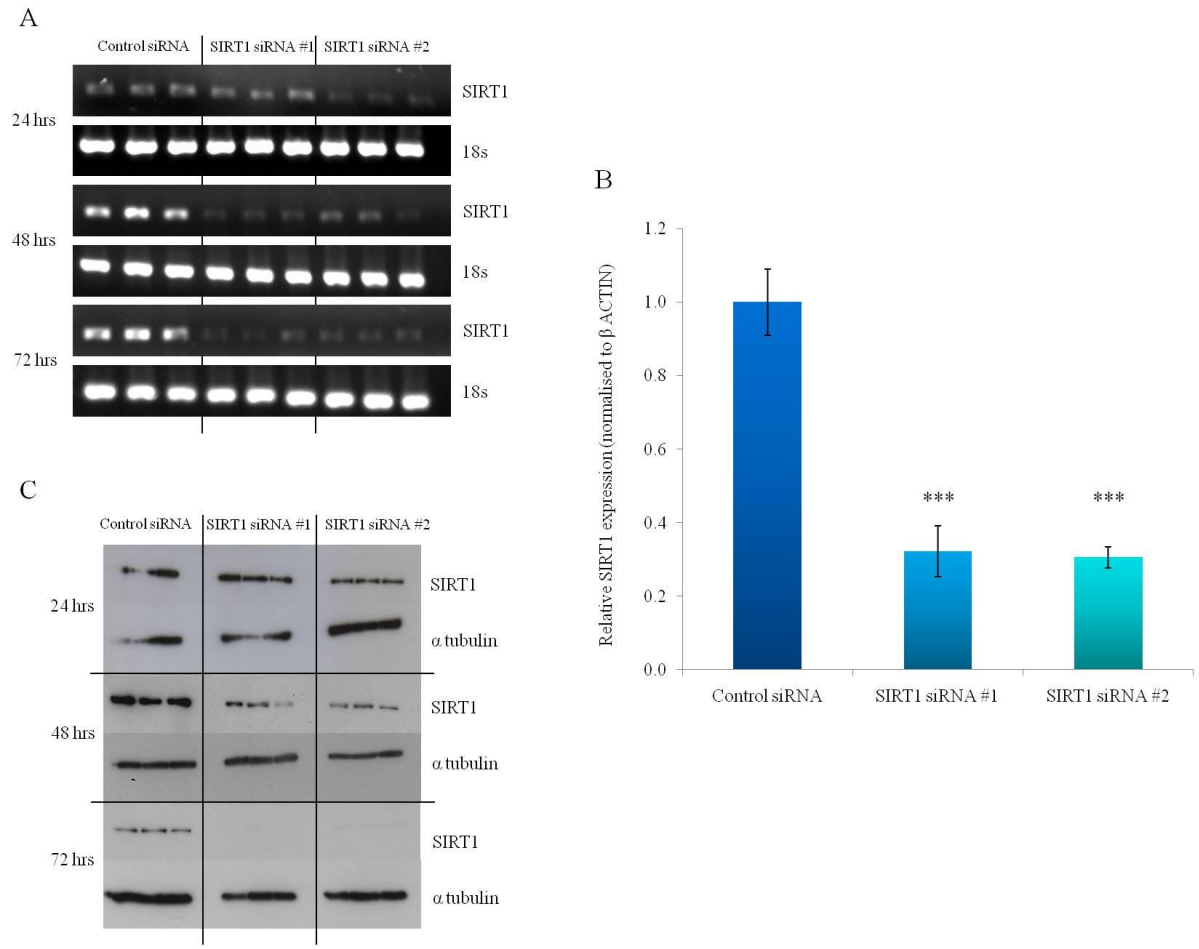

Figure 3.4. Confirmation of (A) SIRT1 mRNA expression knockdown in transiently transfected Caco-2 cells by RT-PCR and (B) RT-qPCR and (C) SIRT1 protein knockdown by western blot. *A – RT-PCR products were analysed by agarose gel electrophoresis. As indicated, lanes contained products generated from Caco-2 cells transiently transfected with either SIRT1-targeting siRNA or with a Stealth RNAi™ siRNA negative control of similar GC content at either 24, 48 or 72 hours after transfection. Primer pairs (SIRT1 –SIRT1F and SIRT1R or 18s –18sF and 18sR – see Table 2.2B) were included in the reaction as indicated along with MMLVRT. A comparison of band intensity between cells transfected with either SIRT1-targeting siRNA and those transfected with the Stealth RNAi™ siRNA negative control indicate SIRT1 mRNA knockdown. B – RT products were analysed quantitatively for SIRT1 and β ACTIN mRNA expression using the Roche LightCycler® 480, LightCycler® 480 SYBR Green I Master and primer pairs (SIRT1 –SIRT1F and SIRT1R or 18s –18sF and 18sR – see Table 2.2C). Relative levels of SIRT1 expression were calculated in each sample using levels of SIRT1 expression normalised to β ACTIN. A comparison between SIRT1 mRNA expression levels between cells transfected with either of the two SIRT1-targeting siRNAs and those transfected with the control indicates statistically significant SIRT1 mRNA knockdown; ***$p < 0.001$ by one way ANOVA followed by Tukey. All data are mean ± SEM for $n = 9$. C – Protein extracted from Caco-2 cells transiently transfected with either SIRT1-targeting siRNA or with a Stealth RNAi™ siRNA negative control of similar GC content at either 24, 48 or 72 hours after transfection was separated by SDS-PAGE gel electrophoresis. SIRT1 expression was analysed by probing with an antibody to the SIRT1 protein followed by reprobing with an antibody to alpha tubulin as a loading control. A comparison of band intensity between cells transfected with either SIRT1-targeting siRNA and those transfected with the Stealth RNAi™ siRNA negative control indicate SIRT1 mRNA knockdown.*

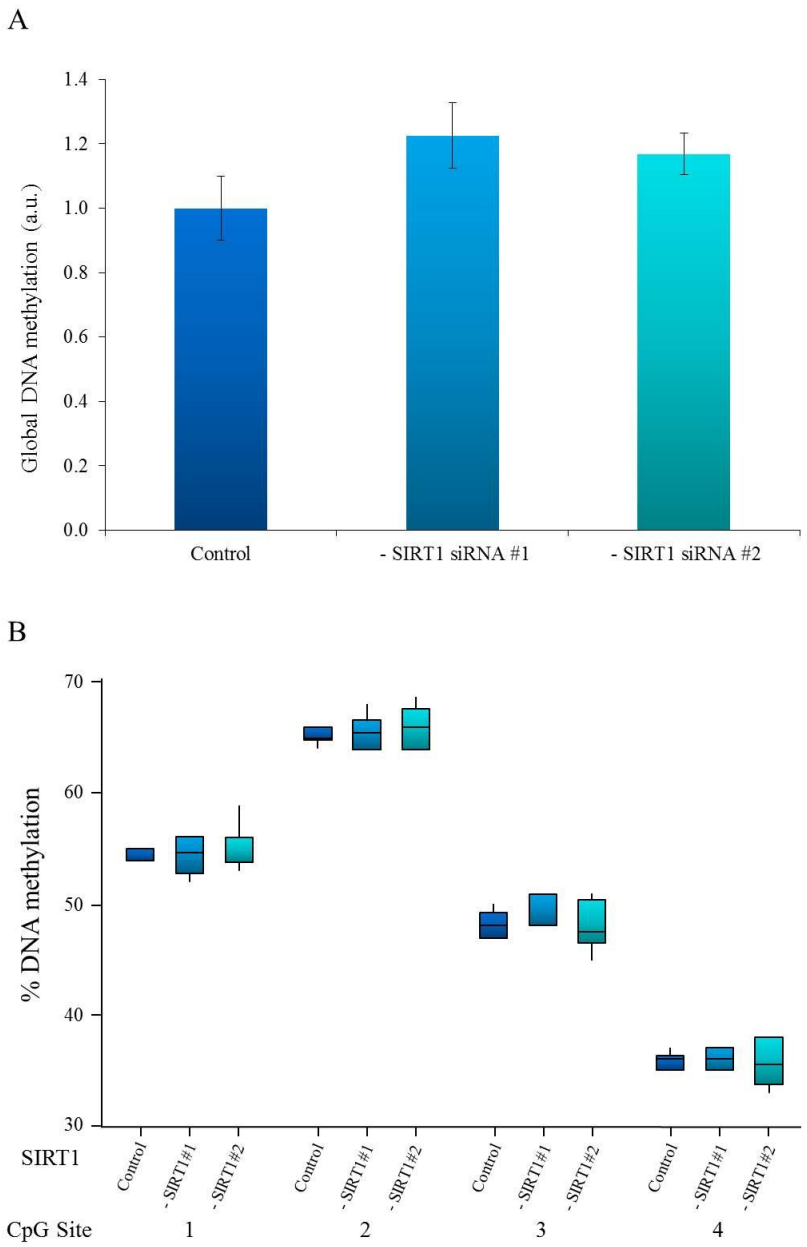

Figure 3.5. Effect on genomic DNA methylation of SIRT1 knockdown using (A) COBRA and (B) the LINE-1 pyrosequencing assay. *A – COBRA analysis showed no statistically signification difference between DNA methylation levels in Caco-2 cells transfected with SIRT1-targeting siRNA (blue and light blue) for 72 hours when compared with a Stealth RNAi™ siRNA negative control of similar GC content (dark blue) (p > 0.05 by* one way *ANOVA followed by Bonferroni's multiple comparisons test). All data are mean ± SEM for n = 6. B – The LINE-1 pyrosequencing assay showed no statistically signification difference between DNA methylation levels in Caco-2 cells transfected with SIRT1-targeting siRNA (blue and light blue) for 72 hours when compared with a Stealth RNAi™ siRNA negative control of similar GC content (dark blue) (p > 0.05 by one way ANOVA followed by Bonferroni's multiple comparisons test). All data are mean ± SEM for n = 6.*

3.4.2 Effects on genomic DNA methylation of overexpression of SIRT1

To achieve stable SIRT1 overexpression in the Caco-2 cell line, a plasmid comprising the pCMV6-ENTRY vector containing the *SIRT1* open reading frame (ORF) was purchased from Origene. The pCMV6-ENTRY-SIRT1 plasmid was propagated through *E. coli* as described in Section 2.1 and 2.2. The presence of *SIRT1* within the plasmid construct was confirmed by restriction mapping with *BglII* and *MluI* (*Figure 3.6*) and also through sequencing using primers to the SIRT1 sequence (*Table 2.2B*).

Caco-2 cells seeded 24 hours previously at 3.5 x 10^5 cells/well in a six well plate (area = 9.6 cm^2/well) were successfully transfected with 2 μg SIRT1 expression construct or with 2 μg control vector without a *SIRT1* insert, pCMV6-Neo, that also confers resistance to G418 (Section 2.3.3). Cells were selected using G418 at a concentration of 750 μg/ml, determined empirically to be the lowest effective concentration for cell death. When the G418 treatment had led to cell death in the untransfected population, cells transfected with either the SIRT1 expression construct or the control vector were lysed and RNA was extracted. RNA was analysed by RT-PCR as described previously (Section 3.4.1) to establish if *SIRT1* overexpression had been achieved. An increased intensity of the SIRT1-specific band from cells transfected with the SIRT1 expression construct compared with the band generated from the control cells indicated that *SIRT1* mRNA overexpression had been achieved (*Figure 3.7A*).

SIRT1 overexpression at the protein level was assessed using a total cell lysate preparation from the stably-transfected cell lines; the samples were analysed by western blot as previously described (Section 3.4.1). Initially, cells transfected with the SIRT1 overexpression construct showed an increase in the levels of SIRT1 expression in comparison to the negative control; however in subsequent passages there appeared to be a return of SIRT1 expression to an endogenous level similar to that of the negative control (*Figure 3.7B*).

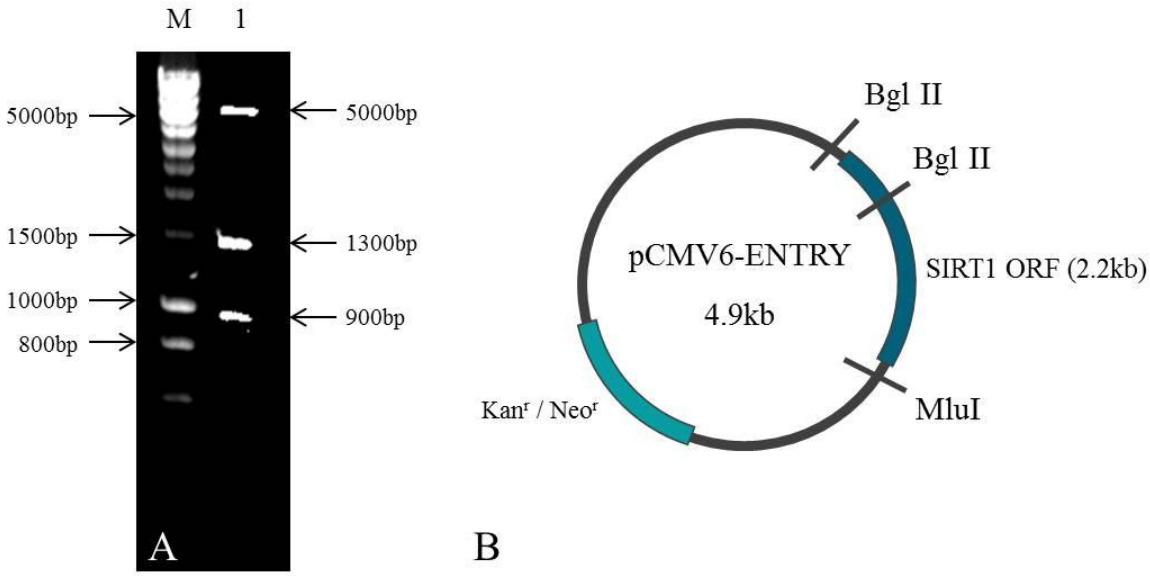

Figure 3.6. Confirmation of the presence of the SIRT1 ORF in the recombinant pCMV6-ENTRY-based construct through restriction mapping. *A – Digestion of the pCMV6-ENTRY vector containing the SIRT1 ORF with BglII and MluI. Products (5 kb, 1.3 kb and 900 bp) confirmed the presence of SIRT1. A DNA molecular weight marker (Hyperladder I Bioline, sizes indicated) was run in the lane marked 'M'. B – Diagrammatic representation of the digestion of the SIRT1 expression construct with BglII and MluI, sites indicated.*

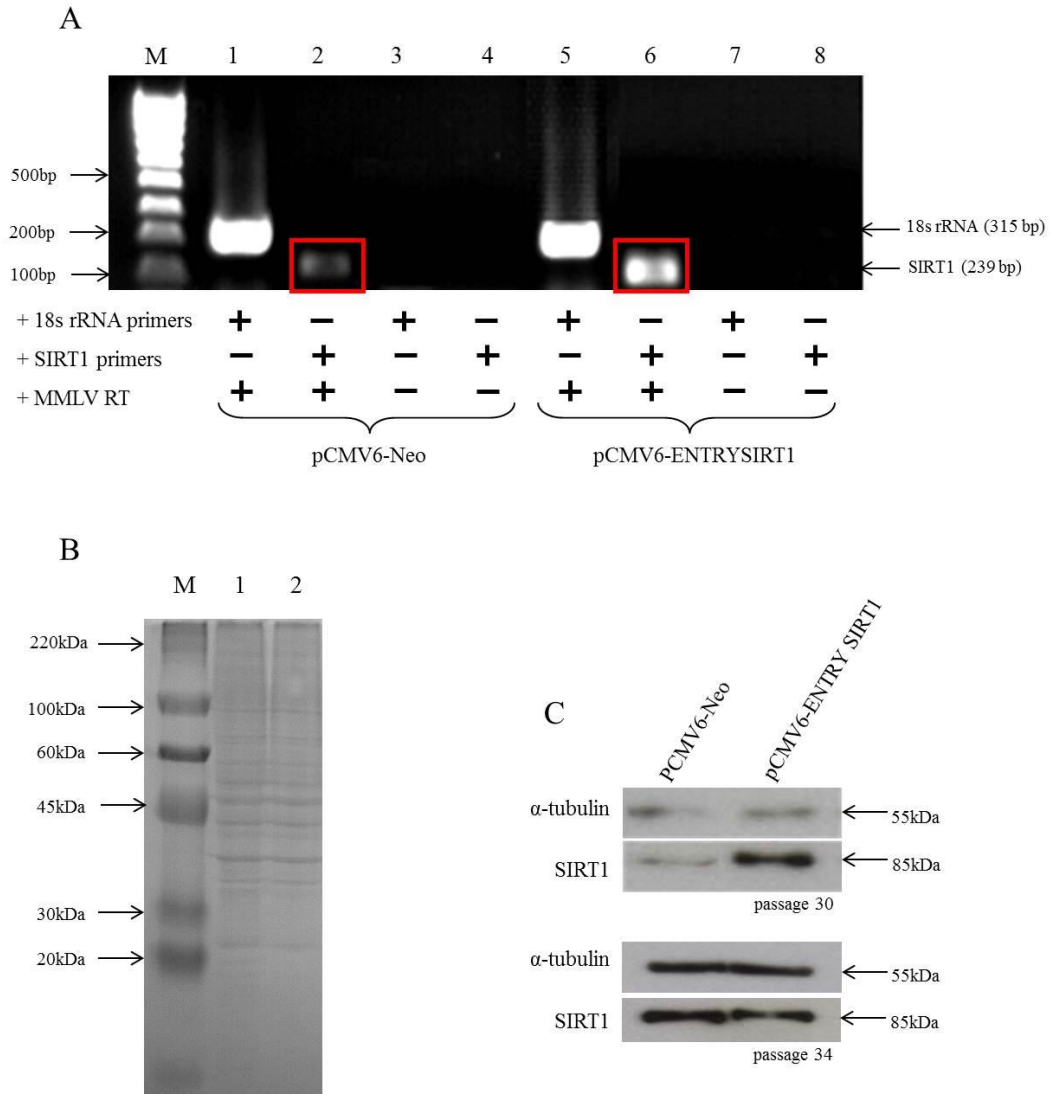

Figure 3.7. Confirmation of (A) SIRT1 mRNA overexpression in stably transfected Caco-2 cells by RT-PCR, (B) equal protein loading concentrations by colloidal blue staining and of (C) SIRT1 protein overexpression in stably transfected Caco-2 cells by western blot. *RT-PCR products were analysed by agarose gel electrophoresis. In lane 1 a DNA molecular weight marker (Hyperladder IV, Bioline; sites indicated) was run. As indicated, lanes 2 - 9 contained products generated from Caco-2 cells stably transfected with either the control vector pCMV6-Neo or the SIRT1 expression construct pCMV6-ENTRYSIRT1. Primer pairs (SIRT1F, SIRT1R, 18sF, 18sR – see Table 2.2B) and MMLVRT were included in the reaction as indicated. A comparison of band intensity between cells transfected with the SIRT1 expression construct and those transfected with the control vector indicate SIRT1 mRNA overexpression. B – Colloidal blue staining of an SDS-PAGE gel was used to confirm equal loading of the protein samples. A wide range protein electrophoresis molecular weight marker (ColourBurst 8-220 kDa, Sigma) was run in the lane marked 'M' (sizes indicated). C – After selection with G418, protein extracted from Caco-2 cells containing the SIRT1 overexpressing construct or the negative control vector were separated by SDS-PAGE gel electrophoresis and SIRT1 expression was analysed by probing with an antibody to the SIRT1 protein followed by reprobing with an antibody to alpha tubulin as an additional loading control to the colloidal blue staining (sizes indicated). SIRT1 overexpression was analysed at two passages to check reliability of overexpression construct.*

As *SIRT1* overexpression appeared to have been lost quickly in the G418-selected cells over a few passages it was reasoned that transient transfection of the same SIRT1 expression construct may be a more reliable approach to achieve SIRT1 overexpression during cell experimentation given that time was not available for clonal selection following G418 treatment. To verify SIRT1 overexpression from the plasmid construct under conditions of transient transfection, Caco-2 cells were transfected with 2 µg SIRT1 expression construct (pCMV6-ENTRYSIRT1) or with 2 µg control vector without a *SIRT1* insert (pCMV6-Neo). After 72 hours cells were lysed and RNA and total cell lysate were extracted from parallel experiments as described previously (Section 3.4.1). RNA was used to assess *SIRT1* overexpression at the mRNA level by RT-PCR as described previously (Section 3.4.1). An increased intensity of the SIRT1-specific band from cells transfected with the *SIRT1* expression construct compared with the band generated from the control cells indicated that SIRT1 mRNA overexpression had been achieved (*Figure 3.8A*). SIRT1 overexpression at the mRNA level was also assessed by RT-qPCR (*Figure 3.8B*) as described previously (Section 3.4.1) confirming RT-PCR observations. Total cell lysate was used to confirm SIRT1 overexpression at the protein level by western blot (*Figure 3.8C*) as described previously (Section 3.4.1). This transfection model was continued as a means to overexpress SIRT1 within cells in further experiments.

Global methylation status of the extracted DNA from Caco-2 cells transfected with either the SIRT1 expression construct or with the control vector was assessed by LINE-1 COBRA and the LINE-1 pyrosequencing assay as described in Sections 1.5.2 and 2.6.2 and 1.5.3 and 2.6.8 respectively. SIRT1 overexpression alone had no apparent effect on LINE-1 methylation measured using either technique ($p > 0.05$) (*Figures 3.9A* and *Figure 3.9B*).

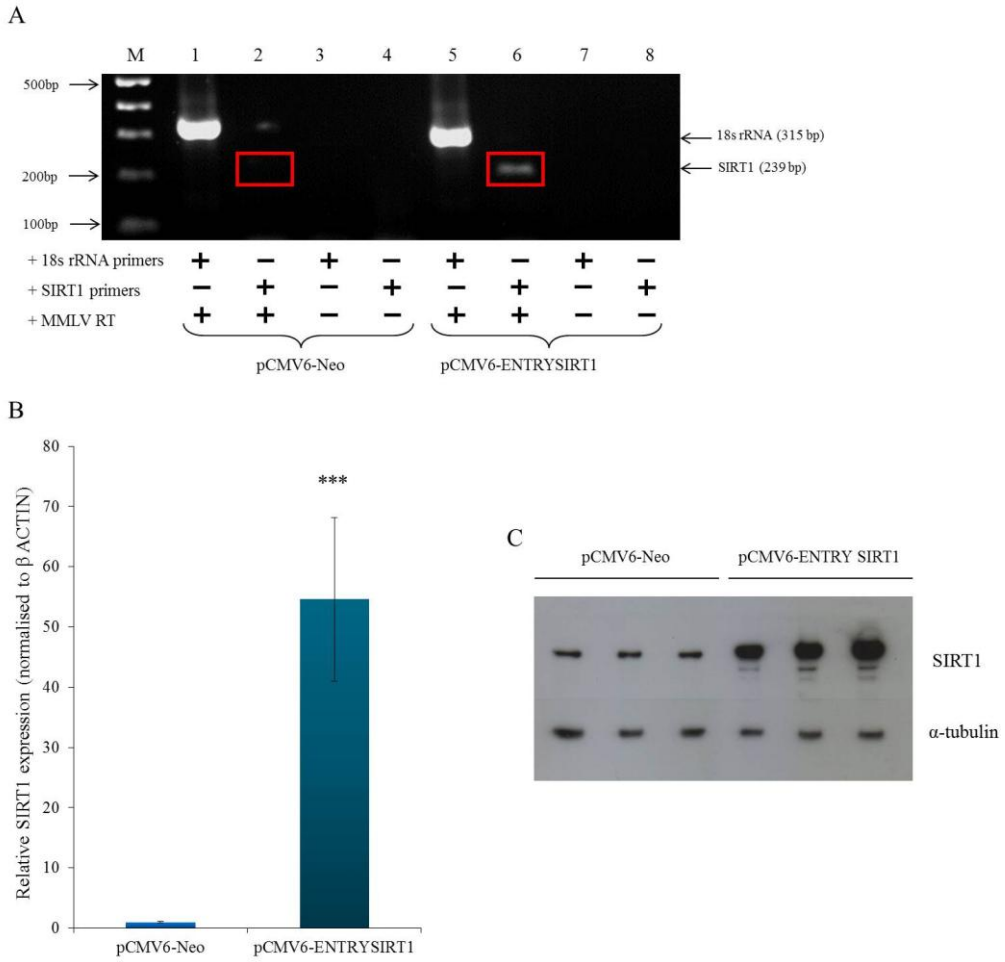

Figure 3.8. Confirmation of (A) SIRT1 mRNA overexpression in transiently transfected Caco-2 cells by RT-PCR and (B) RT-qPCR and (C) SIRT1 protein overexpression by western blot. *A – RT-PCR products were analysed by agarose gel electrophoresis. As indicated, lanes contained products generated from Caco-2 cells transiently transfected with either the control vector pCMV6-Neo or the SIRT1 expression construct pCMV6-ENTRY + SIRT1. Primer pairs (RTPCRSIRT1F, RTPCRSIRT1R, RTPCR18sF, RTPCR18sR – see Table 2.2B) and MMLVRT were included in the reaction as indicated. A comparison of band intensity between cells transfected with the SIRT1 expression construct and those transfected with the control vector indicate SIRT1 mRNA overexpression. B – RT products were analysed quantitatively for SIRT1 and β ACTIN mRNA expression using the Roche LightCycler® 480, LightCycler® 480 SYBR Green I Master and primer pairs (SIRT1 –SIRT1F and SIRT1R or 18s –18sF and 18sR – see Table 2.2D). Relative levels of SIRT1 expression were calculated in each sample using levels of SIRT1 expression normalised to β ACTIN. A comparison between SIRT1 mRNA expression levels between cells transfected with the SIRT1 expression construct pCMV6-ENTRYSIRT1 and those transfected with the control vector pCMV6-Neo indicates statistically significant SIRT1 mRNA overexpression; ***p < 0.0001 by Student's unpaired t-test. All data are mean ± SEM for n = 9. C – Protein extracted from Caco-2 cells transiently transfected with either the control vector pCMV6-Neo or the SIRT1 expression construct pCMV6-ENTRYSIRT1 was separated by SDS-PAGE gel electrophoresis. SIRT1 expression was analysed by probing with an antibody to the SIRT1 protein followed by reprobing with an antibody to alpha tubulin as a loading control. A comparison of band intensity between cells transfected with either the control vector pCMV6-Neo or the SIRT1 expression construct pCMV6-ENTRYSIRT1 indicate SIRT1 mRNA overexpression.*

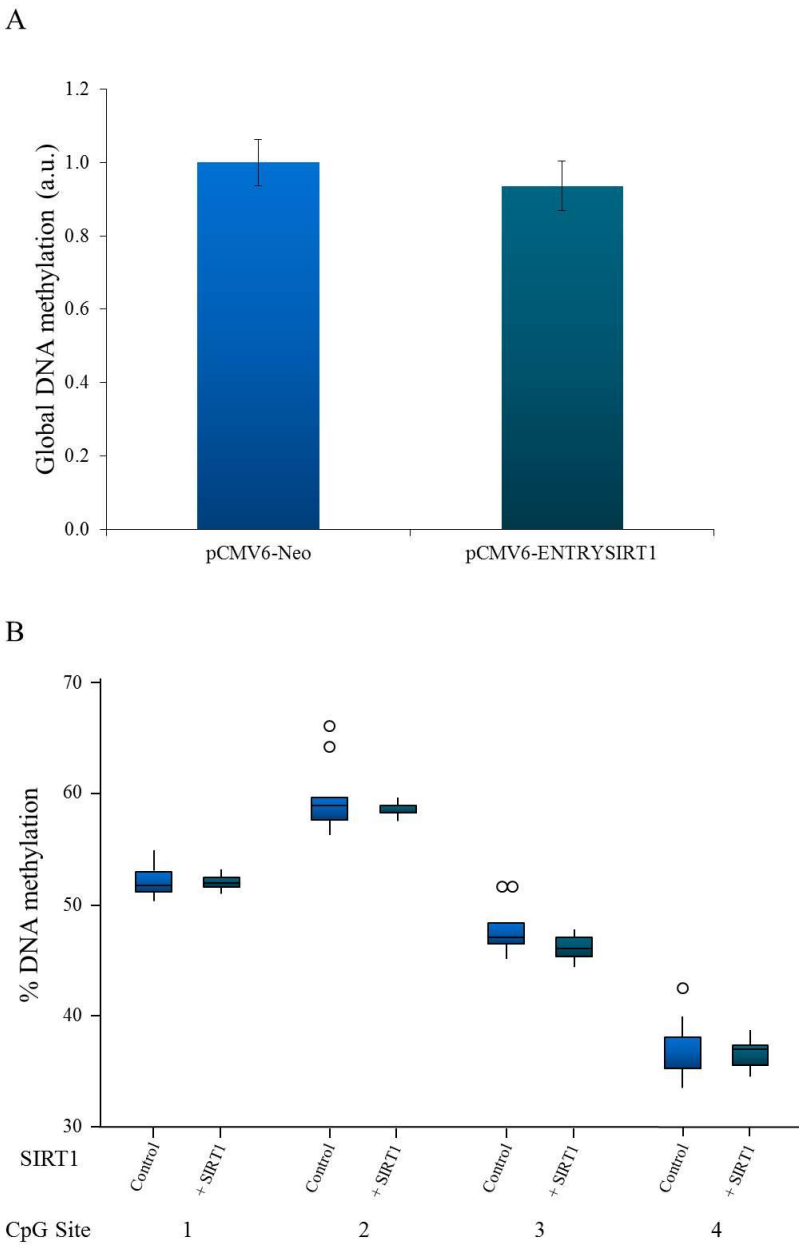

Figure 3.9. Effect on genomic DNA methylation of SIRT1 overexpression measured using (A) COBRA and (B) the LINE-1 pyrosequencing assay. *A – COBRA analysis showed no statistically signification difference between DNA methylation levels in Caco-2 cells transfected with SIRT1 expression construct pCMV6-ENTRYSIRT1 (teal) for 72 hours when compared with the control vector pCMV6-Neo (blue) ($p > 0.05$ by student's t-test). All data are mean ± SEM for $n = 21$. B – The LINE-1 pyrosequencing assay showed no statistically signification difference between DNA methylation levels in Caco-2 cells transfected with SIRT1 expression construct pCMV6-ENTRYSIRT1 (teal) for 72 hours when compared with the control vector pCMV6-Neo (blue) ($p > 0.05$ by student's t-test). All data are mean ± SEM for $n = 12$.*

3.5 Effects on genomic DNA methylation of treating Caco-2 cells with the polyphenols genistein, daidzein and resveratrol, in parallel with manipulation of SIRT1 expression levels

As previously discussed, substantial inter-individual variation in age-related DNA methylation may be due to different environmental and lifestyle factors, including diet (Issa, 2002). The identification of the plant polyphenol resveratrol as a possible SIRT1 activator (Howitz et al., 2003) and reported observations that the isoflavones genistein and daidzein can have effects on DNA methylation (Fang et al., 2005) identifies these dietary agents as potential mimetics of some aspects of the longevity response to DR. To test our hypothesis that effects on DNA methylation may contribute to the longevity effects of DR through histone acetylation mediated by SIRT1, and that these effects may be mimicked by plant polyphenolic compounds, Caco-2 cells were treated with the polyphenols in the presence and absence of SIRT1 manipulation and global DNA methylation was measured. Resveratrol (10 μM, Sigma), genistein (50 μM, LC Laboratories) and daidzein (50 μM, LC Laboratories) from 10 mM filter-sterilised stock solutions were prepared in DMSO (Section 2.3.5). For treatment with the polyphenols, the cell culture medium was substituted for a phenol red-free equivalent to that ensure any effects seen were due to the added polyphenols and not the phenol-red dye.

Caco-2 cells seeded 24 hours previously at 3.5 x 10^5 cells/well in a six well plate (area = 9.6 cm^2/well) transfected with SIRT1-targeted siRNA (Sections 2.3.2 and 3.4.1) or the SIRT1 overexpression construct (Sections 2.3.3 and 3.4.2) and relevant controls were treated after 24 hours with the polyphenols resveratrol (10 μM), genistein (50 μM), daidzein (50 μM) or a control of 0.1 % v/v DMSO and levels of DNA methylation were assessed by LINE-1 COBRA (Sections 1.5.2 and 2.6.2) and the LINE-1 pyrosequencing assay (Sections 1.5.3 and 2.6.8) after a further 72 hours.

An increase in DNA methylation was measured following treatment of Caco-2 cells, transfected with vector only (no manipulation of SIRT1 expression), with resveratrol (10μM); this increase in DNA methylation at the LINE-1 element was measured only using COBRA ($p < 0.001$) (*Figure 3.10A*) and was not detected by LINE-1 pyrosequencing ($p > 0.05$) (*Figure 3.11A*). When SIRT1 was overexpressed, the resveratrol-induced increase in LINE-1 methylation was abrogated. Genistein (50μM) and daidzein (50μM) had no effects against the control background (vector only) but in the presence of either compound and SIRT1 overexpression reduced LINE-1 methylation measured only using COBRA ($p < 0.01$ and $p < 0.05$ respectively) (*Figure 3.10B* and *Figure 3.10C*) and was not detected by LINE-1 pyrosequencing ($p > 0.05$) (*Figure 3.11B* and *Figure 3.11C*).

Resveratrol, genistein or daidzein had no effect on LINE-1 methylation under conditions of SIRT1 knockdown measured using either technique (*Figure 3.12* and *Figure 3.13*). Notably, the increase seen in LINE-1 methylation in response to resveratrol measured in cells transfected with the pCMV6-Neo

vector using COBRA (*Figure 3.10A* and L J Ions, L A Wakeling and D Ford; unpublished observations) was not observed when cells were transfected with the control siRNA.

.

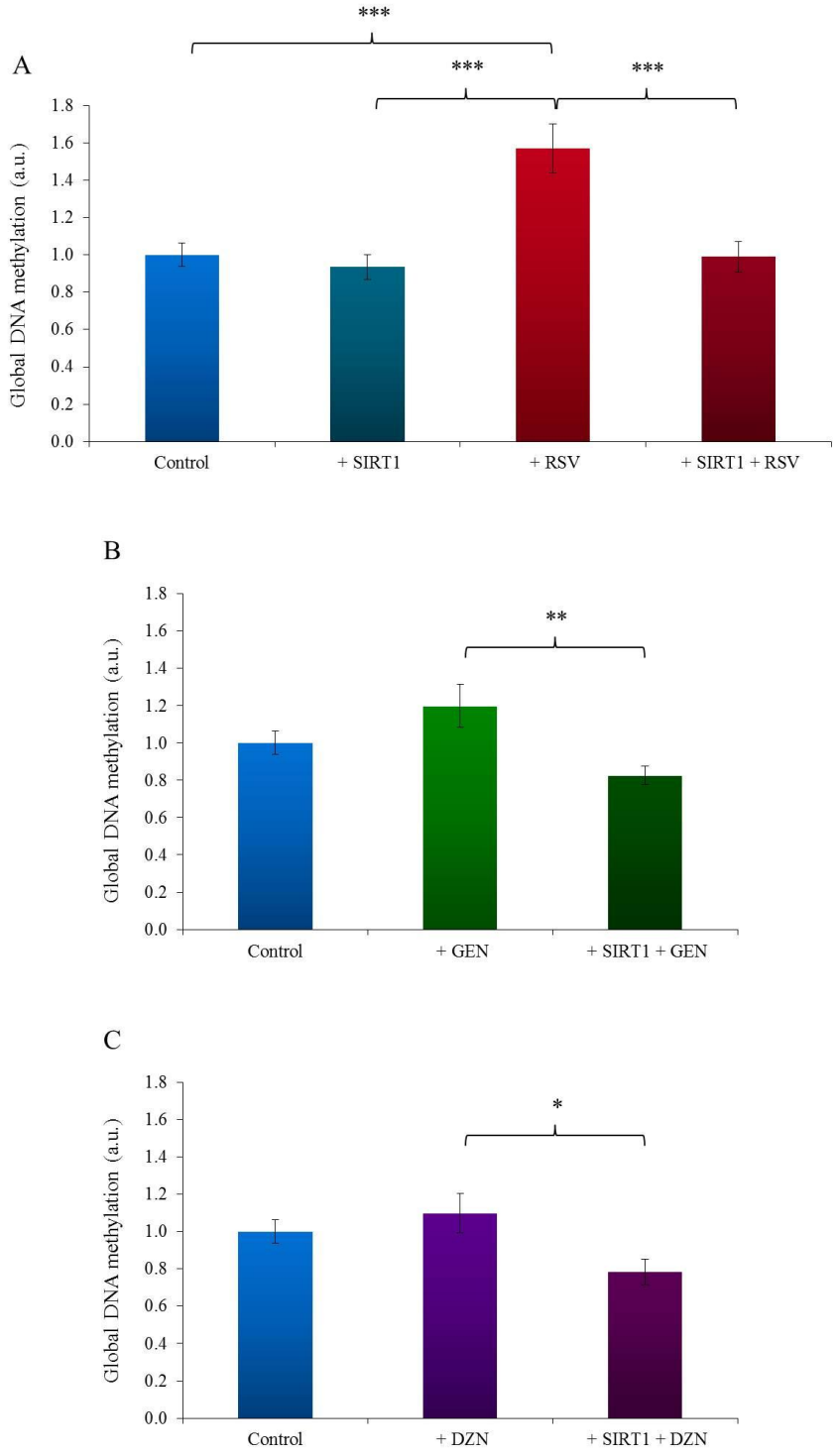

Figure 3.10 Effect on genomic DNA methylation of resveratrol, genistein or daidzein treatment in the presence of SIRT1 overexpression in Caco-2 cells using COBRA. *SIRT1 overexpression (teal) did not affect the measured level of LINE-1 DNA methylation compared to the control vector without a SIRT1 insert (blue), but treatment of cells with resveratrol resulted in a significant increase (A). Against a background of SIRT1 overexpression DNA methylation was reduced when Caco-2 cells were treated with (A) resveratrol (red) (RSV; 10 µM); ***p < 0.001 n = 21 by one way ANOVA then Bonferroni's multiple comparisons test, (B) genistein (green) (GEN; 50 µM); **p < 0.01 n = 9 by Student's unpaired t-test and (C) daidzein (purple) (DZN; 50 µM); *p < 0.05 by Student's unpaired t-test. All data are mean ± SEM for n = 9 or 21 as indicated.*

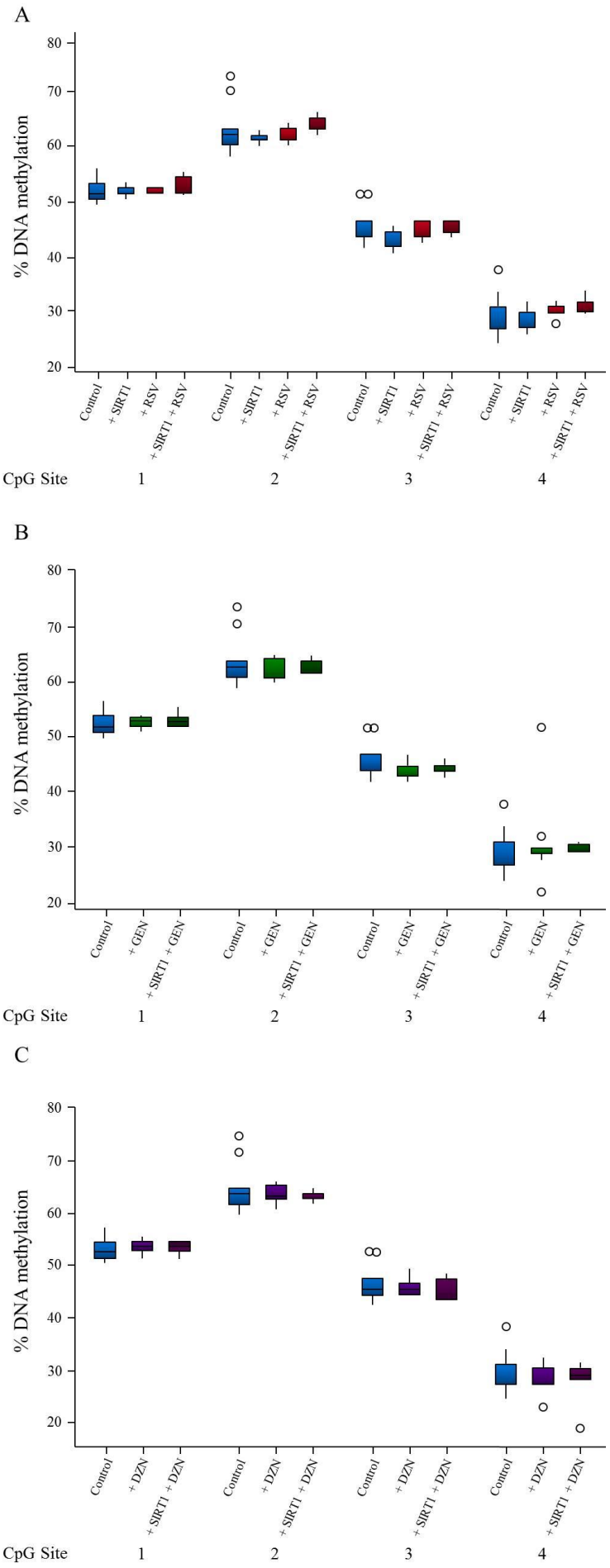
A
% DNA methylation
80
70
60
50
40
30
20
Control
+ SIRT1
+ RSV
+ SIRT1 + RSV
CpG Site
1
2
3
4
B
% DNA methylation
Control
+ GEN
+ SIRT1 + GEN
CpG Site
C
% DNA methylation
Control
+ DZN
+ SIRT1 + DZN
CpG Site

Figure 3.11 Effect on genomic DNA methylation of resveratrol, genistein or daidzein treatment in the presence of SIRT1 overexpression in Caco-2 cells using the LINE-1 pyrosequencing assay. *The LINE-1 pyrosequencing assay showed no statistical differences between DNA methylation levels in Caco-2 cells transfected with a SIRT1 overexpression construct (teal) and treated with (A) resveratrol (red) (RSV; 10 µM), (B) genistein (green) (GEN; 50 µM) or (C) daidzein (purple) (DZN; 50 µM) 24 h after transfection when compared to the control (blue) ($p > 0.05$ by one way ANOVA then Bonferroni's multiple comparisons test). All data are mean ± SEM for n = 12.*

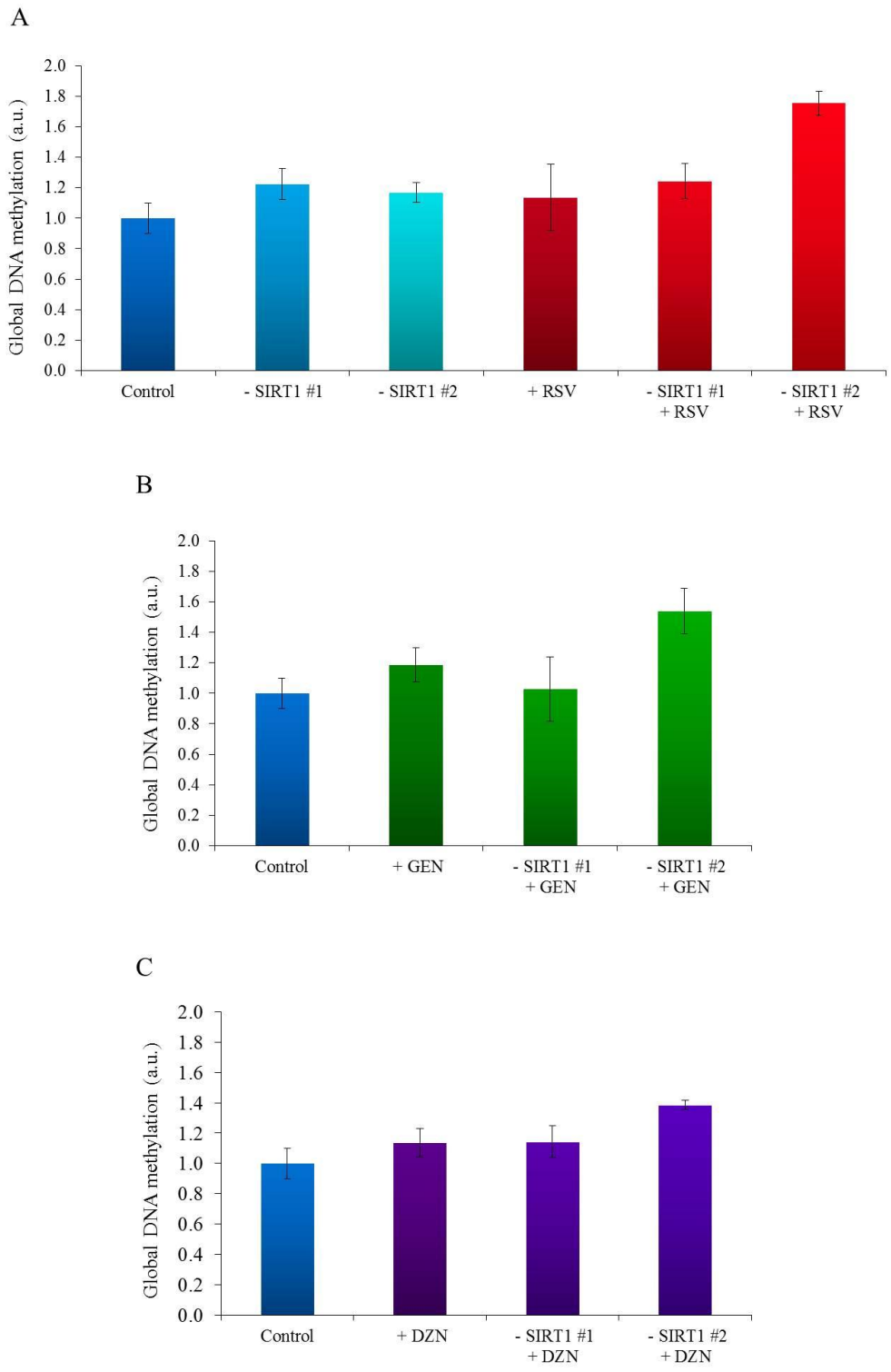

Figure 3.12 Effect on genomic DNA methylation of SIRT1-targeted siRNA knockdown and resveratrol, genistein or daidzein treatment in Caco-2 cells measured using COBRA. *No statistically significant differences were measured between DNA methylation levels in Caco-2 cells transfected cells transfected with an siRNA negative control (dark blue) or either of the two validated non-overlapping SIRT1 siRNAs (blue and light blue) and treated with (A) resveratrol (red) (RSV; 10 µM), (B) genistein (green) (GEN; 50 µM) or (C) daidzein (purple) (DZN; 50 µM) 24 h after transfection when compared with the control ($p > 0.05$ by one way ANOVA then Bonferroni's multiple comparisons test). All data are mean ± SEM for n = 3.*

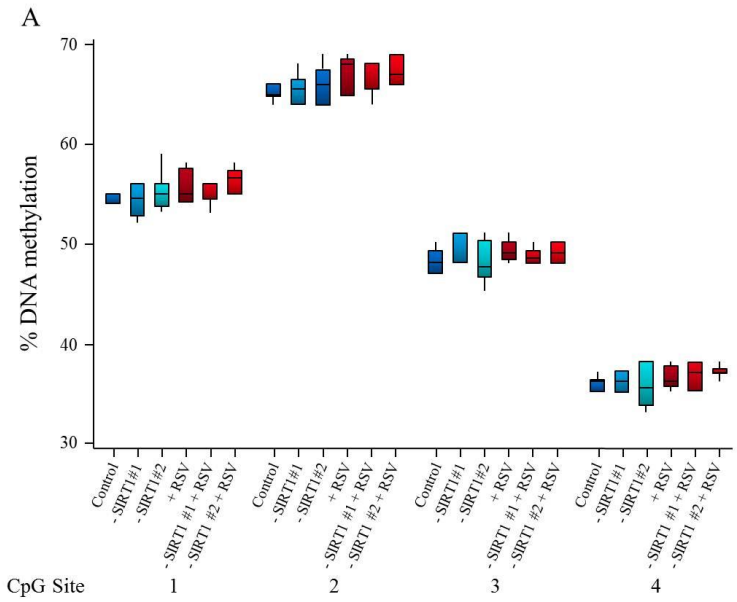
A
% DNA methylation
70
60
50
40
30
Control
- SIRT1#1
- SIRT1#2
+ RSV
- SIRT1 #1 + RSV
- SIRT1 #2 + RSV
CpG Site
1
2
3
4

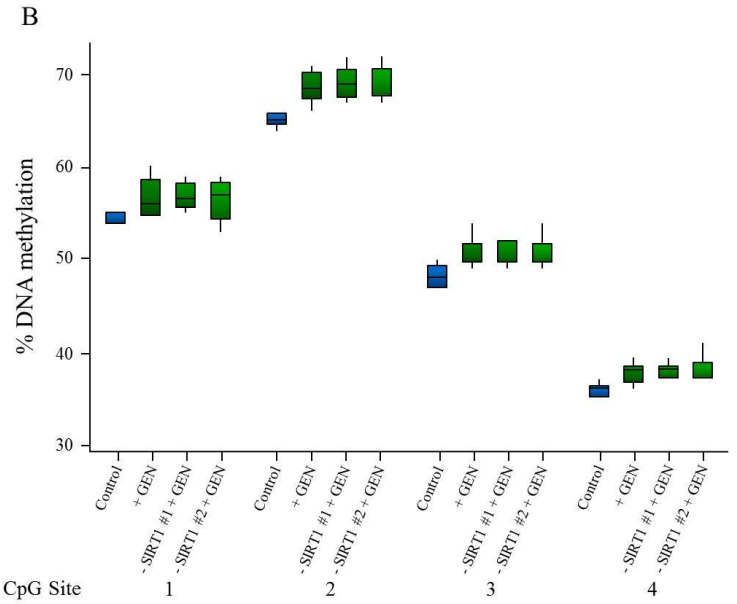
B
% DNA methylation
70
60
50
40
30
Control
+ GEN
- SIRT1 #1 + GEN
- SIRT1 #2 + GEN
CpG Site
1
2
3
4

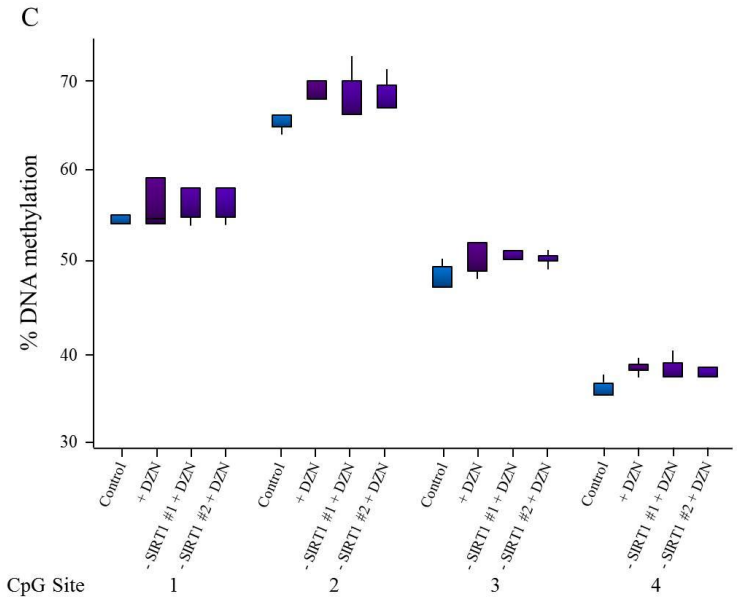
C
% DNA methylation
70
60
50
40
30
Control
+ DZN
- SIRT1 #1 + DZN
- SIRT1 #2 + DZN
CpG Site
1
2
3
4

Figure 3.13 Effect on genomic DNA methylation of SIRT1-targeted siRNA knockdown and resveratrol, genistein or daidzein treatment in Caco-2 cells measured using the LINE-1 pyrosequencing assay. *The LINE-1 pyrosequencing assay showed no statistical differences between DNA methylation levels in Caco-2 cells transfected with an siRNA negative control (dark blue) or either of the two validated non-overlapping SIRT1 siRNAs (blue and light blue) and treated with (A) resveratrol (red) (RSV; 10 µM), (B) genistein (green) (GEN; 50 µM), or (C) daidzein (purple) (DZN; 50 µM) 24 h after transfection when compared with the control ($p > 0.05$ by one way ANOVA then Bonferroni's multiple comparisons test). All data are mean ± SEM for $n = 3$.*

3.6 Discussion

The Caco-2 human epithelial colorectal adenocarcinoma cell line was selected from a screen of cell lines representing a range of tissues to investigate DNA methylation. The cell lines tested showed no significant difference in global DNA methylation levels as measured by the pyrosequencing of CpG sites within the LINE-1 retrotransposon and the LUMA assay. Enterocytes are the predominant cell type of the epithelial lining of the mucosa of the intestine and their morphological and physiological properties are exhibited by the Caco-2 cell line, which therefore may provide a suitable model for the intestinal response to DR or, in the case of this study, potential dietary mimetics of DR whose first encounter upon consumption would be with the intestinal cell wall. All cell lines were from tumour cell populations and so due to well documented changes in DNA methylation in cancerous tissue perhaps did not show a true representation of DNA methylation levels of the corresponding tissue; indeed this factor was also the main limitation associated with using the Caco-2 cell line.

Investigating the effects of manipulating SIRT1, through blocking the enzymatic activity of the SIRT1 protein with Sirtinol, on levels of global DNA methylation as measured through the repetitive LINE-1 surrogate marker, revealed no significant response. Interpretation of the result of this experiment is limited, however, by our inability to measure directly if the Sirtinol treatment was effective in reducing SIRT1 activity. Attempts to generate a Caco-2 cell line stably overexpressing SIRT1 failed. Depending upon the integration point of the SIRT1 transgene a mixed population of different levels of SIRT1 expression would arise within the selected cell line. The loss of SIRT1 overexpression after several rounds of passage may indicate that a shift had occurred towards those cells in which the SIRT1 transgene, due to the location of integration, was expressed at a lower level. A possible approach to overcome this limitation would be the selection of clonal cell lines after transfection, measuring the levels of SIRT1 expression within these cell lines and selecting those expressing SIRT1 at the highest levels. However time constraints did not permit this approach. Manipulating the levels of SIRT1 through transient expression from an overexpression plasmid construct and siRNA mediated knockdown had no significant effect on levels of LINE-1 DNA methylation. A publication identifying sites in the genome to which SIRT1 binds (Oberdoerffer et al., 2008) did not reveal the LINE-1 element as a site of SIRT1 binding. Perhaps therefore the LINE-1 repetitive element as a measure of global methylation is not an appropriate site at which to measure effects of SIRT1 on DNA methylation. A recent report investigating the role of SIRT1 in telomere maintenance and repair in mice deficient or overexpressing SIRT1 measured DNA methylation in response to SIRT1 manipulation. SIRT1 manipulation did not have an effect on global DNA methylation when measured at the B1-SINE1 element using COBRA as a surrogate marker of global DNA methylation (Palacios et al., 2010). Overall, therefore, our own observations and those of other researchers provide no evidence that SIRT1 alone can affect global DNA methylation, but a definitive conclusion cannot yet be reached as a result of experimental limitations.

The effects of the polyphenols resveratrol, genistein and daidzein, alone or in combination with SIRT1 manipulation, on DNA methylation in the Caco-2 cell line were measured by COBRA and the LINE-1 pyrosequencing assay. Caco-2 cells were treated with resveratrol, genistein or daidzein with the aim to establish whether the plant polyphenols played a role in mimicking some of the beneficial effects of DR, potentially through SIRT1 and/or changes in DNA methylation levels. In Caco-2 cells transfected with an empty vector, resveratrol (10μM, 48 hours) caused an increase in DNA methylation at the LINE-1 element. In Caco-2 cells treated with resveratrol (10 μM, 48 hours), genistein or daidzein (50 μM, 48 hours) a reduction in LINE-1 DNA methylation in response to SIRT1 overexpression was measured using COBRA. However, measurement using pyrosequencing indicated that LINE-1 methylation was unaffected by all of these treatments. Copies of the LINE-1 retrotransposon throughout the genome show sequence variability (Khan et al., 2006). Different primer pairs were used for the two assays, so a possible explanation for the discordance between measurements using the two methods is, therefore, preferential primer binding to different sequences that are differentially affected by the polyphenols tested. The findings demonstrate that choice of assay for measuring DNA methylation may have an impact on the conclusions drawn and highlight the potential pitfalls of relying on a single approach to detect the fairly subtle effects typical of the actions of dietary components on LINE-1 methylation.

Overall, these observations support a general view that SIRT1 can influence DNA methylation in the presence of the dietary polyphenols tested and at elevated, but not reduced, levels of SIRT1 expression in Caco-2 cells, revealing complex interactions. Moreover, detection of such effects is assay-dependent. As previously discussed, it is possible that other genome regions may be better markers of effects of SIRT1 on global DNA methylation. In addition, measurement of gene-specific DNA methylation may be required to identify sites modified by SIRT1, such as investigated in following chapters (Chapter 5 and Chapter 6).

4 An investigation of factors that may affect SIRT1 expression

4.1 Outline

In the previous chapter effects of the manipulation of *SIRT1* activity and expression on global DNA methylation were investigated. *In vivo*, effects (for example of DR) on *SIRT1* may also be at both the level of enzyme activation/inhibition and/or at the level of gene expression. We thus sought to improve understanding of how *SIRT1* is regulated at both levels.

We hypothesise that some effects of DR may be mimicked by dietary polyphenols. One potential mechanism for such effects is through these compounds affecting *SIRT1* gene transcription. Such effects may, potentially, modify the effects of SIRT1-polyphenol interactions on DNA methylation (and of other SIRT1-mediated responses to DR).

It is known that the methylation status of a gene promoter region can affect gene expression. Proposed underlying mechanisms include the direct physical prevention of transcription factor binding by the methylated CpG site or by proteins that bind to methylated CpG sites (Tate and Bird, 1993). Our overarching hypothesis proposes that SIRT1 affects DNA methylation through histone deacetylation activity, resulting in altered expression of downstream gene targets. We questioned if the *SIRT1* gene was subject to regulation by promoter methylation, which may potentially affect levels of expression with increased age and/or be a mechanism through which other factors – such as dietary compounds or indeed levels of *SIRT1* activity itself – may modulate expression.

It is well established that methylation patterns across the genome change with ageing. The majority of earlier published work suggested there is an overall decrease in methylation with age (Wilson et al., 1987; Vanyushin et al., 1973), but emerging evidence reveals site-specific increases, as well as reductions, with age (Maegawa et al., 2010; Rakyan et al., 2010; Teschendorff et al., 2010; Christensen et al., 2009; Kwabi-Addo et al., 2007). Regardless of the direction of DNA methylation change, an effect on the expression of the affected gene is possible. It was of relevance in the context of our overarching hypothesis, therefore, to investigate if the expression of SIRT1 itself was changed with age.

We thus studied the transcriptional activity of *SIRT1* in response to polyphenols, changes in promoter methylation and investigated any change in expression with age.

Furthermore, with a view to studying regulation of SIRT1 at the level of enzyme activation/inhibition, and also to confirm functional consequences of changes in expression in our experimental cell line

models, we attempted to employ a commercially available assay to measure SIRT1 deacetylation activity.

4.2 Effects on SIRT1 transcriptional activity of polyphenols resveratrol, genistein and daidzein

To test the effects of polyphenols on the *SIRT1* promoter a *SIRT1* promoter-reporter plasmid construct was generated comprising the region –1011 to +53 (relative to the start of transcription) of the human *SIRT1* gene upstream of the β-galactosidase reporter gene in the plasmid pBlue-TOPO (Invitrogen). The 1064 bp region of the *SIRT1* promoter (*Figure 4.1*) was PCR amplified (Section 2.5.1.1) and subcloned into the pBlue-TOPO® vector (Invitrogen) (Section 2.2.1) to produce this promoter reporter plasmid construct. Amplification and subcloning of the required sequence was verified by sequencing (*Figure 4.2*).

A GAPDH promoter-reporter plasmid construct comprising the region –517 to +67 (relative to the start of transcription) of the human GAPDH gene upstream of the β-galactosidase reporter gene in the plasmid pBlue-TOPO® was used as a control. The 584 bp region of the GAPDH promoter (*Figure 4.3*) was used to produce a promoter reporter plasmid construct as above. Amplification and subcloning of the required sequencing was verified by sequencing (*Figure 4.4*).

A transcriptionally inert pBlue-TOPO® construct containing a segment of DNA sequence known to have no promoter activity was used as a negative control (J Tyson, Newcastle University, Personal communication).

Caco-2 cells seeded 24 hours previously at 3.5 x 10^5 cells/well in a six well plate (area = 9.6 cm^2/well) were transfected transiently with the SIRT1 promoter-reporter plasmid construct or the GAPDH control. After 24 hours cells were treated with the polyphenols resveratrol (10 μM), genistein (50 μM), daidzein (50 μM) or a control of 0.1 % v/v DMSO (vehicle only, at the same concentration as for the addition of the test polyphenols) and reporter gene activity was measured after a further 48 hours. Total cell lysate was used to measure reporter gene activity (β-galactosidase), as described in Section 2.8.2. Total cell lysate was extracted (Section 2.8.2.1) and protein concentration determined by Bradford assay (Section 2.8.1.4). Twenty microlitres of total cell lysate was incubated at 37 ºC with 130 μl 1.2 ng/ml chlorophenol red- β-D-galactopyranoside (Section 2.8.2.3). Reporter gene activity was expressed as nmoles of chlorophenol red formed per minute per mg of total protein and normalised to the reporter gene activity measured in Caco-2 cells grown in control medium.

Resveratrol and genistein, but not daidzein, had an effect on *SIRT1* promoter activity in this system and reduced reporter gene expression (*Figure 4.5A*) ($p < 0.05$ and $p < 0.001$ respectively). However,

though not significant, resveratrol and genistein reduced reporter gene expression also from the *GAPDH* promoter (*Figure 4.5B*) ($p > 0.05$), indicating a likely effect on gene transcription that is not specific to *SIRT1*. When measures of reporter gene activity driven by the SIRT1 promoter under the different conditions were normalised relative to the measured activity from the GAPDH promoter no differences between treatments were observed (*Figure 4.5C*) ($p > 0.05$). Thus, we find no evidence for effects of the polyphenols tested on *SIRT1* gene transcription specifically.

SIRT1 Sequence

Chr10+: 69643377 - 69644576

-1050 GAGTCACAGT GTGCCAGAAT TTCAGGGAGA GAGGAAAGTG GAAGGGCTTT

-1000 CCACTAAGCC TTTTGAACTA CTAGGTACCC CTCGTTTTAC ATCTGGTTAT

-950 CTCATTTAAA TCTATGACGT TTTAAAATAC TTATTACCAT TTAAGACATG

-900 AGAAAAATTA AGTTTAGAAA CGGCTAGATA GCTCACGCTA GAAAGGAAGG

-850 ACTCCAAATT TTAACCAAGG GCAGATGTGC ATGGAGGCCA AGTCATTTCC

-800 TTCCCATGCT CTCATACTGA CCCAACAAAC CCATTCTGCA CGTGAGAAAA

-750 CTGAGGCCCG GAGGAGGGAA TTCACACACG TTTGAAGCCA AGCTGGGGCC

-700 AGAAAGTAGA TCGGCTGATC TCCAAACCTC CACGTCAAAG GTCTTCCCAG

-650 GAGGACATAT GCCTTCAAGG ATTTTACAAT GTATACCACC CTACAAGTGA

-600 TGGGAGAGAG GGGAAAAAAG CAACCGACTA AGGAGAAAAG CAAGGAGCAG

-550 AAAAAGGAGC AAAAGAGGAG CTGTCAGAAC GGTGTGAGGA GAGTGGGAAA

-500 GGAGCCGCCT CCTTTTGCCT CTCTTCCTAC TTATTAACAA AACAGAACGA

-450 CTATCCAACG TATTTCAGGG AGCTAAGTCT TAGCCAGCTT CAGCTGTGTT

-400 TTAACCCTTA GCTAAATATA GACAAGGCTA AGGCAGGCCA GGTGTACACT

-350 TCAGGAAGAC GTGGAAATTC CCAGGGCGGA CCAAAACTTG AGCTGTTCCG

-300 GCGGTAGTGA TTTGAGGTCA GTTTGAAAGA GAAGTTGAGA AAGCGGCCGA

-250 GGGGCGAATT TGGCTGCACT ACACGCTCGC CACAAAGAGG AAGGGCCGCC

-200 GGCCGCCGGG GCCGAGTGCG CTTCCAGCCC AGGCGGAGCG GTAGACGCAA

-150 CAGCCTCCGC CCGCCACGTG ACCCGTAGTG TTGTGGTCTG GCCCGCGTGG

-100 GTGGCGGGAG CGCCGAGAGG GCGGGGGCGG CGATGGGGCG GGTCACGTGA

-50 TGGGGTTTAA ATCTCCCGCA GCCGGAGCCG CGGGGGCGCC AGTGCCGCGC

+1 gtcgagcggg agcagaggag gcgagggagg agggccagag aggcagttgg

+50 aagatggcgg acgaggcggc cctcgccctt cagcccggcg gctccccctc

+100 ggcggcgggg gccgacaggg aggccgcgtc gtcccccgcc ggggagccgc

+150 tccgcaagag gccgcggaga gatggtcccg gcctcgagcg gagcccgggc

Figure 4.1. The SIRT1 promoter region sequence. *The -1050 to +100 bp SIRT1 promoter sequence taken from the human genome sequence is shown. The genomic region upstream of the start of transcription as identified by alignment of the transcript sequence NM_02238 (lowercase) is represented in uppercase letters. Primers were designed for amplification by PCR of a 1064 bp region of the SIRT1 sequence (SIRT1PromoterF - light red and SIRT1PromoterR - dark red) to generate a PCR product to sub-clone into the pBlue-TOPO® reporter vector. Primers and annealing temperatures are given in Table 2.2B.*

Aligned SIRT1 Insert Sequence in pBLUE-TOPO

Figure 4.2. The SIRT1 promoter sequence inserted into pBlue-TOPO® and related primers. *The region of the SIRT1 promoter sequence (non-italicised uppercase and lowercase) inserted into the pBlue-TOPO® vector (italicised uppercase) is shown aligned to the original genomic sequence. Primers were designed to sequence the SIRT1 region in pBlue-TOPO® (SIRT1PromoterF - light red and SIRT1PromoterR - dark red). A reverse primer was designed for PCR to the pBlueTOPO vector (pBlueTOPOR – dark red; italicised uppercase) sequence for sequence verification. Primers and annealing temperatures are given in Table 2.2B.*

GAPDH Sequence

Chr12+:6642657 - 6643957

-1000 GGAGGGACTT CCGCCCTCAC GTCCCGCTCT TCGCCCCAGG CTGGATGGAA

-950 TGAAAGGCAC ACTGTCTCTC TCCCTAGGCA GCACAGCCCA CAGGTTTCCA

-900 GGAGTGCCTT TGTGGGAGGC CTCTGGGCCC CCACCAGCCA TCCTGTCCTC

-850 CGCCTGGGGC CCCAGCCCGG AGAGAGCCGC TGGTGCACAC AGGGCCGGGA

-800 TTGTCTGCCC TAATTATCAG GTCCAGGCTA CAGGGCTGCA GGACATCGTG

-750 ACCTTCCGTG CAGAAACCTC CCCCTCCCCC TCAAGCCGCC TCCCGAGCCT

-700 CCTTCCTCTC CAGGCCCCCA GTGCCCAGTG CCCAGTGCCC AGCCCAGGCC

-650 TCGGTCCCAG AGATGCCAGG AGCCAGGAGA TGGGGAGGGG GAAGTGGGGG

-600 CTGGGAAGGA ACCACGGGCC CCCGCCCGAG GCCCATGGGC CCCTCCTAGG

-550 CCTTTGCCTG AGCAGTCCGG TGTCACTACC GCA**GAGCCTC GAGGAGAAGT**

-500 **TCC**CCAACTT TCCCGCCTCT CAGCCTTTGA AAGAAAGAAA GGGGAGGGGG

-450 CAGGCCGCGT GCAGCCGCGA GCGGTGCTGG GCTCCGGCTC CAATTCCCCA

-400 TCTCAGTCGT TCCCAAAGTC CTCCTGTTTC ATCCAAGCGT GTAAGGGTCC

-350 CCGTCCTTGA CTCCCTAGTG TCCTGCTGCC CACAGTCCAG TCCTGGGAAC

-300 CAGCACCGAT CACCTCCCAT CGGGCCAATC TCAGTCCCTT CCCCCCTACG

-250 TCGGGGCCCA CACGCTCGGT GCGTGCCCAG TTGAACCAGG CGGCTGCGGA

-150 AAAAAAAAAG CGGGGAGAAA GTAGGGCCCG GCTACTAGCG GTTTTACGGG

-100 CGCACGTAGC TCAGGCCTCA AGACCTTGGG CTGGGACTGG CTGAGCCTGG

-50 CGGGAGGCGG GGTCCGAGTC ACCGCCTGCC GCCGCGCCCC CGGTTTCTAT

+1 aaattgagcc cgcagcctcc cgcttcgctc tctgctcctc ctgttcg**aca**

+50 **gtcagccgca tcttctt**ttg cgtcgccagg tgaagacggg cggagagaaa

+100 cccgggaggc tagggacggc ctgaaggcgg caggggcggg cgcaggccgg

+150 atgtgttcgc gccgctgcgg ggtgggcccg ggcggcctcc gcattgcagg

+200 ggcgggcgga ggacgtgatg cggcgcgggc tgggcatgga ggcctggtgg

+250 gggaggggag gggaggcgtg tgtgtcggcc ggggccacta ggcgctcact

+300 gttctctccc tccgcgcagc cgagccacat cgctcagaca cc**atg**gggaa

Figure 4.3 The GAPDH promoter region sequence. *The -517* to +67 *bp GAPDH promoter sequence taken from the human genome sequence is shown. The genomic region upstream of the start of transcription as identified by alignment of the transcript sequence NM_002046 (lowercase) is represented in uppercase letters. Primers were designed for amplification by PCR of a 584 bp region of the GAPDH sequence (GAPDHPrmomoterF - light red and GAPDHPromoterR - dark red) to generate a PCR product to sub-clone into the pBlue-TOPO® reporter vector. Primers and annealing temperatures are given in Table 2.2B.*

Aligned GAPDH Insert Sequence in pBlue-TOPO

```
-550  CCTTTGCCTG AGCAGTCCGG TGTCACTACC GCAGAGCCTC GAGGAGAAGT
                                        ||||||| ||||||||||
      GGATCCCTAG TCCAGTGTGG TGGAATTGCC CTTGAGCCTC GAGGAGAAGT

-500  TCCCCAACTT TCCCGCCTCT CAGCCTTTGA AAGAAAGAAA GGGGAGGGGG
      |||||||||| |||||||||| |||||||||| |||||||||| ||||||||||
      TCCCCAACTT TCCCGCCTCT CAGCCTTTGA AAGAAAGAAA GGGGAGGGGG

-450  CAGGCCGCGT GCAGCCGCGA GCGGTGCTGG GCTCCGGCTC CAATTCCCCA
      |||||||||| |||||||||| |||||||||| |||||||||| ||||||||||
      CAGGCCGCGT GCAGCCGCGA GCGGTGCTGG GCTCCGGCTC CAATTCCCCA

-400  TCTCAGTCGT TCCCAAAGTC CTCCTGTTTC ATCCAAGCGT GTAAGGGTCC
      |||||||||| |||||||||| |||||||||| |||||||||| ||||||||||
      TCTCAGTCGT TCCCAAAGTC CTCCTGTTTC ATCCAAGCGT GTAAGGGTCC

-350  CCGTCCTTGA CTCCCTAGTG TCCTGCTGCC CACAGTCCAG TCCTGGGAAC
      |||||||||| |||||||||| |||||||||| |||||||||| ||||||||||
      CCGTCCTTGA CTCCCTAGTG TCCTGCTGCC CACAGTCCAG TCCTGGGAAC

-300  CAGCACCGAT CACCTCCCAT CGGGCCAATC TCAGTCCCTT CCCCCCTACG
      |||||||||| |||||||||| |||||||||| |||||||||| ||||||||||
      CAGCACCGAT CACCTCCCAT CGGGCCAATC TCAGTCCCTT CCCCCCTACG

-250  TCGGGGCCCA CACGCTCGGT GCGTGCCCAG TTGAACCAGG CGGCTGCGGA
      |||||||||| |||||||||| |||||||||| |||||||||| ||||||||||
      TCGGGGCCCA CACGCTCGGT GCGTGCCCAG TTGAACCAGG CGGCTGCGGA

-150  AAAAAAAAAG CGGGGAGAAA GTAGGGCCCG GCTACTAGCG GTTTTACGGG
      |||||||||| |||||||||| |||||||||| |||||||||| ||||||||||
      AAAAAAAAAG CGGGGAGAAA GTAGGGCCCG GCTACTAGCG GTTTTACGGG

-100  CGCACGTAGC TCAGGCCTCA AGACCTTGGG CTGGGACTGG CTGAGCCTGG
      |||||||||| |||||||||| |||||||||| |||||||||| ||||||||||
      CGCACGTAGC TCAGGCCTCA AGACCTTGGG CTGGGACTGG CTGAGCCTGG

-50   CGGGAGGCGG GGTCCGAGTC ACCGCCTGCC GCCGCGCCCC CGGTTTCTAT
      |||||||||| |||||||||| |||||||||| |||||||||| ||||||||||
      CGGGAGGCGG GGTCCGAGTC ACCGCCTGCC GCCGCGCCCC CGGTTTCTAT

+1    aaattgagcc cgcagcctcc cgcttcgctc tctgctcctc ctgttcgaca
      |||||||||| |||||||||| |||||||||| |||||||||| ||||||||||
      aaattgagcc cgcagcctcc cgcttcgctc tctgctcctc ctgttcgaca

+50   gtcagccgca tcttcttttg cgtcgccagg tgaagacggg cggagagaaa
      |||||||||| |||||||
      gtcagccgca tcttcttAAG GGCAATTCTG CAGAAAGCTT ACCATGGGGG

+100  cccgggaggc tagggacggc ctgaaggcgg caggggcggg cgcaggccgg

      GTTCTCATCA TCATCATCAT CATGGTATGG CTAGCATGAC TGGTGGACAG
```

Figure 4.4 The GAPDH promoter sequence inserted into pBlue-TOPO® and related primers. *The region of the GAPDH promoter sequence (non-italicised uppercase and lowercase) inserted into the pBlue-TOPO® vector (italicised uppercase) is shown aligned to the original genomic sequence. Primers were designed to sequence the GAPDH region in pBlue-TOPO® (GAPDHPromoterF - light red and GAPDHPromoterR - dark red). A reverse primer was designed for PCR to the pBlueTOPO vector (pBlueTOPOR – dark red; italicised uppercase; part shown) sequence for sequence verification. Primers and annealing temperatures are given in Table 2.2B.*

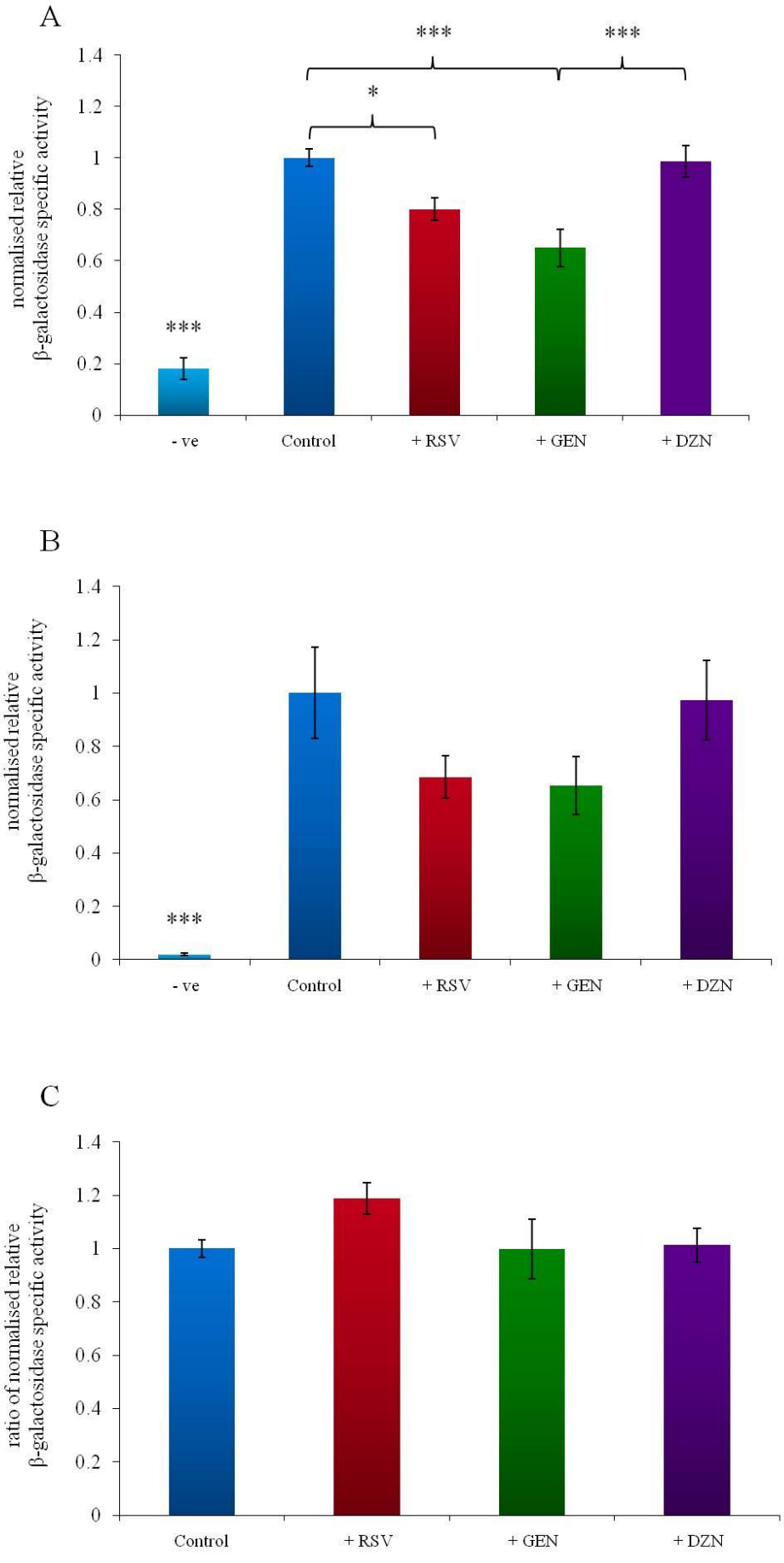
A
***
***
*
normalised relative β-galactosidase specific activity
1.4
1.2
1
0.8
0.6
0.4
0.2
0
***
- ve
Control
+ RSV
+ GEN
+ DZN
B
normalised relative β-galactosidase specific activity
1.4
1.2
1
0.8
0.6
0.4
0.2
0
***
- ve
Control
+ RSV
+ GEN
+ DZN
C
ratio of normalised relative β-galactosidase specific activity
1.4
1.2
1
0.8
0.6
0.4
0.2
0
Control
+ RSV
+ GEN
+ DZN

Figure 4.5. Effect of dietary polyphenols on activity of the human SIRT1 promoter. *Activity of the β-galactosidase reporter gene was measured 72 h after transfection with a promoter-reporter construct comprising either (A) the human SIRT1 promoter region (–1011 to +34, relative to the start of transcription) or (B) the human GAPDH promoter region (-517 to +67, relative to the start of transcription) upstream of the β-galactosidase reporter gene in the plasmid pBlue-TOPO (Invitrogen) or with a corresponding negative control construct ('-ve'), without a promoter sequence insert. Treatment with resveratrol (RSV; 10 µM), genistein (GEN; 50 µM) or daidzein (DZN; 50 µM) was 24 h after transfection. Control cells ('Control') were treated with DMSO vehicle only. All data are mean ± SEM for n = 12-18 and are expressed as a ratio of the protein concentration of the cell lysate, normalised to the control condition. (C) Activity of the SIRT1 promoter region normalised to the activity of the GAPDH promoter region. *p < 0.05, ***p < 0.001 by one way ANOVA followed by Bonferroni's multiple comparisons test.*

4.3 Effects of promoter methylation on SIRT1 transcription

To investigate if levels of SIRT1 expression can themselves be modulated by (potentially SIRT1-mediated) DNA methylation, Caco-2 cells were transfected with a methylated and unmethylated *SIRT1* promoter reporter construct; comprising the *SIRT1* promoter upstream of the *LacZ* gene. An equivalent construct containing the *SLC30A5* (zinc transporter) promoter was used as a positive control; previous work in the laboratory had established that *SLC30A5* promoter activity is repressed by methylation (L J Coneyworth, Newcastle University, PhD Thesis).

The *SIRT1* promoter-reporter plasmid construct previously generated (Section 4.2) comprising the region –1011 to +53 (relative to the start of transcription) of the human *SIRT1* gene upstream of the β-galactosidase reporter gene in the plasmid pBlue-TOPO was used to assess the effect of methylation on *SIRT1* transcription. The *SLC30A5* promoter reporter plasmid construct comprising the region –1000 to +100 (relative to the start of transcription) of the human *SLC30A5* gene (*Figure 4.6*) was used to produce a positive control promoter reporter plasmid construct (*Figure 4.7*) as described previously (Section 4.2). As before, a transcriptionally inert pBlue-TOPO® construct was used as a negative control.

For both *SIRT1* and *SLC30A5* unmethylated promoter-reporter constructs were generated by the propagation of the plasmid through the methylase deficient K12 ER2925 *E. coli* strain as described in Section 2.2.3 and plasmid DNA was prepared as described in Section 2.2.2. Methylated *SIRT1* and *SLC30A5* promoter-reporter constructs were generated through *in vitro* methylation of 2 µg unmethylated plasmid DNA by *SssI* methylase (New England Biolabs) as described in Section 2.2.4. As a control, to ensure that any changes in promoter activity were not due to the enzymatic methylation process, 'mock' methylation reactions were set up and were identical to *in vitro* methylation reactions except the *SssI* methylase was omitted.

Caco-2 cells seeded 24 hours previously at 3.5×10^5 cells/well in a six well plate (area = 9.6 cm^2/well) were transfected transiently with either the unmethylated, 'mock' methylated or methylated *SIRT1* and *SLC30A5* promoter-reporter plasmid construct or the negative control. After 48 hours cells were lysed and reporter gene (β-galactosidase) activity was measured as described in Section 2.8.2. Total cell lysate was extracted (Section 2.8.2.1) and protein concentration was determined by Bradford assay (Section 2.8.1.4). Twenty microlitres of total cell lysate was incubated at 37 ºC with 130 µl 1.2 ng/ml chlorophenol red-β-D-galactopyranoside (Section 2.8.2.3). Reporter gene activity was expressed as nmoles of chlorophenol red formed per minute per mg of total protein.

SLC30A5 Promoter Sequence

Chr5+:68388882 - 68390031

-1000 CTTTAGAAAT CTGGAAATTG CCTTTAGGTT CCCTTAGGAG TAGGAGAGAA

-950 **GGCCATGAAG TTTCGCACGT G**GTCACTCCT AGAAAATTGC CCTGGGATAG

-900 TTTGCTGAGG AGGCAAATTT TGGTCAATAC TAGTTTCTCC TCTCCAAAGT

-850 CCATCAAAGG CATTGTTCAA AAGAAATGGC CGTACCACTA TTTGTAATTG

-800 ATTCTCTACA GCTTCAAAAA TAGTTATCTC TGGTTGGGGG AAGGGCACGT

-750 GAACTTTTAA GACTTCGGGC CTTCTCATCA CAAAAATGAT CCATACTCAC

-700 AAAAACTTAG AGGCAGAGGG TATGTTAACC TAGATTAAGA ATCTCTAGGC

-650 CGAGTGCGGT GGCTCACTCC TGTAATCGCA GCACTTTGGG AGGCCGAGGT

-600 GGGTGGATCA CCTGAGGTCA GGAGTTCGAG ACCAGCCTGA CCAACATGGA

-550 GAAACCCCGT CTCTACTAAA AATACAAAAT TAGCCAGGTG TGGTGGCACA

-500 TGCCTGTAAT CCCAGCTACT TGGGAGACTG AGGCAGGAGA ATCGCTTGAA

-450 CCTGGGAGGT GGAAGTTGCC GTGAGCCGAG ATCGCGCCAT TGCACTCCAG

-400 CCTGGGCAAC AGGAGCGAAA CTCCATCTCA AAACAAAAAA AAAAAGAATC

-350 CCTAACGCAG AGGAAAAGAT TGGTGAGCTT TGTTTAATCA CACACGCTGT

-300 ACATTTTCCA CGCCCTCCCC CTCTGCCCTA CAGGAATCCG CTGTACTTCT

-250 GACGGCCCAT AGGTGGCACT GTAGGGACAG GTAAGTGCAC AGGGAGCGCC

-200 ACCCGGAGAG GCTGATAGGA GGCGGAGCTT CAATGCGACA CAACGTGGCG

-150 GGAGGAGCCT AAGGGACGAG GAAAGGCGAG TGTTCTGCTT GCGCAGACGC

-100 AAGGCTGGGC ACTCCCCCGG GAGTGAGGGT TGCTGGGCCT GATGACGTGG

-50 CTTGGCAACG TCCCTACCGC CGCTGCTTCC CGGGAACCTG GCGCCGCCGG

+1 aactgatcgc ggcctagtcc cgacgc**gtgt gtgctagtga gccggagccg**

+50 gcgacggcgg cagtggcggc ccggcctgca ggagcccgac ggggtctctg

+100 cc**atg**gggga gtgacgcgcc tgcacccgct gttccgcggc agcggcgaga

Figure 4.6. The SLC30A5 promoter region sequence. *The -1000 to +100 bp region of the SLC30A5 promoter sequence taken from the human genome sequence is shown. The genomic region upstream of the start of transcription as identified by alignment of the transcript sequence NM_022902 (lowercase) is represented in uppercase letters. Primers were designed for amplification by PCR of a 1000 bp region of the SLC30A5 sequence (SLC30A5F#1 - light red and SLC30A5R#1 - dark red) to generate a PCR product to sub-clone into the pBlue-TOPO® reporter vector. Primers and annealing temperatures are given in Table 2.2B.*

Figure 4.7. The SLC30A5 promoter sequence inserted into pBlue-TOPO® and related primers. *The region of the SLC30A5 promoter sequence (non-italicised uppercase) inserted into the pBlue-TOPO® vector (italicised uppercase) is shown aligned to the original genomic sequence. Primers were designed for a PCR to a region in the SLC30A5 (SLC30A5PromoterF - light red and SLC30A5PromoterR#1 - dark red; non-italicised uppercase) sequence. A reverse primer was designed for PCR to the pBlueTOPO vector (pBlueTOPOR – dark red; italicised uppercase) sequence for sequence verification. Primers and annealing temperatures are given in Table 2.2B.*

As expected, methylation of the *SLC30A5* promoter reporter construct resulted in a loss of promoter activity ($p < 0.001$). A comparison of 'mock' methylated and unmethylated constructs showed no difference in levels of reporter gene expression. The *SIRT1* promoter showed a modest reduction in activity when methylated ($p < 0.01$) (*Figure 4.8*) revealing the potential for any *SIRT1*-mediated (or other) effects on methylation of the *SIRT1* promoter to affect SIRT1 expression.

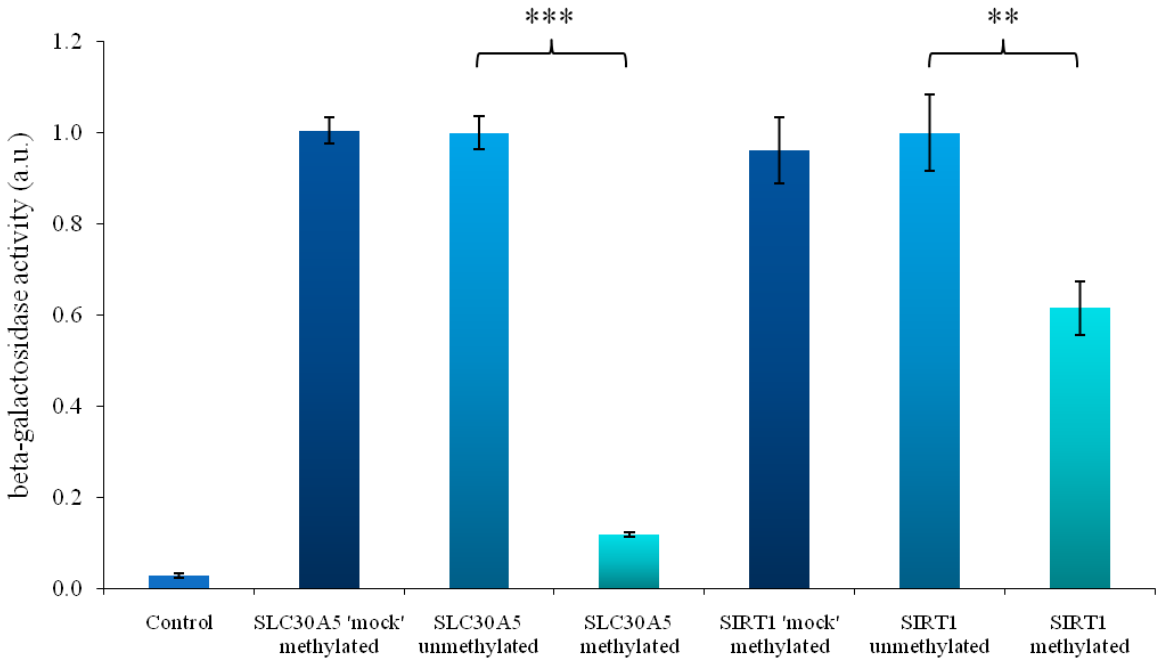

Figure 4.8 Effect on SIRT1 transcriptional activity of promoter methylation. *Cell lysate extracted from Caco-2 cells transfected with methylated or unmethylated SIRT1 promoter reporter constructs or control methylated or unmethylated ZnT5 promoter reporter constructs were assessed for promoter activity using the beta galactosidase activity assay to measure reporter gene expression. As expected, methylated ZnT5 promoter reporter constructs had reduced promoter activity in comparison to unmethylated constructs (***p < 0.001 by student's t-test). The methylated SIRT1 promoter reporter construct also showed a decrease in promoter activity compared with the unmethylated SIRT1 promoter reporter construct (** p < 0.01 by student's t-test). All data are mean ± SEM for n = 3.*

4.4 Relationship between SIRT1 levels and ageing in intestinal mouse tissue

We propose in our hypothesis that the increased levels of SIRT1 seen under DR affect levels of DNA methylation to mediate some of the beneficial effects of reduced dietary intake. It is possible that such an increase in SIRT1 expression opposes an age-related decline in expression. The literature currently available shows a wide variation in the effects of ageing on SIRT1 expression levels in different tissues. Of particular note are: an observed increase in SIRT1 skeletal muscle of rats (proposed by the authors to potentially compensate for the decreased activity of SIRT1/lower levels of NAD^+ substrate with age) (Koltai et al., 2010); an increase in SIRT1 in monkey heart as a protective affect against stress (Alcendor et al., 2007); a decrease in SIRT1 in thymus and heart in mice in response to senescence, part of the cellular process of ageing, (Sasaki et al., 2006; Sakamoto et al., 2004); a decrease during senescence in human fibroblasts (Michishita et al., 2005). To our knowledge there are currently no reports of the levels of SIRT1 in the ageing gut, so SIRT1 expression was measured in samples of intestinal tissue from relatively young and older mice.

Protein lysates extracted from the jejunum and ileum tissue of 12 and 38 month old mice were assessed for changes in SIRT1 levels in response to ageing by western blot as described in Section 2.8. Protein lysate was extracted (Section 2.8.1.1) and protein concentration determined by Bradford assay (Section 2.8.1.4). Ten micrograms of tissue lysate extracted from each tissue sample was separated by SDS-PAGE (Section 2.8.1.5) and blotted onto a polyvinylidene difluride (PVDF) membrane (Section 2.8.1.6), which was then probed with antibodies to SIRT1 and the loading control protein alpha tubulin. Bands revealed on the blot were quantified by densitometry and the arbitrary values obtained for SIRT1 protein expression were expressed as a ratio of the band intensity of the alpha tubulin loading control. Figure 4.9A shows a typical western blot assessing the levels of SIRT1 protein in the intestinal tissue of a single animal from each age group. Data were then normalised against the densitometric signal intensity obtained from the 12 month old mice analysed on the same blot. This analysis revealed no difference in the level of SIRT1 expression between young and old mouse intestinal tissues (*Figure 4.9B*). However, the small pool of three mice per age group was probably not sufficient to accurately represent the inter-individual differences in SIRT1 and alpha tubulin protein expression in the intestinal gut tissues of individual mice, so findings remain inconclusive.

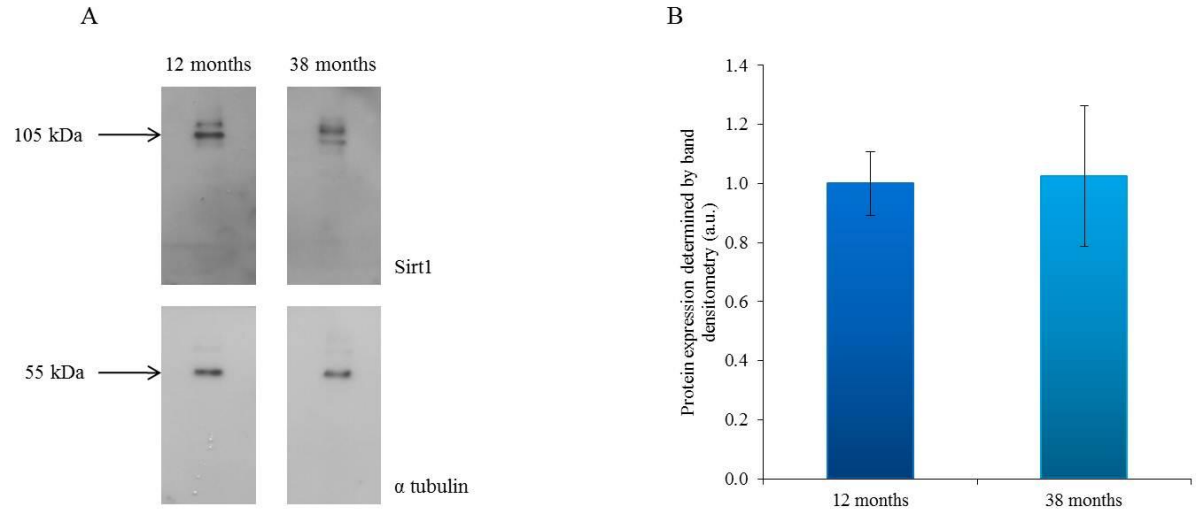

Figure 4.9. Relationship between SIRT1 levels and ageing in mouse intestinal tissue. *A – Protein extracted from 12 month and 38 month jejunum and ileum mouse tissue were separated by SDS-PAGE and SIRT1 expression was analysed by probing with an antibody to the SIRT1 protein followed by reprobing with an antibody to the loading control alpha tubulin. B – The bands revealed on the blot were quantified using densitometry. There was no statistically significant difference between the SIRT1 protein levels in the jejunum and ileum of young and old mice. $p > 0.05$ by student's t-test. All data are mean ± SEM for n = 3.*

4.5 Attempts of measure SIRT1 activity for use in cell line models and mouse tissues

In addition to the investigations described above, we also made attempts to optimise the SIRT1 Fluor de Lys™ fluorescent activity assay (BIOMOL® International) using recombinant SIRT1 (supplied with the kit) with the intention of studying the effects of dietary compounds, promoter methylation and age on SIRT1 deacetylase activity, as well as providing evidence of increased activity in cells overexpressing SIRT1 from plasmid constructs and in response to siRNA knockdown as employed in the work described in Chapter 3, Chapter 6 and Chapter 7.

The SIRT1 fluorescence activity assay has been used widely and reported within the literature as a means to investigate the effects of potential sirtuin-activating compounds (STACs) on SIRT1 deacetylase activity and test/identify synthetic STACs (Milne et al., 2007). The assay is based on the deacetylation and sensitisation of the Fluor de Lys-SIRT1 substrate upon incubation with cell lysate containing endogenous SIRT1 together with the co-substrate NAD^+. Upon treatment with the Fluor de Lys Developer II, a detectable fluorophore is produced (*Figure 4.10*). To assess SIRT1 activity in Caco-2 cells transfected with the SIRT1 overexpression construct, total cell lysate from the overexpression experiments replaced the human recombinant SIRT1 provided with the assay, which was used as a positive control. Fluorescence was also measured when the recombinant SIRT1 was replaced with cell lysate but the apparent reaction rate was independent of the quantity of cells lysate added. We therefore tested for fluorescence emission under assay conditions in the absence of any added protein and the same rate of fluorescence emission was observed, leading to the deduction that the substrate was unstable and that any apparent SIRT1 activity in the lysate was an artefact. Additionally, there has been much controversy surrounding the use of this assay in measuring SIRT1 deacetylase activity, leading to heated discussion within the literature over the authenticity of results. Recent research (Pacholec et al., 2010; Beher et al., 2009) backs up earlier claims (Borra et al., 2005; Kaeberlein et al., 2005a) questioning the reliability of the fluorescent assay to screen for compounds that enhanced SIRT1 deacetylase activity, specifically the use of the fluorescent peptide substrate employed within the Fluor de Lys assay. These studies propose that the non-physiological fluorescent moiety within the substrate creates experimental artefacts through increased binding affinity of the fluorescently labelled peptide irrespective of the presence of the peptide sequence. GlaxoSmithKline subsequently addressed these concerns by running further experiments identifying novel compounds that did not require the fluorophore for increased activity (Dai et al., 2010). Validation of the STACs in this study was through an activity assay employing a different substrate.

Our own observations, along with the uncertainty in the reliability of the assay as reported above, led the SIRT1 Fluor de Lys™ assay to be dismissed as sufficiently robust for measurements of the deacetylase activity of SIRT1 in our experiments.

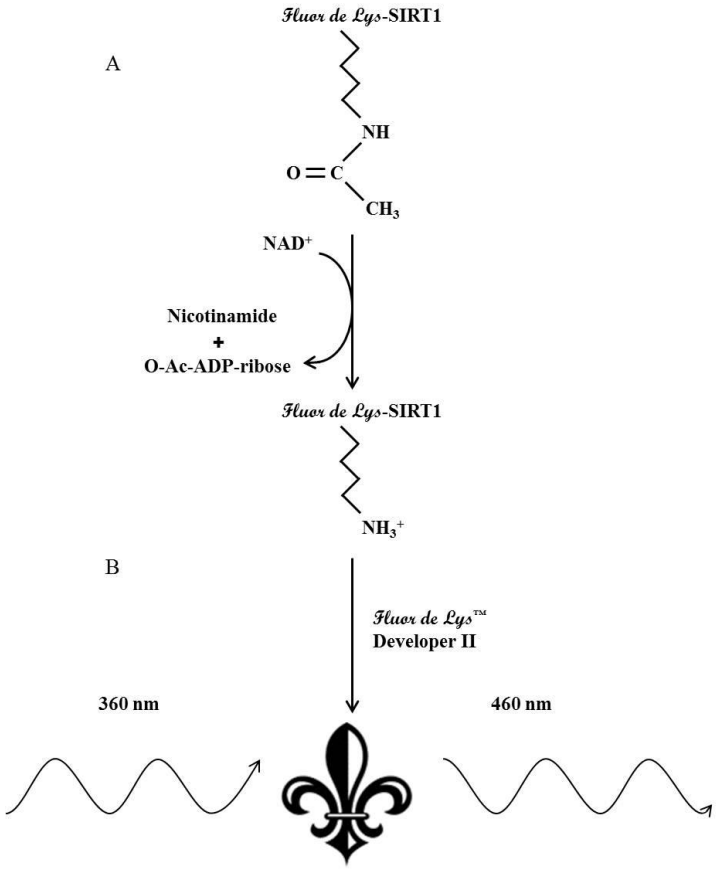

Figure 4.10. Schematic of the SIRT1 Fluorescence Activity Assay. *A – The Fluor de Lys-SIRT1 substrate, which comprises the p53 sequence Arg-His-Lys-Lys(ε-acetyl), is incubated with the human recombinant SIRT1 together with the co-substrate NAD^+ leading to the deacetylation and sensitisation of the Fluor de Lys-SIRT1 substrate. B - Upon treatment with the Fluor de Lys developer II, a detectable fluorophore is produced.*

4.6 Discussion

In this chapter the transcriptional activity of *SIRT1* was investigated in the context of changes to promoter activity in response to polyphenols, effects of promoter methylation and effects of age. The effects of the polyphenols resveratrol, genistein and daidzein on *SIRT1* promoter activity were investigated using the β-galactosidase activity assay. Caco-2 cells were treated with resveratrol, genistein or daidzein in the presence of a promoter-reporter construct containing the promoter region of the human *SIRT1* gene upstream of the β-galactosidase gene with the aim to establish whether the plant polyphenols play a role in modifying *SIRT1* promoter activity and therefore deacetylation of downstream targets of SIRT1 that may be involved in mimicking some of the beneficial effects of DR through *SIRT1*. In Caco-2 cells transfected with the *SIRT1* promoter reporter construct resveratrol (10 μM, 48 hours) and genistein (50 μM, 48 hours) caused a reduction in the level of *SIRT1* promoter activity, however once normalised to the response of the reference gene *GAPDH* these effects were no longer apparent, therefore the polyphenols do not appear to effect the transcriptional activity of the *SIRT1* gene specifically. Both genistein (Akiyama et al., 1987) and resveratrol (Jayatilake et al., 1993) might have a general affect on transcription of the reporter constructs through their known ability to inhibit tyrosine kinases involved in regulating protein activation via phosphorylation.

The consequences of methylation of the *SIRT1* for transcriptional activity of the gene were investigated using a methylated promoter-reporter model (Coneyworth et al., 2009). Caco-2 cells were transfected with the *SIRT1* promoter-reporter construct with the aim to establish if the methylation status of the SIRT1 promoter sequence affected the transcriptional activity of the *SIRT1* gene. In Caco-2 cells transfected with the methylated *SIRT1* promoter reporter construct, the level of *SIRT1* promoter activity was reduced compared to the unmethylated control. This observation suggested that SIRT1 activity can be regulated through the methylation status of the promoter region of the *SIRT1* gene.

The expression levels of SIRT1 in young (12 months) and old mice (38 months) were investigated at the protein level by probing total cell lysate, extracted from intestinal tissue and resolved by SDS-PAGE, with an antibody to the SIRT1 protein. No differences were detected between the levels of SIRT1 in young compared with old mouse intestinal tissue. Our observation that levels of SIRT1 expression within the mouse gut did not differ between younger and older mice does not exclude the possibility that the cell-type or sub-cellular localisation was unaffected, since only total tissues homogeny was used. Furthermore, the availability of only 3 mice per group for this analysis may have provided insufficient power to detect a difference in SIRT1 expression.

The Fluor de Lys™ activity assay system to measure SIRT1 enzymatic activity has been found to be unreliable in other studies as well as through our own observations. There are several other methods through which levels of SIRT1 deacetylation may be measured. Promega have recently developed a

new SIRT1 activity assay, SIRT-Glo™, based on the recognition and deacetylation by SIRT1 of a novel substrate that contains a peptide sequence derived from p53 with an acetylated lysine attached to aminoluciferin. The deacetylation of this peptide results in the production of a substrate that can be cleaved by a developer reagent to release the aminoluciferin, which is then acted upon by luciferase to give a measurable luminescence signal (Halley et al., 2011). Advantages include the addition of a single reagent mixture that contains all the components required for the reaction, a higher sensitivity compared to fluorescent based assays and a steady-state luminescent signal. One of the first investigations into validation of the SIRT1 Fluor de Lys™ fluorescent activity assay utilised additional techniques in parallel to the Fluor de Lys™ system. Coumarin and rhodamine-based fluorescence assays, where the Fluor de Lys-SIRT1 substrate (which contains the human p53 sequence from amino acids 379 to 382 with the acetylated lysine adjacent to the fluorophore) was replaced by either a p53-AMC and p53-R110 substrate respectively, showed the same effect of resveratrol to activate SIRT1-mediated deacetylation. However, when the Fluor de Lys-SIRT1 peptide was replaced by [^{3}H]AcH3 peptide – another deacetylation target for SIRT1 – or an unlabelled p53 peptide, no activation of SIRT1 by resveratrol was observed suggesting that the fluorophore and not the peptide sequence conferred resveratrol activation (Borra et al., 2005). High performance liquid chromatography (HPLC) was utilised to measure the presence of ^{14}C labelled NAD^{+} and the deacetylation product nicotinamide in the reaction using the fluorophore-free ([3H]AcH3) substrate. This assay would have been another possible method to assay SIRT1 deacetylase activity in our own investigations had there not been time constraints.

Several factors that may affect SIRT1 expression are investigated through the research presented in this chapter, however many aspects of SIRT1 regulation – expression of the pre-mRNA, post-transcriptional modification and translation of the protein – have not been investigated in any depth by our own or other research groups and warrant further investigation. The regulation of expression of the *SIRT1* gene to produce the primary transcript is known to rely upon the binding of several transcription factors under different conditions. We observed a repression of transcriptional activity when the *SIRT1* promoter region upstream of the LacZ gene was methylated. Further investigations, to identify the combination of methylated CpG sites crucial for transcriptional suppression are justifiable as downstream experimentation could then determine the effect of the methylation on transcription factor binding. The discovery of microRNAs to target mRNA for degradation preventing protein expression has added another layer to the central dogma of gene regulation. Several SIRT1-targeting microRNAs have now been found and will no doubt play fundamental roles in how and when SIRT1 is expressed and may also explain some discrepancies between data reported.

Studies of sirtuin regulation should extend to other family members, which have also been observed to play fundamental roles in a variety of pathways that may be perturbed during the ageing process.

Recent studies have showed that SIRT4 negatively regulates levels of SIRT1 and downstream fatty acid oxidation in the liver (Nasrin et al., 2010) and the protective effect of DR against oxidative damage in multiple tissues is abolished with DR in SIRT3 knockout mice (Someya et al., 2010) suggesting the other sirtuins perhaps work in concert with SIRT1 to produce the lifespan extension response to DR. Experiments involving knockdown of multiple sirtuins may go some way to addressing the level of the interplay between the seven sirtuins.

In contrast to reports based on analysis of other tissues, we did not observe a change in SIRT1 protein levels with age in a small cohort of mouse intestine, based on analysis of six animals. Sub-cellular localisation of SIRT1 has been shown to differ between numerous tissue and cell types (Tanno et al., 2007) suggesting a mechanism with which the deacetylation of both nuclear and cytoplasmic targets of SIRT1 can be functionally regulated. Use of immunohistochemistry or fluorescent protein tags to visualise the sub-cellular location of SIRT1 in response to age would perhaps reveal other effects of age and possibly shed more light on possible influence of age on the functional actions of SIRT1 not measurable by levels of expression alone.

5 *In silico* analysis of relationships between loci binding SIRT1, genes affected by dietary restriction and genes showing ageing-related changes in methylation

5.1 Outline

As discussed previously dietary restriction (DR) remains one of the most robust dietary interventions proved effective to increase lifespan across evolutionarily distinct species, from yeast to rodents (Guarente and Picard, 2005). The NAD^+-dependent (class III) histone deacetylase SIRT1 in mammals, and its ortholog in other species, may be pivotal in mediating the effect of DR to increase lifespan. Ageing is associated with changes in genome methylation (e.g. (Maegawa et al., 2010), which may be causative in the ageing process. Such observations, in view of the activity of SIRT1 at the level of the epigenome, form the basis for the hypothesis that epigenetic affects of SIRT1 activity mediate some of the beneficial effects of DR that contribute to lifespan extension. The approach to testing this hypothesis in this chapter was to determine, through *in silico* analysis, the overlap between genes that bind SIRT1, those regulated at the mRNA level in response to DR, and those that show an age-related change in methylation status, predicated on the principle that overlaps greater than would be expected by chance would support the hypothesis.

As the intention was to compare gene lists from a wide variety of sources all genes were converted to be represented with the same gene identifier. Ensembl identifiers are one of the most stable and extensively used gene identifiers currently in use and provide a comprehensive and up to date gene ID set on which to base bioinformatic analysis. The Ensembl Biomart Gene Conversion Tool was used to convert genes from their given identifier to the Ensembl format as described in Section 2.9.1. The NimbleGen MM5 array was used as the 'Universe' against which all genes lists analysed were checked to ensure their presence. Genes not represented in the 'Universe' were excluded from further analysis to ensure that sizes of overlaps obtained through gene list comparisons and their statistical analysis were precise and robust. Altogether 17087 genes on the MM5 array could be represented by an Ensembl identifier using the Ensembl Biomart Gene Conversion Tool (Appendix E.I).

5.2 SIRT1-associated genes

A list of gene loci at which SIRT1 binds to the promoter region in mouse embryonic stem cells (ES cells) was obtained from the published data of Oberdoerffer and co-workers (Oberdoerffer et al., 2008) based on use of chromatin immunoprecipitation using an anti-SIRT1 antibody. Mouse embryonic stem cells were cross linked with 1 % formaldehyde, sonicated, incubated with the antibody and immunoprecipitated using an anti-SIRT1 antibody. The immunoprecipitated DNA was co-hybridised with input DNA (not enriched for sites of SIRT1 binding) to a NimbleGen MM5 minimal promoter

tiling array. A list of all loci corresponding to probes for which there was enrichment in the immunoprecipitated DNA fraction was provided as supplementary material. Four hundred and thirty annotated gene loci were identified to which SIRT1 bound and that could be represented by an Ensembl identifier (*Table 5.2* and Appendix E.I).

5.3 Genes responsive to dietary restriction

To investigate the extent to which genes that were associated with SIRT1 in mouse embryonic stem cells overlapped with those regulated at the mRNA level in response to dietary restriction - also in mouse - a literature research was conducted to establish a list for this comparison. Initially, to search for relevant publications the online PubMed database which accesses MEDLINE the online Medical Literature Analysis and Retrieval System (MEDLARS) was used. PubMed (1950 – 2008) searches were conducted using the search terms 'mouse' in conjunction with ('calorie restriction' OR 'caloric restriction' OR 'dietary restriction' OR 'energy restriction') AND ('gene expression' OR 'transcriptional profiling' OR 'microarray'). Relevant references cited in publications and reviews (Swindell, 2008; Han and Hickey, 2005) obtained through this search were also included as potential sources for gene lists. Studies that did not provide full results of the transcriptional profiling within the body of the paper or as easily accessible supplementary material were excluded. This process identified eleven studies from which a single gene list, with duplicates excluded, was compiled (Sharov et al., 2008; Swindell, 2008; Wu et al., 2008; Dhahbi et al., 2006; Fu et al., 2006; Selman et al., 2006; Han and Hickey, 2005; Higami et al., 2004; Massaro et al., 2004; Tsuchiya et al., 2004; Lee et al., 2002) (*Table 5.1*). For each published study the authors' list of regulated genes was accepted using data from any tissues for which it was available; the rationale was that the data available for gene loci binding SIRT1 was based on ES cells, so was not tissue-specific. All gene lists were converted to Ensembl identifiers as described above and duplicates were eliminated to generate a single list of 2613 genes (Appendix E.I) found to respond to DR in mice and also found on the MM5 array 'Universe'.

Reference	Tissue	Design	Gene Identifier	Number of Genes
Dhanbi et al (2006)	Heart	Male B6C3F1 were DR for 2 months (17 % 2 weeks then 45 % 6 weeks) from 29 months of age then killed at 31 months n = 4	GeneBank	106
Fu et al (2006)	Heart, Hypothalamus, Liver	Male C57BL/6 were 40 % DR for 2.5 - 4.5 months from 1.5 months old then killed at 4 - 6 months of age n = 6 per tissue (each pooled from 3 mice)	GeneBank	1116
Han et al (2005)	Anterior Pituitary, Cerebellum, Epididymus, Gastrolcnemius Muscle, Heart, Liver, Lung, Neocortex, WAT	Gene expression data was collected from 15 published studies; male and female 129/sv, Ames, Ames Dwarf, B6C3F1, BALB/c, C3B10RF, C57BL/6 or C57BL/6J were DR. See Han et al 2005 for details of each individual study.	GeneBank	167
Higami et al (2004)	WAT	Male C57BL/6 were 41 % DR for 0.75 - 9 months from 1.5 months old then killed at 10 - 11 months of age n = 5	GeneBank	109
Lee et al (2002)	Heart	Male B6C3F1 were 41 % DR for 16 months from 14-30 months old then killed at 30 months of age n = 5	GeneBank	831
Massaro et al (2004)	Lung	Male C57BL/6 were 66 % DR for 14 days n = 6	GeneBank	257
Selman et al (2006)	Colon, Gastrolcnemius Muscle, Hypothalamus, Liver	Male C57BL/6 were 10-30 % DR for 30 days from 3.5-4 months old then killed at 4.03 months of age n = 3 per tissue (each pooled from 3.3 mice)	HUGO	2072
Sharov et al (2008)	Ovary, Testis	Male and female C57BL/6 were 40 % DR for 0.75 months from 3.5 months old then killed at 6 - 24 months of age n = 6 per tissue	HUGO	136
Swindell (2008)	Cochlea, Colon, Heart, Hippocampus, Hypothalamus, Kidney, Liver, Lung, Muscle, WAT	Gene expression data was collected from 10 published studies; male and female 129/sv, Ames, B6C3F1, B6CBA, C57BL/6, C57BL/6J, or C57BL/6NHsd were DR. See Swindell 2008 for details of each individual study.	HUGO	28
Tsuchiya et al (2004)	Liver	Male and female Ames and Ames Dwarf were 30 % DR for 4 months from 2 months old then killed at 6 months of age n = 8 per mouse strain	GeneBank	77
Wu et al (2008)	Hippocampus	Male B6CBA were 30 % DR for 4 months from 4 months of age then killed at 8 months of age n = 4	GeneBank	146

Table 5.1. Summary of gene profiling studies in dietary restricted mice. *Abbreviations: DR – dietary restriction; WAT – white adipose tissue.*

5.4 Genes with a methylation status changed with age

Publication of a data set listing genes that showed a change in methylation status with ageing in mouse intestine (Maegawa et al., 2010) afforded the opportunity to determine if genes found to associate with SIRT1 and/or to respond to DR were also over-represented in this group. Genomic DNA from intestinal tissue of 3 or 35 month old C57BL/6 mice was fragmented by methylation-sensitive restriction digestion using *Sma*I to produce blunt end fragments, cutting only when the recognition site (CCCGGG) is unmethylated. This digestion was followed by digestion using *Xma*I, the *Sma*I methylation-insensitive isoschizomer, to cut methylated *SmaI* sites and produce CCGG overhangs allowing adaptor ligation. The fragments produced from this digestion process were PCR amplified and samples from young and old mice were co-hybridised to the promoter oligonucleotide array after labelling with Cy3 (green) or Cy5 (red).

Using the same criteria as the authors of this study to designate genes as showing differential methylation between young (3 month) and old (35 month) tissue, Ensembl identifiers were assigned to 1040 genes that showed ageing-related changes in methylation status (Appendix E.I) and were represented in the list of 17087 genes on the NimbleGen MM5 minimal promoter tiling array for which could also be represented by Ensembl identifiers.

5.5 Analysis of overlaps between SIRT1-associated genes, genes responsive to DR and genes with a methylation status changed with age.

Of the 1040 genes that showed ageing-related changes in methylation status, 47 were also in the list of genes found to associate with SIRT1 (*Table 5.2*); the number expected by chance is 26 (i.e. 1040/17087 (or 6.1 %) of the 430 SIRT1-associated genes). Calculation of cumulative hypergeometric probability indicates that the apparent over-representation of genes found to show ageing-related changes in methylation status that also associate with SIRT1 (representation factor of 1.81) is statistically significant ($P = 7.1 \times 10^{-5}$). This analysis indicates that genes to which SIRT1 binds are more likely to show changes in methylation status with increased age. This relationship also supports the hypothesis that responses to DR include epigenetic effects (specifically effects on DNA methylation) resulting from SIRT1 activity.

The 2613 genes identified as responsive to DR represented 15.3 % of the genes interrogated as potential SIRT1 targets (i.e. 2613/17087). Eighty-four genes appeared on both the list of SIRT1 targets and on the list of genes responsive to DR (*Table 5.2*). If the proportion of SIRT1-associated genes responsive to DR were the same as the proportion of all genes responsive to DR (as would be the case if DR-responsiveness and association with SIRT1 were independent variables), then the expected size

of this overlap would be 66 genes (i.e. 15.3 % of the 430 SIRT1-associated genes). Calculation of cumulative hypergeometric probability indicates that the apparent over-representation of genes responsive to DR that also associate with SIRT1 (representation factor of 1.27) is statistically significant (P = 0.0095). This analysis indicates that there is an association between genes that respond to DR and genes that bind SIRT1, which supports the hypothesis that responses to DR include epigenetic effects resulting from SIRT1 activity.

One hundred and ninety one genes appeared on both the lists of genes responsive to DR and found to show an age-related change in methylation status. This figure compared with 159 expected by chance (i.e. 6.1 % of the 2613 genes found to respond to DR or 15.3 % of the 1040 genes found to show an ageing-related change in methylation status), giving a representation factor of 1.20 and cumulative hypergeometric probability of 0.0031. This analysis indicates that genes that respond to DR are more likely than other genes to show changes in methylation status with ageing (or vice versa), consistent with a view that effects of DR include effects on gene methylation status relevant to ageing and therefore in agreement with the overall hypothesis. Numbers of genes, observed/expected values, representation factors and hypergeometric probability values for the above three pairwise comparisons of overlaps are summarised in Table 5.3.

Ten genes fell into the 'three way' overlap between the gene lists compiled (*Table 5.2* and Appendix E.I), compared with an expected number of 4 (i.e. 0.153 x 0.061 x 430), giving a representation factor of 2.5 and cumulative hypergeometric probability of 0.0079. This 'three way' overlap is represented via a Venn diagram in Figure 5.1. Again, the analysis supports the hypothesis that responses to DR include epigenetic effects (specifically effects on DNA methylation) resulting from SIRT1 activity.

Genes associated with SIRT1 AND responsive to DR

ENSMUSG00000025964*	Adam23*	ENSMUSG00000029178	Klf3	ENSMUSG00000019889	Ptprk
ENSMUSG00000053644	Aldh7a1	ENSMUSG00000026866	Kynu	ENSMUSG00000004127	Rg9mtd2
ENSMUSG00000020610	Amz2	ENSMUSG00000032193	Ldlr	ENSMUSG00000026360*	Rgs2*
ENSMUSG00000011958*	Bnip2*	ENSMUSG00000029103*	Lrpap1*	ENSMUSG00000008301	Rnuxa
ENSMUSG00000055172*	C1r*	ENSMUSG00000018819	Lsp1	ENSMUSG00000012848	Rps5
ENSMUSG00000024372	C2	ENSMUSG00000008035	Mid1Ip1	ENSMUSG00000031568	Rwdd4a
ENSMUSG00000029283	Cdc7	ENSMUSG00000059908	Mug1	ENSMUSG00000017707*	Serinc3*
ENSMUSG00000069089	Cdk7	ENSMUSG00000073832	Mup17	ENSMUSG00000033965	Slc16a2
ENSMUSG00000056501	Cebpb	ENSMUSG00000020900*	Myh10*	ENSMUSG00000026205	Slc23a3
ENSMUSG00000028044	Cks1b	ENSMUSG00000061911*	Myt1l*	ENSMUSG00000022664	Slc35a5
ENSMUSG00000022843	Clcn2	ENSMUSG00000021710	Nln	ENSMUSG00000063354	Slc39a4
ENSMUSG00000026317	Cln8	ENSMUSG00000027405	Nol5a/NoP56	ENSMUSG00000006641	Slc5a6
ENSMUSG00000024644	Cndp2	ENSMUSG00000030551	Nr2f2	ENSMUSG00000020027	Socs2
ENSMUSG00000000326*	Comt*	ENSMUSG00000027852	Nras	ENSMUSG00000039218	Srrm2
ENSMUSG00000032330	Cox7a2	ENSMUSG00000041827	Oasl1	ENSMUSG00000018167	Stard3
ENSMUSG00000031446	Cul4a	ENSMUSG00000020131	Pcsk4	ENSMUSG00000047963	Stbd1
ENSMUSG00000029630	Cyp3a59	ENSMUSG00000005615*	Pcyt1a*	ENSMUSG00000022241	Tars
ENSMUSG00000003135	D1bwg0212e	ENSMUSG00000025728	Pigq	ENSMUSG00000018604	Tbx3
ENSMUSG00000046179	E2f8	ENSMUSG00000023452	Pisd	ENSMUSG00000024498	Tcerg1
ENSMUSG00000022053	Ebf2	ENSMUSG00000014503	Pkd2l2	ENSMUSG00000006335*	Tfpt*
ENSMUSG00000035530*	Eif1*	ENSMUSG00000031538	Plat	ENSMUSG00000048007	Timm8a1
ENSMUSG00000021282	Eif5	ENSMUSG00000028691	Prdx1	ENSMUSG00000027801	Tm4sf4
ENSMUSG00000021364	Elovl2	ENSMUSG00000005161	Prdx2	ENSMUSG00000029723*	Tsc22d4*
ENSMUSG00000024360	Etf1	ENSMUSG00000039671	Prkcbp1	ENSMUSG00000062380	Tubb3
ENSMUSG00000055401	Fbxo6	ENSMUSG00000002455	Prpf6	ENSMUSG00000030870	Ubfd1
ENSMUSG00000025059	Gyk	ENSMUSG00000027566	Psma7	ENSMUSG00000001891	Ugp2
ENSMUSG00000031734	Irx3	ENSMUSG00000022193	Psmb5	ENSMUSG00000032376	Usp3
ENSMUSG00000003779	Kif20a	ENSMUSG00000021745	Ptprg	ENSMUSG00000027803*	Wwtr1*

Genes associated with SIRT1 AND showing a change in methylation status with ageing

ENSMUSG00000030249	Abcc9	ENSMUSG00000028344	Invs	ENSMUSG00000038205	Prkab2
ENSMUSG00000054808	Actn4	ENSMUSG00000033365	Ipo13	ENSMUSG00000021745	Ptprg
ENSMUSG00000029094	Afap1	ENSMUSG00000031734	Irx3	ENSMUSG00000025485	Ric8
ENSMUSG00000052414	Atf7	ENSMUSG00000031738	Irx6	ENSMUSG00000057378	Ryr3
ENSMUSG00000057914	Cacnb2	ENSMUSG00000054274	Kif26b	ENSMUSG00000045092	S1pr1
ENSMUSG00000015733	Capza2	ENSMUSG00000029178	Klf3	ENSMUSG00000019913	Sim1
ENSMUSG00000029283	CDC7	ENSMUSG00000032193	Ldlr	ENSMUSG00000063354	Slc39a4
ENSMUSG00000006958	Chrd	ENSMUSG00000026890	Lhx6	ENSMUSG00000040247	Tbc1d10c
ENSMUSG00000045672	Col27a1	ENSMUSG00000038668	Lpar1	ENSMUSG00000000093	Tbx2
ENSMUSG00000029705*	Cux1*	ENSMUSG00000045095	Magi1	ENSMUSG00000018604	Tbx3
ENSMUSG00000030871	Ears2	ENSMUSG00000020900*	Myh10*	ENSMUSG00000032536*	Trak1*
ENSMUSG00000021282	Eif5	ENSMUSG00000005886	Ncoa2	ENSMUSG00000007805	Twist2
ENSMUSG00000028664	Ephb2	ENSMUSG00000026525	Opn3	ENSMUSG00000008604	Ubqln4
ENSMUSG00000059003	Grin2a	ENSMUSG00000005615*	Pcyt1a*	ENSMUSG00000006270	Vax1
ENSMUSG00000056755	Grm7	ENSMUSG00000056204	Pgpep1	ENSMUSG00000022023	Wbp4
ENSMUSG00000069308	Hist1h2bp	ENSMUSG00000018547	Pip4k2b		

Genes associated with SIRT1 AND responsive to DR AND showing a change in methylation status with ageing

ENSMUSG00000029283	Cdc7	ENSMUSG00000032193	Ldlr	ENSMUSG00000021745	Ptprg
ENSMUSG00000021282	Eif5	ENSMUSG00000020900*	Myh10*	ENSMUSG00000063354	Slc39a4
ENSMUSG00000031734	Irx3	ENSMUSG00000005615*	Pcyt1a*	ENSMUSG00000018604	Tbx3
ENSMUSG00000029178	Klf3				

Table 5.2. Lists of SIRT1-associated genes also responsive to DR or showing a change in methylation status with ageing or responsive to DR AND showing a change in methylation status with ageing. Both ENSEMBL identifiers and gene symbols are stated. **Denotes genes found also to be deregulated with age in mouse neocortex.*

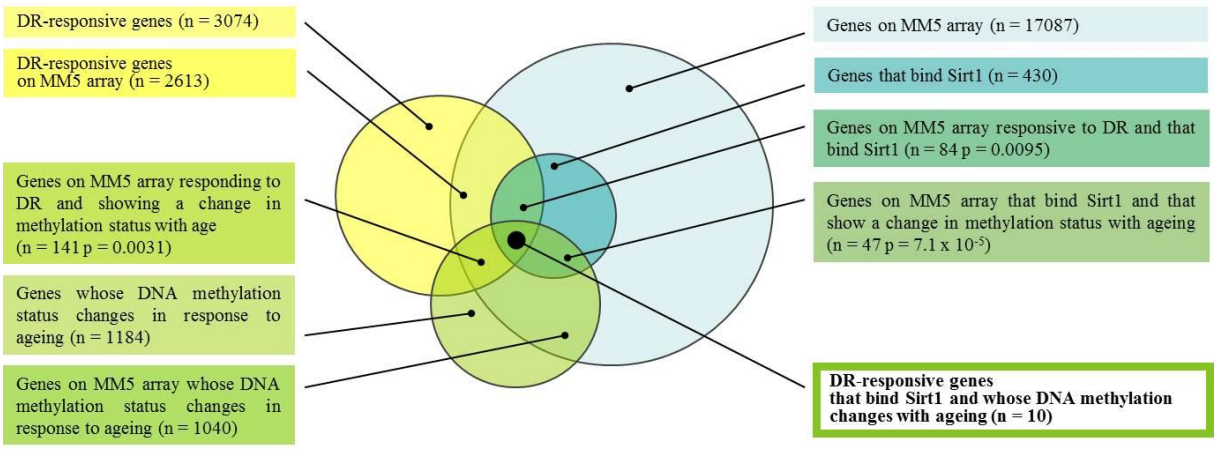

Figure 5.1. Diagrammatic representation of the 'three way' overlap of genes found to be associated with SIRT1 and found to be responsive to DR and found to show an ageing-related change in methylation status. *'n' indicates the number of genes common to both groups; 'p' indicates the cumulative hypergeometric probability.*

Gene set interrogated n = 17087 (see Appendix E.I)	Genes responsive to DR n = 2613 (see Appendix E.I)	Genes showing a change in methylation status with ageing n = 1040 (see Appendix E.I)
SIRT1-associated genes n = 430 (see *Table 5.2*)	OBS/EXP = 84/66 = 1.27 p = 0.0095	OBS/EXP = 47/26 = 1.81 p = 7.1 x 10^{-5}
Genes showing a change in methylation status with ageing n = 1040 (see Appendix E.I)	OBS/EXP = 191/159 = 1.20 p = 0.0031	

Table 5.3. Overlaps between genes responsive to DR, genes that SIRT1 binds to and genes that show changes in methylation status with ageing, based on in silico analysis. *'n' indicates the number of genes common to both groups; Observed (OBS) over calculated expected (EXP) values, the representation factor, are shown; 'p' indicates the cumulative hypergeometric probability.*

5.6 Genes identified as targets for SIRT1-binding that responds to DR and undergo an age-related change in methylation status.

Genes falling within the 'three way' overlap identified through our *in silico* analysis may be particularly strong candidates for mediating affects of DR on lifespan/healthspan through the SIRT1-mediated effects on methylation that we propose. Each of these 10 genes is thus considered briefly below, noting the nature of the observed response to DR and with emphasis on possible or speculative roles in ageing and/or modulation of healthy lifespan.

5.6.1 Cell division cycle 7

The *Cdc7* gene showed increased expression in response to DR in mouse hippocampus (Wu et al., 2008) and encodes the conserved cell division cycle 7 kinase, which is required in parallel with the cyclin-dependent kinase (CDK) to establish replication forks during DNA replication. During G1 phase the MCM2-7 (minichromosome maintenance 2-7) DNA helicase complex is loaded onto the origin of replication in an inactive form. CDC7 and CDK are essential to activate this replicative helicase and also for recruitment of co-factors required for chromosome replication (Labib, 2010). Inactivation of CDC7 results in genomic instability (Costanzo et al., 2003) and cell death (Montagnoli et al., 2004) so possible links with ageing – through effects on cell survival – are likely though, to our knowledge, not established.

5.6.2 Eukaryotic translation initiation factor 5

Eukaryotic translation initiation factor 5 (Eif5), which showed increased expression in response to DR in mouse liver (Fu et al., 2006) regulates the activity of the conserved guanosine triphosphate (GTP)-binding eukaryotic translation initiation factor 2 protein eIF2. eIF2 is composed of three subunits (αβγ) and initiates eukaryotic protein translation through binding (to the γ subunit) and delivering initiator methionyl tRNA (met-tRNA) to the ribosome. eIF2 forms a pre-initiation complex (PIC) with the 40s ribosomal subunit and initiation factors eIFs 1, 1A, 3 and 5 (through the β subunit) after binding met-tRNA. eIF5 acts as a GDP dissociation inhibitor (GDI) and GTPase accelerating protein (GAP) regulating the translation initiation process through eIF2 activity via hydrolysis of the eIF2-bound GTP required for release of the 40s ribosomal subunit for 60s interaction and transcription initiation. eIF5 then later prevents eIF2-bound GDP release, which would result in the downstream reactivation of eIF2 and subsequent translation initiations. Mutation of *Eif5* results in dysregulation and stalling of transcription initiation resulting in slowed cell growth (Jennings and Pavitt, 2010) a process that could feasibly alter the ageing trajectory. Additionally, the *C. elegans* homologue of the human eukaryotic translation initiation factor eIF4H, drr-2 has been shown to respond to DR and increase longevity in worms, highlighting the importance of transcription initiation in lifespan (Ching et al., 2010).

5.6.3 Iroquois related homeobox 3

The *Irx3* gene showed increased expression in response to DR in mouse heart (Lee et al., 2002). Translation of the *Irx3* gene in progenitor cells during early embryonic development produces the Iroquois related homeobox 3 protein, a member of the Iroquois transcription factor family. Irx genes are responsible for a variety of developmental processes such as organisation of the heart, eye and, in the case of *Irx3*, the dorso-ventral patterning of neural tube (the precursor to the central nervous system) via strict direction of motor neuron generation (Cavodeassi et al., 2001). Although Irx3 is required for aspects of embryonic development, other Iroquois transcription factors have been implicated in regulation of gene expression in adult cells; most notably, Irx5 has a role in contraction of the heart, where it negatively regulates the expression of potassium channels to control depolarisation and repolarisation of endocardial (septal base of heart) and epicardial (ventricular apex of heart) myocytes (Costantini et al., 2005). It is possible that Irx3 may also have roles in the regulation of gene expression in adult cells with functional consequences of relevance to ageing, though to our knowledge such factors have not yet been identified.

5.6.4 Krüppel-like factor 3

Klf3 showed increased expression in response to DR in mouse liver (Selman et al., 2006). The family of Krüppel-like factor (KLF) transcription factors bind DNA, specifically promoters and enhancers of genes, through three highly-conserved zinc fingers, which allow the KLF proteins to regulate gene expression through activation and repression. The Krüppel-like factor 3 (KLF3) regulates gene expression of target sequences through recruitment of the C-terminal binding protein CtBP, binding of co-factors including histone methyl transferases and deacetylases, and sumoylation of KLF3 lysines, together forming a repressor complex. KLF3 plays roles in i) regulation of adipogenesis by repression of the adipogenic genes PPARγ, C/EBPα and β inhibiting fat cell formation, ii) generation of red blood cells by binding and repression of embryonic and adult β-globins and iii) differentiation of B cells through downstream activation of KLF3 after the activation and initiation of the B cell response. Conversely, KLF3 appears to act as an activator in development of muscle cells, binding the muscle creatine kinase (MCK) promoter, which mediates the transfer of energy from the mitochondria to muscle cells, promoting muscle differentiation (Pearson et al., 2011). Given the wide range of biological processes and tissues in which KLF3 functions, it is easy to propose links between expression of this transcription factor and factors of ageing, particularly with respect to haematopoiesis and the reliance of the human body on this system for immunity; however, to our knowledge, such links have not yet been addressed explicitly.

5.6.5 Low density lipoprotein receptor

The low density lipoprotein (LDL) receptor (LDLR) is a transmembrane glycoprotein that is expressed at the cell surface in a wide variety of tissues within the body - specifically the liver - and acts as the main regulator of cholesterol homeostasis within the plasma. The *Ldlr* showed decreased expression in

response to DR in mouse white adipose tissue (Higami et al., 2004). LDLR binds and transports via endocytosis the major carrier of cholesterol, LDL, from the plasma into the cell for lysosomal degradation. Mutations in *Ldlr* cause hypercholesterolemia, an increase in blood cholesterol levels that can also be caused by environmental factors such as poor diet and obesity and ultimately can lead to cardiovascular disease with increasing age. Thus, affecting LDLR expression levels may be a mechanism through which DR affects the ageing process.

5.6.6 Myosin, heavy chain 10

Myh10 showed decreased expression in response to DR in mouse liver (Selman et al., 2006). The myosin motor protein superfamily is essential in cellular processes requiring migration along actin filaments, a major cytoskeletal component of the cell. Class II myosin is present in all non muscle eukaryotic cells in addition to playing a major role in contraction of cardiac, skeletal and smooth muscle. Non muscle myosin II (NM II) has the same structure as muscle myosin; composed of heavy and light chains forming bipolar filaments to which actin can then bind, forming the sliding filaments of muscle tissue. *Myh9, Myh10* and *Myh14,* encode the NM II heavy chain isoforms A, B and C respectively (NMHC IIA-C) and define the NM II isoforms (NM IIA-C). NM IIB (encoded by *Myh10*) gives structure to the centre and rear of the migrating cell, assists with cell adhesion, mediates nuclear localisation and establishes Golgi apparatus and microtubule-organising centre positioning, ensuring correct migration, adhesion, and polarity of the cell respectively (Vicente-Manzanares et al., 2009). Ablation of NMHC IIB in a mouse model results in incorrect myocardialisation of the heart (Tullio et al., 1997) and brain architecture (Tullio et al., 2001) in early development. Known roles of this gene product, therefore, are of a fundamental nature and while specific functions directly relating to ageing have not, to our knowledge, been identified it is feasible that perturbation of function in older organisms may contribute to an ageing phenotype and that restriction of function through DR may have beneficial consequences.

5.6.7 Phosphate cytidylyltransferase 1 choline alpha isoform

Pcyt1a showed increased expression in response to DR in mouse liver (Fu et al., 2006). Phosphatidylcholines are a key membrane lipid component of the cell, the biosynthesis of which is catalysed by cytidine 5'-triphosphate (CTP):phosphocholine cytidylyltransferase alpha (CTα) (Sugimoto et al., 2008). Phosphatidylcholine biosynthesis plays a crucial role as cells divide and an increase in membrane phospholipids is required for cells to proceed through G1. Reducing the bioavailability of choline in fibroblasts (Tercé et al., 1994) or reducing the activation and expression of *Pcyt1a* (Banchio et al., 2003) greatly impairs the progress of cells through G1 and S phase respectively. Dysregulation of such mechanisms facilitating progression of the cell cycle is likely to lead to genomic instability and adverse changes such as oncogenesis and other pathological challenges related to those of an ageing cell, so it is feasible that beneficial effects of DR may be mediated through affects on *Pcyt1a* expression

5.6.8 Protein tyrosine phosphatase receptor type G

Ptprg showed increased in response to DR in mouse hippocampus (Wu et al., 2008). The protein tyrosine phosphatase receptor type G – encoded by *Ptprg* – transduces signals across the cell membrane through removal of phosphate groups from tyrosine residues on proteins. *PTPRG* has been proposed as a tumour suppressor gene due to its location in a frequently deleted section of human chromosome 3 associated with renal and lung carcinomas. Additionally, reduction in *PTPRG* expression is associated with chronic myeloid leukaemia characterised by a decrease in methylation at gene promoter CpG sites recorded in 55 % of patients assessed (Della Peruta et al., 2010). Such observations suggest an important role for correct expression of *Ptprg* in prevention of cancers, which become more prevalent with age, and providing a potential link between effects of DR on expression of the gene and ageing-related disease.

5.6.9 Solute carrier 39, member 4

Slc39a4 showed decreased expression in response to DR in mouse liver (Selman et al., 2006). Zinc availability plays a major role in many cellular processes due to the requirement of zinc in protein structure and function. Indeed, up to 10 % of the human genome may code for zinc-associated proteins (Andreini et al., 2006). The regulation of zinc homeostasis is dependent upon the expression of genes to take up, store and efflux zinc from the cytoplasm. The Slc39 solute carrier family encode the ZIP proteins, which transport zinc into the cell or release it from intracellular stores. The zinc transporter ZIP4, encoded by *Slc39a4*, plays an important role in intestinal zinc absorption through the apical membrane of enterocytes (Eide, 2004). Mutations in the *Slc39a4* gene result in acrodermatitis enteropathica, an inherited disorder of dietary zinc absorption (Dufner-Beattie et al., 2003). It remains an unproven, yet feasible, hypothesis that altered methylation of *Slc39a4* in the ageing gut leads to impaired zinc absorption, which may explain zinc-related features of ageing, notably compromised immune function (Fairweather-Tait et al., 2008).

5.6.10 T-box3 transcription factor

Tbx3 showed decreased expression in response to DR in mouse ovary (Sharov et al., 2008). T-box genes code for transcription factors that, through a conserved T-box DNA binding domain, activate or repress the promoter or enhancer of genes required in early embryonic development. The T-box 3 transcription factor - encoded by *Tbx3* - is required in limb bud formation, specifically digit development. Haploinsufficiency of the *Tbx3* gene in development results in ulnar-mammary syndrome and congenital malformations (King et al., 2006). Dysregulation of *Tbx3* in adult plays a role in tumourigenesis through inhibition of senescence via the ARF/MDM2/p53/$p21^{CIP1}$ pathway (Lu et al., 2010), providing a link between the function of this transcription factor and the ageing process.

5.7 Discussion

Genes were selected and converted to a common identifier from studies identifying genes that associated with SIRT1 (Oberdoerffer et al., 2008), were responsive to DR at the mRNA level (Sharov et al., 2008; Swindell, 2008; Wu et al., 2008; Dhahbi et al., 2006; Fu et al., 2006; Selman et al., 2006; Han and Hickey, 2005; Higami et al., 2004; Massaro et al., 2004; Tsuchiya et al., 2004; Lee et al., 2002) or whose methylation changed with ageing (Maegawa et al., 2010) generating three gene lists for which overlaps were identified. An overlap of 84 genes between the list of genes identified as sites of binding by SIRT1 and the list of genes found to respond to DR was found to be greater than would be expected by chance ($p = 0.0095$). The overlap of 47 genes associated with SIRT1 that also showed ageing-related changes in methylation status was also greater than expected by chance ($p = 7.1 \times 10^{-5}$). An overlap of 191 DR-responsive genes and genes showing a change in methylation with ageing ($p = 0.0031$) was also greater than expected by chance. Similarly, the overlap between the three lists of ten genes was again greater than would be expected by chance ($p = 0.0079$). Overall, this *in silico* analysis supported the hypothesis that SIRT1-mediated effects of DR include effects on DNA methylation.

The genes highlighted through this *in silico* analysis by virtue of appearing on all three lists encode proteins involved in a diverse range of cellular processes such as the fundamental regulation of the cell cycle (CDC7, EIF5), structure (MYH10, PCYT1A), and signalling (PTPRG), control of gene expression in early development (IRX3, TBX3) or general transcriptional regulation (KLF3) and regulation of dietary components (LDLR, SLC39A4). To our knowledge, previous studies have identified none of these genes as pivotal in determining lifespan or features of ageing, but hypotheses can be proposed. Thus, each gene provides a starting point for further investigation into how its methylation status may be a factor linking SIRT1, DR and their effects on the ageing cell.

The following chapter describes investigation of these gene loci individually to examine directly if SIRT1 expression can influence methylation status and/or expression levels, to attempt to uncover further evidence to support the overarching hypothesis and to highlight further if there is a strong argument favouring further research on these genes as possible mediators of lifespan or healthspan.

6 Gene-targeted *in vitro* investigation of links between SIRT1 expression, gene-specific DNA methylation and gene expression

6.1 Outline

This chapter describes investigation of the 10 genes identified by *in silico* analysis described in Chapter 5 to determine if they respond to SIRT1 manipulation, by having altered methylation at CpG sites within their promoter regions and/or to show affected gene expression levels.

To investigate if levels of SIRT1 expression can affect DNA methylation, SIRT1 was overexpressed and knocked down in the Caco-2 cell line. SIRT1 overexpression and knockdown in Caco-2 cells was confirmed at the mRNA level by RT-qPCR and at the protein level by western blot. DNA methylation at selected CpG sites was measured by pyrosequencing at CpG dinucleotides immediately upstream of the start of transcription in eight of the ten genes (*CDC7, EIF5, IRX3,* KLF3*, PCYT1A, PTPRG, SLC39A4, TBX3*) highlighted by the *in silico* analysis. Robust assays were not achieved for the measurement of methylation within the *LDLR* and *MYH10* promoter regions. Reverse transcription-qPCR was used to determine if expression at the mRNA level of the same genes was affected by manipulation of SIRT1 expression levels.

6.2 Gene specific DNA methylation and mRNA expression

To achieve SIRT1 knockdown, Caco-2 cells seeded 24 hours previously at 3.5 x 10^5 cells/well in a six well plate (area = 9.6 cm^2/well) were transfected transiently with 100 pmol SIRT1-targeting siRNA or with 100 pmol of a Stealth RNAi™ siRNA negative control of similar GC content. After 72 hours cells were lysed and DNA, RNA and total cell lysate were extracted from parallel experiments. Genomic DNA and total RNA were used to assess affects of SIRT1 knockdown on DNA methylation levels and expression of the target genes, respectively. First, RNA and protein were used to confirm SIRT1 knockdown at the transcriptional and translational level. RNA was used to assess SIRT1 knockdown at the mRNA level by RT-qPCR as described in Section 2.7.2. Total RNA was extracted from Caco-2 cells using TRIzol® reagent followed by the Invitrogen PureLink™ RNA Mini Kit (Section 2.4.3). Four and a half micrograms of DNase-treated RNA (Section 2.7.1.2) was reverse transcribed using Superscript™ III RNase H- Reverse Transcriptase (Invitrogen) (Section 2.7.1.3). Reverse transcribed cDNA was then PCR amplified (Section 2.5.1.1) using primers specific to a 128 bp region of the *SIRT1* gene (SIRT1F and SIRT1R). Measurements were normalised against the reference gene *ACTB* (β ACTIN) using primers that amplified a 90 bp region. Primer sequences and annealing temperatures are outlined in Table 2.2B.

Reverse transcription-qPCR analysis of SIRT1 and β ACTIN was performed using the Roche LightCycler® 480 (Section 2.7.2.4). Standard curves were generated for SIRT1 and β ACTIN to confirm linear amplification of PCR products and were run in parallel with the experimental samples. To generate standard curves undiluted cDNA extracted from untreated Caco-2 cells was used to create an 8 point 2-fold dilution series (Section 2.7.2.5), each dilution within this series was then used in qPCR amplification for each gene, and each reaction was performed in duplicate. (See Appendix D for typical amplification and standard curves for SIRT1 and β ACTIN.) As before, relative levels of SIRT1 transcript in the Caco-2 cells transfected with either of the two siRNAs showed a statistically significant reduction (~70 %) in SIRT1 mRNA compared with the control siRNA (*Figure 3.4B*) ($p < 0.001$).

Total cell lysate was used to assess SIRT1 knockdown at the protein level by western blot as described in Section 2.8. Total cell lysate was extracted (Section 2.8.2.2) and protein concentration determined by Bradford assay (Section 2.8.1.4). Ten micrograms of total cell lysate was separated by SDS-PAGE (Section 2.8.1.5) and blotted onto a polyvinylidene difluride (PVDF) membrane (Section 2.8.1.6), which was then probed with antibodies to SIRT1 and the loading control protein alpha tubulin. SIRT1 protein knockdown was confirmed by a reduced signal intensity revealed by the SIRT1 antibody in cells transfected transiently with the SIRT1-targeting siRNA compared with cells transfected transiently with the Stealth RNAi™ siRNA negative control. (See Chapter 3 *Figure 3.4C* for typical western blot confirmation of SIRT1 knockdown.)

To achieve SIRT1 overexpression, Caco-2 cells seeded 24 hours previously at 3.5×10^5 cells/well in a six well plate (area = 9.6 cm^2/well) were transfected transiently with 2 μg SIRT1 expression construct (pCMV6-ENTRYSIRT1) or with 2 μg control vector without a SIRT1 insert (pCMV6-Neo). After 72 hours cells were lysed and DNA, RNA and total cell lysate were extracted from parallel experiments as described above. Genomic DNA and total RNA were used to assess affects of SIRT1 overexpression on methylation levels and expression of the target genes, respectively. Total RNA and cell lysate were used to confirm SIRT1 overexpression at the mRNA level by RT-qPCR and protein level by western blot as described above. (See Chapter 3 *Figure 3.8B* and *Figure 3.8C* for typical RT-qPCR and western blot confirmation of SIRT1 overexpression.)

Having obtained DNA and RNA samples with confirmed SIRT1 knockdown and overexpression, DNA methylation was measured by pyrosequencing at the CpG sites immediately upstream of the start of transcription in eight of the ten genes (*CDC7, EIF5, IRX3, KLF3, PCYT1A, PTPRG, SLC39A4, TBX3*) highlighted by the *in silico* analysis described in Chapter 5. Primers were designed to amplify ~1000 bp sequence to cover approximately 900 bp upstream and 100 bp downstream of the start of transcription of each gene, representing the classically-defined promoter region. Pyrosequencing

assays were designed using the PyroMark Assay Design Software 2.0 (Qiagen) using this ~1000 bp sequence as a template. This starting sequence, before being entered into the design software, was converted to corresponding bisulfite modified sequence in Microsoft Word by using the 'Find' and 'Replace All' functions to first replace 'CG' (CpG sites) with 'C/TG', then replace 'C' with 'T' then replace 'T/' with 'C/', to give a sequence where 'C/T' represents a site that, depending on the original methylation pattern, may or may not have been deaminated by bisulfite treatment. Representing the CpG site in this way allows the design software to recognise it as a polymorphism that can then be checked by sequencing producing a ratio of 'C' vs. 'T' and therefore a percentage of cytosines protected by a methyl group at this site within the sample population – percentage DNA methylation. Upon running the assay design the software generated possible primer sets ('F#2', 'R#2' and 'Seq'). The set with the best score and widest CpG site coverage was selected for use and uploaded onto the PyroMark MD™ system (Qiagen). For *CDC7, EIF5, IRX3* and *PTPRG* these CpG dinucleotides were within predicted CpG islands (Section 2.9.3). Robust assays were not achieved for the measurement by pyrosequencing of methylation within the *LDLR* and *MYH10* promoter regions. In parallel with measurements of DNA methylation, RT-qPCR was used to determine if expression at the mRNA level of the same genes was affected by manipulation of SIRT1 expression levels.

Pyrosequencing was carried out as described in Section 1.5.3 and 2.6.8. Percentage DNA methylation was measured at consecutive CpG sites within the sequence. Each pyrosequencing assay consisted of a two stage PCR reaction. The first PCR generated a ~1000 bp product, and contained 25 µl HotStar Taq MasterMix (Qiagen), 0.25 µM sense and antisense primers ('YF#1' and 'YR#1') using 4 µl of bisulfite-modified genomic DNA (Section 2.6.1) as a template. This reaction was followed by a second, nested PCR generating a ~200 bp product, and contained 25 µl HotStar Taq MasterMix (Qiagen), 0.25 µM sense primer and 0.20 µM antisense biotinylated primer ('F#2' and 'R#2') using 4 µl of the first PCR reaction as a template. Primer sequences and annealing temperatures are stated in Table 2.2C and gene-specific assay details are given in each corresponding following section. Pyrosequencing using the gene-specific sequencing primer ('Seq') was carried out in duplicate for each sample.

Standard curves were generated to confirm linear amplification of methylated and unmethylated sequences. Unmethylated DNA template was generated by PCR amplification of a ~1000 bp region ('F#1' and 'R#1') of the target sequence from genomic DNA as described above. Two micrograms of unmethylated PCR product was methylated *in vitro* as described in Section 2.2.4. Nine microlitres of methylated or 25 µl unmethylated PCR product was then bisulfite modified as described in Section 2.6.1. The nested PCR using primers to produce a smaller product focusing in on the specific CpG sites was performed as described above. Reactions were combined to give appropriate percentages of methylated DNA (0, 5, 10, 25, 50, 75, 90, 95, 100 %) in a total volume of 10 µl. Pyrosequencing using

the gene-specific sequencing primer was carried out in duplicate for each standard and a standard curve was generated.

Total RNA was used to measure gene expression at the mRNA level by RT-qPCR using primers specific to a ~200 bp region of each target gene as described above. Primers were designed to span an intron. Values were normalised to the *WNT11* gene, which was found to be stably expressed regardless of SIRT1 manipulation in microarray analysis (see Chapter 7), using primers that amplified a 214 bp region (WNT11F and WNT11R). Primer sequences and annealing temperatures are outlined in Table 2.2D. Figure 6.3 shows the amplification and standard curve for WNT11; reference to gene-specific amplification and standard curves is provided in each relevant subsection below.

Details of the results of pyrosequencing to measure DNA methylation and qRT-PCR to determine levels of expression are provided below for each of the individual 8 genes whose response to SIRT1 manipulation was analysed.

6.2.1 Effects of SIRT1 manipulation on CDC7

Percentage DNA methylation was measured at eight consecutive CpG sites within the PCR amplified *CDC7* sequence spanning - 248 to + 53, occurring at - 58, - 51, - 49, - 43, - 27, - 10, - 7 and - 4 bp relative to the start of transcription of the *CDC7* sequence (*Figure 6.1* and Section 2.6.4). The first PCR generated a 912 bp product (CDC7YF#1 and CDC7YR#1) and the second, nested PCR generated a 301 bp product (CDC7F#2 and CDC7R#2). Pyrosequencing was carried out using the CDC7 sequencing primer (CDC7Seq). Methylation standard curves for CDC7 can be found in Appendix C.

Total RNA was used to assess CDC7 expression at the mRNA level by RT-qPCR using primers specific to a 211 bp region of the *CDC7* gene (CDC7F and CDC7R) as described above. Primer sequences and annealing temperatures are outlined in Table 2.2D. Amplification and standard curves for CDC7 can be found in Appendix D.

The 8th CpG site upstream of the *CDC7* transcript at position -58 relative to the start of transcription showed altered levels of DNA methylation in response to SIRT1 knockdown compared with control (*Figure 6.2A*). Table 6.1 summarises the data for CpG sites at which significant effects of SIRT1 expression level were measured. *CDC7* gene expression was also changed in response to SIRT1 manipulation. SIRT1 overexpression caused an increase in levels of *CDC7* transcript compared with the control ($p < 0.05$) and SIRT1 knockdown elicited the opposite response causing a decrease in levels of *CDC7* transcript compared with the control ($p < 0.05$); the data for the two extremes (overexpression and knockdown) also showed a statistically significant difference ($p < 0.001$) (*Figure 6.2B*).

CDC7 Sequence

-1000 CTATTTCCTC TGCTTCCACA CTTGCCCCTC TACAATCCAT TCTCTTCATA
-950 ACAGATAGAT CATATTACTC CCTTGCTTTA AAACTTTCAA ATAGCTTCCA
-900 ATTGTACTCA GAACAAACAC TAAACTTCTT ACCCTGGCTT TCAAGGACCC
-850 TGGTCTGGCT TCTGCCTAAC TCTCCACCTT CATCTATCTG GGACTATCTT
-800 GCGGCTCACT **CACTATGCTT CCCCCACACT GGCCTTTCCT GCCCTGCCCC**
-750 TGCAACATAC CAAGTTCCTC TTTCTCTCTG CATTTGCCCT ATCCTTTCTT
-700 TGCCAGGACA ACAGTCTCCC TACCAGCTCT TTCTCATCCA GGTCTCTTTG
-650 AGAGGGCTTC CCTGACCATC TAGATGCCAC CTTCCTGGTC AGTATTTCCC
-600 TCAAGTAGTA ATCAATGCCG GAAAGAATAC TGTTCATTTA TTCATCCGTT
-550 ATTGTCATCG CTTCATTGGA ATTTAGCTTC CTACAGGGAT GGTGTTTATC
-500 TTGCTCACTA TGATTCCAGC CCCTAGAAAA ACCCACCTAC CTCATAGCCA
-450 AGGGCTCAGT AAATAGTATA CACTGCCTTC CTGCCACTGT GCTAATTTCT
-400 ACTAACACAG CCACAAACAA TCAGCAATTA CATTTTCTGC TTGTTTTTAA
-350 CGGGGAAGTA GGGCACTCAA CGAAAAGGAA ATAAAAGCAG AGTCAAGAAA
-300 GTGCCTTTTA TCCATGGAGT GCCCAATGTG TTGTGCGGCC GGCCACGTAT
-250 AT**AGGGATGT GTCAGCACCT GAGATT**TTTC CTTCTCTGAG CTAGCTTCTT
-200 TCCTGGAAAT CATGCTGGGC CCTTAGCCTT ATGGTTCACC CTGTTTTTTA
-150 AGATCATCCA CGGGCTTCAT TCCCGTAACC GCTCTTCTAG CTGGCCAAGG
-100 CGGCGGGAAG AAACCCCACC CTCTTGCGCA AACGCCCAGT AG**CG**GAATC**C**
-50 **GCG**GGGT**CG**A GGGCTTTAGT GTG**CG**CATGT GCAACCAGAG **CG**G**CG**G**CG**G**G**
+1 **aagtgttgcg caggcg**catc cgatcgactc gg**taggtggg gatctcttgg**
+50 **aga**cggcgac ccaggcatct ggggagccac agaagtcgta ctcccttaaa
+100 cc**GTGAGTTT CCGACGGTTT GTT**CCATGGC GCGGGATTGT GAGGGATTAG
+150 GAACGAATTC TGGATCGTGA CTTCGGTTTT CTCGCCGTGC AGTTCCTTTT

Figure 6.1. The CDC7 sequence and related primers for use in the CDC7 pyrosequencing assay. *The CDC7 sequence taken from the human genome sequence is shown. Primers were designed for a PCR to a region in the CDC7 sequence (CDC7YF#1 – light blue and CDC7YR#1 – dark blue) and a nested PCR (CDC7F#2 – light green and CDC7R#2 – dark green) to focus in on eight specific CpG sites (pink) within the CDC7 sequence. A sequencing primer was designed for use in the pyrosequencing reaction (CDC7Seq - orange). Primers and annealing temperatures are given in Table 2.2C.*

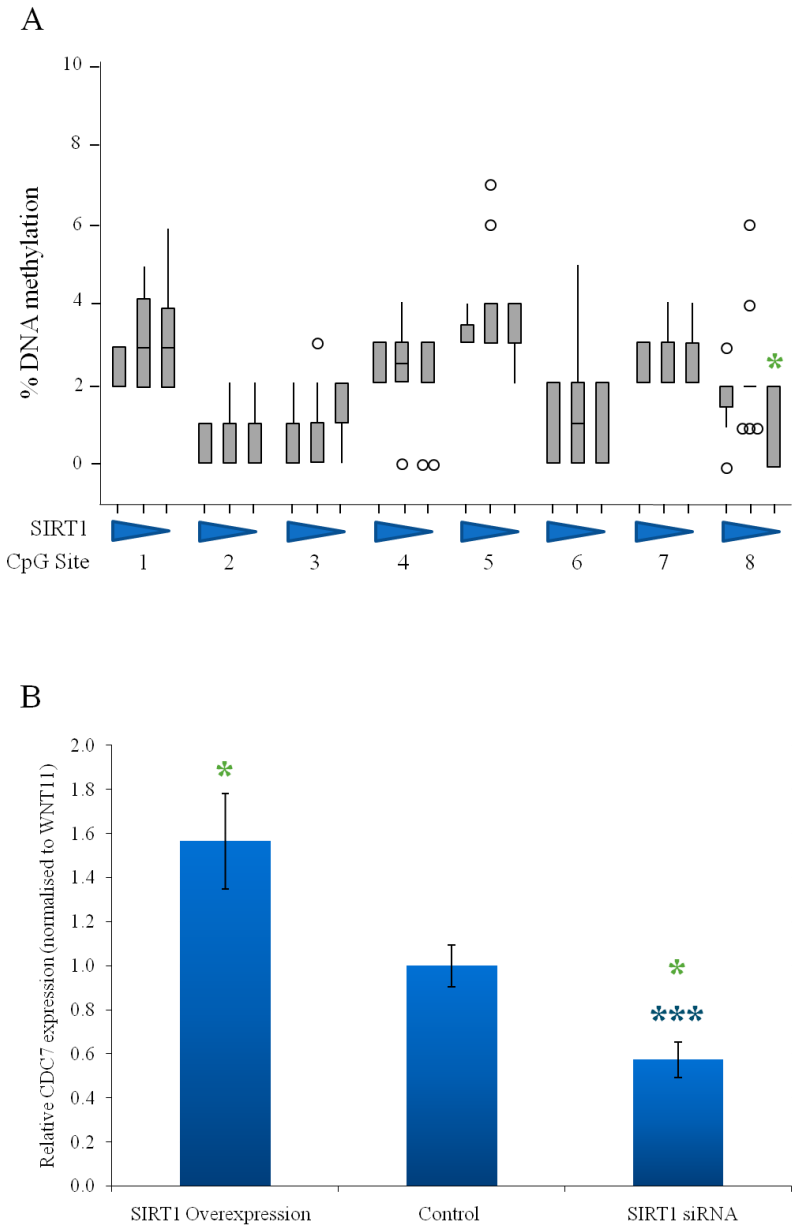

Figure 6.2. Effect of SIRT1 overexpression or SIRT1 knockdown by siRNA on A) percentage methylation at CpG sites within the CDC7 gene as measured by pyrosequencing and B) mRNA levels for CDC7 as measured by RT-qPCR. *A – Methylation is expressed as the percentage of unmethylated cytosines converted to thymines as a result of bisulfite modification determined by pyrosequencing. Data are medians ± upper and lower quartile ranges for each CpG site (n = 9). For the set of data corresponding to each CpG site the first (left-hand-most) bar corresponds to SIRT1 overexpression, the second to control and the third to SIRT1 knockdown as indicated by the triangular symbols beneath each set to indicate a progressive decrease in SIRT1 expression. Outliers are represented by ○. *p < 0.05, compared with control (green) by Kruskal Wallis then Dunn's multiple comparison. B – Gene expression is measured as the PCR cycle number at which the fluorescence signal increases above the background threshold (C_T values). Data are mean ± SEM (n = 9) normalised to the C_T value of the reference gene WNT11 measured in the same samples. *p < 0.05, ***p < 0.001 compared with control (green) or SIRT1 overexpression (blue) by one way ANOVA then Bonferroni's multiple comparison.*

6.2.2 Effects of SIRT1 manipulation on EIF5

Percentage DNA methylation was measured at eight consecutive CpG sites within the PCR amplified *EIF5* sequence spanning - 282 to + 20, occurring at -60, -58, -48, -41, -38, -32, -21 and -17 bp relative to the start of transcription of the *EIF5* sequence (*Figure 6.3* and Section 2.6.5). The first PCR generated a 949 bp product (EIF5YF#1 and EIF5YR#1) and the nested PCR generated a 302 bp product (EIF5F#2 and EIF5R#2). Pyrosequencing was carried out using the EIF5 sequencing primer (EIF5Seq). Standard curves for EIF5 can be found in Appendix C.

Total RNA was used to assess EIF5 expression at the mRNA level by RT-qPCR using primers specific to a 200 bp region of the *EIF5* gene (EIF5F and EIF5R) as described above. Primer sequences and annealing temperatures are outlined in Table 2.2D. Amplification and standard curves for EIF5 can be found in Appendix D.

The 1st, 2nd and 4th CpG site upstream of the *EIF5* transcript at positions -17, -21 and -38 relative to the start of transcription showed altered levels of DNA methylation in response to SIRT1 manipulation (*Figure 6.4A*). Table 6.1 summarises the data for CpG sites at which significant effects of SIRT1 expression level were measured. *EIF5* gene expression was also changed in response to SIRT1 manipulation. SIRT1 overexpression caused an increase in levels of *EIF5* transcript compared with the control ($p < 0.05$) and SIRT1 knockdown elicited the opposite response causing a decrease in levels of *EIF5* transcript compared with the control ($p < 0.05$); the data for the two extremes (overexpression and knockdown) also showed a statistically significant difference ($p < 0.001$) (*Figure 6.4B*).

EIF5 Sequence

-1000 TCCCAAAGTG CTGGGATTAC AGACGTGAGC CACCGCGACC GGCCTAAATA

-950 ATAGTAATTT TCAACGGAAT ACATTGGAAT CTCATTATAA ATGCCTGCTC

-900 TGGGCTACGA TTTGCTTATC AAAGAATTCA CAAGTCATAA ACTAGAGGGG

-850 GTGGACTCGA CGTGA**TGCCC ACTAGGAGAA AGGTG**ACAAG AGAAGCACGA

-800 AGGATAGCGC TTTTCAACCC TGGGAGAGCA GGGAGGCCTT CACCAGAAGG

-750 TGGGAACCCA CCACGAAGCG CCTTCAGGAG GCCCCAGGAT TCCAAACCAA

-700 TTAAGGGCCT CCTCTTCCGA AAACGGGAGG CGACGCGCTG AGCTAAGCGC

-650 GCAGGCTGGG TTGCGGGCCG ACACCGAGGC GGCGCGGCCT CGCGACCGCC

-600 CTGGGCGGTC ACTGGCGAGT CACGGACTCG TTCCGCCAGC GGCCAATCCA

-550 CCCCGAGTCC GAAACAGAAG ACGTCCCTGG GATGAAAGAC CCAGGCCTGG

-500 GGCTTAAGGT GGAAAAACAA CTCATTCCTC GAGGCCCGGA GTCGGGCGTC

-450 CCGGGAGAAC GGGAAAGGGA GATGAGCGCC CGCTGCGGGG AGAACGCGGT

-400 CGGGTTCCTC TCCCCGAAGG TGGCAGCCGC AAAAACACGG CCTCGAAAGC

-350 AGTTTCGAGG ACGATGGCTC CTGCGTCCCG GGAGTCGCCA TGACGCCGCG

-300 GCCTGTCCCA GACCCGGC**GA GGGAGGGGAC CAACCACCAT** CTCCCCCTCA

-250 AGGCCCAAAC CGACAAAGAA CGGCCCCCGG TACCCCGGCC CCGCCACCAG

-200 GGCCACTCCG GGTCTCGCGA GACCCAAGGG CTGCGCCGCG AAGACCTCTG

-150 GGAAAGGCGG GGGGAGGGGA GAGGAAGGAA GCGAGACCGG GGCTGGAGGC

-100 GGGCCGAGGC CGCGAGTTGA GCCTCAGGAA GCAGAAGGGG **CGCG**GAAAGA

-50 TG**CG**ATTGA**C** **G**T**CG**CAAG**CG** AACCAATGA**C** **G**AG**CG**AGCTG TGGCAGGCCT

+1 **ccagccaatg ggcagtgagg** cctgacgcgg ggggcggacg ctggggccga

+50 gggtagcttg agcgcggcgg cggcgttgtt cagtcagagc gaga**acattc**

+100 **cagagGTGAG TCCGG**TGAAG GGGCGGCCCC CTGCCCGGTG CTTCCCGCCC

+150 CCTCGACCCC TCGGGCCGCT GGCTGGCGGG GAAGGTGCAC TCCCCGACCG

Figure 6.3. The EIF5 sequence and related primers for use in the EIF5 pyrosequencing assay. *The EIF5 sequence taken from the human genome sequence is shown. Primers were designed for a PCR to a region in the EIF5 sequence (EIF5YF#1 – light blue and EIF5YR#1 – dark blue) and a nested PCR (EIF5F#2 – light green and EIF5R#2 – dark green) to focus in on eight specific CpG sites (pink) within the EIF5 sequence. A sequencing primer was designed for use in the pyrosequencing reaction (EIF5Seq - orange). Primers and annealing temperatures are given in Table 2.2C.*

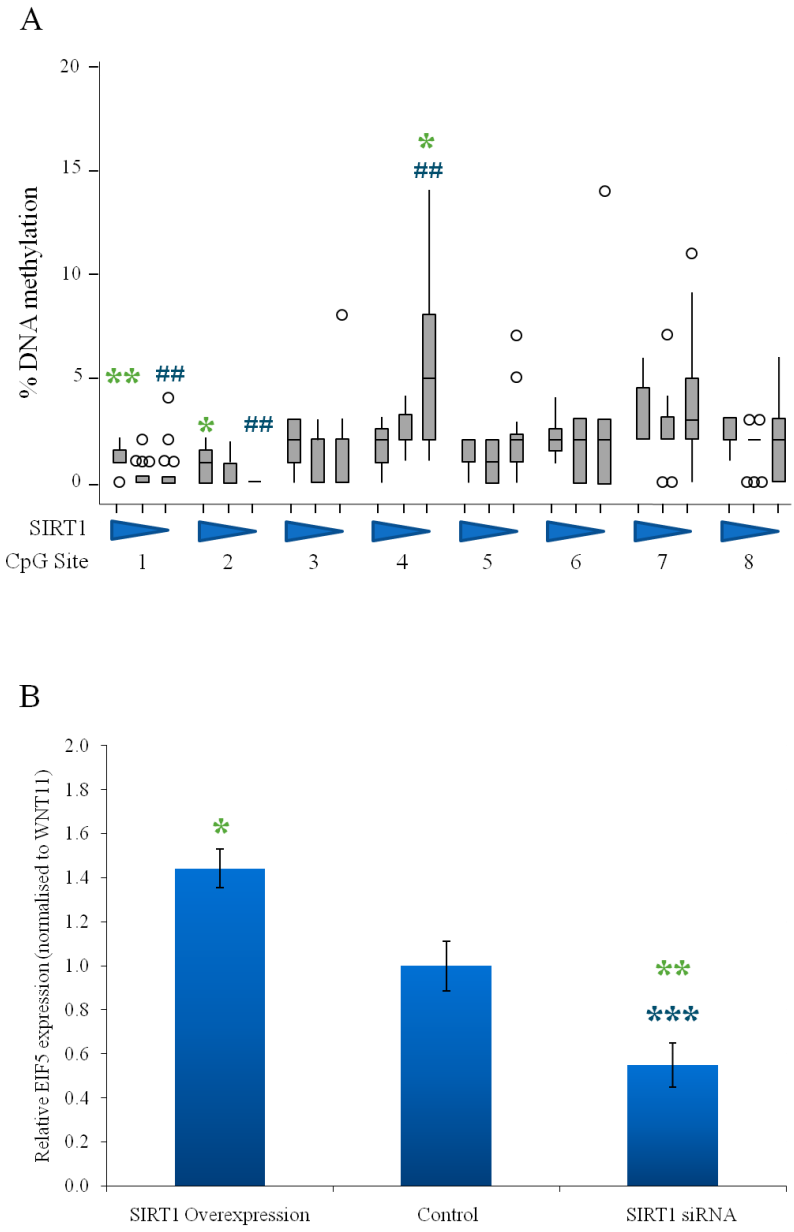

Figure 6.4. Effect of SIRT1 overexpression or SIRT1 knockdown by siRNA on A) percentage methylation at CpG sites within the EIF5 gene as measured by pyrosequencing and B) mRNA levels for EIF5 as measured by RT-qPCR. *A – Methylation is expressed as the percentage of unmethylated cytosines converted to thymines as a result of bisulfite modification determined by pyrosequencing. Data are medians ± upper and lower quartile ranges for each CpG site (n = 9). For the set of data corresponding to each CpG site the first (left-hand-most) bar corresponds to SIRT1 overexpression, the second to control and the third to SIRT1 knockdown as indicated by the triangular symbols beneath each set to indicate a progressive decrease in SIRT1 expression. Outliers are represented by ○. *p < 0.05, **p < 0.01 compared with control (green); $^{\#}p < 0.05$, $^{\#\#}p < 0.01$ compared with SIRT1 overexpression (blue), by Kruskal Wallis then Dunn's multiple comparison. B – Gene expression is measured as the PCR cycle number at which the fluorescence signal increases above the background threshold (C_T values). Data are mean ± SEM (n = 9) normalised to the C_T value of the reference gene WNT11 measured in the same samples. *p < 0.05, **p < 0.01, ***p < 0.001 compared with control (green) or SIRT1 overexpression (blue) by one way ANOVA then Bonferroni's multiple comparison.*

6.2.3 Effects of SIRT1 manipulation on IRX3

Percentage DNA methylation was measured at three consecutive CpG sites within the PCR amplified *IRX3* sequence spanning - 426 to + 11, occurring at - 64, - 19 and - 16 bp relative to the start of transcription of the *IRX3* sequence (*Figure 6.5* and Section 2.6.6). The first PCR generated a 993 bp product (IRX3YF#1 and IRX3YR#1) and the nested PCR generated a 437 bp product (IRX3F#2 and IRX3R#2). Pyrosequencing was carried out using the IRX3 sequencing primer (IRX3Seq). Standard curves for IRX3 can be found in Appendix C.

Total RNA was used to assess IRX3 expression at the mRNA level by RT-qPCR using primers specific to a 150 bp region of the *IRX3* gene (IRX3F and IRX3R) as described above. Primer sequences and annealing temperatures are outlined in Table 2.2D. Amplification and standard curves for IRX3 can be found in Appendix D.

The 1st and 3rd CpG site upstream of the *IRX3* transcript at positions -16 and -64 relative to the start of transcription showed altered levels of DNA methylation in response to SIRT1 manipulation (*Figure 6.6A*). Table 6.1 summarises the data for CpG sites at which significant effects of SIRT1 expression level were measured. *IRX3* gene expression changed in response to SIRT1 manipulation. SIRT1 knockdown caused a decrease in levels of *IRX3* transcript compared with SIRT1 overexpression ($p < 0.05$) (*Figure 6.6B*).

IRX3 Sequence

-1000 CCAAACACTC CCTACAACTT CTTCAAGTCA AACTTGGGCA AGGTTGGCTG

-950 GCTGACTGCG AGAGGAAAAA GAGGGCGCGG AGGGGGCGCG GCGCGCGGCC

-900 GGGTGTAGAG GCCACGGAGG CGAGGCGCCG AGCGTCCCCT TTGTCCTGTA

-850 GAGGGAGCTC CAGCCCCAAA TTTCCCTGCT GCCTCCCCCG GCCCGCCCAC

-800 CCCAGGCCCG CCTGGAGCCG GAATCCCGGC TGGAAAGGTG CGGCGGTCTG

-750 ACACCCCCGC AACCCCCGCG CCGGGGCCTT AGCAGGATGC CTCTTCTAGG

-700 GCACGTGGGA AAACCCACCA GGGTGCCAAG ACGCACAGAT GCTCCCAGGA

-650 CCCGGGCTCC CCAACTCTCA ACTAGAGCTG GGCAGTCACA CATCATCTAG

-600 AGGATTATGT ACCCCTAGGC GACCCTCTTC TCCATATCCG CCTCCACCGT

-550 CACCCCACAC CCTGGCATCT ATAAAGAGGG AAGGGGGGCA ACCGGGTTGG

-500 AAGGAGGATG GAATCTGGGC TTGCACAGCC TCTTATAGGT AACAGTGAGA

-450 AAGCCTCAAC TGTGTCGATC AAAGAATGGG GACGAAGGGA GTGATGAGAA

-400 CACGACCCCG CCACCCGCGC AGGCTAACCC CGTTGTGTCC AGACCCTTCT

-350 CTAAATCTCT TGGCAAGGTC ACCAGAGAAG GATCCAAGCC CCCGCGGTTG

-300 CTCCCGTAGA CAAGCGGGTC GGGCCCAGAT TCCCGGCTCT CAGCAAAGAA

-250 GCTTGCCGGG GTCTCCCACC TGTCTCCTGC TCCCGTTTTC TCGGCCGCCC

-200 CAGGTACTTT TCCAGCCACC TCTCCTGCTG CGGCGCCCCC AGCCCCGCCA

-150 CTTCTGCGCC TCCTCAGCTA TTGCTGTCCT TTGACTACTC GGTCCCGATT

-100 CGTCTCTCGT CCTTTCCCGC GAATTCTTCA AACAACCGAG GGGAGAAAAA

-50 ACCCAAAAAA CAAAAAACCA CCAAACAGAT CCGTCGAGGG GGCAGACAGG

+1 cgggttatag tcaaagtggc agcagctcat ttatttagcc aaaaatagat

+50 actttctcgt acaatttggt tcacacatat gtacatttct ctgtatatat

+100 acacacacac aaaggcagac acgtttattc tcactgaaac tccacccccc

+150 aaaatcaacc ggacaaacaa acctcacagc gaatgcgggg tgccacagaa

Figure 6.5. The IRX3 sequence and related primers for use in the IRX3 pyrosequencing assay. *The IRX3 sequence taken from the human genome sequence is shown. Primers were designed for a PCR to a region in the IRX3 sequence (IRX3YF#1 – light blue and IRX3YR#1 – dark blue) and a nested PCR (IRX3F#2 – light green and IRX3R#2 – dark green) to focus in on three specific CpG sites (pink) within the IRX3 sequence. A sequencing primer was designed for use in the pyrosequencing reaction (IRX3Seq - range). Primers and annealing temperatures are given in Table 2.2C.*

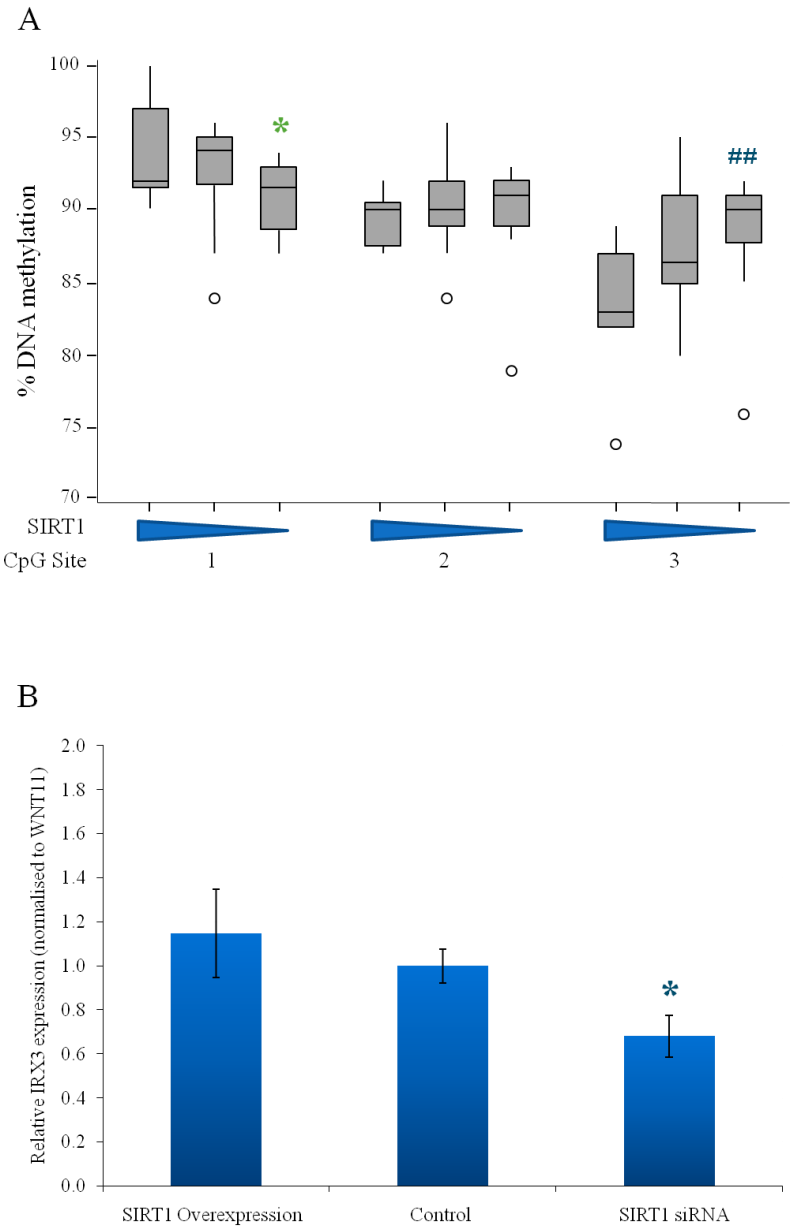

Figure 6.6. Effect of SIRT1 overexpression or SIRT1 knockdown by siRNA on A) percentage methylation at CpG sites within the IRX3 gene as measured by pyrosequencing and B) mRNA levels for IRX3 as measured by RT-qPCR. *A – Methylation is expressed as the percentage of unmethylated cytosines converted to thymines as a result of bisulfite modification determined by pyrosequencing. Data are medians ± upper and lower quartile ranges for each CpG site (n = 9). For the set of data corresponding to each CpG site the first (left-hand-most) bar corresponds to SIRT1 overexpression, the second to control and the third to SIRT1 knockdown as indicated by the triangular symbols beneath each set to indicate a progressive decrease in SIRT1 expression. Outliers are represented by ○. *p < 0.05, **p < 0.01 compared with control (green); $^{\#}p < 0.05$, $^{\#\#}p < 0.01$ compared with SIRT1 overexpression (blue), by Kruskal Wallis then Dunn's multiple comparison. B – Gene expression is measured as the PCR cycle number at which the fluorescence signal increases above the background threshold (C_T values). Data are mean ± SEM (n = 9) normalised to the C_T value of the reference gene WNT11 measured in the same samples. *p< 0.05 compared with SIRT1 overexpression (blue) by one way ANOVA then Bonferroni's multiple comparison.*

6.2.4 Effects of SIRT1 manipulation on KLF3

Percentage DNA methylation was measured at six consecutive CpG sites within the PCR amplified *KLF3* sequence spanning - 238 to + 71, occurring at -69, -60, -56, -52, -50 and -47 bp relative to the start of transcription of the *KLF3* sequence (*Figure 6.7* and Section 2.6.7). The first PCR generated a 904 bp product (KLF3YF#1 and KLF3YR#1) and the nested PCR generated a 309 bp product (KLF3F#2 and KLF3R#2). Pyrosequencing was carried out using the KLF3 sequencing primer (KLF3Seq). Standard curves for KLF3 can be found in Appendix C.

Total RNA was used to assess KLF3 expression at the mRNA level by RT-qPCR using primers specific to a 166 bp region of the *KLF3* gene (KLF3F and KLF3R) as described above. Primer sequences and annealing temperatures are outlined in Table 2.2D. Amplification and standard curves for KLF3 can be found in Appendix D.

The 3rd CpG site upstream of the *KLF3* transcript at position -52 relative to the start of transcription showed altered levels of DNA methylation in response to SIRT1 overexpression compared with control (*Figure 6.8A*). Table 6.1 summarises the data for CpG sites at which significant effects of SIRT1 expression level were measured. *KLF3* gene expression was also changed in response to SIRT1 manipulation. SIRT1 overexpression caused an increase in levels of *KLF3* transcript compared with the control ($p < 0.001$) and SIRT1 knockdown elicited the opposite response causing a decrease in levels of *KLF3* transcript compared with the control ($p < 0.05$); the data for the two extremes (overexpression and knockdown) also showed a statistically significant difference ($p < 0.001$) (*Figure 6.8B*).

KLF3 Sequence

-1000 GTTTGCCAAG TTTCCAGGCA AGCCCAACTG CGCAAATGCC GCTTTTTAGC
-950 TCCAGCGGCA GGCCTGGCCC GTGGGAGTTT TGCCCCAGGG GTCTCCGGGC
-900 CTTCAAAGAA AAGTCCCACG AGGTGGGGGG CGCCGCCTGG GCCGCCGGCC
-850 AGGGGGACCC GTCGCCCCAG GGCACAAAGA AAGAGCGCGC CTACAGGGTG
-800 TCCCCTGACC CCGGCGACTC GGGGCCAGGG AGGCTCGGCG CGCCCCAGCG
-750 GCCGCTCTTC CCCTCCCGAA CCCGCCCGGC CCACTCGCTC CTGCACCGCG
-700 GCCGCCTCGG CTCGGCTTTT CTCTTGCAGT GAGCTGAGTG CGCTCAGCCG
-650 AGGAGGGGCC GCGCCGCGCC GCGCCGGCCG CGGGGCCCAG CCCTTCCCGC
-600 CGCGCCCGGG GCCGCCCTTC CCGCTGGAGC CGGCTGATCG ATGGCCCTGG
-550 CAGCCCGCGC CCCCCGCCTC GGCTCGCCCG CGAGCCCGGC TGTGTGTTTT
-500 GGAAGCAGCG CAGCGGGCCG CAGCCGTGTG ACGCCCGGAG CGGGCAGCGC
-450 CGCCCTTCCT TCCCCCCGGG CTCGGGCGGC GGCGCGGCGG CTGGGCCGGG
-400 CGGGAGGGCT GGCGGGGCGC GGACTCCGGG GAGGAGGGCG CGGGGAGGGG
-350 ACGCGGGCGG GGACGCGGGC GGGGGGCGGA GGCCGCGCCG CGCACGCCCA
-300 GCCCCACGGC CGCGCCGCGC CTCGTGGGAC AGGTTGGGCC GGCGGGGCGG
-250 CGCCCGGCTC CGGGGAATAA TGAGTGTCTG TCAGGCCGTC CCCGGGTGAC
-200 TGGGCGGGGC GGGGCGGAGG CGGCGCGGGA GGCGGGGGTG GCGGGGGAAG
-150 GGCGCAGGGC GGGGTGCGTG TTTGCGCGAG TGACTCGGCC GACCCCTCCG
-100 GCGGCTGCCT CCACCCAAGT GGGTGGGGAC CCGCCCAGCC CGGGCGGCCG
-50 CGGCGGCTCC CTCTCCCCTC CCTGACCCTC CCACCCCGGG TCCCAGCCTC
+1 tacttacccc gccagccccg ggaggctcgc agagcgagcg gcgccggcgt
+50 catgtgactg cccggagttg gtgccaggag ccagagggga gccaggagcg
+100 gagccgcgcg gagccggggc ccgagccgga gcgcagcgag agcgcccgcc
+150 gcacgcgcgc ccgtccccgt cccctgcggc cgccaacgcc gcccggactg

Figure 6.7. The KLF3 sequence and related primers for use in the KLF3 pyrosequencing assay. *The KLF3 sequence taken from the human genome sequence is shown. Primers were designed for a PCR to a region in the KLF3 sequence (KLF3YF#1 – light blue and KLF3YR#1 – dark blue) and a nested PCR (KLF3F#2 – light green and KLF3R#2 – dark green) to focus in on six specific CpG sites (pink) within the KLF3 sequence. A sequencing primer was designed for use in the pyrosequencing reaction (KLF3Seq - orange). Primers and annealing temperatures are given in Table 2.2C.*

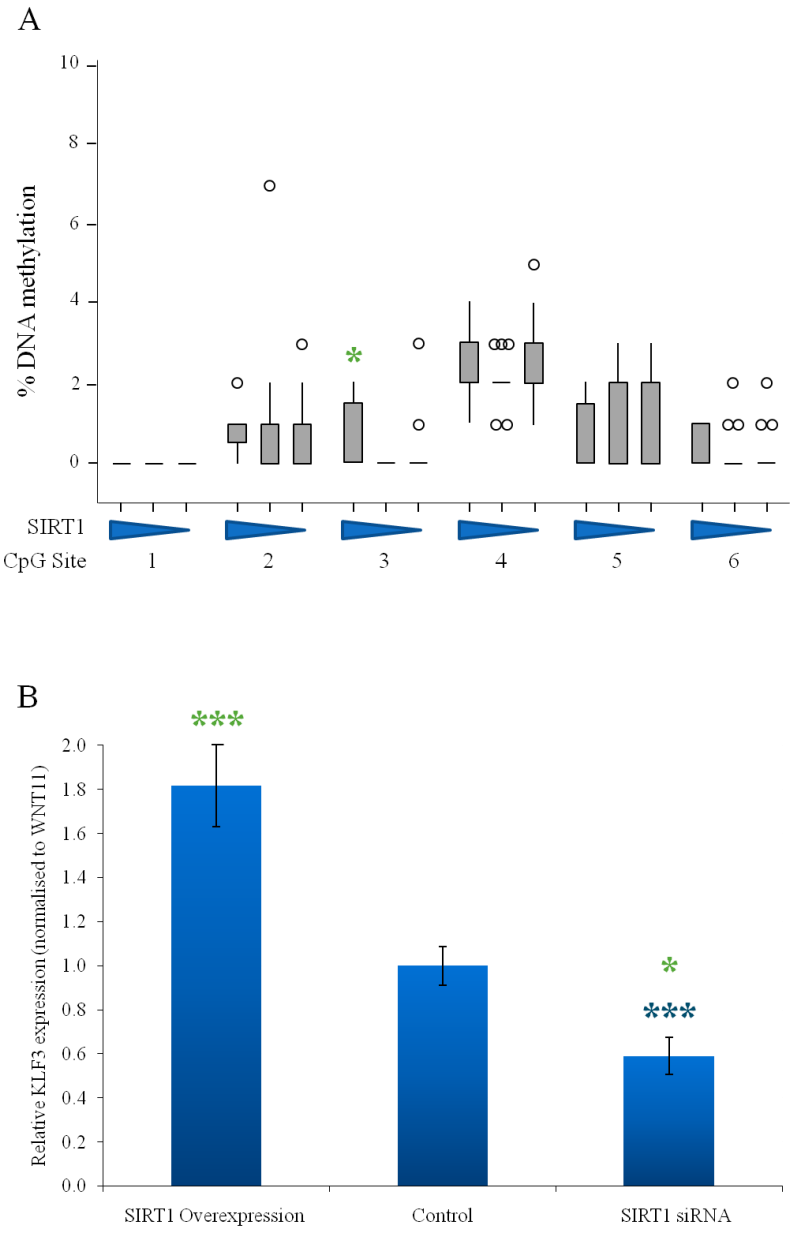

Figure 6.8. Effect of SIRT1 overexpression or SIRT1 knockdown by siRNA on A) percentage methylation at CpG sites within the KLF3 gene as measured by pyrosequencing and B) mRNA levels for KLF3 as measured by RT-qPCR. *A – Methylation is expressed as the percentage of unmethylated cytosines converted to thymines as a result of bisulfite modification determined by pyrosequencing. Data are medians ± upper and lower quartile ranges for each CpG site (n = 9). For the set of data corresponding to each CpG site the first (left-hand-most) bar corresponds to SIRT1 overexpression, the second to control and the third to SIRT1 knockdown as indicated by the triangular symbols beneath each set to indicate a progressive decrease in SIRT1 expression. Outliers are represented by ○.*p < 0.05, **p < 0.01 compared with control (green); $^{\#}p < 0.05$, $^{\#\#}p < 0.01$ compared with SIRT1 overexpression (blue), by Kruskal Wallis then Dunn's multiple comparison. B – Gene expression is measured as the PCR cycle number at which the fluorescence signal increases above the background threshold (C_T values). Data are mean ± SEM (n = 9) normalised to the C_T value of the reference gene WNT11 measured in the same samples. *p < 0.05, ***p < 0.001 compared with control (green) or SIRT1 overexpression (blue) by one way ANOVA then Bonferroni's multiple comparison.*

6.2.5 Effects of SIRT1 manipulation on PCTY1A

Percentage DNA methylation was measured at two consecutive CpG sites within the PCR amplified *PCYT1A* sequence spanning - 369 to + 64, occurring at - 88 and - 21 bp relative to the start of transcription of the *PCYT1A* sequence (*Figure 6.9* and Section 2.6.10). The first PCR generated a 939 bp product (PCYT1AYF#1 and PCYT1AYR#1) and the nested PCR generated a 433 bp product (PCYT1A F#2 and PCYT1A R#2). Pyrosequencing was carried out using the PCYT1A sequencing primer (PCYT1A Seq). Standard curves for PCYT1A can be found in Appendix C.

Total RNA was used to assess PCYT1A expression at the mRNA level by RT-qPCR using primers specific to a 168 bp region of the *PCYT1A* gene (PCYT1A F and PCYT1A R) as described above. Primer sequences and annealing temperatures are outlined in Table 2.2D. Amplification and standard curves for PCYT1A can be found in Appendix D.

No statistically significant effect was measured in DNA methylation levels at either of the 2 CpG site assayed upstream of the *PCYT1A* transcript in response to altered SIRT1 expression levels ($p > 0.05$) (*Figure 6.10A*). Table 6.1 summarises the data for CpG sites at which significant effects of SIRT1 expression level were measured. *PCYT1A* gene expression was changed in response to SIRT1 manipulation. SIRT1 knockdown caused a decrease in levels of *PCYT1A* transcript compared with the control ($p < 0.01$), the difference between the two extremes (overexpression and knockdown) was also statistically significant ($p < 0.001$) (*Figure 6.10B*).

PCYT1A Sequence

-1000 GAGGAGCAGC AGAGGGAGGT CCCTGCCAGC TGCAGCTCTC AGAGGAAAAG
-950 AAAGATGTGG AGCACTGGTT CCAGGGAAGA ATGTTCTGAA GAGGGACAGA
-900 GGTCAAGGTG ATAAGGCTGT TGCTTTAGAA AGGAAGGTGT TTCCTATGCT
-850 TTTGCCTTTA CATTCTGTGC AAATCTCTCT AATATGGCTA TGACCAAAAT
-800 GGATTAACAT CAAGTTCCAA CAGCAGACAT TTACAAAGTA TCCTTTGTAA
-750 AAGGCTAGGT AATATTAATA GCATTCAAAT AGGAGTAGCA GGGCCAGGCA
-700 CTTACTCCCA GTAGGAAACT AATCTCAATC GACTTGGTAT AGGATTGAGT
-650 ATTGTCCCGC TCCTCTCCTC ATCATTGTAA CTCTAAAAGT GTTCCTTCCT
-600 TCGAAGGTAG ATGGCACGAA AGAGACTGAC AAAAGCTCCC AAAGAACTGG
-550 GTCACAGAGT TTTCTGAGAA GATGAACACA GCAGAAACAC TGCAGTTGAT
-500 GCCATGGGTC TGCTTCCATC CCCATCAGTG TCTTCATGGA CCCCATTGGG
-450 TCCAACAAGA AACTCCTCAG GGAGTAAGAA AAGTTAGGTT CAGATCTCCT
-400 TCCCGCAGCC ACAATGACAC TGGTGACAGC AGTACGTTCA GGGGATTTGT
-350 GACTGTAACT CTGCTTTTCG CTTTTCCTTA AGGAAATCAA AATTAAGATA
-300 TTTCTCCACA AATTACCCAT CAGCGTGGCT CATTTCGTGA AGGACTTGGC
-150 AAGCCACATA GCTTCAGAAC GGAAGGCAAA TGCTATAGTA TACCGGGAAG
-100 AAAAGGCCTC TGCGTATTAC ACTACCTCCT TCTTCTGCCC ACTCCTCAGG
-50 GGCAAAAAAT TAGTTCTACA TTTGAAAGAC GAATTTTTTA AAAAATTAAT
+1 gaaaatgaca attccctgt tgagatcacg tgaacataaa cagtgaaaca
+50 aagcccttgg gggggggtaa atggatgcag agcaggcttc taaggtgcag
+100 tccccctcct tcgtgtgggt gagtgatgtc acttgcagga caggctgttt
+150 gggttccccc agtcctaggt cttctttccc cagttgtctt tcctttgtag

Figure 6.9. The PCYT1A sequence and related primers for use in the PCYT1A pyrosequencing assay. *The PCYT1A sequence taken from the human genome sequence is shown. Primers were designed for a PCR to a region in the PCYT1A sequence (PCYT1AYF#1 – light blue and PCYT1AYR#1 – dark blue) and a nested PCR (PCYT1AF#2 – light green and PCYT1AR#2 – dark green) to focus in on two specific CpG sites (pink) within the PCYT1A sequence. A sequencing primer was designed for use in the pyrosequencing reaction (PCYT1ASeq - orange). Primers and annealing temperatures are given in Table 2.2C.*

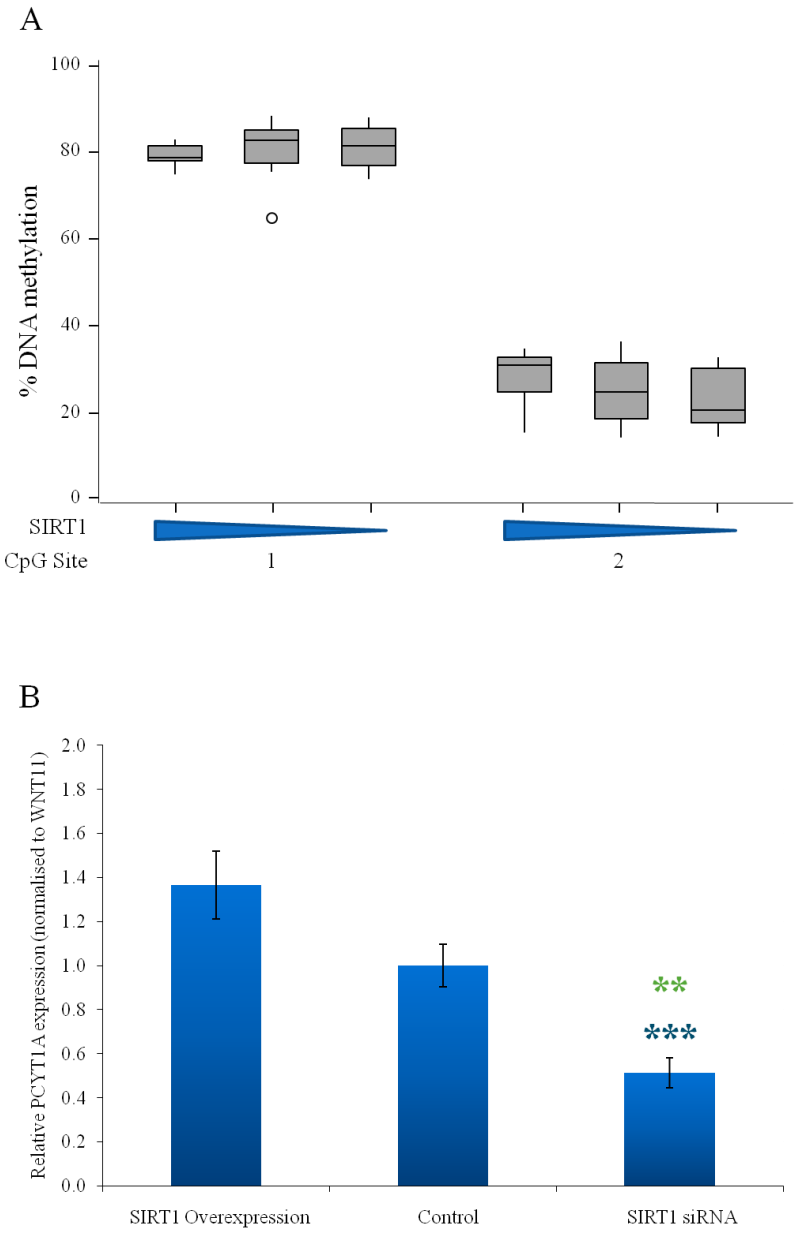

Figure 6.10. Effect of SIRT1 overexpression or SIRT1 knockdown by siRNA on A) percentage methylation at CpG sites within the PCYT1A gene as measured by pyrosequencing and B) mRNA levels for PCTY1A as measured by RT-qPCR. *A – Methylation is expressed as the percentage of unmethylated cytosines converted to thymines as a result of bisulfite modification determined by pyrosequencing. Data are medians ± upper and lower quartile ranges for each CpG site (n = 9). For the set of data corresponding to each CpG site the first (left-hand-most) bar corresponds to SIRT1 overexpression, the second to control and the third to SIRT1 knockdown as indicated by the triangular symbols beneath each set to indicate a progressive decrease in SIRT1 expression. Outliers are represented by ○. p > 0.05 compared between SIRT1 overexpression, control and SIRT1 knockdown by Kruskal Wallis then Dunn's multiple comparison. B – Gene expression is measured as the PCR cycle number at which the fluorescence signal increases above the background threshold (C_T values). Data are mean ± SEM (n = 9) normalised to the C_T value of the reference gene WNT11 measured in the same samples. **p < 0.01, ***p < 0.001 compared with control (green) or SIRT1 overexpression (blue) by one way ANOVA then Bonferroni's multiple comparison.*

6.2.6 Effects of SIRT1 manipulation on PTPRG

Percentage DNA methylation was measured at nine consecutive CpG sites within the PCR amplified *PTPRG* sequence spanning - 472 to + 29, occurring at - 72, - 66, - 64, - 62, - 51, - 47, - 39, - 35 and - 32 bp relative to the start of transcription of the *PTPRG* sequence (*Figure 6.11* and Section 2.6.11). The first PCR generated a 917 bp product (PTPRGYF#1 and PTPRGYR#1) and the second, nested PCR generated PCR generating a 501 bp product, (PTPRGF#2 and PTPRGR#2). Pyrosequencing was carried out using the PTPRG sequencing primer (PTPRGSeq). Standard curves for PTPRG can be found in Appendix C.

Total RNA was used to assess PTPRG expression at the mRNA level by RT-qPCR using primers specific to a 205 bp region of the *PTPRG* gene (PTPRG F and PTPRG R) as described above. Primer sequences and annealing temperatures are outlined in Table 2.2D. Amplification and standard curves for PTPRG can be found in Appendix D.

The 9th CpG site upstream of the *PTPRG* transcript at position -72 relative to the start of transcription showed altered levels of DNA methylation in response to SIRT1 manipulation (*Figure 6.12A*). Table 6.1 summarises the data for CpG sites at which significant effects of SIRT1 expression level were measured. *PTPRG* gene expression was also changed in response to SIRT1 manipulation. SIRT1 overexpression caused an increase in levels of *PTPRG* transcript compared with the control ($p < 0.05$) and SIRT1 knockdown elicited the opposite response causing a decrease in levels of *PTPRG* transcript compared with the control ($p < 0.05$); the data for the two extremes (overexpression and knockdown) also showed a statistically significant difference ($p < 0.001$) (*Figure 6.12B*).

PTPRG Sequence

-1000 CTTAGAAGTC TAAGCGATAA AGATCTTCTT ACCGAGAGCC AAGGGACAAA
-950 ACTCATTACA GATAAGCCTA GTCCTCCCAT TTCCCCCGGA CGCCTCTCCC
-900 CGATTGCTAA AGAAGCAGCC GCTCCCCGGG TAGCTGCCAG GAAATCAGTC
-850 CGGCCCCGCG GCGCTGCTTT CACCCTGCAG GGTGTAAGAG GCGCACTTCC
-800 TGCGCCCTCC CCGCGGCCAA ACCGGGGTGC GGGAACCTTC TCCAGAGAAG
-750 CTGCGAGTTG GGGAAACTCC GCCACCGATC CATCGTGGCG CCGGGAAAGG
-700 GGATGCGGGG CTCGGAAGGG CTAGATTTCG CAATCCTGGG ATCGACATTC
-650 CTCCCCTCCC CCACTTTCCC CAGCCTTGGA CTGGGCCAAT GAAAGCCCGA
-600 AAAAGAAAAA AAAAAAAAAT TAAATCTCAA TGTAGCCGGA GTGCAAAGGC
-550 CGCTCGGCTT TGTTTCCCGG CGGGGGAATG CGCTGTGTTG GAGGCGCGAA
-500 CAGGAGCCGC AGACGGTGAG CCTCACCGCT GCAAATGCCA GGGCAGTGAA
-450 GCCGAACAGA AAACCCCATC GCTTTAAAAA GGCAGCTGTC CGCCCTCCCC
-400 CTTTCCCCTC GCCAGGGCGA GGGGCCCCTC AAGTCCGGGA TCCGCGAGCT
-350 GCGCGGAGGA TCTCGCCAAA CCCGAGCACC GTGCGGCGTC TTTTAAGAGC
-300 TCGAACAACG GGAATCCAGC AAAAAACAAG CCGGCCCCAG AAGGCAGCCT
-250 CCCTCCTCTC TCCGCGCACG GGCTACAATC GCCCCCAGTC CCCAAACTGT
-200 CCCAGTAGAG GCCGCGCGGA GAGAGCAGAG CCGAGGGACC CAGCGCAAGG
-150 CGGGAGCCAA GCGCGGCTGC TTTAAGAACG CGGAGAGCGC GCGCCCGCCG
-100 CCAGCTGGCC CGGGCTGCGC GCCCCCGCCG CCACCGCGCG CCCCCTGTTC
-50 GCTCGCTCCT TCGCTCGCCG GCTTTAAAGT CTCTGCCAGG ATCCATGCTC
+1 acatgttact tcctgtatgg aggcatggcc agtttccagc cccgcgctct
+50 tcgttccttc ccagcctgcg ccggagccac aactttcagg agcatggact
+100 gaaggcgccc tcgccccagc gcccctctga gatcctttgt gttttcctcc
+150 gtttccctccg gccgtttcta ttttgggggg ctctccgctc cccctgcctc

Figure 6.11. The PTPRG sequence and related primers for use in the PTPRG pyrosequencing assay. *The PTPRG sequence taken from the human genome sequence is shown. Primers were designed for a PCR to a region in the PTPRG sequence (PTPRGYF#1 – light blue and PTPRGYR#1 – dark blue) and a nested PCR (PTPRGF#2 – light green and PTPRGR#2 – dark green) to focus in on nine specific CpG sites (pink) within the PTPRG sequence. A sequencing primer was designed for use in the pyrosequencing reaction (PTPRGSeq - orange). Primers and annealing temperatures are given in Table 2.2C.*

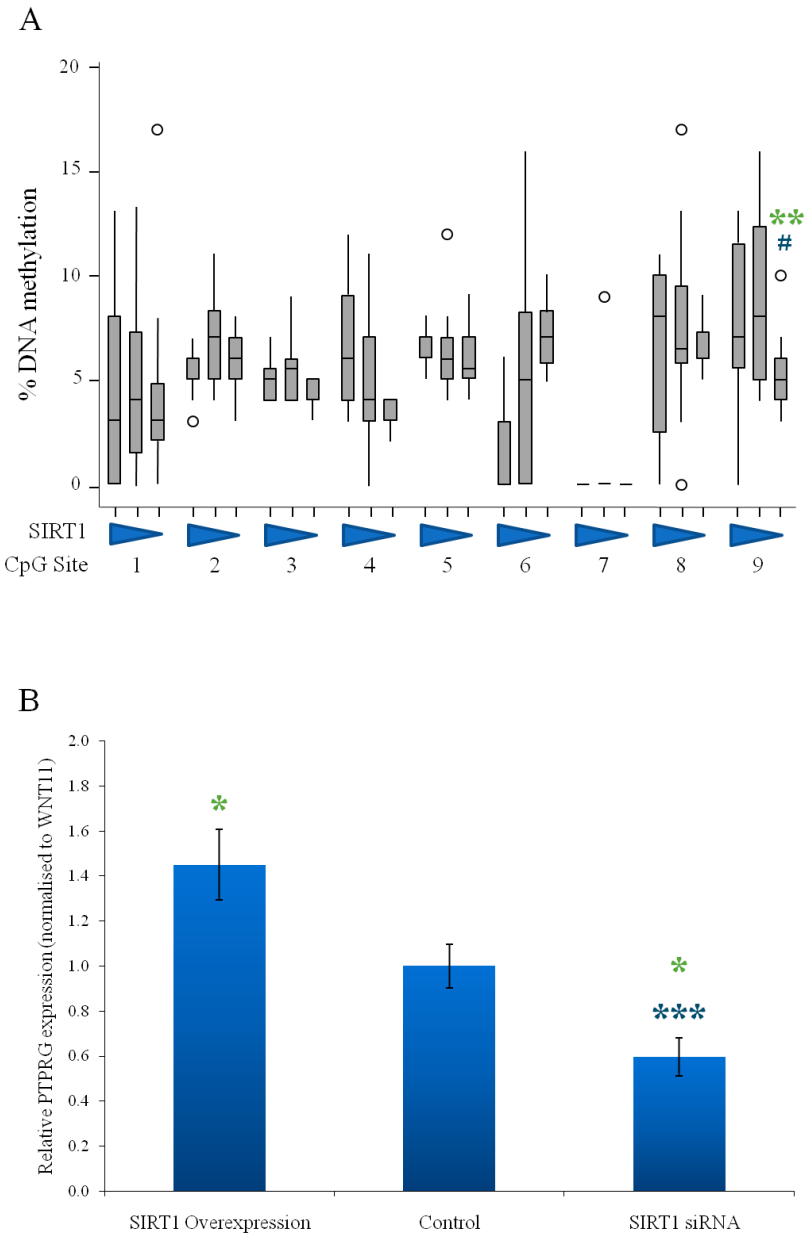

Figure 6.12. Effect of SIRT1 overexpression or SIRT1 knockdown by siRNA on A) percentage methylation at CpG sites within the PTPRG gene as measured by pyrosequencing and B) mRNA levels for PTPRG as measured by RT-qPCR. *A – Methylation is expressed as the percentage of unmethylated cytosines converted to thymines as a result of bisulfite modification determined by pyrosequencing. Data are medians ± upper and lower quartile ranges for each CpG site (n = 9). For the set of data corresponding to each CpG site the first (left-hand-most) bar corresponds to SIRT1 overexpression, the second to control and the third to SIRT1 knockdown as indicated by the triangular symbols beneath each set to indicate a progressive decrease in SIRT1 expression. Outliers are represented by ○. *p < 0.05, **p < 0.01 compared with control (green); $^{\#}p < 0.05$, $^{\#\#}p < 0.01$ compared with SIRT1 overexpression (blue), by Kruskal Wallis then Dunn's multiple comparison. B – Gene expression is measured as the PCR cycle number at which the fluorescence signal increases above the background threshold (C_T values). Data are mean ± SEM (n = 9) normalised to the C_T value of the reference gene WNT11 measured in the same samples. *p < 0.05, **p < 0.01, ***p < 0.001 compared with control (green) or SIRT1 overexpression (blue) by one way ANOVA then Bonferroni's multiple comparison.*

6.2.7 Effects of SIRT1 manipulation on SLC39A4

Percentage DNA methylation was measured at three consecutive CpG sites within the PCR amplified *SLC39A4* sequence spanning - 242 to + 39, occurring at - 91, - 81 and - 61 bp relative to the start of transcription of the *SLC39A4* sequence (*Figure 6.13* and Section 2.6.12). The first PCR generated a 900 bp product (SLC39A4YF#1 and SLC39A4YR#1) and the nested PCR generated PCR generating a 281 bp product, (SLC39A4F#2 and SLC39A4R#2). Pyrosequencing was carried out using the SLC39A4 sequencing primer (SLC39A4Seq). Standard curves for SLC39A4 can be found in Appendix C.

Total RNA was used to assess SLC39A4 expression at the mRNA level by RT-qPCR using primers specific to a 171 bp region of the *SLC39A4* gene (SLC39A4F and SLC39A4R) as described above. Primer sequences and annealing temperatures are outlined in Table 2.2D. Amplification and standard curves for SLC39A4 can be found in Appendix D.

No statistically significant effect was measured in DNA methylation levels at any of the 3 CpG site assayed upstream of the SLC39A4 transcript in response to altered SIRT1 expression levels ($p > 0.05$) (*Figure 6.14A*). Table 6.1 summarises the data for CpG sites at which significant effects of SIRT1 expression level were measured. *SLC39A4* gene expression changed in response to SIRT1 manipulation. SIRT1 knockdown caused a decrease in levels of *SLC39A4* transcript compared with SIRT1 overexpression ($p < 0.01$) (*Figure 6.14B*).

SLC39A4 Sequence

-1000 AATGGCTCAC ACCTGTAATC CTAGCACTTT GGGAGATCGA GGTGGGTGGA
-950 TTACCTGAGG TCAGGAGATC GAGACCAGCC TGGCCAACAT GGTGAAACCC
-900 CGTCCTACTA AAAATATAAA AATTAACTGG GCGTGGTGGC GGGTGCCTGT
-800 AATCCCAGCT ACTCGGGAGG CTGATGCAGA ATTGCTTGAA CCTGGGAGGC
-750 AGAGGTTGCA GTGAGCCGAG ATGGTGCCAC TGTACTCCAG CCGGGGCGAC
-700 AGAGTGAAGC TCTGTCTCAA AAGAAGAAAG AAAAGAAAAG GGGAGGGGAT
-650 GGGAGGGAAG GTCATGTGAA GACAAAGGCA GGGATTGGAG TCATACTGCC
-600 CACAAACCAA GGAACACCTG GGGCCACCAG TAGCCAGGAA AGGCTCATGG
-550 AACAGACTGT TTCCTAGAGA CTTCAGAGAG AGCATTGCTC TCCTGACACT
-500 TTGATTCCTA ACTTTCAGCC TCCAGAACTG TGAGAATAAG TTTCTGGTTT
-450 TAAGGCACTC AGTTTATGGT AGGCTTTGTT AAGGTAGCCC TAGGAGGCCA
-400 CCACACAGGC ACTCAGGATT AACGCCTCAG AGTCAGAAGA GGCTGGCGTC
-350 CCAGGAACCG TGGGCTGCCA CACACTCTGG TCTGACGATC TCCAGGTTTG
-300 CTTTCCATGA CAGAGAAATA AGCCCTCGGC TGTGTAAGCA GTTATAGGTA
-250 AGCAAGTTTG ATTCCTGTTT GGGGACAGGT CCCACCTGCT GCCCACACAC
-200 CCGGGTGAAT TTCCCTGACC CCACTCCTCA GGCAGGCAGG GTCTCCATAT
-150 CAAAGAGGGG GCACCTGAGG CTGGCTGCCT GGGGGTCCTG AGTGCAGCTC
-100 TCCTGGCTTC GAGGCACCCC GATGGGGAGA AGGCAGTGCC GCAATTGTCC
-50 TTTCTCAGCT GAGGGCCCTT CCCACCCAGC AAGGAGAGCA CAGCCATGCT
+1 ccaaggacaa gagtgtcttt actggagttg ggactggggc ctctataggg
+50 gcttctggtt tctgggctgt aggtttgtga ggtgtgggat cttaagtcaa
+100 aggtggggga ctagggcagg gtatcagaag gtgatgtcat cctcgtacag
+150 ggacagcagc agcaggacgg tccagccgcc cagcaggccc acgttgtgca

Figure 6.13. The SLC39A4 sequence and related primers for use in the SLC39A4 pyrosequencing assay. *The SLC39A4 sequence taken from the human genome sequence is shown. Primers were designed for a PCR to a region in the SLC39A4 sequence (SLC39A4YF#1 – light blue and SLC39A4YR#1 – dark blue) and a nested PCR (SLC39A4F#2 – light green and SLC39A4R#2 – dark green) to focus in on three specific CpG sites (pink) within the SLC39A4 sequence. A sequencing primer was designed for use in the pyrosequencing reaction (SLC39A4Seq - orange). Primers and annealing temperatures are given in Table 2.2C.*

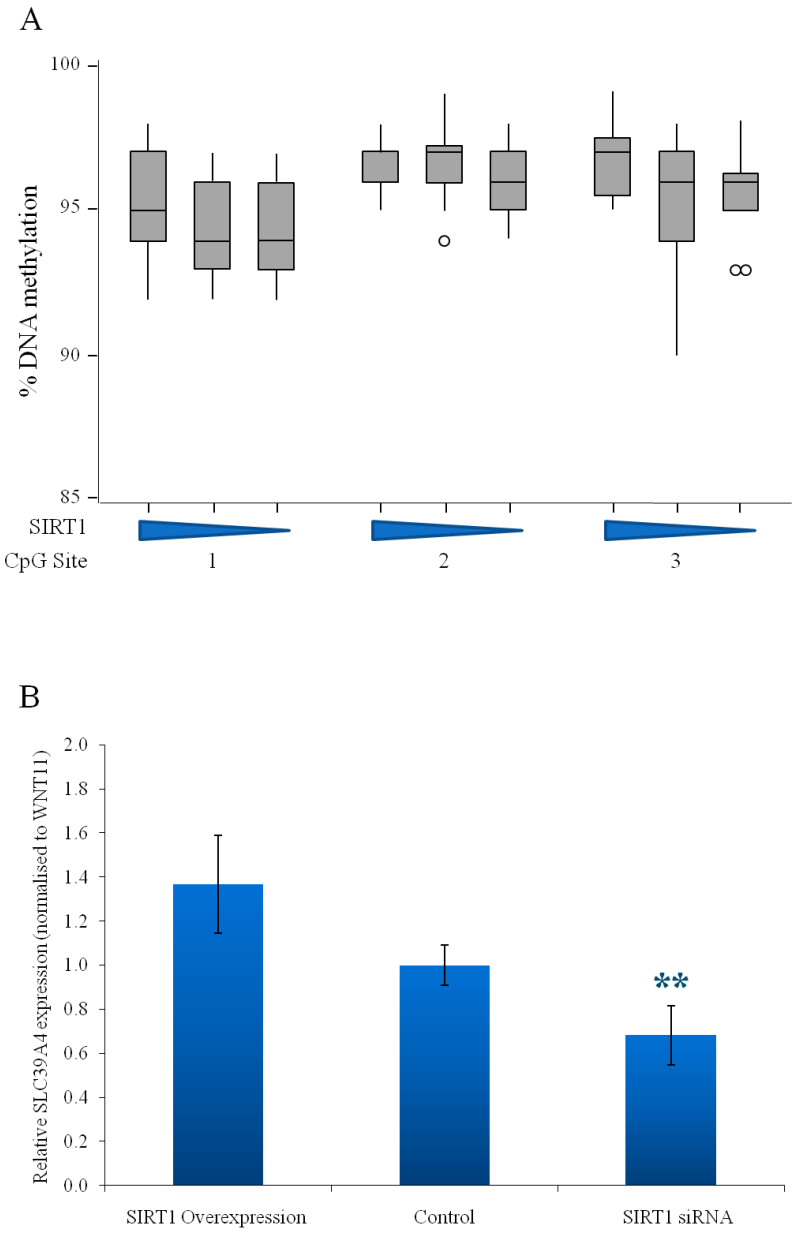

Figure 6.14. Effect of SIRT1 overexpression or SIRT1 knockdown by siRNA on A) percentage methylation at CpG sites within the SLC39A4 gene as measured by pyrosequencing and B) mRNA levels for SLC39A4 as measured by RT-qPCR. *A – Methylation is expressed as the percentage of unmethylated cytosines converted to thymines as a result of bisulfite modification determined by pyrosequencing. Data are medians ± upper and lower quartile ranges for each CpG site (n = 9). For the set of data corresponding to each CpG site the first (left-hand-most) bar corresponds to SIRT1 overexpression, the second to control and the third to SIRT1 knockdown as indicated by the triangular symbols beneath each set to indicate a progressive decrease in SIRT1 expression. Outliers are represented by ○. p > 0.05 compared between SIRT1 overexpression, control and SIRT1 knockdown by Kruskal Wallis then Dunn's multiple comparisons test. B – Gene expression is measured as the PCR cycle number at which the fluorescence signal increases above the background threshold (C_T values). Data are mean ± SEM (n = 9) normalised to the C_T value of the reference gene WNT11 measured in the same samples. **p < 0.01 compared with SIRT1 overexpression (blue) by one way ANOVA then Bonferroni's multiple comparison.*

6.2.8 Effects of SIRT1 manipulation on TBX3

Percentage DNA methylation was measured at three consecutive CpG sites within the PCR amplified *TBX3* sequence spanning - 187 to + 53, occurring at - 137, - 125 and - 105 bp relative to the start of transcription of the *TBX3* sequence (*Figure 6.15* and *Section 2.6.13*). The first PCR generated a 912 bp product (TBX3YF#1 and TBX3YR#1) and the nested PCR generated a 440 bp product (TBX3F#2 and TBX3R#2). Pyrosequencing was carried out using the TBX3 sequencing primer (TBX3Seq). Standard curves for TBX3 can be found in Appendix C.

Total RNA was used to assess TBX3 expression at the mRNA level by RT-qPCR using primers specific to a 198 bp region of the *TBX3* gene (TBX3F and TBX3R) as described above. Primer sequences and annealing temperatures are outlined in Table 2.2D. Amplification and standard curves for TBX3 can be found in Appendix D.

The 1st, 2nd and 3rd CpG site upstream of the *TBX3* transcript at positions -105, -125 and -137 relative to the start of transcription showed altered levels of DNA methylation in response to SIRT1 manipulation (*Figure 6.16A*). Table 6.1 summarises the data for CpG sites at which significant effects of SIRT1 expression level were measured. *TBX3* gene expression was also changed in response to SIRT1 manipulation. SIRT1 overexpression caused an increase in levels of *TBX3* transcript compared with the control ($p < 0.001$) and SIRT1 knockdown had the opposite response causing a decrease in levels of *TBX3* transcript compared with the control ($p < 0.05$); the data for the two extremes (overexpression and knockdown) also showed a statistically significant difference ($p < 0.001$) (*Figure 6.16B*).

TBX3 Sequence

-1000 CCTTCCCGTG CCGCCCCCGC CCCCCAACAG ACACACACCT CGGAGGCGAG
-950 GCTGGGGGTC GGGAGACCAA AAGACTGACA GTGCCTCATC ATTTTTTATT
-900 GAATGTTTCA AAGATAAATT GAACTTCAAA AGGCAACTCC CCGAACAGCC
-850 TGGAGACGGG TTTGAAGGGG AGACTAGGGG AGGATGTCAG CCTCCTGGGT
-800 GACTTTTGCC GTGGAGGGGG TGAAATGTGC ACCCTGGAAT TACCTTTCCC
-750 CTTTCGGGGA TAATTTCCCT CCTCCCTCGC GTGACACAGC TAAGTTTTCG
-700 CGGAGCTGGC CGCGCTTTGC ACGCACAACT CGGGATGGAT GGGGCCTCGT
-650 AGGGGCGCCT TGGGCCAGCC GGGTTCAATT TGAGGCACCA GGGACTGCAG
-600 GCTGTGTGGG GGGTTGCCGA GTGGAAAGGC GTTGCGTCTT GTCCACTTCT
-550 ACAACCTGGA GGGTTGCTGC CTAGCCAAGC CCGCTCGGAC TGCTGGGGCA
-500 TTCTGCTGGC CTTTTCCCCG AGCCAAACAC ACTGGTGCAA GAAGGTATTT
-450 TCGACTTGGA TTCGCCAGAT TGATGTCAAA ACTGAGGGCG AGCTTAAAAC
-400 GAAAAACATT CGTACTTGCC GAGCTTACTT TTGGTCGGAT TCGGGTGGGA
-350 AAACCTGACT TAGGGAGCAC ATCAGTCTTT TTCCATTAAA ACTTAAAAGT
-300 ATCTGAAATT ACCCTTCTTT CTGTATTCTC ATCAGGCCCC TTTCCGTCTC
-250 CCTGCTTTGC TCCCTAATTT AAAGGAAAAG TAATTTCAGA TTGAAGTGGC
-200 TCCCTTCGCT CAAGTAAGGG ACTTTTGTTT TTAGCTTTGT AACTTGAGTG
-150 ACATCTCATT TTGGTTCGCT GGGGGCGGTC TTAATTATTT AAAGGCGAAG
-100 GGAAGGGGGT AAACTCAGAA CAAGAAGATA CTAAACCCTC CCCTGACTGT
-50 CCATCTTCAG GAAAGGTTCC CAAAGAAAAA ACATTTAACA CAAGGCCCAA
+1 agacatttca ataaaaattt attgaaattt cagtgatgtt ttaaagagag
+50 gggaaaaat acagaaaacc aaagaactca tcaacaacta taacacaaaa
+100 tataccttca tgaatttgtc tttaaaccat ctctcagcac ctgacttttg
+150 aactgtgaat atatctctat aggcaggcac caattcaaaa caccgatact

Figure 6.15. The TBX3 sequence and related primers for use in the TBX3 pyrosequencing assay. *The TBX3 sequence taken from the human genome sequence is shown. Primers were designed for a PCR to a region in the TBX3 sequence (TBX3YF#1 – light blue and TBX3YR#1 – dark blue) and a nested PCR (TBX3F#2 – light green and TBX3R#2 – dark green) to focus in on three specific CpG sites (pink) within the TBX3 sequence. A sequencing primer was designed for use in the pyrosequencing reaction (TBX3Seq - orange). Primers and annealing temperatures are given in Table 2.2C.*

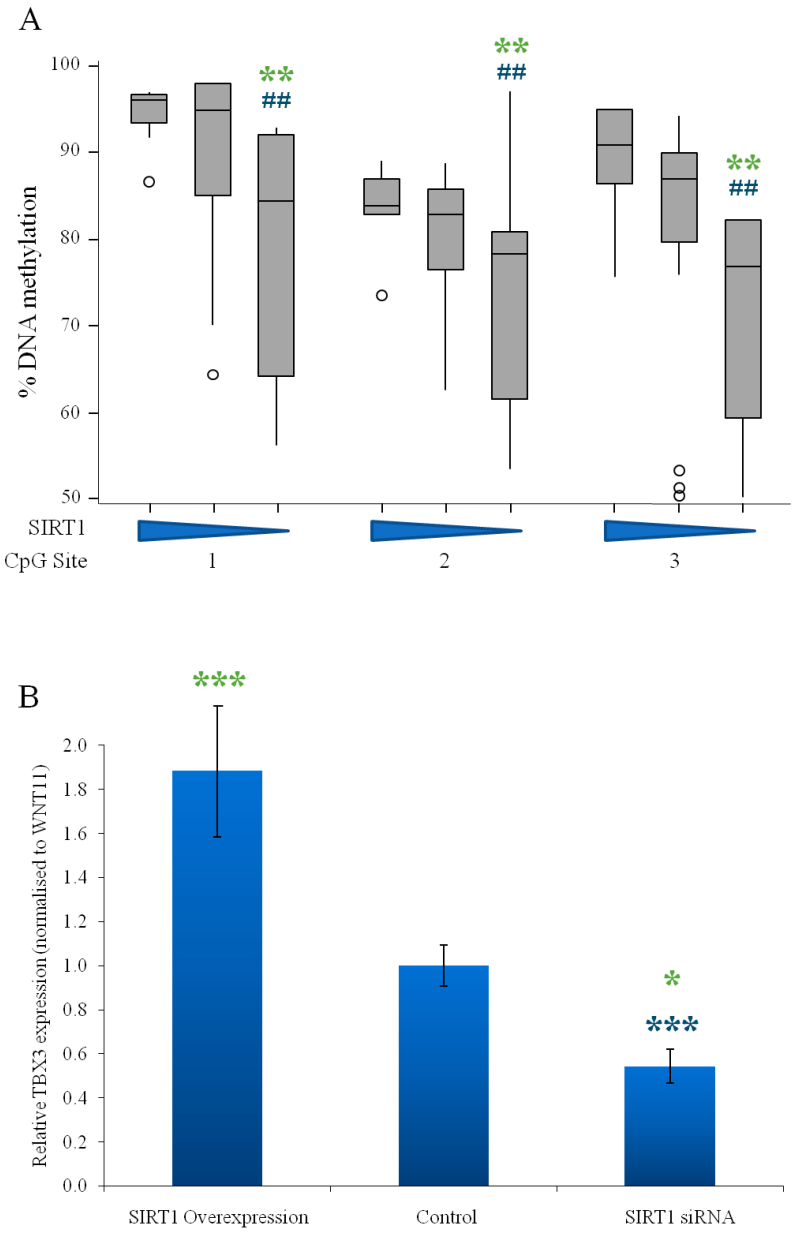

Figure 6.16. Effect of SIRT1 overexpression or SIRT1 knockdown by siRNA on A) percentage methylation at CpG sites within the TBX3 gene as measured by pyrosequencing and B) mRNA levels for TBX3 as measured by RT-qPCR. *A – Methylation is expressed as the percentage of unmethylated cytosines converted to thymines as a result of bisulfite modification determined by pyrosequencing. Data are medians ± upper and lower quartile ranges for each CpG site (n = 9). For the set of data corresponding to each CpG site the first (left-hand-most) bar corresponds to SIRT1 overexpression, the second to control and the third to SIRT1 knockdown as indicated by the triangular symbols beneath each set to indicate a progressive decrease in SIRT1 expression. Outliers are represented by ○. *p < 0.05, **p < 0.01 compared with control (green); $^{\#}p < 0.05$, $^{\#\#}p < 0.01$ compared with SIRT1 overexpression (blue), by Kruskal Wallis then Dunn's multiple comparison. B – Gene expression is measured as the PCR cycle number at which the fluorescence signal increases above the background threshold (C_T values). Data are mean ± SEM (n = 9) normalised to the C_T value of the reference gene WNT11 measured in the same samples. *p < 0.05, ***p < 0.001 compared with control (green) or SIRT1 overexpression (blue) by one way ANOVA then Bonferroni's multiple comparison.*

6.2.9 Summary of the effects of SIRT1 manipulation on gene-specific DNA methylation

The effects of SIRT1 manipulation on DNA methylation levels on each target gene as measured by pyrosequencing is summarised in Table 6.1.

Gene	Region analysed (relative to tss)	Number of CpG sites analysed	CpG sites affected by manipulating level of SIRT1 expression			
			CpG number (relative to tss)	Methylation (%) in cells with SIRT1 o/e (median (Q1,Q3); n = 9)	Methylation (%) in control cells (median (Q1,Q3); n = 9)	Methylation (%) in cells with reduced SIRT1 expression (median (Q1,Q3); n = 18)
CDC7	-59 to +1	8	8	2 (1.5, 2)	2 (2, 2)	1.5 (0, 2) *
EIF5	-61 to +1	8	1 2 4	1 (1, 1.5) ** 1 (0, 1.5) * 2 (1, 2.5)	0 (0, 0.25) 0 (0, 1) 2 (2, 3.25)	0 (0, 0.25) ## 0 (0, 0) ## 5 (2, 8) *##
IRX3	-65 to +1	3	1 3	92 (91.5, 97) 83 (82, 87)	94 (91.75, 95) 86.5 (85, 91)	91.5 (88.7, 93) * 90 (87.75, 91) ##
KLF3	-70 to -45	6	3	0 (0, 1.5) *	0 (0, 0)	0 (0, 0)
PCYT1A	-89 to +1	2	none affected			
PTPRG	-73 to +1	9	9	7 (5.5, 11.5)	8 (5, 12.25)	5 (4, 6) **#
SLC39A4	-92 to +1	3	none affected			
TBX3	-135 to +1	3	1 2 3	96 (93.5, 96.5) 84 (83, 87) 91 (86.5, 95)	95 (85, 98) 83 (76.75, 86) 87 (79.75, 90)	84.5 (64.75, 92) **## 78.5 (61.75, 81) **## 77 (59.5, 82.25) **##

Table 6.1. Summary of the effects of SIRT1 overexpression or SIRT1 knockdown by siRNA on percentage methylation at CpG sites in Caco-2 cells. *Data are stated only for CpG sites at which significant effects of SIRT1 expression level were measured. tss – transcription start site; o/e – overexpression; Q1 – first quartile; Q3 – third quartile.*p < 0.05, **p < 0.01 compared with control (green); $^{\#}p < 0.05$, $^{\#\#}p < 0.01$ compared with SIRT1 overexpression (blue), by Kruskal Wallis then Dunn's multiple comparisons tests.*

6.3 Relationship between CpG site density and DNA methylation levels

Inspection of values for gene-specific CpG site methylation across the eight genes studied revealed an apparent relationship between the intervals separating CpG sites and the percentage methylation, such that CpG sites clustered close together within a sequence appeared to have lower levels of methylation. Collating the data for mean DNA methylation at CpG sites at each of the eight loci revealed a linear relationship with the density at which they occurred ($p = 0.0046$) (*Figure 6.17*). This preliminary observation was confirmed by publication of a whole-genome study, where through a novel method – Methyl-MAPS (methylation mapping analysis by paired-end sequencing) using methyl sensitive and methyl dependent enzyme digestion followed by deep sequencing – it was established that overall CpG methylation increased with CpG site density until density reached 0.07 (indicating there is a cytosine at least once every 15 nucleotides) after which CpG site methylation decreased rapidly (Edwards et al., 2010).

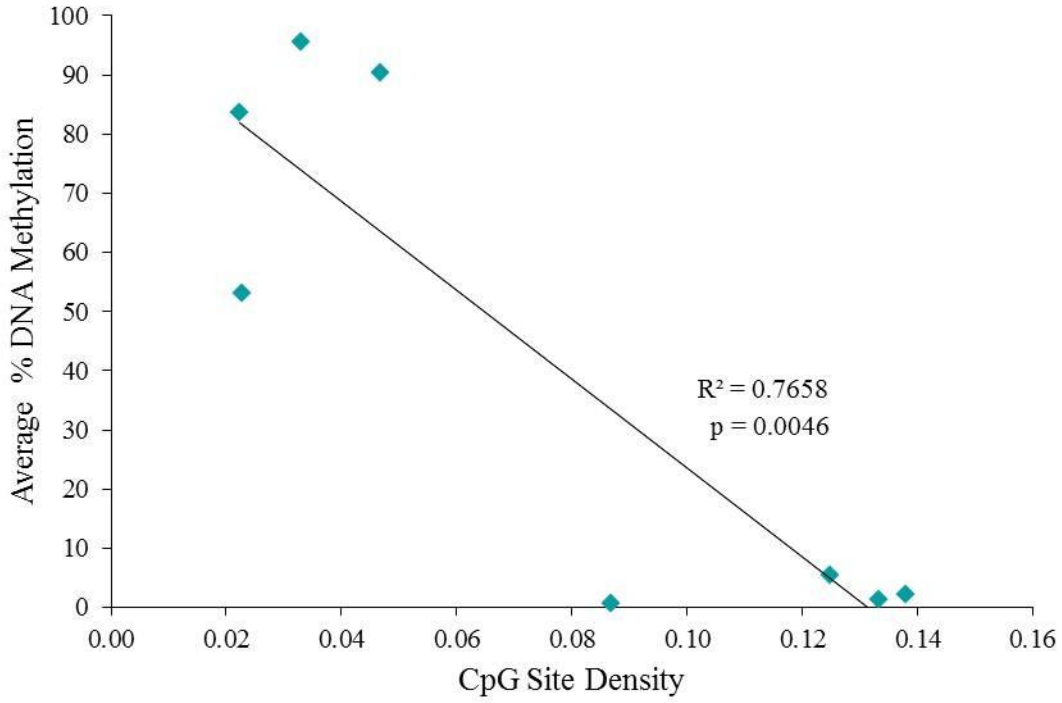

Figure 6.17. Relationship between CpG site density and average percentage DNA methylation. *CpG site density was calculated by dividing the number of CpG sites in a sequence by the length of the sequence and plotted against the average % DNA methylation measured in the sequence. The R^2 and p values are indicated.*

6.4 Discussion

The effects of SIRT1 overexpression or knockdown in Caco-2 cells on DNA methylation was investigated and changes in methylation were detected at CpG sites in the promoter regions for six of the eight genes (*CDC7, EIF5, IRX3, KLF3, PTPRG, TBX3*) in the 'three way' overlap highlighted by the *in silico* analysis presented in Chapter 5. Significant effects of SIRT1 manipulation on methylation were observed on at least 1 site in six of the eight promoter regions examined. No effects of SIRT1 manipulation on DNA methylation was measured at the CpG sites of *PCYT1A* and *SLC39A4.* Methylation was measured at specific CpG sites within the promoter regions within a 50 - 100 bp region, so there is the chance that SIRT1 manipulation may have affected methylation status of CpG sites not captured in the assays for *PCYT1A* and *SLC39A4*. Expression at the mRNA level of all of the eight genes was affected significantly by SIRT1 overexpression and/or knockdown (*CDC7, EIF5, KLF3, PCYT1A, PTPRG, TBX3*) or when SIRT1 overexpression and knockdown were compared (*IRX3* and *SLC39A4*). These experiments thus provide proof of concept that changes in SIRT1 expression, such as is reported to occur under conditions of DR, can influence both gene-specific DNA methylation and corresponding gene expression. A relationship between CpG site density and percentage methylation was also observed.

A limitation of the observations thus far is that we have established no causal link between the SIRT1-dependent changes in gene methylation and expression that we observe. Approaches to establishing such a relationship could include utilising the methylated promoter reporter construct model, described in Section 4.3, to investigate the effects of *in vitro* methylation on the promoters of *CDC7, EIF5, IRX3, KLF3, PCYT1A, PTPRG, SLC39A4* and *TBX3* when driving expression of β galactosidase in a transfected cell line. Other evidence that would establish a causal link between promoter methylation and gene expression would be to show that those genes with highly methylated promoter regions (*IRX3, PCYT1A, SLC39A4* and *TBX3*) have altered gene expression in Caco-2 cells treated with a DNA-demethylating agent such as 5-aza-2'-deoxycytidine. There is an opportunity – based on the existing data – to carry out analysis using a tool to predict transcription factor binding sites such as RegionMiner (Genomatix, Germany) to determine if sites methylated differentially by changed SIRT1 levels lie within transcription factor binding sites which would provide some indirect evidence of a likely causal link between DNA methylation and gene expression.

Speculative suggestions concerning the downstream consequences of the SIRT1-mediated changes in DNA methylation or expression of the genes studied here can be made but would require experimental investigation, since none of the genes highlighted through the *in silico* analysis (Chapter 5) and thus studied here have any specific, clear links to the ageing process or modification of lifespan. Beneficial effects of DR on lifespan could feasibly involve these genes however through maintenance of cell cycle control (*CDC7* and *EIF5*), cellular structure (*MYH10* and *PCYT1A*) and signalling (*PTPRG*),

control of gene expression (*IRX3*, *KLF3* and *TBX3*) and regulation of dietary components (*LDLR* and *SLC39A4*).

As determination of DNA methylation status of CpG sites by pyrosequencing is limited to only a small region of the gene, a criticism may be that the measurements provided are only a snapshot of the methylation pattern across the entire promoter region. Analysis of CpG sites in a much larger region of each promoter may reveal more complex patterns and relationships, as demonstrated by the gene suppression caused by methylation in CpG islands (Saxonov et al., 2006) and CpG shores (Irizarry et al., 2009) which have been described as CpG dense regions up to 2 kb upstream of genes affected by their methylation status. A second obvious limitation relating to the targeted CpG site methylation measurements made thus far is that, given we have now established proof of principle that SIRT1 can affect gene-specific DNA methylation, effects across the entire genome (i.e. effects at the level of the 'methylome') should be considered. Chapter 7 describes experiments that investigate these more global effects using a microarray-based approach to assess effects of SIRT1 manipulation on DNA methylation and gene expression across the genome.

7 An investigation of genome-wide effects of SIRT1 on DNA methylation and gene expression

7.1 Outline

Chapter 3 reported investigation of the levels of global DNA methylation using the LINE-1 retrotransposon as a surrogate marker, which we found did not change in response to SIRT1 manipulation but revealed some effects of dietary polyphenols that were influenced by SIRT1 expression levels. We also investigated in work which was presented in Chapter 6 changes in gene-specific DNA methylation but only assayed a small number of the CpG sites that could theoretically be methylated and undergo changes in methylation in response to altered SIRT1 expression. To gain a more comprehensive view of the extent to which DNA methylation at specific loci may be affected by SIRT1 expression levels we carried out microarray-based analysis of the methylation pattern across the genome under conditions where SIRT1 was expressed at different levels. In parallel we measured the response to expressing SIRT1 at different levels at the level of the transcriptome.

To investigate the effect of levels of SIRT1 expression on genome-wide DNA methylation and gene expression, SIRT1 was overexpressed and knocked down in the Caco-2 cell line. SIRT1 overexpression and knockdown in Caco-2 cells was confirmed at the mRNA level by RT-qPCR and at the protein level by western blot. Genome-wide DNA methylation changes were measured by Methylated DNA Immunoprecipitation (MeDIP) followed by co-hybridisation of differential dye-labelled input and methylation-enriched DNA samples to microarrays. Genome-wide transcript levels were compared at different levels of SIRT1 expression by hybridisation of RNA to microarrays.

7.2 Investigating the genome-wide effects of SIRT1 on DNA methylation

We tested our overarching hypothesis that changes in SIRT1 expression levels (as occurs under conditions of DR) can influence DNA methylation (which may mediate some of the beneficial effects of DR) on a genome-wide scale by manipulating the levels of SIRT1 within Caco-2 cells by overexpression from a transgene or siRNA-mediated knockdown then investigating the effects of DNA methylation at specific sites across the genome via hybridisation of input and methylation-enriched DNA to microarrays.

The MeDIP protocol, through which the methylated fraction of DNA is immunoprecipitated using an anti-5-methylcytidine antibody was initially described by (Weber et al., 2005) and further developed to include internal positive and negative controls to assess the reproducibility of enrichment within a sample set (S Lisanti, Newcastle University, Personal Communication) as described in Section 1.5.5 and 2.6.14.

7.2.1 Experimental design

Caco-2 cells seeded 24 hours previously at 3.5 x 10^5 cells/well in a six well plate (area = 9.6 cm^2/well) were transfected transiently with 100 pmol SIRT1-targeting siRNA or with 100 pmol of a Stealth RNAi™ siRNA negative control of similar GC content to achieve SIRT1 knockdown or with 2 µg SIRT1 expression construct (pCMV6-ENTRYSIRT1) to achieve SIRT1 overexpression or with 2 µg control vector with no SIRT1 insert (pCMV6-Neo). After 72 hours cells were lysed and DNA and total cell lysate were extracted from parallel experiments. Total cell lysate was used to assess SIRT1 manipulation at the protein level by western blot as described in Section 2.8. Total cell lysate was extracted (Section 2.8.2.2) and protein concentration determined by Bradford assay (Section 2.8.1.4). Ten micrograms of total cell lysate was separated by SDS-PAGE (Section 2.8.1.5) and blotted onto a polyvinylidene difluride (PVDF) membrane (Section 2.8.1.6), which was then probed with antibodies to SIRT1 and the loading control protein alpha tubulin. Changes in SIRT1 protein levels were confirmed by differences in signal intensity when blots were probed with SIRT1 antibody. Typical western blot confirmation of SIRT1 knockdown or overexpression is shown in Figure 3.4 and Figure 3.8 (Chapter 3) respectively. DNA for methylation analysis was prepared from three independent experiments pooled to produce three biological repeats for each condition (SIRT1 overexpression; SIRT1 knockdown and corresponding controls), of which those with the highest quality were selected for MeDIP.

Having obtained DNA samples with confirmed SIRT1 knockdown and overexpression, a profile of DNA methylation across the genome was obtained using the DNA Methylation Service provided by NimbleGen Roche (Reykjavik, Iceland) as described in Section 2.6.14. Each DNA sample was subjected to MeDIP before site-specific DNA methylation across the genome was analysed by hybridisation to microarrays.

To prepare samples for MeDIP DNA was sonicated using an ultrasonic homogeniser and purified as described in Section 2.6.14.2 to produce DNA fragments ranging from 200 – 1000 bp in length, confirmed by agarose gel electrophoresis (*Figure 7.1A*). Purified fragmented DNA (4.4 µg) was then spiked with unmethylated and methylated internal controls generated from Lambda phage dam dcm- genomic DNA (*Figure 7.1B*) and denatured at 95 °C as described in Section 2.6.14.3 and 2.6.14.4. Forty five microlitres of spiked fragmented DNA was stored at 4 °C to act as the input; the remaining spiked fragmented DNA was incubated with mouse anti-5-methylcytidine then with sheep anti-mouse IgG-coated superparamagnetic polystyrene beads, which were captured using a magnetic rack (Section 2.6.14.4).

Whole genome amplification of 2 ng/µl input or immunoprecipitated DNA was performed using the GenomePlex® Complete Whole Genome Amplification kit (Sigma) to increase the yield of each DNA

sample (Section 2.6.15.5). The retention of the fragmentation size was confirmed by agarose gel electrophoresis (*Figure 7.1C*).

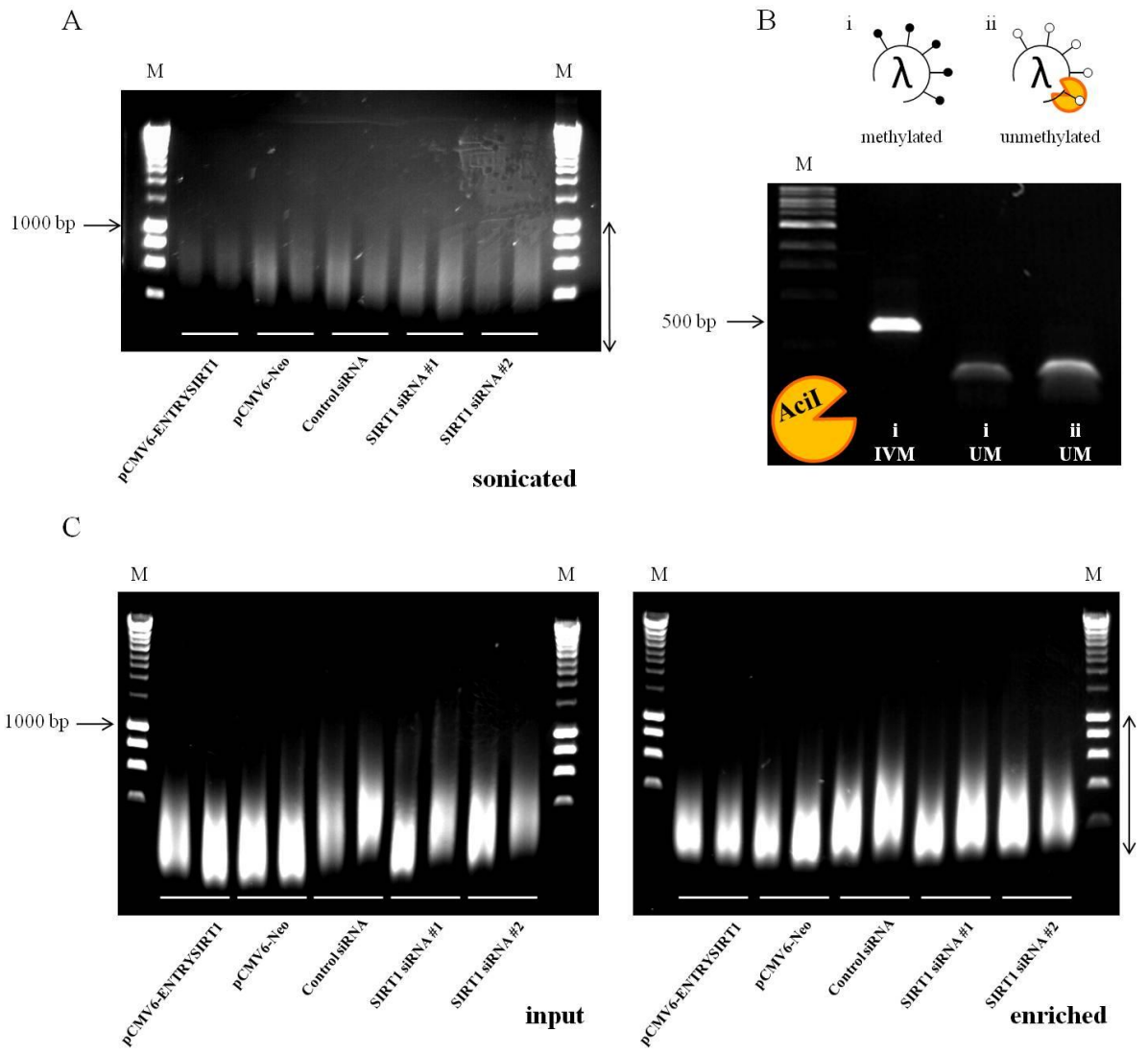

Figure 7.1. Confirmation of (A) DNA fragmentation by ultrasonic homogenisation, (B) methylation status of lambda phage internal controls and (C) retained DNA fragmentation after Whole Genome Amplification (WGA). *A – Sonication products were analysed by agarose gel electrophoresis. B – Methylation status of in vitro methylated (i IVM; closed circles) and unmethylated (ii UM; open circles) internal controls for MeDIP was analysed by agarose gel electrophoresis before adding to the sonicated DNA. Two fragments (i and ii) were generated from Lambda phage dam dcm- genomic DNA (λ) by PCR amplification of two 500 bp regions, one of which was then in vitro methylated (i). Methylation status was confirmed by digestion with the methylation sensitive restriction enzyme AciI. A comparison of band size after digestion between unmethylated and methylated fragment i (i UM and i IVM) or between methylated fragment i and the unmethylated internal control fragment ii (ii UM) confirmed methylation. C – Sonicated WGA products (immunoprecipitated with an anti-5-methylcytidine antibody in the case of the enriched sample) were analysed by agarose gel electrophoresis to confirm retention of DNA fragmentation. As indicated for A and C, lanes contained products generated from Caco-2 cells transfected transiently with either SIRT1-targeting siRNA or with a Stealth RNAi™ siRNA negative control of similar GC content or the SIRT1 expression construct pCMV6-ENTRYSIRT1or control vector pCMV6-Neo at 72 hours after transfection. M – DNA molecular weight marker (Hyperladder I, Bioline; sites indicated). The double-headed arrow on the right hand side of panel A and C indicates the range of DNA fragment sizes required for downstream array hybridisation.*

Enrichment analysis was performed by qPCR to assess the efficiency of MeDIP enrichment using primers to the internal spike controls (*Figure 7.2A*) and known endogenous sequences of high (H19 and L1.2) and low (UBE2B) levels of methylation (*Figure 7.2B* and *Figure 7.2C*). qPCR analysis of these genes was performed using the Roche LightCycler® 480 (Section 2.7.2.4). Primer sequences and annealing temperatures are stated in Table 2.2D. Amplification curves for the unmethylated and methylated Lambda Phage fragments, H19, L1.2 and UBE2B are shown in Appendix D. Enrichment was calculated using the C_T values generated for each input and methylation-enriched sample by subtraction of negative control values from the value for each input or methylation-enriched sample, then subtraction of the corrected C_T value of the enriched from the input sample giving a value x for which enrichment was calculated as 2^x. Enrichment results using the comparison of the internal spike controls or the highly methylated sequences H19 and L1.2 versus the low methylation of UBE2B are shown in Figure 7.2A-C respectively. Enrichment values varied substantially across the ten samples analysed (two biological repeats for each of the five test conditions) and this variability was as substantial between biological duplicates of the same condition as between different conditions, so was not related to the manipulations in SIRT1 applied. However, all enrichments values exceeded the 10-fold criteria required for further analysis. As each input and enriched sample are compared directly these variable levels of enrichment should not affect the analysis in a fundamental way, but may lead to difference in the sensitivity with which differences in DNA can be detected on the individual microarrays.

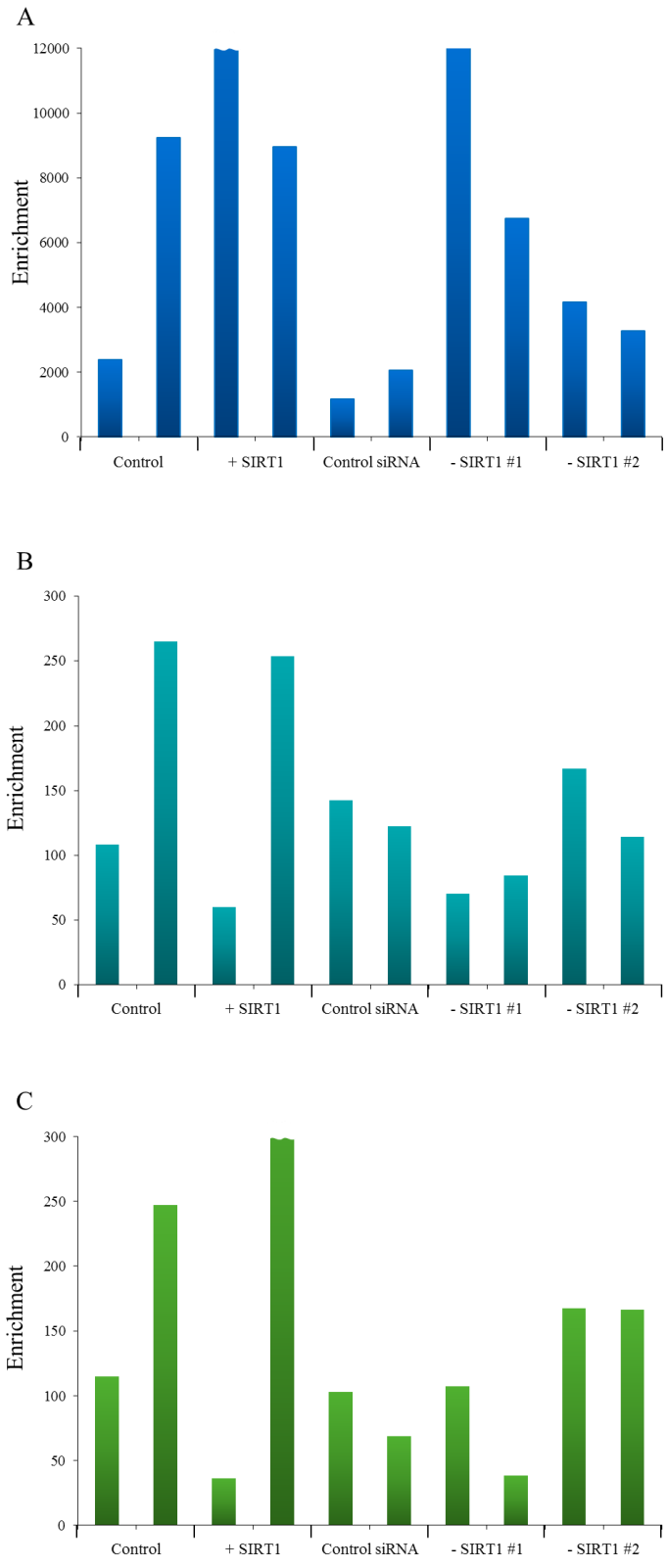

Figure 7.2. Enrichment of methylated DNA after MeDIP compared to input DNA. *Levels of enrichment were calculated in each sample using C_T values for negative controls subtracted from values for samples. Enriched sample values were subtracted from input values ($\boldsymbol{x}$) and enrichment expressed as 2 $\boldsymbol{x}$. A – Lambda Phage controls. B – H19/UBE2B. C – L1.2/UBE2B. Data for the two biological replicates prepared and analysed for each condition are shown.*

7.2.2 Array design and hybridisation by NimbleGen

After confirmation of enrichment and quality assessment by retention of fragmentation and acceptable measures of absorbance (A_{260}/A_{280}), DNA samples were sent to NimbleGen Roche for analysis by hybridisation to the NimbleGen 3x720K CpG Island Plus RefSeq Promoter Array. This array consists of 3 identical arrays per chip targeting 720,000 probes covering 30,848 transcripts, 22,532 promoters and 27,728 CpG Islands. DNA samples from cells overexpressing SIRT1 and corresponding vector only controls or cells in which SIRT1 expression was reduced by siRNA and corresponding controls were hybridised as biological duplicates over three chips. DNA from cells transfected with a second SIRT1-targeting siRNA was hybridised to a fourth array. Input DNA was labelled with Cy3 and immunoprecipitated DNA with Cy5 and samples were co-hybridised to the arrays.

7.2.3 Data analysis

The raw data scanned from the array chips was supplied electronically. The summary report of the peak data mapped to the transcription start site of genes was imported into Excel (Microsoft) and duplicates were removed. Genes were supplied with Entrez identifiers. A stringent two-step approach was then taken to identify genes that were methylated at different levels under conditions of SIRT1 knockdown or overexpression compared to control. In the first instance sequences enriched by MeDIP were identified as being represented on both biological duplicates and in the case of the SIRT1-targetting siRNAs were required to appear in the list for both siRNAs. The resulting list of methylated genes whose signal intensity met the minimum p-value cut-off consisted of 4707 genes under control conditions (pCMV6-Neo), 5080 genes under conditions of SIRT1 overexpression (pCMV6-ENTRYSIRT1), 5385 genes under control siRNA conditions (negative scrambled control) and 4766 genes under conditions of SIRT1 knockdown (SIRT1-targeting siRNAs #1 & #2). Genes that underwent a change in methylation in response to either SIRT1 overexpression or SIRT1 knockdown were identified as those for which enrichment of methylation was detected on the array under only one of the two conditions being compared. A total of 4102 genes appeared on the lists of methylated genes for both separate control conditions suggesting the DNA methylation status was relatively unaffected by the transfection procedure alone. A total of 1555 genes were found to be differentially methylated under conditions of SIRT1 overexpression compared with control (Appendix E.II). A total of 1681 genes were found to be differentially methylated under conditions of SIRT1 knockdown compared with control (Appendix E.II). A total of 490 genes were present on the lists of genes whose methylation changed in response to both SIRT1 overexpression and knockdown (*Figure 7.3A* and Appendix E.II).

A total of 356 of the 490 genes whose methylation status was affected by SIRT1 manipulation in Caco-2 cells could be assigned mouse Ensembl identifiers and were present on the MM5 ‘Universe’ allowing comparisons with the previous *in silico* lists of genes that bound SIRT1 and genes responsive

to DR used for the *in silico* analysis presented in Chapter 5. Overlaps were observed of 12 (r.f. 1.34; p = 0.18) and 56 (r.f. 1.02; p = 0.43) genes respectively (*Figure 7.3A* and Appendix E.II) and were not statistically significant. Thus the overlap between genes whose methylation status was found to be affected by SIRT1 and those found to bind with SIRT1 or respond to DR did not exceed the number expected by chance. A total of 1051 of the 1219 mouse genes that showed an ageing related change in methylation status (Maegawa et al., 2010), used in the *in silico* analysis present in Chapter 5 and to guide selection of genes studied in the work presented in Chapter 6, could be represented by a comparable human Entrez identifier and were present on the 'Universe' of 11407 genes that were methylated in our DNA methylation microarray or the list generated by (Maegawa et al., 2010) (*Figure 7.3A* and Appendix E.II). Of these genes, 38 appeared on the list of 490 human genes that showed an SIRT1 manipulation-related change in methylation status, giving a representation factor of 0.84 and hypergeometric probability of 0.89 (*Figure 7.3B*). Thus the overlap between genes whose methylation status was found to be affected by SIRT1 and those showing a change in methylation in older compared with younger mouse intestine did not exceed the number expected by chance.

The less stringent lists composed of genes whose DNA methylation changed in response to SIRT1 overexpression only (Appendix E.II) or SIRT1 knockdown only (Appendix E.II) were also investigated for the significance of the overlap with the gene expression data when only manipulating SIRT1 one way.

Of the 1555 genes that showed a change in DNA methylation status in response to SIRT1 overexpression 1060 could be converted to mouse Ensembl identifiers and were present on MM5 allowing comparisons with the previous in silico lists of genes that bound SIRT1 and genes responsive to DR used for the *in silico* analysis presented in Chapter 5. Overlaps were observed of 15 (r.f. 0.56; p = 0.99) and 157 (r.f. 0.96; p = 0.68) genes respectively (Appendix E.II) and were not statistically significant. Thus the overlap between genes whose methylation status was found to be affected by SIRT1 overexpression and those found to bind with SIRT1 or respond to DR did not exceed the number expected by chance. Comparing the 1555 genes that showed a change in DNA methylation status in response to SIRT1 overexpression with the list of 1051 genes from the (Maegawa et al., 2010) paper that could be represented by a human Entrez identifier and were present on the 'Universe' of genes that could be methylated an overlap of 103 genes was observed (r.f. 0.72; p = 0.99). Thus the overlap between genes whose methylation status was found to be affected by SIRT1 and those showing a change in methylation in older compared with younger mouse intestine did not exceed the number expected by chance.

Of the 1681 genes that showed a change in DNA methylation status in response to SIRT1 knockdown 1163 could be converted to mouse Ensembl identifiers and were present on MM5 allowing

comparisons with the lists of genes that bound SIRT1 and genes responsive to DR used for the *in silico* analysis presented in Chapter 5. Overlaps were observed of 35 (r.f. 1.19; p = 0.155) and 200 (r.f. 1.12; p = 0.035) genes respectively (Appendix E.II). Thus the overlap between genes whose methylation status was found to be affected by SIRT1 knockdown and those found to bind with SIRT1 did not exceed the number expected by chance. However, the gene methylation profile of Caco-2 cells affected by SIRT1 knockdown matches, to an extent greater than expected by chance, genes that respond to DR across a range of different mouse tissues, suggesting that changes in the level of SIRT1 has an effect on the methylation status of some of the genes that are responsive to DR (*Figure 7.3B*). Comparing the 1681 genes that showed a change in DNA methylation status in response to SIRT1 knockdown with the list of 1051 genes from the (Maegawa et al., 2010) paper that could be represented by a human Entrez identifier and were present on the 'Universe' of genes that could be methylated an overlap of 102 genes was observed (r.f. 0.77; p = 0.99).

The lists of genes that changed either in response to SIRT1 overexpression or SIRT1 knockdown showed much the same trend in results as the list of 490 genes that changed in response to SIRT1 overexpression and knockdown when overlapped in the same way, however, only genes whose methylation changed under conditions of SIRT1 knockdown were over represented on the list of genes found to be responsive to DR complied from the *in silico* in Chapter 5.

A

Genes affected by SIRT1 manipulation

Human Gene Symbol	Human Entrez ID		Mouse Ensembl ID
AAMP	14	†	ENSMUSG00000006299
AKAP12	9590		ENSMUSG00000038587
APOBR	55911		ENSMUSG00000042759
CA10	56934		ENSMUSG00000056158
CADM3	57863		ENSMUSG00000005338
CBLN2	147381		ENSMUSG00000024647
CBLN4	140689		ENSMUSG00000067578
CDK5	1020	†	ENSMUSG00000028969
CHRM1	1128		ENSMUSG00000032773
CLN3	1201		ENSMUSG00000030720
FBN2	2201		ENSMUSG00000024598
FGF2	2247		ENSMUSG00000037225
FOXL1	2300		ENSMUSG00000043867
FZD5	7855		ENSMUSG00000045005
GATA3	2625		ENSMUSG00000015619
GBX1	2636		ENSMUSG00000067724
GLI3	2737		ENSMUSG00000021318
HOXD13	3239		ENSMUSG00000001819
IL23A	51561		ENSMUSG00000025383
ISL2	64843		ENSMUSG00000032318
KCNMA1	3778		ENSMUSG00000063142
LRRC14	9684		ENSMUSG00000033728
MEGF11	84465		ENSMUSG00000036466
ODZ4	26011		ENSMUSG00000048078
PAN2	9924		ENSMUSG00000005682
PAPLN	89932		ENSMUSG00000021223
REEP2	51308		ENSMUSG00000038555
RORC	6097	†	ENSMUSG00000028150
RSPO3	84870		ENSMUSG00000019880
SALL1	6299		ENSMUSG00000031665
SCUBE1	80274		ENSMUSG00000016763
SHC3	53358		ENSMUSG00000021448
SLC31A2	1318		ENSMUSG00000066152
ST8SIA4	7903		ENSMUSG00000040710
SYNC	81493		ENSMUSG00000001333
TBX15	6913		ENSMUSG00000027868
ZDHHC24	254359		ENSMUSG00000006463
ZER1	10444		ENSMUSG00000039686
AADACL3	126767		ENSMUSG00000078507
ABCC3	8714		ENSMUSG00000020865
ABTB1	80325		ENSMUSG00000030083
ACP5	54		ENSMUSG00000001348
ACRBP	84519		ENSMUSG00000072770
ADAMTS3	9508		ENSMUSG00000043635
ADHFE1	137872		ENSMUSG00000025911
ADRA2C	152		ENSMUSG00000045318
AES	166		ENSMUSG00000054452
AGER	177		ENSMUSG00000015452
AGFG1	3267		ENSMUSG00000026159
AIM1	202		ENSMUSG00000019866
AIRE	326		ENSMUSG00000000731
AK4	205	†	ENSMUSG00000028527
ALOX15B	247		ENSMUSG00000020891
ALPK3	57538		ENSMUSG00000038763
ALS2CR11	151254		
ALX1	8092		ENSMUSG00000036602
ANKRD11	29123		ENSMUSG00000035569
ANKRD9	122416		ENSMUSG00000037904
APOL1	8542		
ARL17A	51326		
ARMC7	79637		ENSMUSG00000057219
ASCL2	430		ENSMUSG00000009248
ASF1A	25842	†	ENSMUSG00000019857
ASMTL-AS1	80161		
ATP10A	57194		ENSMUSG00000025324
ATP11A	23250	†	ENSMUSG00000031441
B4GALNT4	338707		ENSMUSG00000055629
BAALC	79870		ENSMUSG00000022296
BAHCC1	57597		ENSMUSG00000039741
BANP	54971		ENSMUSG00000025316
BCAS4	55653		
BID	637	†	ENSMUSG00000004446
BMP3	651		ENSMUSG00000029335
BUB1	699	†	ENSMUSG00000027379
BUB3	9184		ENSMUSG00000066979
BZW1P2	151579		
C10orf93	255352		
C11orf66	220004		ENSMUSG00000035179
C12orf10	60314		ENSMUSG00000001285
C14orf48	256369		
C15orf24	56851		ENSMUSG00000055943

Continued…

Human Gene Symbol	Human Entrez ID		Mouse Ensembl ID
C19orf53	28974		ENSMUSG00000019362
C20orf165	128497		ENSMUSG00000017767
C20orf24	55969	†	ENSMUSG00000027637
C22orf43	51233		
C2orf18	54978		ENSMUSG00000029175
C4orf42	92070		
C8orf56	157556		
C9orf140	89958		ENSMUSG00000026955
C9orf142	286257	†	ENSMUSG00000047617
C9orf163	158055		
C9orf37	85026		
CADPS	8618		ENSMUSG00000054423
CALCA	796		ENSMUSG00000030669
CAMK1	8536		ENSMUSG00000030272
CAPN13	92291		ENSMUSG00000043705
CASP9	842	†	ENSMUSG00000028914
CCDC147	159686		ENSMUSG00000046585
CCDC65	85478		ENSMUSG00000003354
CCDC82	79780		ENSMUSG00000079084
CCL22	6367		ENSMUSG00000031779
CCT6P1	643253		
CD22	933		ENSMUSG00000030577
CD63	967		ENSMUSG00000025351
CDC45	8318		ENSMUSG00000000028
CDH15	1013		ENSMUSG00000031962
CDK5RAP1	51654		ENSMUSG00000027487
CELA2A	63036		ENSMUSG00000058579
CELF2	10659		ENSMUSG00000002107
CEP57L1	285753		ENSMUSG00000019813
CGNL1	84952		ENSMUSG00000032232
CHGA	1113		ENSMUSG00000021194
CHRNA4	1137		ENSMUSG00000027577
CILP2	148113		ENSMUSG00000044006
CLDN9	9080		ENSMUSG00000066720
CLEC2L	154790		ENSMUSG00000079598
CLN5	1203	†	ENSMUSG00000022125
CLU	1191	†	ENSMUSG00000022037
CNTN4	152330		ENSMUSG00000064293
COL11A1	1301		ENSMUSG00000027966
COL4A2	1284		ENSMUSG00000031503
COL9A3	1299		ENSMUSG00000027570
COX19	90639	†	ENSMUSG00000045438
CRYBA1	1411		ENSMUSG00000000724
CSNK2B	1460		ENSMUSG00000024387
CSTB	1476		ENSMUSG00000005054
CTBP1	1487		ENSMUSG00000037373
CTCF	10664	*	ENSMUSG00000005698
CTLA4	1493		ENSMUSG00000026011
CTRB2	440387		ENSMUSG00000031957
CTRL	1506		ENSMUSG00000031896
CTSA	5476		ENSMUSG00000017760
CTU2	348180		ENSMUSG00000049482
DBF4B	80174		
DCAF4L1	285429		
DCBLD2	131566		ENSMUSG00000035107
DDI1	414301		ENSMUSG00000047619
DERL2	51009	†	ENSMUSG00000018442
DIRC2	84925		ENSMUSG00000022848
DKK4	27121		ENSMUSG00000031535
DNAJB12	54788		ENSMUSG00000020109
DNAJC16	23341		ENSMUSG00000040697
DOCK2	1794		ENSMUSG00000020143
DPP6	1804		ENSMUSG00000061576
DUSP21	63904		ENSMUSG00000025043
ECHDC2	55268		ENSMUSG00000028601
EFNA3	1944		ENSMUSG00000028039
EHD1	10938		ENSMUSG00000024772
EPB41L4B	54566		ENSMUSG00000028434
EPHA1	2041		ENSMUSG00000029859
EPN2	22905		ENSMUSG00000001036
EPPK1	83481		
ERAS	3266		ENSMUSG00000031160
ERCC1	2067		ENSMUSG00000003549
ERCC4	2072		ENSMUSG00000022545
ESYT3	83850		ENSMUSG00000037681
ETNK2	55224		ENSMUSG00000070644
ETV3L	440695		
FAM173A	65990		ENSMUSG00000057411
FAM193B	54540	†	ENSMUSG00000021495
FAM22A	728118		
FAM48B2	170067		

Continued…

Human Gene Symbol	Human Entrez ID		Mouse Ensembl ID
FAM57B	83723		ENSMUSG00000058966
FAM86C2P	645332		
FAM86EP	348926		
FAM89A	375061	†	ENSMUSG00000043068
FBL	2091		ENSMUSG00000046865
FBLL1	345630		ENSMUSG00000051062
FBP2	8789	†	ENSMUSG00000021456
FBXW8	26259		ENSMUSG00000032867
FEM1B	10116		ENSMUSG00000032244
FERMT1	55612		ENSMUSG00000027356
FKBP1A	2280	†	ENSMUSG00000032966
FLJ32063	150538		
FLJ45983	399717		
FOLR1	2348		ENSMUSG00000001827
FZR1	51343		ENSMUSG00000020235
GDAP2	54834		ENSMUSG00000027865
GGT5	2687		ENSMUSG00000006344
GHDC	84514		ENSMUSG00000017747
GNB3	2784		ENSMUSG00000023439
GNG2	54331		ENSMUSG00000043004
GORAB	92344		ENSMUSG00000040124
GP1BB	2812	†	ENSMUSG00000050761
GPCPD1	56261		ENSMUSG00000027346
GPER	2852		ENSMUSG00000053647
GPR161	23432		ENSMUSG00000040836
GPR179	440435		ENSMUSG00000070337
GPR32	2854		
GPR89C	728932		
GPRASP1	9737		ENSMUSG00000043384
GPRC5D	55507		ENSMUSG00000030205
GPT2	84706	†	ENSMUSG00000031700
GRIA3	2892		ENSMUSG00000001986
GRIK4	2900		ENSMUSG00000032017
GRK7	131890		
GRM2	2912		ENSMUSG00000023192
GTF2I	2969	†	ENSMUSG00000060261
H2BFXP	767811		
HDAC7	51564		ENSMUSG00000022475
HDGFL1	154150		ENSMUSG00000045835
HIBCH	26275	†	ENSMUSG00000041426
HIC2	23119		ENSMUSG00000050240
HIST1H2BH	8345		ENSMUSG00000064168
HIST1H4G	8369		
HIVEP3	59269		ENSMUSG00000028634
HMGN2	3151		ENSMUSG00000090620
HPR	3250		ENSMUSG00000031722
HS3ST2	9956		ENSMUSG00000046321
HSD17B3	3293		ENSMUSG00000033122
HSPBAP1	79663		ENSMUSG00000022849
HTRA1	5654	†	ENSMUSG00000006205
IER5L	389792		ENSMUSG00000089762
IGF2BP2	10644		ENSMUSG00000033581
IL34	146433		ENSMUSG00000031750
INSC	387755	†	ENSMUSG00000048782
ITGAV	3685		ENSMUSG00000027087
ITGB4	3691		ENSMUSG00000020758
ITPKA	3706	†	ENSMUSG00000027296
JMJD8	339123		ENSMUSG00000025736
JRKL	8690		
KAL1	3730		
KATNAL2	83473		ENSMUSG00000025420
KCNE4	23704		ENSMUSG00000047330
KCNF1	3754		ENSMUSG00000051726
KCNMB2	10242		ENSMUSG00000037610
KCTD10	83892	*	ENSMUSG00000001098
KIAA1609	57707		ENSMUSG00000034105
KIAA1671	85379		ENSMUSG00000051339
KIRREL	55243		ENSMUSG00000041734
KLC3	147700		ENSMUSG00000040714
KLHDC5	57542		ENSMUSG00000040102
KLHL34	257240		ENSMUSG00000047485
KLK10	5655		ENSMUSG00000030693
KLK12	43849		ENSMUSG00000044430
KLK7	5650		ENSMUSG00000030713
KRT24	192666		ENSMUSG00000020913
KRT31	3881		ENSMUSG00000048981
KRTAP5-5	439915		
KRTCAP3	200634		ENSMUSG00000029149
L1CAM	3897		ENSMUSG00000031391

Continued…

Human Gene Symbol	Human Entrez ID		Mouse Ensembl ID
LACRT	90070		
LAT2	7462		ENSMUSG00000040751
LCA10	643736		ENSMUSG00000019971
LDHAL6A	160287		
LEPREL4	10609		ENSMUSG00000006931
LGI3	203190		ENSMUSG00000033595
LIFR	3977		ENSMUSG00000054263
LIMK1	3984		ENSMUSG00000029674
LOC100192378	100192378		
LOC100270710	100270710		
LOC219347	219347		ENSMUSG00000072678
LOC729020	729020		
LYRM1	57149		ENSMUSG00000030922
LYSMD1	388695		ENSMUSG00000053769
MAGEF1	64110		
MAN2B1	4125		ENSMUSG00000005142
MAP4	4134		ENSMUSG00000032479
MAPK9	5601		ENSMUSG00000020366
MAST4	375449		ENSMUSG00000034751
MC1R	4157	*	ENSMUSG00000074037
MCHR1	2847	*	ENSMUSG00000050164
METTL10	399818		ENSMUSG00000030960
METTL19	152992		ENSMUSG00000029097
METTL21B	25895		
MGAT3	4248	*	ENSMUSG00000042428
MGAT4B	11282	†	ENSMUSG00000036620
MGC14436	84983		
MGC16121	84848		
MLXIPL	51085	†	ENSMUSG00000005373
MMGT1	93380		ENSMUSG00000061273
MORF4	10934		
MORN3	283385		ENSMUSG00000029477
MSH4	4438		ENSMUSG00000005493
MTMR11	10903		ENSMUSG00000045934
MTMR7	9108		ENSMUSG00000039431
NAT9	26151		ENSMUSG00000015542
NAV1	89796		ENSMUSG00000009418
NCRNA00245	100131213		
NDUFA4	4697		ENSMUSG00000029632
NDUFV1	4723	†	ENSMUSG00000037916
NFKBIB	4793		ENSMUSG00000030595
NKAPL	222698		ENSMUSG00000059395
NKG7	4818		ENSMUSG00000004612
NLRP12	91662		ENSMUSG00000078817
NLRX1	79671		ENSMUSG00000032109
NOB1	28987		ENSMUSG00000003848
NPR1	4881		ENSMUSG00000027931
NR1D2	9975	†	ENSMUSG00000021775
NR1H4	9971	†	ENSMUSG00000047638
NR2C2	7182		ENSMUSG00000005893
NUDT8	254552		ENSMUSG00000024869
NUDT9P1	119369		
NUP153	9972		ENSMUSG00000021374
NUP214	8021		ENSMUSG00000001855
ODZ3	55714	†	ENSMUSG00000031561
OPCML	4978		ENSMUSG00000062257
OR1F1	4992		
OR1L8	138881		ENSMUSG00000075380
OR2A4	79541		ENSMUSG00000043605
OR2T33	391195		ENSMUSG00000056959
OR5P3	120066		ENSMUSG00000063764
OR6B1	135946		ENSMUSG00000049168
OSCP1	127700		ENSMUSG00000042616
PABPC1P2	728773		
PAGE2B	389860		
PAK4	10298		ENSMUSG00000030602
PANX1	24145		ENSMUSG00000031934
PAQR8	85315		ENSMUSG00000025931
PARVA	55742		ENSMUSG00000030770
PARVG	64098		ENSMUSG00000022439
PCDHGA10	56106		
PCDHGB5	56101		
PCDHGB6	56100		ENSMUSG00000023036
PCNXL2	80003		ENSMUSG00000060212
PDE11A	50940		ENSMUSG00000075270
PGAM4	441531		
PGBD3	267004		
PHKA1	5255		ENSMUSG00000034055
PHYHD1	254295		ENSMUSG00000079484

Continued…

Human Gene Symbol	Human Entrez ID		Mouse Ensembl ID
PIM1	5292	†	ENSMUSG00000024014
PIP5KL1	138429		ENSMUSG00000046854
PKDCC	91461	†	ENSMUSG00000024247
PKIG	11142	†	ENSMUSG00000035268
PKN1	5585		ENSMUSG00000057672
PLAT	5327	*†	ENSMUSG00000031538
PLEKHN1	84069		ENSMUSG00000078485
PLK5	126520		ENSMUSG00000035486
PLXND1	23129		ENSMUSG00000030123
PNKD	25953	†	ENSMUSG00000026179
PRDX2	7001	*†	ENSMUSG00000005161
PRDX4	10549		ENSMUSG00000025289
PRNP	5621		ENSMUSG00000079037
ProSAPiP1	9762		ENSMUSG00000037703
PRR22	163154		
PSIMCT-1	100101490		
PSMB9	5698	†	ENSMUSG00000024337
PSMD5	5711		ENSMUSG00000026869
PTGDS	5730		ENSMUSG00000015090
PTP4A3	11156	†	ENSMUSG00000059895
PTPRJ	5795		ENSMUSG00000025314
PTPRVP	148713		ENSMUSG00000066885
RAB36	9609		ENSMUSG00000020175
RAD23A	5886	†	ENSMUSG00000003813
RAMP1	10267	†	ENSMUSG00000034353
RCC2	55920		ENSMUSG00000040945
RETN	56729	†	ENSMUSG00000012705
RFWD2	64326		ENSMUSG00000040782
RG9MTD3	158234		ENSMUSG00000035601
RGS14	10636		ENSMUSG00000052087
RHOC	389		ENSMUSG00000002233
RMND5B	64777		ENSMUSG00000001054
RNASEH2A	10535	*	ENSMUSG00000052926
RNF39	80352		ENSMUSG00000036492
RPH3AL	9501		ENSMUSG00000020847
RPL12	6136		ENSMUSG00000080054
RPL8	6132		ENSMUSG00000003970
RPS27A	6233		ENSMUSG00000055093
RRAS2	22800		ENSMUSG00000055723
RSPH10B	222967		
RSPH10B2	728194		ENSMUSG00000075569
RSPH6A	81492		ENSMUSG00000040866
RTDR1	27156		ENSMUSG00000009070
RUSC1-AS1	284618		
RUVBL2	10856	*	ENSMUSG00000003868
S100A16	140576		ENSMUSG00000074457
SAE1	10055	†	ENSMUSG00000052833
SCNM1	79005		ENSMUSG00000005629
SCTR	6344		ENSMUSG00000026387
SCXA	100129885		ENSMUSG00000034161
SCXB	642658	†	ENSMUSG00000034161
SEMA6D	80031		ENSMUSG00000027200
SERP2	387923		ENSMUSG00000052584
SERPINB13	5275		ENSMUSG00000048775
SERPINE2	5270		ENSMUSG00000026249
SFRP2	6423		ENSMUSG00000027996
SFTA3	253970		
SFTPC	6440		ENSMUSG00000022097
SGCD	6444		ENSMUSG00000020354
SGSH	6448		ENSMUSG00000005043
SIAH3	283514		ENSMUSG00000091722
SIGLEC10	89790		ENSMUSG00000030468
SIGLEC15	284266		ENSMUSG00000091055
SIGLEC5	8778		ENSMUSG00000039013
SIRT2	22933		ENSMUSG00000015149
SLC11A1	6556		ENSMUSG00000026177
SLC12A8	84561		ENSMUSG00000035506
SLC22A13	9390		ENSMUSG00000074028
SLC25A10	1468		ENSMUSG00000025792
SLC25A16	8034		ENSMUSG00000071253
SLC27A1	376497	†	ENSMUSG00000031808
SLC29A4	222962		ENSMUSG00000050822
SLC2A9	56606		ENSMUSG00000005107
SLC39A14	23516		ENSMUSG00000022094
SLC41A1	254428	†	ENSMUSG00000013275
SLC4A2	6522		ENSMUSG00000028962
SLC4A5	57835		ENSMUSG00000068323
SLC5A7	60482		ENSMUSG00000023945
SMPD3	55512		ENSMUSG00000031906

Continued…

Human Gene Symbol	Human Entrez ID		Mouse Ensembl ID
SNAPC2	6618		ENSMUSG00000011837
SNORA12	677800		
SNORA62	6044		ENSMUSG00000064925
SNORA84	100124534		
SNORD116-16	100033428		
SNORD63	26785		
SNX29	92017		ENSMUSG00000071669
SOX14	8403		
SPARC	6678	†	ENSMUSG00000018593
SRL	6345		ENSMUSG00000022519
SSTR2	6752		ENSMUSG00000047904
STAC2	342667		ENSMUSG00000017400
STOX2	56977	†	ENSMUSG00000038143
SULT1A2	6799		
SURF6	6838		ENSMUSG00000036160
SUSD1	64420		ENSMUSG00000038578
SV2B	9899		ENSMUSG00000053025
SYCP1	6847	*	ENSMUSG00000027855
SYNGR2	9144		ENSMUSG00000048277
T	6862		ENSMUSG00000062327
TAC3	6866		ENSMUSG00000025400
TAOK2	9344		ENSMUSG00000059981
TBCA	6902	†	ENSMUSG00000042043
TBL2	26608	†	ENSMUSG00000005374
TBX1	6899	†	ENSMUSG00000009097
TCEAL2	140597		
TCEB3B	51224		
TEAD4	7004		ENSMUSG00000030353
TGM3	7053		ENSMUSG00000027401
TGM6	343641		ENSMUSG00000027403
TM6SF2	53345		ENSMUSG00000036151
TMEFF1	8577		ENSMUSG00000028347
TMEM104	54868		ENSMUSG00000045980
TMEM151B	441151		ENSMUSG00000050405
TMEM173	340061		ENSMUSG00000024349
TMEM176A	55365		ENSMUSG00000023367
TMEM176B	28959		ENSMUSG00000029810
TMEM223	79064		ENSMUSG00000075043
TMEM31	203562		
TMEM81	388730		ENSMUSG00000048174
TMEM87B	84910		ENSMUSG00000014353
TNFRSF8	943		ENSMUSG00000028602
TNFSF12	8742		ENSMUSG00000090170
TNFSF13	407977		ENSMUSG00000090170
TNNC2	7125		ENSMUSG00000017300
TRAF5	7188		
TSPO2	222642		ENSMUSG00000023995
TTC24	164118		ENSMUSG00000051036
TTLL10	254173		ENSMUSG00000029074
TUBB1	81027		ENSMUSG00000016255
UAP1L1	91373		ENSMUSG00000026956
UBE2L3	7332	†	ENSMUSG00000038965
UBE2V1	7335		ENSMUSG00000078923
UBE3B	89910	*	ENSMUSG00000029577
UCMA	221044		ENSMUSG00000026668
UFSP1	402682		ENSMUSG00000051502
UGCG	7357		ENSMUSG00000028381
UNC5CL	222643		ENSMUSG00000043592
UPK1A	11045		ENSMUSG00000006313
UQCR10	29796		ENSMUSG00000059534
USF2	7392		ENSMUSG00000058239
VPS13B	157680		ENSMUSG00000037646
VRK1	7443		ENSMUSG00000021115
VWF	7450	†	ENSMUSG00000001930
WDR3	10885		ENSMUSG00000033285
WIF1	11197		ENSMUSG00000020218
XBP1	7494	†	ENSMUSG00000020484
XPA	7507		ENSMUSG00000028329
XRCC2	7516		ENSMUSG00000028933
YY2	404281		ENSMUSG00000091736
ZFAND2A	90637	†	ENSMUSG00000053581
ZFP57	346171		ENSMUSG00000036036
ZFP90	146198		ENSMUSG00000031907
ZMAT1	84460		ENSMUSG00000052676
ZNF286B	729288		
ZNF30	90075		
ZNF304	57343		
ZNF323	64288		
ZNF567	163081		

Continued…

Human Gene Symbol	Human Entrez ID		Mouse Ensembl ID
ZNF580	51157	*	ENSMUSG00000055633
ZNF581	51545		ENSMUSG00000035228
ZNF605	100289635		ENSMUSG00000023284
ZNF628	89887		ENSMUSG00000074406
ZNF646	9726		ENSMUSG00000049739
ZNF652	22834		ENSMUSG00000075595
ZNF668	79759		ENSMUSG00000049728
ZNF670	93474		
ZNF705D	728957		
ZNF721	170960		
ZNF83	55769		
ZW10	9183		ENSMUSG00000032264

B

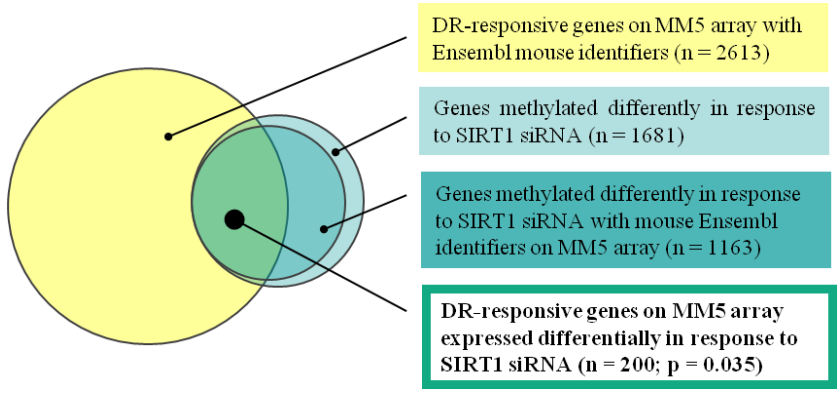

Figure 7.3. Analysis by the 'most stringent pathway' of DNA methylation affected by SIRT1 manipulation (siRNA or overexpression construct) and by ageing. *A – Genes with changed methylation over 72 hours in response to manipulated SIRT1 expression in Caco-2 cells by siRNA and overexpression are listed. Genes identified through the in silico analysis as differentially methylated in older tissue are in shaded cells. Genes identified through the in silico analysis as sites of SIRT1-binding (*) or as responsive to DR (†) are highlighted by dashed underlining. Human gene symbols and Entrez identifiers and mouse Ensembl identifiers are stated. B – Overlaps between genes identified as responsive to DR and genes differently methylated under conditions of SIRT1 knockdown are represented in a Venn diagram. 'n' indicates the number of genes common to both group; 'p' indicates the cumulative hypergeometric probability***..**

7.3 Investigating the genome-wide effects of SIRT1 on gene expression

To complement investigations into our hypothesis that SIRT1 may be mediating the beneficial effects of DR on gene regulation via DNA methylation we investigated the direct effects of SIRT1 manipulation on gene expression. Microarray-based techniques allowed for the genome-wide effects of SIRT1 manipulation to be probed, profiling global gene expression changes in response to SIRT1 levels. Such approaches would detect changes in gene expression brought about by changing the level of SIRT1 expression through all active mechanisms – not only effect on gene methylation. For example, multiple cellular substrates undergo SIRT1-mediated deacetylation, including transcription factors and co-regulators that are required for gene expression. For example, the forkhead transcription factors are down regulated by SIRT1 preventing the activation of gene transcription and subsequent downstream processes such as cell differentiation and apoptosis (Brunet et al., 2004; Motta et al., 2004).

The approach to data analysis to address our hypothesis that some effects of SIRT1 on gene expression are through DNA methylation was to compare the list of genes we found to be differentially methylated in response to changing levels of SIRT1 expression (as described in the preceding sections of this chapter) with the list of genes we found to be differentially expression in response to changing levels of SIRT1 expression.

7.3.1 Experimental design

RNA for transcriptome analysis under conditions of SIRT1 overexpression or knockdown was obtained from cells treated exactly as described for preparation of DNA for methylome analysis (Section 7.2.1). Samples for DNA methylome analysis and transcriptome analysis were obtained from cells processed in parallel. RNA for expression analysis was prepared from three independent experiments pooled to produce 3 biological repeats for each condition (SIRT1 overexpression; SIRT1 knockdown and corresponding controls), of which all three biological replicates for SIRT1 overexpression and controls and two biological replicates for each of the SIRT1 siRNAs and control were hybridised to the expression array.

Having obtained RNA samples with confirmed SIRT1 knockdown and overexpression, gene expression was measured using the Illumina Gene Expression Service provided by Service XS (Leiden, The Netherlands) as described in Section 2.7.3. Each RNA sample was subjected to quality and integrity checks before global gene expression was measured by microarray analysis. RNA quality was assessed by spectrophotometry (Section 2.4.4) and integrity was assessed using the Bioanalyser (Section 2.4.5); the integrity output of the Bioanalyser for the samples analysed by microarray hybridisation is shown in Figure 7.4.

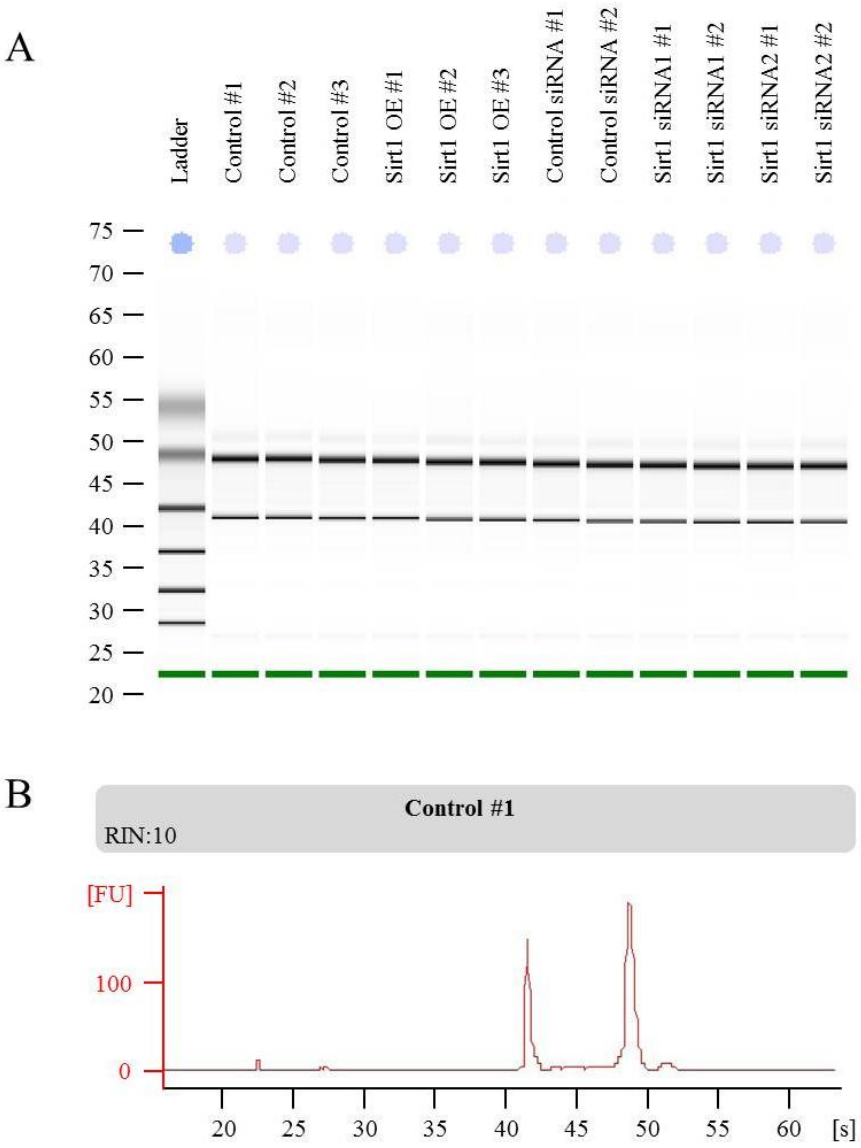

Figure 7.4. RNA integrity. *A – Gel-like image generated from bioanalyser electropherogram output. B – Typical bioanalyser electropherogram output. A RIN of 7 or more indicates RNA of sufficient quality.*

7.3.2 Microarray design and hybridisation by Service XS

After confirmation of integrity and quality, RNA samples were sent to Service XS for analysis. The Illumina HumanHT-12 v4 Expression BeadChip consists of 12 identical arrays targeting over 47,000 probes covering genes, gene candidates and splice variants from the 2009 NCBI RefSeq Release 38. RNA samples were reverse transcribed to produce a cDNA template that was then *in vitro* transcribed amplified to incorporate biotin-labelled nucleotides. RNA samples from cells overexpressing SIRT1 and corresponding vector only controls were hybridised as biological triplicates onto individual arrays, RNA samples from cells in which SIRT1 expression was reduced by one of two siRNAs and the corresponding control were hybridised as biological duplicates onto individual arrays within the HumanHT-12 v4 Expression BeadChip (Illumina), then the signal was developed with Streptavidin-Cy3 and the BeadChip scanned. Gene expression data from the scan images and the intensity value for each probe was calculated.

7.3.3 Data analysis

The raw data scanned from the array chips was supplied electronically and was deposited in GEO (accession GSE30486). Using RankProd analysis (Hong et al., 2006) on a quality filtered subset of microarray probes (Section 2.7.3.3), 95 genes were identified whose expression was reduced (*Figure 7.5A* and Appendix E.III) and 62 genes identified whose expression was increased (*Figure 7.5B* and Appendix E.III) by a factor of 1.5-fold or greater under conditions of SIRT1 knockdown. Under conditions of SIRT1 overexpression there was no statistically significant difference between gene expression in samples where SIRT1 was overexpressed compared with the control. The absence of any deviation, even to the extent that would be expected between biological replicates, suggested that an element of the gene expression profiling had failed and the experiment should be repeated, which time constraints did not permit. To allow comparison with the previous mouse data sets of genes that bound SIRT1 and genes responsive to DR used for the *in silico* analysis presented in Chapter 5, the genes differentially expressed under conditions of SIRT1 knockdown were assigned equivalent mouse Ensembl identifiers. A total of 107 of the 119 genes that were differentially expressed under conditions of SIRT1 knockdown were present on the MM5 microarray (*Figure 7.5A* and *Figure 7.5B* and Appendix E.III). Of these genes, 39 appeared on the list of 2613 mouse genes that respond to DR (*Figure 7.5A* and *Figure 7.5B*; shaded cells), giving a representation factor of 1.98 and hypergeometric probability of 2.67×10^{-5} (*Figure 7.5C*). Thus the gene profile of Caco-2 cells affected by SIRT1 manipulation matches, to an extent substantially greater than expected by chance, genes that respond to DR across a range of different mouse tissues, both providing validity to Caco-2 cells with altered SIRT1 expression as an *in vitro* model of DR and lending support to the view that SIRT1 is a key mediator of the response of mammalian cells to DR. Overlaps between the 107 genes assigned mouse Ensembl identifiers affected by SIRT1 knockdown in Caco-2 cells and genes identified through the *in silico* analysis as binding SIRT1 (3 genes; r.f. 1.11; $p = 0.507$) or between these 107 genes and the set

of genes reported to show ageing-related changes in methylation status used for the *in silico* analysis (7 genes; r.f. 1.07; p = 0.478) (*Figure 7.5A* and *Figure 7.5B;* denoted by * or # respectively and Appendix E.III) did not exceed the level expected by chance.

A

Genes affected by reduced SIRT1 expression (siRNA)

Human Gene Symbol	Human Entrez ID		Mouse Ensembl ID	Fc ↓
ISG15	9636		ENSMUSG00000035692	2.28
IFIT1	3434		ENSMUSG00000034459	2.25
NPPB	4879		ENSMUSG00000029019	2.19
IFI27	3429		ENSMUSG00000064215	2.01
P4HA2	8974		ENSMUSG00000018906	1.95
RCN2	5955		ENSMUSG00000032320	1.93
PRIC285	85441		ENSMUSG00000027580	1.80
SIVA	10572		ENSMUSG00000064326	1.79
FAM96A	84191		ENSMUSG00000032381	1.79
LAMP2	3920		ENSMUSG00000016534	1.77
TXNIP	10628		ENSMUSG00000038393	1.76
PRODH	5625		ENSMUSG00000003526	1.76
UGT1A6	54578		ENSMUSG00000054545	1.75
TMED10	10972		ENSMUSG00000021248	1.74
GSTA2	2939		ENSMUSG00000057933	1.70
IGFBP6	3489		ENSMUSG00000023046	1.62
CIDEC	63924		ENSMUSG00000030278	1.61
CDKN1A	1026	*	ENSMUSG00000023067	1.60
UQCRQ	27089		ENSMUSG00000044894	1.59
PTEN	5728		ENSMUSG00000013663	1.57
ERGIC1	57222		ENSMUSG00000001576	1.57
ACSL5	51703		ENSMUSG00000024981	1.57
TPT1	7178	*	ENSMUSG00000060126	1.56
LOX	4015		ENSMUSG00000024529	2.47
ANKRD37	353322		ENSMUSG00000050914	2.43
APOA4	337		ENSMUSG00000032080	2.34
CSF1R	1436		ENSMUSG00000024621	2.34
CEACAM6	4680			2.30
IFITM1	8519		ENSMUSG00000025491	2.26
AQP10	89872			2.19
APOC3	345		ENSMUSG00000032081	2.10
GNRH2	2797		ENSMUSG00000015812	2.09
GPX2	2877	*	ENSMUSG00000042808	2.05
SIRT1	23411		ENSMUSG00000020063	2.00
MORF4L1	10933		ENSMUSG00000062270	1.97
NQO1	1728		ENSMUSG00000003849	1.97
AKR1C2	1646		ENSMUSG00000021207	1.96
NDRG4	65009		ENSMUSG00000036564	1.92
CEACAM1	634		ENSMUSG00000074272	1.91
GSTA1	2938		ENSMUSG00000074183	1.90
OAS3	4940		ENSMUSG00000032661	1.89
MYPOP	339344		ENSMUSG00000048481	1.89
WSB1	26118		ENSMUSG00000017677	1.89
EEF1A2	1917		ENSMUSG00000016349	1.88
LOC644799	644799			1.88
LGALS14	56891			1.87
RPS29	6235		ENSMUSG00000034892	1.87
C5orf28	64417			1.86
ALB	213		ENSMUSG00000029368	1.85
PRKRIR	5612		ENSMUSG00000030753	1.84
HN1	51155		ENSMUSG00000020737	1.83
B3GNT1	11041		ENSMUSG00000047379	1.83
OKL38	29948		ENSMUSG00000074063	1.80
FOXQ1	94234		ENSMUSG00000038415	1.80
LOC644363	644363			1.78
MIR1978	100302173			1.78
GAST	2520		ENSMUSG00000017165	1.76
CANX	821		ENSMUSG00000020368	1.76
MX1	4599		ENSMUSG00000000386	1.76
TMED10P	286102			1.75
ITGA2	3673		ENSMUSG00000015533	1.75
ISG20	3669		ENSMUSG00000039236	1.72
WBSCR22	114049		ENSMUSG00000005378	1.70
IFRD2	7866		ENSMUSG00000010048	1.69
IL13RA1	3597		ENSMUSG00000017057	1.69
LOC440145	440145			1.68
CDK2	1017		ENSMUSG00000025358	1.68
NAT13	80218		ENSMUSG00000022698	1.68
CD68	968		ENSMUSG00000018774	1.68
UTS2	10911		ENSMUSG00000028963	1.68
TMBIM6	7009	#	ENSMUSG00000023010	1.68
N-PAC	84656		ENSMUSG00000022536	1.67
OSBPL8	114882		ENSMUSG00000020189	1.66
IPO11	51194		ENSMUSG00000042590	1.66
SCARNA14	692149			1.65
MAL2	114569	*	ENSMUSG00000024479	1.65
LOC644844	644844			1.65
LOC285074	285074			1.62
RAB32	10981		ENSMUSG00000019832	1.62
SEPHS2	22928		ENSMUSG00000049091	1.61
CDC2L6	23097		ENSMUSG00000038481	1.61
TM4SF5	9032		ENSMUSG00000018919	1.61

Continued...

Human Gene Symbol	Human Entrez ID	Mouse Ensembl ID	Fc ↓
NDUFA7	4701	ENSMUSG00000041881	1.60
REEP1	65055	ENSMUSG00000052852	1.59
IRF9	10379	ENSMUSG00000002325	1.59
VAMP8	8673	ENSMUSG00000050732	1.58
ANAPC1	64682	ENSMUSG00000014355	1.58
RPL8	6132	ENSMUSG00000003970	1.57
GGCT	79017	ENSMUSG00000002797	1.57
CALM1	801	ENSMUSG00000001175	1.57
RYBP	23429	ENSMUSG00000072872	1.56
SCARNA18	677765		1.56
HDHD1A	8226	ENSMUSG00000048875	1.55
CCND1	595	ENSMUSG00000070348	1.55
TFDP1	7027	ENSMUSG00000038482	1.52

B

Genes affected by reduced SIRT1 expression (siRNA)

Human Gene Symbol	Human Entrez ID		Mouse Ensembl ID	Fc ↑
UGP2	7360	#	ENSMUSG00000001891	1.90
FABP5	2171		ENSMUSG00000027533	1.90
GGH	8836		ENSMUSG00000073987	1.86
CYP51A1	1595	*	ENSMUSG00000001467	1.73
LAPTM4B	55353		ENSMUSG00000022257	1.69
VIM	7431		ENSMUSG00000026728	1.69
COL3A1	1281		ENSMUSG00000026043	1.68
SERPINI1	5274		ENSMUSG00000027834	1.67
CA2	760		ENSMUSG00000027562	1.66
CTSZ	1522		ENSMUSG00000016256	1.65
FAM98A	25940		ENSMUSG00000002017	1.59
TUBA3D	113457		ENSMUSG00000067338	1.59
BNIP3L	665		ENSMUSG00000022051	1.57
TAGLN	6876		ENSMUSG00000032085	1.55
PDGFRA	5156		ENSMUSG00000029231	1.54
HRSP12	10247		ENSMUSG00000022323	1.53
LOC387934	387934			2.09
UBD	10537		ENSMUSG00000035186	2.08
UQCRH	7388	*	ENSMUSG00000063882	1.93
CLEC2D	29121	#	ENSMUSG00000030157	1.93
LOC100131672	100131672			1.91
LOC653737	653737			1.87
RPLP1	6176	*	ENSMUSG00000007892	1.85
LOC441743	441743			1.85
RGS4	5999		ENSMUSG00000038530	1.84
KIAA1199	57214		ENSMUSG00000052353	1.79
LOC645231	645231			1.75
LOC642738	642738			1.75
CCNO	10309		ENSMUSG00000042417	1.73
FGG	2266		ENSMUSG00000033860	1.69
OSTCL	202459			1.69
ANXA2P1	303			1.69
LOC730996	730996			1.68
FGA	2243		ENSMUSG00000028001	1.67
ARL6IP1	23204		ENSMUSG00000030654	1.67
LOC100134273	100134273			1.66
KCNJ8	3764		ENSMUSG00000030247	1.66
LOC727984	727984			1.64
TULP3	7289		ENSMUSG00000001521	1.64
MYO1D	4642		ENSMUSG00000035441	1.64
PI3	5266			1.64
LOC646527	646527			1.62
ZNF738	148203			1.62
LOC646966	646966			1.61
YY1	7528		ENSMUSG00000021264	1.61
LOC390735	390735			1.60
LOC100133803	100133803			1.60
LOC727821	727821			1.60
LOC653631	653631			1.59
RPL12P6	440176			1.59
LOC100131905	100131905			1.59
LOC644937	644937			1.59
UBE2E1	7324		ENSMUSG00000021774	1.59
LOC389322	389322			1.58
TRMT11	60487		ENSMUSG00000019792	1.57
ODAM	54959		ENSMUSG00000009580	1.56
LOC647307	647307			1.56
ANKRD1	27063		ENSMUSG00000024803	1.55
LOC100129599	100129599			1.53
PRPS1	5631		ENSMUSG00000031432	1.53
AIDA	64853		ENSMUSG00000042901	1.53
TAF15	8148		ENSMUSG00000020680	1.51

C

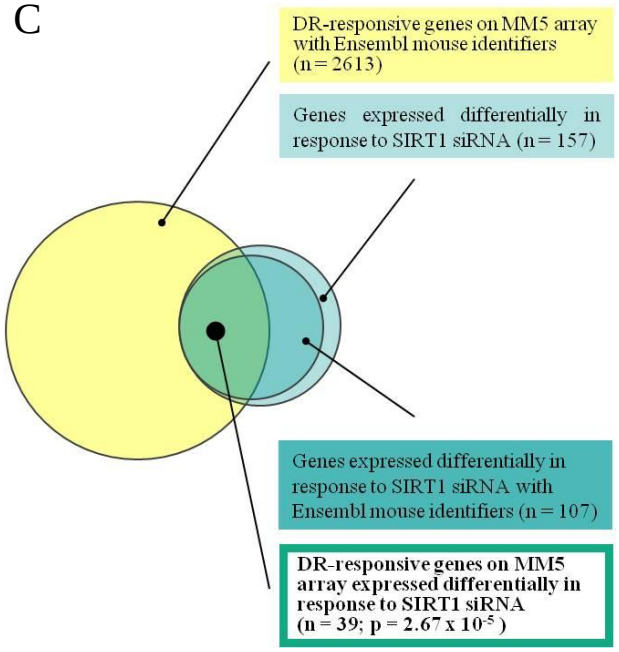

Figure 7.5. Analysis of genes affected by reduced SIRT1 expression (siRNA) and by DR. *Genes with expression reduced (A) or increased (B) by 1.5-fold or greater (ranked) over 72 hours in response to reducing SIRT1 expression in Caco-2 cells by siRNA are listed. Genes identified through the in silico analysis as responsive to DR are in shaded cells. Genes identified through the in silico analysis as sites of SIRT1-binding (*) or as differentially methylated in older tissue (#) are highlighted by dashed underlining. Human gene symbols and Entrez identifiers and mouse Ensembl identifiers are stated. Overlaps between genes identified as responsive to DR and genes affected by SIRT1 knockdown are represented in a Venn diagram (C). 'n' indicates the number of genes common to both groups; 'p' indicates the cumulative hypergeometric probability.*

7.4 Relationship between the genome-wide effects of SIRT1 on DNA methylation and gene expression

One of the primary goals of obtaining parallel data on gene methylation and expression in Caco-2 cells in response to changed levels of SIRT1 expression was to investigate the relationship between the two measures. The two data sets were overlapped using the Entrez gene identifier annotations provided (Appendix E.IV). For the purpose statistical analysis by calculation of hypogeometric probability, a universal list of genes was generated by identifying all of the 9838 that were enriched for methylation under any of our experimental conditions that were represented also on the transcriptome (Illumina) array. The rationale for excluding any genes on the transcriptome array that were not identified as methylated under any of our conditions was to avoid a statistical bias in favour of a significant overlap between genes undergoing both a change in methylation and expression in response to SIRT1 manipulation by virtue of using a universal gene set that included genes for which there was no evidence of methylation *per se*. Of the 9838 genes, 9659 were also on the transcriptome array (Appendix E.IV). Of the 1555 genes for which we detected changes in methylation under conditions of SIRT1 overexpression (compared with control) 1524 were on the transcriptome array (gene list 'A' – Appendix E.IV). Of the 1681 genes for which we detected changes in methylation under conditions of SIRT1 knockdown (compared with control) 1657 were on the transcriptome array (gene list 'B' – Appendix E.IV). Of the 490 genes (*Figure 7.4*) for which we detected changes in methylation under conditions of both SIRT1 overexpression and knockdown (compared with control), 482 were on the transcriptome array (gene list 'C' – Appendix E.IV). Of the 157 genes that we found to be expressed differentially in response to SIRT1 knockdown, 53 (*Figure 7.6*) were represented within the pool of 9659 genes that showed enrichment for methylation under any of our experimental conditions (and were represented on the transcriptome array). None of the overlaps between these 53 genes and gene lists 'A', 'B' or 'C' as defined above were statistically significant (for gene list 'A': 9 genes, r.f. 1.08, $p = 0.46$; for gene list 'B': 7 genes, r.f. 0.77, $p = 0.82$; for gene list 'C': 1 gene, r.f. 0.38, $p = 0.93$; for gene lists and overlaps see Appendix E.IV). A possible explanation is that whilst SIRT1 affects both gene methylation and expression, there is no causal relationship; rather SIRT1 acts through independent mechanisms to bring about both effects. However, as discussed in more depth in the following section, analysis of the methylome data is still at a preliminary stage and refinement of the data analysed may uncover large overlaps.

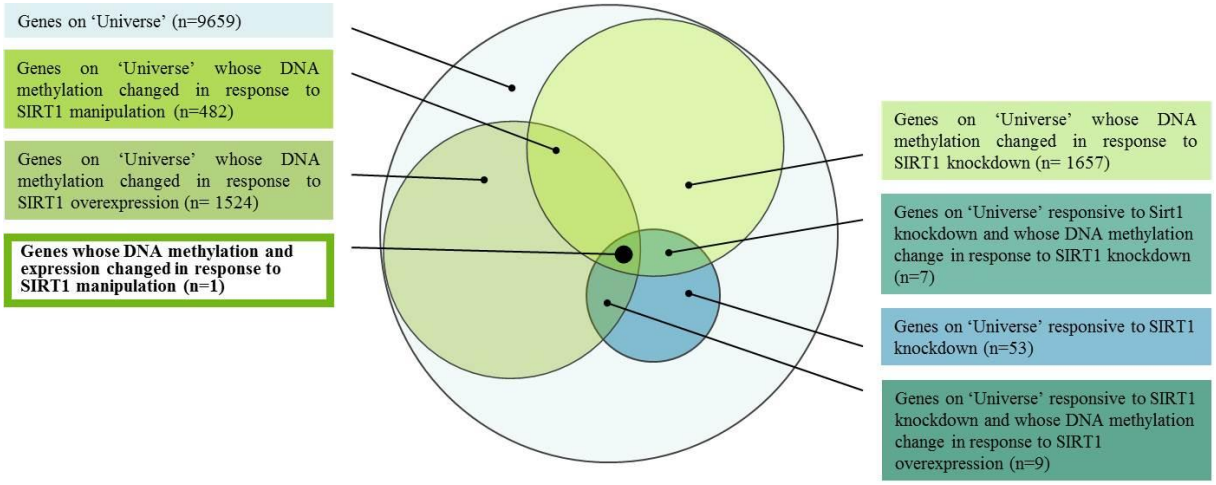

Figure 7.6. Analysis of gene expression and DNA methylation affected by SIRT1 manipulation. *Diagrammatic representation of the overlaps between genes identified as affected by SIRT1 manipulation either in expression levels or DNA methylation status. 'n' indicates the number of genes common to both groups.*

7.5 Discussion

The effects of SIRT1 manipulation on DNA methylation and gene expression on a genome-wide scale were investigated. Genes whose expression changed in response to SIRT1 knockdown were represented to an extent greater than would be expected by chance on the list of genes previously generated through work presented in Chapter 5 whose expression changed in response to DR. This observation supports the view that manipulation of SIRT1 in the Caco-2 cell line provides a model of DR. Genes whose DNA methylation changed in response to SIRT1 manipulation (siRNA knockdown or overexpression) were not represented to an extent greater than would be expected by chance on the list genes generated whose DNA methylation status changed with age.

The criteria applied to identify differentially methylated loci were particularly stringent. Genes were considered as methylated only if enrichment peaks were reported based on analysis of hybridisation to all replicate arrays and were identified as undergoing a SIRT1-dependent change in methylation only if a peak became absent under the condition being compared. Thus, in this preliminary analysis we did not take into account any quantitative difference in peak enrichment intensity between conditions being compared; rather we took an 'all or none' approach. Application of a more quantitative approach is likely to increase the list of genes identified as differentially methylated in response to changing levels of SIRT1 expression and may uncover other significant associations with other data sets. Such changes will be undertaken through research beyond the scope or available timescale of the current project.

The large number of candidate gene targets generated through analysis presented in this chapter open many avenues for further exploration. Follow up investigations could focus on the broad analysis of separating responses according to the direction of the methylation change in response to an increase in SIRT1 from knockdown to endogenous levels or endogenous to overexpressed levels. More specific analysis could focus in on select gene targets generated from the above directional studies and, as discussed previously in Chapter 6, effects of SIRT1 on expression of target genes could be measured by RT-qPCR and effects on DNA methylation measured by pyrosequencing. Additionally, a causal link between DNA methylation and gene expression could be addressed using *in vitro* methylation of promoter-reporter constructs and/or by the treatment of cells with demethylating agents such as 5-aza-2'-deoxycytidine, followed by RT-qPCR to examine effects on target gene expression.

8 Discussion and conclusions

This study set out to investigate effects of the SIRT1 histone deacetylase and dietary compounds on DNA methylation in the context of dietary restriction (DR) and longevity. The SIRT1 protein acts to remove acetyl groups from the lysine residues on histone tails, as well as an array of other protein substrates and this action may be a mechanism through which some of the beneficial effects of DR are mediated. DNA methylation changes with ageing and is associated with histone deacetylation, the two mechanisms working in juxtaposed roles to regulate gene expression. The work outlined in this thesis investigated in detail the relationship between manipulation of SIRT1 expression and DNA methylation at global and site-specific levels in the human intestinal cell line Caco-2.

The role of SIRT1 in lifespan extension received much attention after initial discoveries in yeast (Kaeberlein, 1999), worms (Tissenbaum and Guarente, 2001) and flies (Rogina and Helfand, 2004) showed that increasing the levels of the equivalent SIRT1 homologue (Sir2) resulted in longer lifespan. The response to increasing the levels of Sir2 showed many other parallels with the response of these organisms to DR, including a reduction in fertility.

DR also increases lifespan in rodents, and parallel observed increases in SIRT1 levels (Barger et al., 2008; Kanfi et al., 2008; Nisoli et al., 2005; Cohen et al., 2004) suggest that SIRT1 may also play a role in this response in mammals. Such observations further fuelled interest in SIRT1, and in particular if activating SIRT1 would mimic some of the beneficial responses associated with the DR. Our initial studies, presented in Chapter 3, aimed to determine if SIRT1, alone or in combination with, specific dietary compounds, reported previously in the literature to activate SIRT1 (resveratrol) or that had a similar structure and were implicated in DNA methylation (genistein/daidzein), could alter DNA methylation levels, indicating a possible mechanism through which healthspan-enhancing aspects of DR might be mediated. Several cell lines derived from a variety of tissues were assessed for the levels of global DNA methylation with the aim of identifying cell models with a range of endogenous levels of DNA methylation and select cell lines with very high and low levels of methylation to investigate the effects of SIRT1 expression at these extremes. No significant differences were found in levels of global DNA methylation measured by the LINE-1 and LUMA pyrosequencing assays. The human intestinal Caco-2 cell line was therefore selected as a model for testing the effects dietary polyphenols on DNA methylation. This cell line has the morphological and physiological properties of enterocytes, the absorptive cell in the epithelial lining of the intestine, and so provided, in part, a suitable model for the intestinal response to DR, or, in the case of this study, potential dietary mimetics of DR whose first encounter upon consumption would be with the intestinal epithelial barrier. The major limitation with using a tumour-derived cell line model in any scientific investigation, (excluding those into the related

cancer from which the cell line was derived) is that changes associated with oncogenesis may influence findings. This limitation must be borne in mind particularly in studies involving measurement of DNA methylation, because it is well established that changes in DNA methylation occur with oncogenesis (Cheung et al., 2009). Thus a limitation of the current study is that observed changes in DNA methylation would be against a background that was already different from normal enterocytes. Nonetheless, we reasoned that the model was adequate at least to demonstrate proof of concept that SIRT1 and/or dietary polyphenols can influence DNA methylation and also identify affected genes for more targeted investigations, ultimately (beyond the scope of this project) in normal tissues.

We established that SIRT1 manipulation alone in the Caco-2 cell line had no effect on global DNA methylation levels. This perhaps was unsurprising as the LINE-1 element used as a surrogate marker of global DNA methylation was not identified as a site at which SIRT1 bound to the genome (in mouse embryonic stem cells) (Oberdoerffer et al., 2008). Subsequent investigations into the effects of polyphenols alone or in combination with SIRT1 manipulation yielded complex results, though only when assessed by gel-based LINE-1 COBRA. Specifically, resveratrol (10μM, 48 hours) caused an increase in DNA methylation at the LINE-1 element. This response was abrogated when SIRT1 overexpression was combined with resveratrol treatment returning DNA methylation levels back to baseline. SIRT1 overexpression in the presence of genistein or daidzein (50 μM, 48 hours) caused a decrease in DNA methylation, suggesting that polyphenols can interact with SIRT1 to have effects on mechanisms involved in the process of methylating and demethylating cytosine residues. The nature of such possible interactions is unclear, but the complexity in the pattern observed may indicate effects through multiple pathways, some of which become predominant at particular ratios of SIRT1 to specific polyphenols.

Measurement of global DNA methylation with a surrogate marker such as the LINE-1 element also has drawbacks in terms of coverage of only one sequence (albeit frequent) and its possible altered methylation status in the Caco-2 cell line compared with normal tissue. Comparisons with values for methylation of the LINE-1 element in normal tissue reported in the literature are difficult because levels of methylation at specific, adjacent CpG sites appear to be substantially different. For example in the assay we applied values at the different CpG sites varied from ~30 % to ~70 % in the Caco-2 cell line. Reports of methylation at individual CpG sites in the LINE-1 element are frequently not available for comparison as CpG site methylation is reported as an average of the individual values. Comparison is further complicated by the fact that different investigations have measured methylation at different CpG sites within the LINE-1 sequence. A further possible limitation associated with use of the LINE-1 element to probe effects on global DNA methylation is that the sequence may be particularly refractory to methylation changes. For example, although reports in the literature show

many changes in DNA methylation across different sites as individuals grow older (Maegawa et al., 2010; Rakyan et al., 2010; Teschendorff et al., 2010; Christensen et al., 2009; Kwabi-Addo et al., 2007), a longitudinal study in humans aged between 55 and 92 years showed no change in the levels of LINE-1 DNA methylation observed in individuals over an 8 year period (Bollati et al., 2009) and no change was measured in the levels of LINE-1 methylation levels between different age groups in biopsied normal human colon (Figueiredo et al., 2009).

As the number of reported investigations into the possible ability of SIRT1 and its homologues to increase lifespan have increased, so has the level of discordance within the published literature as to the exact role, if any, it plays in determining lifespan different species. In 2010, a review article on the role played by nutrient sensing pathways in the longevity response to DR by Fontana et al (Fontana et al., 2010) sparked a series of communications in the journal Science after the failure to include consideration of the role of sirtuins. Thirty-three scientists involved in research on sirtuins argued that the numerous observations that have implicated the sirtuin family in nutrient-sensing and life extension pathways, backed up by a large body of peer reviewed evidence, warranted inclusion in the review. However, the authors countered that effects of SIRT1 on lifespan extension in mammals had yet to be demonstrated and so did not fit into the discussion of conserved pathways. The ability of the SIRT1 homologues to extend lifespan in worms and flies has recently been questioned as procurement and study of strains with Sir2 overexpression, originally reported to have extended lifespan, showed that these effected were not reproduced when specific genetic crosses were made (Burnett et al; Nature, 2011; in press). This genetic approach led to identification of the Dyf gene in *C. elegans*, and not Sir2, as co-segregating with the extended-lifespan phenotype. Observations that SIRT1 protein increased with DR in rodents have not been unchallenged. Moreover SIRT1-overexpressing transgenic mice do not appear to live longer than control animals. However, numerous beneficial effects mimicking those seen in DR, including reduced fasting levels of insulin, glucose and cholesterol and improved glucose homeostasis (Bordone et al., 2007), are commensurate with better health in older age which is highly pertinent to our ageing society.

Further controversy surrounding sirtuins arose in the debate over activation of SIRT1 by resveratrol and related synthetic compounds. Multiple publications based observations of increased SIRT1 deacetylase activity in response to resveratrol treatment appear to have been based on a flawed fluorescence activity assay, where resveratrol-mediated activation of SIRT1 was only observed when SIRT1 was attached to the fluorescent moiety. In our own investigation we encountered different problems with the assay in that fluorescence emission was completely independent of the addition of recombinant SIRT1 or cell lysate. While there may have been an opportunity to further optimise the assay – perhaps to obtain fluorescence emission above this ‘background’ level – the accumulating evidence concerning the lack of robustness of the assay led us to abandon this approach. A limitation

of several aspects of the present study, therefore, is that although we established unequivocally that SIRT1 mRNA and protein levels were affected substantially in the Caco-2 cell line model of SIRT1 overexpression and knockdown that we employed to measure effect on both DNA methylation and gene expression, we did not demonstrate that these changes resulted in the (expected) altered level of SIRT1 enzymatic activity. Other reports of studies that did not rely on the fluorescence-based assay of SIRT1 activation do support the view that this polyphenol can activate SIRT1. For example, resveratrol was shown to change the levels of SIRT1 mRNA and protein in coronary arterial endothelial cells and cultured arteries, promoting mitochondrial biogenesis (Csiszar et al., 2009), and the Krüppel-like factor 2 (KLF2), whose deficiency has been show to induce atherosclerosis, is upregulated by resveratrol in a SIRT1-dependent manner (Gracia-Sancho et al., 2010), suggesting that some of the beneficial effects of resveratrol are through SIRT1.

To better understand mechanisms through which SIRT1 expression could be regulated, the transcriptional activity of the *SIRT1* promoter was investigated in response to polyphenols and changes in promoter methylation. We also aimed to determine if there are changes in expression of SIRT1 with increased age. We established that the plant polyphenols investigated did not affect *SIRT1* activity at the transcriptional level. Caco-2 cells transfected with a promoter-reporter construct containing the *SIRT1* promoter then treated with the polyphenols resveratrol, genistein and daidzein showed no change in reporter gene expression. The generation of the *SIRT1* promoter-reporter construct allowed further investigations into effects on *SIRT1* transcriptional activity with respect to the influence of promoter methylation. Caco-2 cells transfected with a methylated SIRT1 promoter report construct had significantly reduced levels of reporter gene activity compared with an unmethylated control, suggesting SIRT1 activity can be regulated through the methylation status of the promoter region upstream of the *SIRT1* gene.

Our hypothesis proposes that the increased levels of SIRT1 seen under DR affect levels of DNA methylation to mediate the beneficial effects of reduced dietary intake. There is documented evidence of levels of SIRT1 fluctuating with age (Alcendor et al., 2007; Sasaki et al., 2006; Michishita et al., 2005; Sakamoto et al., 2004) though to our knowledge there is currently no literature that reports the effects of age in the gut, a tissue which, if dietary intake was effecting healthy lifespan – potentially through SIRT1 levels – would be the first barrier responsible for regulating the downstream response of the body to dietary restriction. We addressed the possibility that an increase in SIRT1 expression may oppose an age-related decline in expression using mouse intestinal tissue. We found no effect of age on the expression of SIRT1 at the protein level in mouse intestinal tissue extracted from young and old mice. These measurements were made in a small sample set, so increased sample numbers, as well as exploring SIRT1 levels in various tissue types, would be required to draw a more robust conclusion.

Having obtained only very limited data supporting possible effects of SIRT1 (in combination with polyphenols) on methylation at the LINE-1 element in our cell line model, we proposed that it was important to address the possibility that effects of SIRT1 on DNA methylation may be predominantly at other sites, particularly at specific gene loci. Targets to investigate for site-specific methylation changes in response to SIRT1 manipulation were identified through use of published resources to identify genes that bind to SIRT1 but also show a response to DR and change in methylation status with ageing, as described in Chapter 5. Ten genes (*CDC7, EIF5, IRX3, KLF3, LDLR, MYH10, PCYT1A, PTPRG, SLC39A4,* and *TBX3*) were found to fit all three of these criteria and were involved in a diverse range of cellular processes. To our knowledge, these genes have not previously been highlighted in the context of lifespan, DR or SIRT1 function. In addition to identifying specific genes for further study this *in silico* analysis also lent support to our hypothesis because overlaps between all pairs of gene lists, as well as the 'three way' overlap, were all significantly greater than expected by chance. Further investigation of promoter DNA methylation and gene expression of these genes highlighted by the *in silico* analysis in response to SIRT1 manipulation, described in Chapter 6, revealed that changing the level of SIRT1 expressed in Caco-2 cells for six of the eight genes for which we measured promoter DNA methylation resulted in a significant change at at least one of the CpG sites captured in the assay and also had an effect on the expression, at the mRNA level, of all eight of these genes. These data support our hypothesis that some effects of DR mediated by SIRT1 are through effects on DNA methylation resulting in altered gene expression. A major limitation of these observations, however, is that a causal link between the observed changes in DNA methylation and gene expression is not established. The changes in DNA methylation observed, although statistically significant, were small. In some cases these differences were at CpG sites that showed low levels of methylation (e.g. *EIF5*: 2 % to 5 %) and in other instances at CpG sites that showed high levels of methylation (e.g. *TBX3*: 77 % to 91 %). There is wide discussion about whether or not such changes, which are typical responses to other dietary manipulations or changes seen in ageing, are likely to have functional consequences with respect to gene expression. Because DNA methylation is a binary phenomenon (a CpG site is methylated or not methylated in a single cell) then any change within a single cell is a large change, and differences in percentage methylation reflect a shift in cell population, so may have biological consequences at the level of tissue function.

Evidence for direct causal links between changes in promoter methylation of these genes and their expression could be sought though the use of promoter-reporter constructs; comparison of the level of reporter gene expression between unmethylated and *in vitro*-methylated constructs, as presented in Chapter 4 for a SIRT1-promoter-reporter construct, could provide evidence that gene expression is affected by the methylation status of the promoter region. However, a major limitation of this approach is that it does not easily allow manipulation of the methylation status of selected CpG sites. Another approach to link changes in promoter methylation with gene expression could be to use the

demethylating agent 5-aza-2'-deoxycytidine in those genes with highly methylated promoter regions (*IRX3*, *PCYT1A*, *SLC39A4* and *TBX3*) then measure the effects of this treatment on gene expression.

The analysis of the response of surrogate global and selected site-specific levels of DNA methylation in response to SIRT1 manipulation was logically preceded by the use of micro-array based technology, described in Chapter 7, to investigate the DNA methylation pattern across the genome under conditions of SIRT1 manipulation. We aimed to gain through this approach a more extensive understanding of the effects of SIRT1 levels on DNA methylation. In parallel, we measured the response to altering the SIRT1 expression at the level of the transcriptome. Genes whose expression changed in response to SIRT1 knockdown were represented to an extent greater than would be expected by chance on the list of genes previously generated through the work presented in Chapter 5 whose expression changed in response to DR. Moreover, genes whose methylation status changed in response to SIRT1 knockdown were also represented to an extent greater than would be expect by change in this same list of DR-responsive genes. These exciting observations provide firstly evidence in support of the view that SIRT1 plays a role (at least in mammals) in the response to DR. As noted above in this chapter, this premise is the topic of recent vigorous challenge. The observations also support our overarching hypothesis that some of the functional consequences of DR are mediated via SIRT1 through effect at the level of DNA methylation. The data reveal a large number of gene targets for which causal links between these modifications and roles in modulating the ageing process could be investigated. Future lines of investigation should, include a more detailed bioinformatics analysis of the gene lists generated through the methylomic and transcriptomic studies and identified gene targets with likely roles in modifying aspects of the ageing process should be investigated using basic and advanced molecular biology to uncover the mechanisms directly linking the change in SIRT1 with changes at the level of transcription and epigenetic modifications.

The ageing processes is a vastly complex series of physiological changes from the cell to whole organism level stemming from multiple changes in cellular pathways causing aberrant functional changes and ultimately, diminished health. The multiple deacetylation targets of SIRT1, some involved in other nutrient-sensing pathways, suggest a complex network of pathway changes and cell regulation would be affected by DR-altered SIRT1 levels. We propose effects on DNA methylation to be only one mechanism through which SIRT1 can affect the ageing process. A full understanding of the role of SIRT1 in ageing requires that this full network of interactions is studied in more detail and taken into account. Systems biology approaches may provide a means to better understand the functions of SIRT1 at this level of complexity. In light of the roles played by other members of the sirtuin family in healthy ageing, as discussed in Chapter 1, SIRT1 could be working in concert with other sirtuins, and such interactions should also be included.

In conclusion, the work presented in this thesis has indicated that effects of SIRT1 on methylation of specific genes may correspond with altered expression under conditions of dietary restriction and that many of the same genes undergo a change in methylation level with increased age. The data reveal a large number of gene targets for which causal links between these modifications roles in modulating the ageing process could be investigated.

References

Abdelmohsen, K., et al. (2007) 'Phosphorylation of HuR by Chk2 Regulates SIRT1 Expression', *Molecular Cell,* 25, (4), pp. 543-557.

Ahmet, I., et al. (2005) 'Cardioprotection by Intermittent Fasting in Rats', *Circulation,* 112, (20), pp. 3115-3121.

Akiyama, T., et al. (1987) 'Genistein, a specific inhibitor of tyrosine-specific protein kinases', *Journal of Biological Chemistry,* 262, (12), pp. 5592-5595.

Alcendor, R. R., et al. (2007) 'Sirt1 Regulates Aging and Resistance to Oxidative Stress in the Heart', *Circulation Research,* 100, (10), pp. 1512-1521.

Andreini, C., et al. (2006) 'Counting the zinc-proteins encoded in the human genome', *Journal of Proteome Research,* 5, (1), pp. 196-201.

Anson, R. M., et al. (2003) 'Intermittent fasting dissociates beneficial effects of dietary restriction on glucose metabolism and neuronal resistance to injury from calorie intake', *Proceedings of the National Academy of Sciences,* 100, (10), pp. 6216-6220.

Araki, T., et al. (2004) 'Increased Nuclear NAD Biosynthesis and SIRT1 Activation Prevent Axonal Degeneration', *Science,* 305, (5686), pp. 1010-1013.

Babushok, D. V. and Kazazian, H. H., Jr. (2007) 'Progress in understanding the biology of the human mutagen LINE-1', *Human Mutation,* 28, (6), pp. 527-39.

Balaghi, M. and Wagner, C. (1993) 'DNA methylation in folate deficiency: use of CpG methylase', *Biochemical & Biophysical Research Communications,* 193, (3), pp. 1184-90.

Banchio, C., et al. (2003) 'Activation of CTP:Phosphocholine Cytidylyltransferase α Expression during the S Phase of the Cell Cycle Is Mediated by the Transcription Factor Sp1', *Journal of Biological Chemistry,* 278, (34), pp. 32457-32464.

Barger, J. L., et al. (2008) 'A low dose of dietary resveratrol partially mimics caloric restriction and retards aging parameters in mice', *PLoS ONE,* 3, (6), pp. e2264.

Bass, T. M., et al. (2007) 'Effects of resveratrol on lifespan in Drosophila melanogaster and Caenorhabditis elegans', *Mechanisms of Ageing and Development,* 128, (10), pp. 546-552.

Bauer, J. H., et al. (2004) 'An accelerated assay for the identification of lifespan-extending interventions in Drosophila melanogaster', *Proceedings of the National Academy of Sciences of the United States of America,* 101, (35), pp. 12980-12985.

Baur, J. A., et al. (2006) 'Resveratrol improves health and survival of mice on a high-calorie diet.', *Nature,* 444, (7117), pp. 337-42.

Bedalov, A., et al. (2001) 'Identification of a small molecule inhibitor of Sir2p', *Proceedings of the National Academy of Sciences,* 98, (26), pp. 15113-15118.

Beher, D., et al. (2009) 'Resveratrol is Not a Direct Activator of SIRT1 Enzyme Activity', *Chemical Biology & Drug Design,* 74, (6), pp. 619-624.

Bird, A., et al. (1985) 'A fraction of the mouse genome that is derived from islands of nonmethylated, CpG-rich DNA', *Cell,* 40, (1), pp. 91-99.

Blanc, S., et al. (2003) 'Energy expenditure of rhesus monkeys subjected to 11 years of dietary restriction.', *Journal of Clinical Endocrinology & Metabolism,* 88, (1), pp. 16-23.

Blüher, M., et al. (2003) 'Extended Longevity in Mice Lacking the Insulin Receptor in Adipose Tissue', *Science,* 299, (5606), pp. 572-574.

Bock, C., et al. (2006) 'CpG Island Methylation in Human Lymphocytes Is Highly Correlated with DNA Sequence, Repeats, and Predicted DNA Structure', *PLoS Genet,* 2, (3), pp. e26.

Bock, C., et al. (2008) 'Inter-individual variation of DNA methylation and its implications for large-scale epigenome mapping', *Nucleic Acids Research,* 36, (10), pp. e55.

Bollati, V., et al. (2009) 'Decline in genomic DNA methylation through aging in a cohort of elderly subjects', *Mechanisms of Ageing and Development,* 130, (4), pp. 234-239.

Bordone, L., et al. (2007) 'SIRT1 transgenic mice show phenotypes resembling calorie restriction', *Aging Cell,* 6, (6), pp. 759-67.

Bordone, L., et al. (2006) 'Sirt1 regulates insulin secretion by repressing UCP2 in pancreatic beta cells.', *Plos Biology*, 4, (2), pp. e31.

Borra, M. T., et al. (2005) 'Mechanism of Human SIRT1 Activation by Resveratrol', *Journal of Biological Chemistry*, 280, (17), pp. 17187-17195.

Bravo, S. A., et al. (2004) 'In-depth evaluation of Gly-Sar transport parameters as a function of culture time in the Caco-2 cell model', *European Journal of Pharmaceutical Sciences*, 21, (1), pp. 77-86.

Breitling, R., et al. (2004) 'Rank products: a simple, yet powerful, new method to detect differentially regulated genes in replicated microarray experiments', *FEBS Letters*, 573, (1-3), pp. 83-92.

Briske-Anderson, M. J., et al. (1997) 'The influence of culture time and passage number on the morphological and physiological development of Caco-2 cells', *Proceedings of the Society for Experimental Biology & Medicine*, 214, (3), pp. 248-57.

Brunet, A., et al. (2004) 'Stress-Dependent Regulation of FOXO Transcription Factors by the SIRT1 Deacetylase', *Science*, 303, (5666), pp. 2011-2015.

Byles, V., et al. (2010) 'Aberrant cytoplasm localization and protein stability of SIRT1 is regulated by PI3K/IGF-1R signaling in human cancer cells', *International Journal of Biological Sciences*, 6, (6), pp. 599-612.

Cavodeassi, F., et al. (2001) 'The Iroquois family of genes: from body building to neural patterning', *Development*, 128, (15), pp. 2847-2855.

Cervoni, N., et al. (2002) 'The oncoprotein Set/TAF-1beta, an inhibitor of histone acetyltransferase, inhibits active demethylation of DNA, integrating DNA methylation and transcriptional silencing', *Journal of Biological Chemistry*, 277, (28), pp. 25026-31.

Cervoni, N. and Szyf, M. (2001) 'Demethylase activity is directed by histone acetylation', *Journal of Biological Chemistry*, 276, (44), pp. 40778-87.

Chen, D., et al. (2005a) 'Increase in activity during calorie restriction requires Sirt1.', *Science*, 310, (5754), pp. 1641.

Chen, D., et al. (2009) 'HIF-1 Modulates Dietary Restriction-Mediated Lifespan Extension via IRE-1 in Caenorhabditis elegans', *PLoS Genet,* 5, (5), pp. e1000486.

Chen, W. Y., et al. (2005b) 'Tumor Suppressor HIC1 Directly Regulates SIRT1 to Modulate p53-Dependent DNA-Damage Responses', *Cell,* 123, (3), pp. 437-448.

Cheung, H.-H., et al. (2009) 'DNA methylation of cancer genome', *Birth Defects Research,* Part C, Embryo Today: Reviews. 87, (4), pp. 335-50.

Ching, T.-T., et al. (2010) 'drr-2 encodes an eIF4H that acts downstream of TOR in diet-restriction-induced longevity of C. elegans', *Aging Cell,* 9, (4), pp. 545-557.

Christensen, B. C., et al. (2009) 'Aging and Environmental Exposures Alter Tissue-Specific DNA Methylation Dependent upon CpG Island Context', *PLoS Genet,* 5, (8), pp. e1000602.

Civitarese, A. E., et al. (2007) 'Calorie restriction increases muscle mitochondrial biogenesis in healthy humans', *PLoS Medicine / Public Library of Science,* 4, (3), pp. e76.

Clancy, D. J., et al. (2001) 'Extension of Life-Span by Loss of CHICO, a Drosophila Insulin Receptor Substrate Protein', *Science,* 292, (5514), pp. 104-106.

Clark, S. J., et al. (1994) 'High sensitivity mapping of methylated cytosines', *Nucleic Acids Research,* 22, (15), pp. 2990-7.

Cohen, H. Y., et al. (2004) 'Calorie restriction promotes mammalian cell survival by inducing the SIRT1 deacetylase', *Science,* 305, (5682), pp. 390-2.

Colman, R. J., et al. (2009) 'Caloric Restriction Delays Disease Onset and Mortality in Rhesus Monkeys', *Science,* 325, (5937), pp. 201-204.

Colman, R. J., et al. (1999) 'Body fat distribution with long-term dietary restriction in adult male rhesus macaques', *Journals of Gerontology Series A-Biological Sciences & Medical Sciences,* 54, (7), pp. B283-90.

Coneyworth, L. J., et al. (2009) 'Does promoter methylation of the SLC30A5 (ZnT5) zinc transporter gene contribute to the ageing-related decline in zinc status?', *Proceedings of the Nutrition Society,* 68, (02), pp. 142-147.

Costantini, D. L., et al. (2005) 'The Homeodomain Transcription Factor Irx5 Establishes the Mouse Cardiac Ventricular Repolarization Gradient', *Cell,* 123, (2), pp. 347-358.

Costanzo, V., et al. (2003) 'An ATR- and Cdc7-Dependent DNA Damage Checkpoint that Inhibits Initiation of DNA Replication', *Molecular Cell,* 11, (1), pp. 203-213.

Csiszar, A., et al. (2009) 'Resveratrol induces mitochondrial biogenesis in endothelial cells', *American Journal of Physiology - Heart and Circulatory Physiology,* 297, (1), pp. H13-H20.

Dai, H., et al. (2010) 'SIRT1 activation by small molecules - kinetic and biophysical evidence for direct interaction of enzyme and activator', *Journal of Biological Chemistry*.

Davis, C. D., et al. (2000) 'Dietary selenium and arsenic affect DNA methylation in vitro in Caco-2 cells and in vivo in rat liver and colon.', *Journal of Nutrition,* 130, (12), pp. 2903-9.

Day, J. K., et al. (2002) 'Genistein alters methylation patterns in mice', *Journal of Nutrition,* 132, (8 Suppl), pp. 2419S-2423S.

Della Peruta, M., et al. (2010) 'Protein Tyrosine Phosphatase Receptor Type γ Is a Functional Tumor Suppressor Gene Specifically Downregulated in Chronic Myeloid Leukemia', *Cancer Research,* 70, (21), pp. 8896-8906.

Descamps, O., et al. (2005) 'Mitochondrial production of reactive oxygen species and incidence of age-associated lymphoma in OF1 mice: Effect of alternate-day fasting', *Mechanisms of Ageing and Development,* 126, (11), pp. 1185-1191.

Dhahbi, J. M., et al. (2006) 'Gene expression and physiologic responses of the heart to the initiation and withdrawal of caloric restriction', *Journals of Gerontology Series A-Biological Sciences & Medical Sciences,* 61, (3), pp. 218-31.

Dolinoy, D. C., et al. (2006) 'Maternal genistein alters coat color and protects Avy mouse offspring from obesity by modifying the fetal epigenome', *Environmental Health Perspectives,* 114, (4), pp. 567-72.

Dong, E., et al. (2007) 'Histone hyperacetylation induces demethylation of reelin and 67-kDa glutamic acid decarboxylase promoters', *Proceedings of the National Academy of Sciences*, 104, (11), pp. 4676-4681.

Dryden, S. C., et al. (2003) 'Role for Human SIRT2 NAD-Dependent Deacetylase Activity in Control of Mitotic Exit in the Cell Cycle', *Mol. Cell. Biol.*, 23, (9), pp. 3173-3185.

Dufner-Beattie, J., et al. (2003) 'The Acrodermatitis Enteropathica Gene ZIP4 Encodes a Tissue-specific, Zinc-regulated Zinc Transporter in Mice', *Journal of Biological Chemistry*, 278, (35), pp. 33474-33481.

Eades, G., et al. (2011) 'miR-200a Regulates SIRT1 Expression and Epithelial to Mesenchymal Transition (EMT)-like Transformation in Mammary Epithelial Cells', *Journal of Biological Chemistry*, 286, (29), pp. 25992-26002.

Eden, A., et al. (2003) 'Chromosomal instability and tumors promoted by DNA hypomethylation.', *Science*, 300, (5618), pp. 455.

Edwards, J. R., et al. (2010) 'Chromatin and sequence features that define the fine and gross structure of genomic methylation patterns', *Genome Research*, 20, (7), pp. 972-980.

Eide, D. (2004) 'The SLC39 family of metal ion transporters', *Pflügers Archiv European Journal of Physiology*, 447, (5), pp. 796-800.

Fairweather-Tait, S. J., et al. (2008) 'Does ageing affect zinc homeostasis and dietary requirements?', *Experimental Gerontology*, 43, (5), pp. 382-388.

Fang, M. Z., et al. (2005) 'Reversal of hypermethylation and reactivation of p16INK4a, RARbeta, and MGMT genes by genistein and other isoflavones from soy', *Clinical Cancer Research*, 11, (19 Pt 1), pp. 7033-41.

Fang, M. Z., et al. (2003) 'Tea polyphenol (-)-epigallocatechin-3-gallate inhibits DNA methyltransferase and reactivates methylation-silenced genes in cancer cell lines', *Cancer Research*, 63, (22), pp. 7563-70.

Figueiredo, J. C., et al. (2009) 'Global DNA Hypomethylation (LINE-1) in the Normal Colon and Lifestyle Characteristics and Dietary and Genetic Factors', *Cancer Epidemiology Biomarkers & Prevention,* 18, (4), pp. 1041-1049.

Flanagan, J. M., et al. (2006) 'Intra- and Interindividual Epigenetic Variation in Human Germ Cells', *The American Journal of Human Genetics,* 79, (1), pp. 67-84.

Fogh, J., et al. (1977) 'One hundred and twenty-seven cultured human tumor cell lines producing tumors in nude mice', *Journal of the National Cancer Institute,* 59, (1), pp. 221-6.

Fontana, L., et al. (2004) 'Long-term calorie restriction is highly effective in reducing the risk for atherosclerosis in humans', *Proceedings of the National Academy of Sciences of the United States of America,* 101, (17), pp. 6659-63.

Fontana, L., et al. (2010) 'Extending Healthy Life Span—From Yeast to Humans', *Science,* 328, (5976), pp. 321-326.

Ford, E., et al. (2006) 'Mammalian Sir2 homolog SIRT7 is an activator of RNA polymerase I transcription', *Genes & Development,* 20, (9), pp. 1075-1080.

Ford, J., et al. (2008) 'JNK2-dependent regulation of SIRT1 protein stability', *Cell Cycle,* 7, (19), pp. 3091-3097.

Fraga, M. F., et al. (2005) 'Epigenetic differences arise during the lifetime of monozygotic twins.', *Proceedings of the National Academy of Sciences of the United States of America,* 102, (30), pp. 10604-9.

Froy, O., et al. (2009) 'Effect of intermittent fasting on circadian rhythms in mice depends on feeding time', *Mechanisms of Ageing and Development,* 130, (3), pp. 154-160.

Frye, R. A. (1999) 'Characterization of five human cDNAs with homology to the yeast SIR2 gene: Sir2-like proteins (sirtuins) metabolize NAD and may have protein ADP-ribosyltransferase activity', *Biochemical & Biophysical Research Communications,* 260, (1), pp. 273-9.

Frye, R. A. (2000) 'Phylogenetic classification of prokaryotic and eukaryotic Sir2-like proteins', *Biochemical & Biophysical Research Communications,* 273, (2), pp. 793-8.

Fu, C., et al. (2006) 'Tissue specific and non-specific changes in gene expression by aging and by early stage CR', *Mechanisms of Ageing & Development,* 127, (12), pp. 905-16.

Gao, Z., et al. (2011) 'Sirtuin 1 (SIRT1) Protein Degradation in Response to Persistent c-Jun N-terminal Kinase 1 (JNK1) Activation Contributes to Hepatic Steatosis in Obesity', *Journal of Biological Chemistry,* 286, (25), pp. 22227-22234.

Gentleman, R. C., et al. (2004) 'Bioconductor: open software development for computational biology and bioinformatics', *Genome Biology,* 5, (10), pp. R80.

Ghosh, H. S., et al. (2010) 'SIRT1 Negatively Regulates the Mammalian Target of Rapamycin', *PLoS ONE,* 5, (2), pp. e9199.

Giannakou, M. E., et al. (2008) 'Role of dFOXO in lifespan extension by dietary restriction in Drosophila melanogaster: not required, but its activity modulates the response', *Aging Cell,* 7, (2), pp. 187-198.

Gonzalo, S., et al. (2006) 'DNA methyltransferases control telomere length and telomere recombination in mammalian cells', *Nature Cell Biology,* 8, (4), pp. 416-24.

Gracia-Sancho, J., et al. (2010) 'Activation of SIRT1 by resveratrol induces KLF2 expression conferring an endothelial vasoprotective phenotype', *Cardiovascular Research,* 85, (3), pp. 514-519.

Grandison, R. C., et al. (2009) 'Amino-acid imbalance explains extension of lifespan by dietary restriction in Drosophila', *Nature,* 462, (7276), pp. 1061-1064.

Gresl, T. A., et al. (2001) 'Dietary restriction and glucose regulation in aging rhesus monkeys: a follow-up report at 8.5 yr', *American Journal of Physiology - Endocrinology & Metabolism,* 281, (4), pp. E757-65.

Grozinger, C. M., et al. (2001) 'Identification of a Class of Small Molecule Inhibitors of the Sirtuin Family of NAD-dependent Deacetylases by Phenotypic Screening', *Journal of Biological Chemistry,* 276, (42), pp. 38837-38843.

Grozinger, C. M. and Schreiber, S. L. (2002) 'Deacetylase enzymes: biological functions and the use of small-molecule inhibitors', *Chemistry & Biology,* 9, (1), pp. 3-16.

Gruber, J. A. N., et al. (2007) 'Evidence for a Trade-Off between Survival and Fitness Caused by Resveratrol Treatment of Caenorhabditis elegans', *Annals of the New York Academy of Sciences*, 1100, (1), pp. 530-542.

Grubisha, O., Smith, B.C., and Denu, J.M. (2005) 'Small molecule regulation of Sir2 protein deactylases.', *FEBS J.*, 272, pp. 4607-4616.

Guarente, L. and Picard, F. (2005) 'Calorie restriction--the SIR2 connection', *Cell*, 120, (4), pp. 473-82.

Guerra, B., et al. (2010) 'SIRT1, AMP-activated protein kinase phosphorylation and downstream kinases in response to a single bout of sprint exercise: influence of glucose ingestion', *European Journal of Applied Physiology*, 109, (4), pp. 731-743.

Guo, X., et al. (2010) 'DYRK1A and DYRK3 promote cell survival through phosphorylation and activation of SIRT1', *Journal of Biological Chemistry*.

Haigis, M. C., et al. (2006) 'SIRT4 Inhibits Glutamate Dehydrogenase and Opposes the Effects of Calorie Restriction in Pancreatic [beta] Cells', *Cell*, 126, (5), pp. 941-954.

Halley, F., et al. (2011) 'A Bioluminogenic HDAC Activity Assay: Validation and Screening', *Journal of Biomolecular Screening*.

Han, E.-S. and Hickey, M. (2005) 'Microarray evaluation of dietary restriction', *Journal of Nutrition*, 135, (6), pp. 1343-6.

Han, L., et al. (2010) 'SIRT1 is regulated by a PPARγ–SIRT1 negative feedback loop associated with senescence', *Nucleic Acids Research*, 38, (21), pp. 7458-7471.

Higami, Y., et al. (2004) 'Adipose tissue energy metabolism: altered gene expression profile of mice subjected to long-term caloric restriction', *FASEB Journal*, 18, (2), pp. 415-7.

Hirschey, M. D., et al. (2010) 'SIRT3 regulates mitochondrial fatty-acid oxidation by reversible enzyme deacetylation', *Nature*, 464, (7285), pp. 121-125.

Holzenberger, M., et al. (2003) 'IGF-1 receptor regulates lifespan and resistance to oxidative stress in mice', *Nature*, 421, (6919), pp. 182-187.

Hong, F., et al. (2006) 'RankProd: a bioconductor package for detecting differentially expressed genes in meta-analysis', *Bioinformatics*, 22, (22), pp. 2825-2827.

Hosono, R., et al. (1989) 'Alterations of life span in the nematode Caenorhabditis elegans under monoxenic culture conditions', *Experimental Gerontology*, 24, (3), pp. 251-264.

Houthoofd, K., et al. (2002) 'Axenic growth up-regulates mass-specific metabolic rate, stress resistance, and extends life span in Caenorhabditis elegans', *Experimental Gerontology*, 37, (12), pp. 1371-1378.

Howitz, K. T., et al. (2003) 'Small molecule activators of sirtuins extend Saccharomyces cerevisiae lifespan.', *Nature*, 425, (6954), pp. 191-6.

Huhtiniemi, T., et al. (2006) 'Comparative and pharmacophore model for deacetylase SIRT1', *Journal of Computer-Aided Molecular Design*, 20, (9), pp. 589-99.

Illingworth, R., et al. (2008) 'A Novel CpG Island Set Identifies Tissue-Specific Methylation at Developmental Gene Loci', *PLoS Biol*, 6, (1), pp. e22.

Inoki, K., et al. (2002) 'TSC2 is phosphorylated and inhibited by Akt and suppresses mTOR signalling', *Nat Cell Biol*, 4, (9), pp. 648-657.

Irizarry, R. A., et al. (2009) 'The human colon cancer methylome shows similar hypo- and hypermethylation at conserved tissue-specific CpG island shores', *Nature Genetics*, 41, (2), pp. 178-86.

Issa, J.-P. (2002) 'Epigenetic variation and human disease', *Journal of Nutrition*, 132, (8 Suppl), pp. 2388S-2392S.

Ja, W. W., et al. (2009) 'Water- and nutrient-dependent effects of dietary restriction on Drosophila lifespan', *Proceedings of the National Academy of Sciences*, 106, (44), pp. 18633-18637.

Jarolim, S., et al. (2004) 'A novel assay for replicative lifespan in Saccharomyces cerevisiae', *FEMS Yeast Research*, 5, (2), pp. 169-177.

Jayatilake, G. S., et al. (1993) 'Kinase Inhibitors from Polygonum cuspidatum', *Journal of Natural Products*, 56, (10), pp. 1805-1810.

Jennings, M. D. and Pavitt, G. D. (2010) 'eIF5: A dual function GAP and GDI for eukaryotic translational control', *Small GTPases*, 1, (2), pp. 118-123.

Jin, Q., et al. (2007) 'Cytoplasm-localized SIRT1 enhances apoptosis', *Journal of Cellular Physiology*, 213, (1), pp. 88-97.

Jin, Q., et al. (2010) 'C/EBP[alpha] regulates SIRT1 expression during adipogenesis', *Cell Res*, 20, (4), pp. 470-479.

Jing, E., et al. (2007) 'SIRT2 Regulates Adipocyte Differentiation through FoxO1 Acetylation/Deacetylation', *Cell Metabolism*, 6, (2), pp. 105-114.

Johnson, T. E. (1990) 'Increased life-span of age-1 mutants in Caenorhabditis elegans and lower Gompertz rate of aging', *Science*, 249, (4971), pp. 908-912.

Jones, P. L., et al. (1998) 'Methylated DNA and MeCP2 recruit histone deacetylase to repress transcription', *Nature Genetics*, 19, (2), pp. 187-91.

Kaeberlein, M., et al. (2005a) 'Substrate-specific Activation of Sirtuins by Resveratrol', *Journal of Biological Chemistry*, 280, (17), pp. 17038-17045.

Kaeberlein, M., et al. (2005b) 'Regulation of Yeast Replicative Life Span by TOR and Sch9 in Response to Nutrients', *Science*, 310, (5751), pp. 1193-1196.

Kaeberlein, M. M., M., and Guarente, L. (1999) 'The SIR2/3/4 complex and SIR2 alone promote longevity in Saccharomyces cerevisae by two different mechanisms.', *Genes & Dev*, 13, pp. 2570-2580.

Kanfi, Y., et al. (2008) 'Regulation of SIRT1 protein levels by nutrient availability', *FEBS Letters*, 582, (16), pp. 2417-23.

Kang, H., et al. (2009) 'CK2 Is the Regulator of SIRT1 Substrate-Binding Affinity, Deacetylase Activity and Cellular Response to DNA-Damage', *PLoS ONE*, 4, (8), pp. e6611.

Kapahi, P., et al. (2004) 'Regulation of Lifespan in Drosophila by Modulation of Genes in the TOR Signaling Pathway', *Current Biology,* 14, (10), pp. 885-890.

Karimi, M., et al. (2006) 'LUMA (LUminometric Methylation Assay)--a high throughput method to the analysis of genomic DNA methylation', *Experimental Cell Research,* 312, (11), pp. 1989-95.

Kenyon, C., et al. (1993) 'A C. elegans mutant that lives twice as long as wild type', *Nature,* 366, (6454), pp. 461-464.

Khan, H., et al. (2006) 'Molecular evolution and tempo of amplification of human LINE-1 retrotransposons since the origin of primates', *Genome Research,* 16, (1), pp. 78-87.

Kim, E.-J., et al. (2007) 'Active Regulator of SIRT1 Cooperates with SIRT1 and Facilitates Suppression of p53 Activity', *Molecular Cell,* 28, (2), pp. 277-290.

Kim, H.-S., et al. (2010) 'Hepatic-Specific Disruption of SIRT6 in Mice Results in Fatty Liver Formation Due to Enhanced Glycolysis and Triglyceride Synthesis', *Cell Metabolism,* 12, (3), pp. 224-236.

Kim, J.-E., et al. (2008) 'DBC1 is a negative regulator of SIRT1', *Nature,* 451, (7178), pp. 583-586.

Kim, M. J., et al. (1997) 'Adult-onset energy restriction of rhesus monkeys attenuates oxidative stress-induced cytokine expression by peripheral blood mononuclear cells', *Journal of Nutrition,* 127, (12), pp. 2293-301.

King, M., et al. (2006) 'T-genes and limb bud development', *American Journal of Medical Genetics Part A,* 140A, (13), pp. 1407-1413.

Klar, A. J., Seymour, F. and Macleod, K. (1979) 'MAR1-A regulator of the HMa and HMalpha locus in Saccharomyces cerevisiae.', *Genetics,* 93, pp. 37-50.

Koltai, E., et al. (2010) 'Exercise alters SIRT1, SIRT6, NAD and NAMPT levels in skeletal muscle of aged rats', *Mechanisms of Ageing and Development,* 131, (1), pp. 21-28.

Kuningas, M., et al. (2007) 'Haplotypes in the human Foxo1a and Foxo3a genes; impact on disease and mortality at old age', *Eur J Hum Genet,* 15, (3), pp. 294-301.

Kwabi-Addo, B., et al. (2007) 'Age-Related DNA Methylation Changes in Normal Human Prostate Tissues', *Clinical Cancer Research,* 13, (13), pp. 3796-3802.

Labib, K. (2010) 'How do Cdc7 and cyclin-dependent kinases trigger the initiation of chromosome replication in eukaryotic cells?', *Genes & Development,* 24, (12), pp. 1208-1219.

Lafontaine-Lacasse, M., et al. (2010) 'Effects of age and gender on Sirt 1 mRNA expressions in the hypothalamus of the mouse', *Neuroscience Letters,* 480, (1), pp. 1-3.

Lagouge, M., et al. (2006) 'Resveratrol improves mitochondrial function and protects against metabolic disease by activating SIRT1 and PGC-1alpha.', *Cell,* 127, (6), pp. 1109-22.

Lakowski, B. and Hekimi, S. (1998) 'The genetics of caloric restriction in Caenorhabditis elegans', *Proceedings of the National Academy of Sciences,* 95, (22), pp. 13091-13096.

Lane, M. A., et al. (1996) 'Calorie restriction lowers body temperature in rhesus monkeys, consistent with a postulated anti-aging mechanism in rodents', *Proceedings of the National Academy of Sciences of the United States of America,* 93, (9), pp. 4159-64.

Lane, M. A., et al. (1999) 'Calorie restriction in nonhuman primates: effects on diabetes and cardiovascular disease risk', *Toxicological Sciences,* 52, (2 Suppl), pp. 41-8.

Langley, E., et al. (2002) 'Human SIR2 deacetylates p53 and antagonizes PML/p53-induced cellular senescence', *EMBO Journal,* 21, (10), pp. 2383-96.

Lee, C.-K., et al. (2002) 'Transcriptional profiles associated with aging and middle age-onset caloric restriction in mouse hearts', *Proceedings of the National Academy of Sciences of the United States of America,* 99, (23), pp. 14988-93.

Lee, K. P., et al. (2008) 'Lifespan and reproduction in Drosophila: New insights from nutritional geometry', *Proceedings of the National Academy of Sciences,* 105, (7), pp. 2498-2503.

Lefevre, M., et al. (2009) 'Caloric restriction alone and with exercise improves CVD risk in healthy non-obese individuals', *Atherosclerosis,* 203, (1), pp. 206-213.

Li, W., et al. (2007) 'Sirtuin 2, a Mammalian Homolog of Yeast Silent Information Regulator-2 Longevity Regulator, Is an Oligodendroglial Protein That Decelerates Cell Differentiation through Deacetylating α-Tubulin', *The Journal of Neuroscience,* 27, (10), pp. 2606-2616.

Lin, S.-J., et al. (2000) 'Requirement of NAD and SIR2 for Life-Span Extension by Calorie Restriction in Saccharomyces cerevisiae', *Science,* 289, (5487), pp. 2126-2128.

Liu, W., et al. (2010) 'High-affinity Na+-dependent dicarboxylate cotransporter promotes cellular senescence by inhibiting SIRT1', *Mechanisms of Ageing and Development,* 131, (10), pp. 601-613.

Lopez-Lluch, G., et al. (2008) 'Mitochondrial biogenesis and healthy aging', *Experimental Gerontology,* 43, (9), pp. 813-9.

Lu, J., et al. (2010) 'TBX2 and TBX3: The special value for anticancer drug targets', *Biochimica et Biophysica Acta (BBA) - Reviews on Cancer,* 1806, (2), pp. 268-274.

Lynch, C. J., et al. (2010) 'SIRT1 Undergoes Alternative Splicing in a Novel Auto-Regulatory Loop with p53', *PLoS ONE,* 5, (10), pp. e13502.

Maegawa, S., et al. (2010) 'Widespread and tissue specific age-related DNA methylation changes in mice', *Genome Research,* 20, (3), pp. 332-340.

Mair, W., et al. (2005) 'Calories Do Not Explain Extension of Life Span by Dietary Restriction in Drosophila', *PLoS Biol,* 3, (7), pp. e223.

Masoro, E. J. (2002) 'Age-associated diseases', in *Caloric Restriction.* Amsterdam: Elsevier, pp. 93-114.

Massaro, D., et al. (2004) 'Calorie-related rapid onset of alveolar loss, regeneration, and changes in mouse lung gene expression.', *American Journal of Physiology - Lung Cellular & Molecular Physiology,* 286, (5), pp. L896-906.

Menghini, R., et al. (2009) 'MicroRNA 217 Modulates Endothelial Cell Senescence via Silent Information Regulator 1', *Circulation,* 120, (15), pp. 1524-1532.

Meyer, T. E., et al. (2006) 'Long-term caloric restriction ameliorates the decline in diastolic function in humans.', *Journal of the American College of Cardiology,* 47, (2), pp. 398-402.

Michan, S. and Sinclair, D. (2007) 'Sirtuins in mammals: insights into their biological function', *Biochemical Journal,* 404, (1), pp. 1-13.

Michishita, E., et al. (2008) 'SIRT6 is a histone H3 lysine 9 deacetylase that modulates telomeric chromatin', *Nature,* 452, (7186), pp. 492-496.

Michishita, E., et al. (2005) 'Evolutionarily Conserved and Nonconserved Cellular Localizations and Functions of Human SIRT Proteins', *Mol. Biol. Cell,* 16, (10), pp. 4623-4635.

Miller, R. A., et al. (2005) 'Methionine-deficient diet extends mouse lifespan, slows immune and lens aging, alters glucose, T4, IGF-I and insulin levels, and increases hepatocyte MIF levels and stress resistance', *Aging Cell,* 4, (3), pp. 119-125.

Milne, J. C., et al. (2007) 'Small molecule activators of SIRT1 as therapeutics for the treatment of type 2 diabetes', *Nature,* 450, (7170), pp. 712-716.

Milutinovic, S., et al. (2007) 'Valproate induces widespread epigenetic reprogramming which involves demethylation of specific genes', *Carcinogenesis,* 28, (3), pp. 560-571.

Min, K.-J. and Tatar, M. (2006) 'Restriction of amino acids extends lifespan in Drosophila melanogaster', *Mechanisms of Ageing and Development,* 127, (7), pp. 643-646.

Montagnoli, A., et al. (2004) 'Cdc7 Inhibition Reveals a p53-Dependent Replication Checkpoint That Is Defective in Cancer Cells', *Cancer Research,* 64, (19), pp. 7110-7116.

Mostoslavsky, R., et al. (2006) 'Genomic Instability and Aging-like Phenotype in the Absence of Mammalian SIRT6', *Cell,* 124, (2), pp. 315-329.

Motta, M. C., et al. (2004) 'Mammalian SIRT1 Represses Forkhead Transcription Factors', *Cell,* 116, (4), pp. 551-563.

Mutskov, V. J., et al. (2002) 'The barrier function of an insulator couples high histone acetylation levels with specific protection of promoter DNA from methylation', *Genes & Development,* 16, (12), pp. 1540-1554.

Nakagawa, T., et al. (2009) 'SIRT5 Deacetylates Carbamoyl Phosphate Synthetase 1 and Regulates the Urea Cycle', *Cell,* 137, (3), pp. 560-570.

Nakamaru, Y., et al. (2009) 'A protein deacetylase SIRT1 is a negative regulator of metalloproteinase-9', *FASEB Journal,* 23, (9), pp. 2810-9.

Nakumura, T., et al. (2003) 'Gene expression profiles of ABC transporters and cytochrome P450 3A in Caco-2 and human colorectal cancer cell lines', *Pharmaceutical Research,* 20, (2), pp. 324-7.

Nan, X., et al. (1997) 'MeCP2 is a transcriptional repressor with abundant binding sites in genomic chromatin', *Cell,* 88, (4), pp. 471-81.

Nan, X., et al. (1998) 'Transcriptional repression by the methyl-CpG-binding protein MeCP2 involves a histone deacetylase complex.', *Nature,* 393, (6683), pp. 386-9.

Nasrin, N., et al. (2009) 'JNK1 Phosphorylates SIRT1 and Promotes Its Enzymatic Activity', *PLoS ONE,* 4, (12), pp. e8414.

Nasrin, N., et al. (2010) 'SIRT4 Regulates Fatty Acid Oxidation and Mitochondrial Gene Expression in Liver and Muscle Cells', *Journal of Biological Chemistry,* 285, (42), pp. 31995-32002.

Nemoto, S., et al. (2004) 'Nutrient Availability Regulates SIRT1 Through a Forkhead-Dependent Pathway', *Science,* 306, (5704), pp. 2105-2108.

Nisoli, E., et al. (2005) 'Calorie restriction promotes mitochondrial biogenesis by inducing the expression of eNOS', *Science,* 310, (5746), pp. 314-7.

Noriega, L. G., et al. (2011) 'CREB and ChREBP oppositely regulate SIRT1 expression in response to energy availability', *EMBO Rep,* advance online publication.

North, B. J., et al. (2003) 'The Human Sir2 Ortholog, SIRT2, Is an NAD+-Dependent Tubulin Deacetylase', *Molecular Cell,* 11, (2), pp. 437-444.

Oberdoerffer, P., et al. (2008) 'SIRT1 redistribution on chromatin promotes genomic stability but alters gene expression during aging.', *Cell,* 135, (5), pp. 907-18.

Ogura, M., et al. (2010) 'Overexpression of SIRT5 confirms its involvement in deacetylation and activation of carbamoyl phosphate synthetase 1', *Biochemical and Biophysical Research Communications,* 393, (1), pp. 73-78.

Orentreich, N., et al. (1993) 'Low Methionine Ingestion by Rats Extends Life Span', *The Journal of Nutrition,* 123, (2), pp. 269-274.

Ota, H., et al. (2005) 'Sirt1 inhibitor, Sirtinol, induces senescence-like growth arrest with attenuated Ras-MAPK signaling in human cancer cells', *Oncogene,* 25, (2), pp. 176-185.

Ou, J.-N., et al. (2007) 'Histone deacetylase inhibitor Trichostatin A induces global and gene-specific DNA demethylation in human cancer cell lines', *Biochemical Pharmacology,* 73, (9), pp. 1297-1307.

Pacholec, M., et al. (2010) 'SRT1720, SRT2183, SRT1460, and resveratrol are not direct activators of SIRT1', *Journal of Biological Chemistry*.

Palacios, J. A., et al. (2010) 'SIRT1 contributes to telomere maintenance and augments global homologous recombination', *The Journal of Cell Biology,* 191, (7), pp. 1299-1313.

Papaconstantinou, H. T., et al. (2000) 'Prevention of mucosal atrophy: role of glutamine and caspases in apoptosis in intestinal epithelial cells', *Journal of Gastrointestinal Surgery,* 4, (4), pp. 416-23.

Pearson, K. J., et al. (2008) 'Resveratrol Delays Age-Related Deterioration and Mimics Transcriptional Aspects of Dietary Restriction without Extending Life Span', *Cell Metabolism,* 8, (2), pp. 157-168.

Pearson, R. C. M., et al. (2011) 'The mammalian zinc finger transcription factor Krüppel-like factor 3 (KLF3/BKLF)', *IUBMB Life,* 63, (2), pp. 86-93.

Penev, P. D., et al. (1998) 'Chronic circadian desynchronization decreases the survival of animals with cardiomyopathic heart disease', *American Journal of Physiology - Heart and Circulatory Physiology,* 275, (6 44-6), pp. H2334-H2337.

Picard, F., et al. (2004) 'Sirt1 promotes fat mobilization in white adipocytes by repressing PPAR-[gamma]', *Nature,* 429, (6993), pp. 771-776.

Powers, R. W., et al. (2006) 'Extension of chronological life span in yeast by decreased TOR pathway signaling', *Genes & Development,* 20, (2), pp. 174-184.

Pradhan, A. K., et al. (2011) 'EVI1 up-regulates the stress responsive gene SIRT1 which triggers deacetylation and degradation of EVI1', *Biochimica et Biophysica Acta (BBA) - Gene Regulatory Mechanisms*, 1809, (4-6), pp. 269-275.

Pruitt, K., et al. (2006) 'Inhibition of SIRT1 reactivates silenced cancer genes without loss of promoter DNA hypermethylation', *PLoS Genetics*, 2, (3), pp. e40.

Rakyan, V. K., et al. (2010) 'Human aging-associated DNA hypermethylation occurs preferentially at bivalent chromatin domains', *Genome Research*.

Rakyan, V. K., et al. (2008) 'An integrated resource for genome-wide identification and analysis of human tissue-specific differentially methylated regions (tDMRs)', *Genome Research*, 18, (9), pp. 1518-1529.

Rasbach, K. A. and Schnellmann, R. G. (2008) 'Isoflavones promote mitochondrial biogenesis', *Journal of Pharmacology & Experimental Therapeutics*, 325, (2), pp. 536-43.

Richardson, B. (2003) 'Impact of aging on DNA methylation', *Ageing Research Reviews*, 2, (3), pp. 245-61.

Rogina, B. and Helfand, S. L. (2004) 'Sir2 mediates longevity in the fly through a pathway related to calorie restriction', *Proceedings of the National Academy of Sciences of the United States of America*, 101, (45), pp. 15998-16003.

Ross, M. H. (1961) 'Length of life and nutrition in the rat', *Journal of Nutrition*, 75, pp. 197-210.

Roth, S. Y., et al. (2001) 'Histone acetyltransferases', *Annual Review of Biochemistry*, 70, pp. 81-120.

Sakamoto, J., et al. (2004) 'Predominant expression of Sir2[alpha], an NAD-dependent histone deacetylase, in the embryonic mouse heart and brain', *FEBS Letters*, 556, (1-3), pp. 281-286.

Sasaki, T., et al. (2006) 'Progressive loss of SIRT1 with cell cycle withdrawal', *Aging Cell*, 5, (5), pp. 413-422.

Sasaki, T., et al. (2008) 'Phosphorylation Regulates SIRT1 Function', *PLoS ONE*, 3, (12), pp. e4020.

Sato, N., et al. (2003) 'Frequent Hypomethylation of Multiple Genes Overexpressed in Pancreatic Ductal Adenocarcinoma', *Cancer Research,* 63, (14), pp. 4158-4166.

Saunders, L. R., et al. (2010) 'miRNAs regulate SIRT1 expression during mouse embryonic stem cell differentiation and in adult mouse tissues', *Aging,* 2, (7), pp. 415-31.

Saxonov, S., et al. (2006) 'A genome-wide analysis of CpG dinucleotides in the human genome distinguishes two distinct classes of promoters', *Proceedings of the National Academy of Sciences of the United States of America,* 103, (5), pp. 1412-1417.

Schilling, E. and Rehli, M. (2007) 'Global, comparative analysis of tissue-specific promoter CpG methylation', *Genomics,* 90, (3), pp. 314-323.

Schneider, E., et al. (2010) 'Spatial, temporal and interindividual epigenetic variation of functionally important DNA methylation patterns', *Nucleic Acids Research,* 38, (12), pp. 3880-3890.

Schwer, B., et al. (2006) 'Reversible lysine acetylation controls the activity of the mitochondrial enzyme acetyl-CoA synthetase 2', *Proceedings of the National Academy of Sciences,* 103, (27), pp. 10224-10229.

Selker, E. U. (1998) 'Trichostatin A causes selective loss of DNA methylation in Neurospora', *Proceedings of the National Academy of Sciences of the United States of America,* 95, (16), pp. 9430-5.

Selman, C., et al. (2006) 'Coordinated multitissue transcriptional and plasma metabonomic profiles following acute caloric restriction in mice', *Physiological Genomics,* 27, (3), pp. 187-200.

Shah, O. J. and Hunter, T. (2006) 'Turnover of the Active Fraction of IRS1 Involves Raptor-mTOR- and S6K1-Dependent Serine Phosphorylation in Cell Culture Models of Tuberous Sclerosis', *Mol. Cell. Biol.,* 26, (17), pp. 6425-6434.

Sharov, A. A., et al. (2008) 'Effects of aging and calorie restriction on the global gene expression profiles of mouse testis and ovary', *Bmc Biology,* 6, pp. 24.

Someya, S., et al. (2010) 'Sirt3 Mediates Reduction of Oxidative Damage and Prevention of Age-Related Hearing Loss under Caloric Restriction', *Cell,* 143, (5), pp. 802-812.

Sugimoto, H., et al. (2008) 'Transcriptional regulation of phosphatidylcholine biosynthesis', *Progress in Lipid Research,* 47, (3), pp. 204-220.

Suwa, M., et al. (2008) 'Endurance exercise increases the SIRT1 and peroxisome proliferator-activated receptor [gamma] coactivator-1[alpha] protein expressions in rat skeletal muscle', *Metabolism,* 57, (7), pp. 986-998.

Swindell, W. R. (2008) 'Comparative analysis of microarray data identifies common responses to caloric restriction among mouse tissues', *Mechanisms of Ageing & Development,* 129, (3), pp. 138-53.

Szyf, M., et al. (1985) 'Cell cycle-dependent regulation of eukaryotic DNA methylase level', *Journal of Biological Chemistry,* 260, (15), pp. 8653-6.

Tafaro, L., et al. (2009) 'Stress in centenarians', *Archives of Gerontology and Geriatrics,* 48, (3), pp. 353-355.

Taguchi, A., et al. (2007) 'Brain IRS2 Signaling Coordinates Life Span and Nutrient Homeostasis', *Science,* 317, (5836), pp. 369-372.

Tanno, M., et al. (2007) 'Nucleocytoplasmic Shuttling of the NAD+-dependent Histone Deacetylase SIRT1', *Journal of Biological Chemistry,* 282, (9), pp. 6823-6832.

Tatar, M., et al. (2001) 'A Mutant Drosophila Insulin Receptor Homolog That Extends Life-Span and Impairs Neuroendocrine Function', *Science,* 292, (5514), pp. 107-110.

Tate, P. H. and Bird, A. P. (1993) 'Effects of DNA methylation on DNA-binding proteins and gene expression', *Current Opinion in Genetics & Development,* 3, (2), pp. 226-231.

Tercé, F., et al. (1994) 'Requirement of phosphatidylcholine for normal progression through the cell cycle in C3H/10T1/2 fibroblasts', *Journal of Lipid Research,* 35, (12), pp. 2130-42.

Teschendorff, A. E., et al. (2010) 'Age-dependent DNA methylation of genes that are suppressed in stem cells is a hallmark of cancer', *Genome Research*.

Tissenbaum, H. A. and Guarente, L. (2001) 'Increased dosage of a sir-2 gene extends lifespan in Caenorhabditis elegans', *Nature,* 410, (6825), pp. 227-230.

Trapp, J., et al. (2006) 'Adenosine Mimetics as Inhibitors of NAD+-Dependent Histone Deacetylases, from Kinase to Sirtuin Inhibition', *Journal of Medicinal Chemistry,* 49, (25), pp. 7307-7316.

Tsuchiya, T., et al. (2004) 'Additive regulation of hepatic gene expression by dwarfism and caloric restriction', *Physiological Genomics,* 17, (3), pp. 307-15.

Tullio, A. N., et al. (1997) 'Nonmuscle myosin II-B is required for normal development of the mouse heart', *Proceedings of the National Academy of Sciences,* 94, (23), pp. 12407-12412.

Tullio, A. N., et al. (2001) 'Structural abnormalities develop in the brain after ablation of the gene encoding nonmuscle myosin II-B heavy chain', *The Journal of Comparative Neurology,* 433, (1), pp. 62-74.

Vakhrusheva, O., et al. (2008) 'Sirt7 Increases Stress Resistance of Cardiomyocytes and Prevents Apoptosis and Inflammatory Cardiomyopathy in Mice', *Circulation Research,* 102, (6), pp. 703-710.

Vanyushin, B. F., et al. (1973) 'The 5-methylcytosine in DNA of rats. Tissue and age specificity and the changes induced by hydrocortisone and other agents', *Gerontologia,* 19, (3), pp. 138-52.

Vaquero, A., et al. (2007) 'SIRT1 regulates the histone methyl-transferase SUV39H1 during heterochromatin formation', *Nature,* 450, (7168), pp. 440-4.

Vaquero, A., et al. (2004) 'Human SirT1 interacts with histone H1 and promotes formation of facultative heterochromatin', *Molecular Cell,* 16, (1), pp. 93-105.

Vaquero, A., et al. (2006) 'SirT2 is a histone deacetylase with preference for histone H4 Lys 16 during mitosis', *Genes & Development,* 20, (10), pp. 1256-1261.

Vardi, A., et al. (2010) 'Soy Phytoestrogens Modify DNA Methylation of GSTP1, RASSF1A, EPH2 and BRCA1 Promoter in Prostate Cancer Cells', *In Vivo,* 24, (4), pp. 393-400.

Vellai, T., et al. (2003) 'Genetics: Influence of TOR kinase on lifespan in C. elegans', *Nature,* 426, (6967), pp. 620-620.

Vicente-Manzanares, M., et al. (2009) 'Non-muscle myosin II takes centre stage in cell adhesion and migration', *Nat Rev Mol Cell Biol,* 10, (11), pp. 778-790.

Vidali, G., et al. (1968) 'Chemical studies of histone acetylation. The distribution of epsilon-N-acetyllysine in calf thymus histones', *Journal of Biological Chemistry,* 243, (24), pp. 6361-6.

Viswanathan, M., et al. (2005) 'A Role for SIR-2.1 Regulation of ER Stress Response Genes in Determining C. elegans Life Span', *Developmental cell,* 9, (5), pp. 605-615.

Walford, R. L., et al. (2002) 'Calorie Restriction in Biosphere 2', *The Journals of Gerontology Series A: Biological Sciences and Medical Sciences,* 57, (6), pp. B211-B224.

Wang, C., et al. (2006) 'Interactions between E2F1 and SirT1 regulate apoptotic response to DNA damage', *Nat Cell Biol,* 8, (9), pp. 1025-1031.

Wang, Y. and Leung, F. C. C. (2004) 'An evaluation of new criteria for CpG islands in the human genome as gene markers', *Bioinformatics,* 20, (7), pp. 1170-7.

Wang, Y. and Tissenbaum, H. A. (2006) 'Overlapping and distinct functions for a Caenorhabditis elegans SIR2 and DAF-16/FOXO', *Mechanisms of Ageing and Development,* 127, (1), pp. 48-56.

Weber, M., et al. (2005) 'Chromosome-wide and promoter-specific analyses identify sites of differential DNA methylation in normal and transformed human cells', *Nature Genetics,* 37, (8), pp. 853-862.

Wei, M., et al. (2008) 'Life Span Extension by Calorie Restriction Depends on Rim15 and Transcription Factors Downstream of Ras/PKA, Tor, and Sch9', *PLoS Genet,* 4, (1), pp. e13.

Weindruch, R. and Walford, R. L. (1982) 'Dietary restriction in mice beginning at 1 year of age: effect on life-span and spontaneous cancer incidence', *Science,* 215, (4538), pp. 1415-8.

Weindruch, R., et al. (1986) 'The retardation of aging in mice by dietary restriction: longevity, cancer, immunity and lifetime energy intake', *Journal of Nutrition,* 116, (4), pp. 641-54.

Willcox, D. C., et al. (2008a) 'They Really Are That Old: A Validation Study of Centenarian Prevalence in Okinawa', *The Journals of Gerontology Series A: Biological Sciences and Medical Sciences,* 63, (4), pp. 338-349.

Willcox, D. C., et al. (2008b) 'Life at the Extreme Limit: Phenotypic Characteristics of Supercentenarians in Okinawa', *The Journals of Gerontology Series A: Biological Sciences and Medical Sciences*, 63, (11), pp. 1201-1208.

Wilson, V. L. and Jones, P. A. (1983) 'DNA methylation decreases in aging but not in immortal cells', *Science*, 220, (4601), pp. 1055-7.

Wilson, V. L., et al. (1987) 'Genomic 5-methyldeoxycytidine decreases with age', *Journal of Biological Chemistry*, 262, (21), pp. 9948-51.

Witte, A. V., et al. (2009) 'Caloric restriction improves memory in elderly humans', *Proceedings of the National Academy of Sciences*, 106, (4), pp. 1255-1260.

Wood, J. G., et al. (2004) 'Sirtuin activators mimic caloric restriction and delay ageing in metazoans', *Nature*, 430, (7000), pp. 686-689.

Wu, P., et al. (2008) 'Calorie restriction ameliorates neurodegenerative phenotypes in forebrain-specific presenilin-1 and presenilin-2 double knockout mice', *Neurobiology of Aging*, 29, (10), pp. 1502-11.

Wu, Z., et al. (1999) 'Mechanisms controlling mitochondrial biogenesis and respiration through the thermogenic coactivator PGC-1', *Cell*, 98, (1), pp. 115-24.

Xiao, C., et al. (2010) 'SIRT6 Deficiency Results in Severe Hypoglycemia by Enhancing Both Basal and Insulin-stimulated Glucose Uptake in Mice', *Journal of Biological Chemistry*, 285, (47), pp. 36776-36784.

Xiong, S., et al. (2010) 'FoxO1 mediates an auto-feedback loop regulating SIRT1 expression', *Journal of Biological Chemistry*.

Xiong, Z. and Laird, P. W. (1997) 'COBRA: a sensitive and quantitative DNA methylation assay', *Nucleic Acids Research*, 25, (12), pp. 2532-2534.

Yang, A. S., et al. (2004) 'A simple method for estimating global DNA methylation using bisulfite PCR of repetitive DNA elements', *Nucleic Acids Research*, 32, (3), pp. e38.

Yang, Y., et al. (2007) 'SIRT1 sumoylation regulates its deacetylase activity and cellular response to genotoxic stress', *Nat Cell Biol*, 9, (11), pp. 1253-1262.

Youngman, L. D., et al. (1992) 'Protein oxidation associated with aging is reduced by dietary restriction of protein or calories', *Proceedings of the National Academy of Sciences*, 89, (19), pp. 9112-9116.

Yu, B. P., et al. (1985) 'Nutritional Influences on Aging of Fischer 344 Rats: I. Physical, Metabolic, and Longevity Characteristics', *Journal of Gerontology*, 40, (6), pp. 657-670.

Yu, B. P., et al. (1982) 'Life span study of SPF Fischer 344 male rats fed ad libitum or restricted diets: longevity, growth, lean body mass and disease', *Journal of Gerontology*, 37, (2), pp. 130-41.

Zainal, T. A., et al. (2000) 'Caloric restriction of rhesus monkeys lowers oxidative damage in skeletal muscle', *FASEB Journal*, 14, (12), pp. 1825-36.

Zhang, Q., et al. (2007) 'Metabolic regulation of SIRT1 transcription via a HIC1:CtBP corepressor complex', *Proceedings of the National Academy of Sciences*, 104, (3), pp. 829-833.

Zhao, T., et al. (2010) 'MicroRNA-34a induces endothelial progenitor cell senescence and impedes its angiogenesis via suppressing silent information regulator 1', *American Journal of Physiology - Endocrinology And Metabolism*.

Zhao, W., et al. (2008) 'Negative regulation of the deacetylase SIRT1 by DBC1', *Nature*, 451, (7178), pp. 587-590.

Zhu, H., et al. (2011) 'MicroRNA-195 promotes palmitate-induced apoptosis in cardiomyocytes by down-regulating Sirt1', *Cardiovascular Research*.

Zschoernig, B. and Mahlknecht, U. (2009) 'Carboxy-terminal phosphorylation of SIRT1 by protein kinase CK2', *Biochemical and Biophysical Research Communications*, 381, (3), pp. 372-377.

Appendix A: Plasmid Maps

I. pBLUE-TOPO® (Invitrogen)

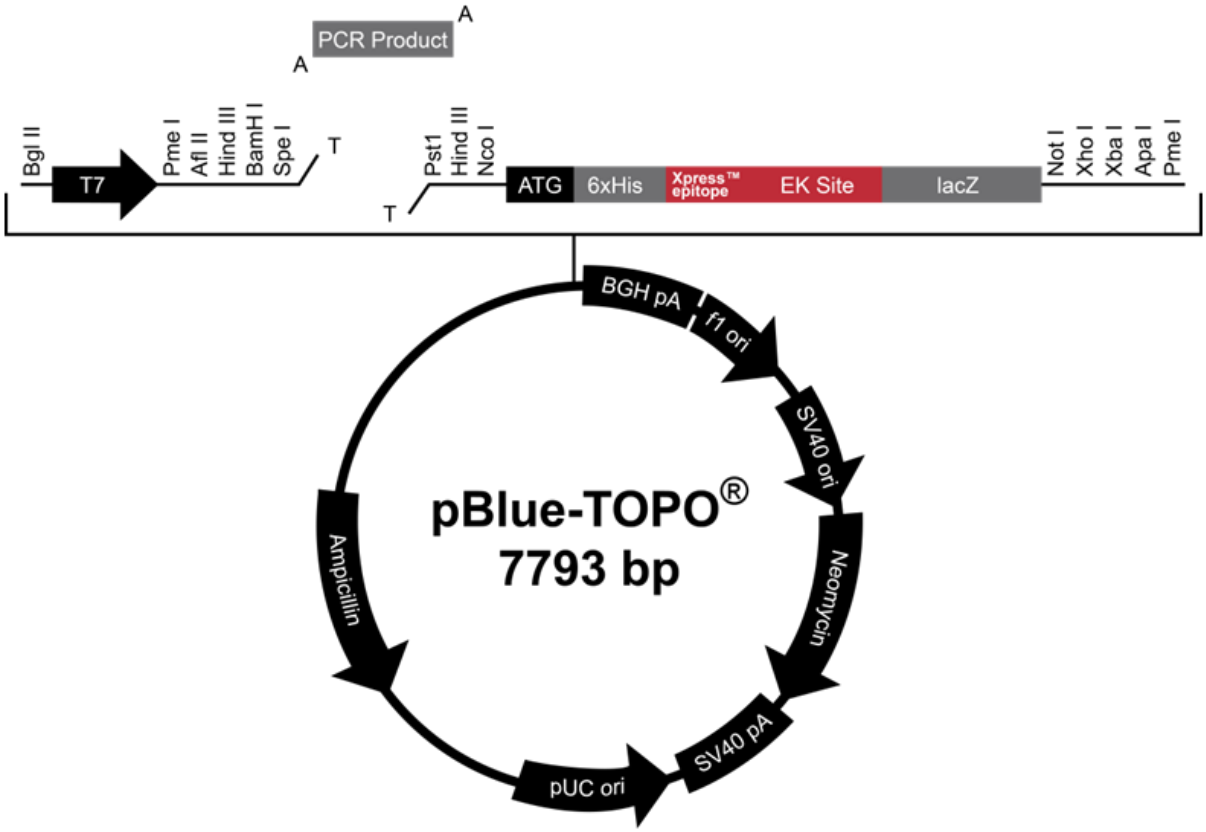

Comments for pBLUE-TOPO®
7793 nucleotides

T7 promoter/priming site: bases 17-36
TOPO® Cloning site: bases 116-117
ATG initiation codon: bases 143-145
Polyhistidine region: bases 155-172
LacZ Reverse priming site: bases 173-191
Xpress™ epitope: bases 212-235
Enterokinase recognition site: bases 211-235
LacZ ORF: bases 264-3313
BGH polyadenylation sequence: bases 3386-3613
F1 origin: bases 3659-4087
SV40 promoter and origin: bases 4141-4423
Neomycin resistance gene: bases 4498-5292
SV40 polyadenylation sequence: bases 5466-5596
pUC origin: bases 5979-6652 (complimentary strand)
Ampicillin resistance gene: bases 6797-7657 (complementary strand)

II. pCMV6-Neo (Origene)

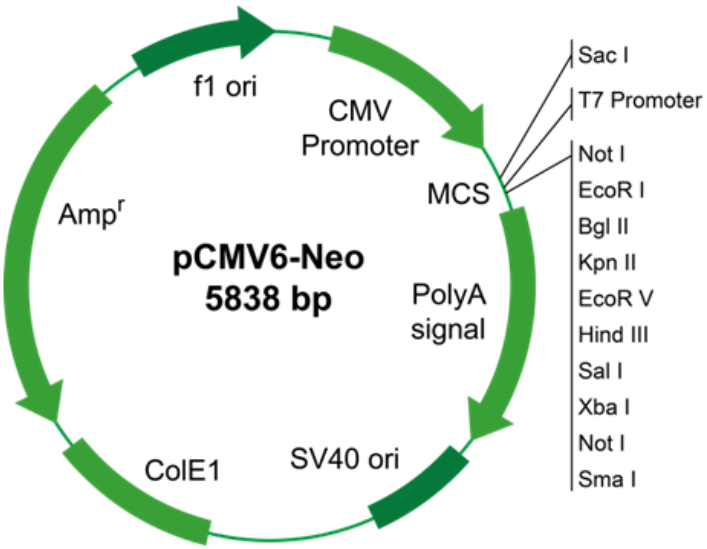

Comments for pCMV6-Neo
5838 nucleotides

CMV promoter: bases 201-926
T7 promoter: bases 953-971
Multiple Cloning Sites: bases 972-1030
Poly-A signal: bases 1063-1648
SV40 origin: bases 1740-2047
Neomycin resistance gene: bases 2120-2904
ColE1 origin: bases 3588-4206
Ampicillin resistance gene: bases 4405-5256

III. pCMV6-ENTRY (Origene)

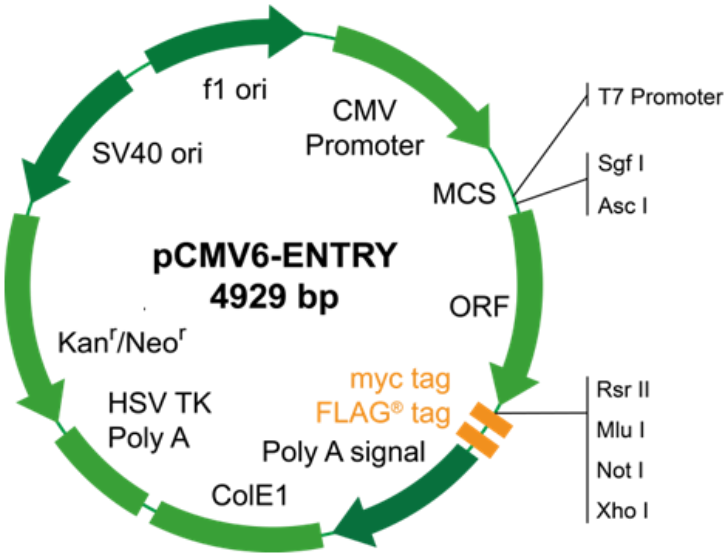

Comments for pCMV6-ENTRY
4929 nucleotides

CMV promoter: bases 201-926
T7 promoter: bases 953-971
Multiple Cloning Sites: bases 978-1153
Poly-A signal: bases 1206-2739
ColE1 origin: bases 2067-2739
SV40 origin: bases 3998-4300
Kanamycin/Neomycin resistance gene: bases 3169-3963

Appendix B: Composition of cell culture medium

DMEM – Dulbecco's Modified Eagle Medium (Caco-2, HeLa, HepG2, MDA)

Components	Concentration (mg/L)	Molarity (mM)
Amino Acids:		
Glycine	30	0.4
L-Alanyl-L-Glutamine	862	3.97
L-Arginine hydrochloride	84	0.398
L-Cystine 2HCl	63	0.201
L-Histidine hydrochloride-H_2O	42	0.2
L-Isoleucine	105	0.802
L-Leucine	105	0.802
L-Lysine hydrochloride	146	0.798
L-Methionine	30	0.201
L-Phenylalanine	66	0.4
L-Serine	42	0.4
L-Threonine	95	0.798
L-Tryptophan	16	0.0784
L-Tyrosine	72	0.398
L-Valine	94	0.803
Vitamins		
Choline chloride	4	0.0286
D-Calcium pantothenate	4	0.00839
Folic Acid	4	0.00907
Niacinamide	4	0.0328
Pyridoxine hydrochloride	4	0.0196
Riboflavin	0.4	0.00106
Thiamine hydrochloride	4	0.0119
i-Inositol	7.2	0.04
Inorganic Salts:		
Calcium Chloride ($CaCl_2$-$2H_2O$)	264	1.8
Ferric Nitrate ($Fe(NO_3)_3$-$9H_2O$)	0.1	0.000248
Magnesium Sulfate ($MgSO_4$-$7H_2O$)	200	0.813
Potassium Chloride (KCl)	400	5.33
Sodium Bicarbonate ($NaHCO_3$)	3700	44.05
Sodium Chloride (NaCl)	6400	110.34
Sodium Phosphate monobasic (NaH_2PO_4-$2H_2O$)	141	0.916
Other Components:		
D-Glucose (Dextrose)	4500	25
Phenol Red	15	0.0399
Sodium Pyruvate	110	1

DMEM – Dulbecco's Modified Eagle Medium no phenol red (Caco-2 polyphenol treatment)

Components	Concentration (mg/L)	Molarity (mM)
Amino Acids:		
Glycine	30	0.4
L-Arginine hydrochloride	84	0.398
L-Cystine 2HCl	63	0.201
L-Histidine hydrochloride-H_2O	42	0.2
L-Isoleucine	105	0.802
L-Leucine	105	0.802
L-Lysine hydrochloride	146	0.798
L-Methionine	30	0.201
L-Phenylalanine	66	0.4
L-Serine	42	0.4
L-Threonine	95	0.798
L-Tryptophan	16	0.0784
L-Tyrosine disodium salt dihydrate	104	0.398
L-Valine	94	0.803
Vitamins		
Choline chloride	4	0.0286
D-Calcium pantothenate	4	0.00839
Folic Acid	4	0.00907
Niacinamide	4	0.0328
Pyridoxine hydrochloride	4	0.0196
Riboflavin	0.4	0.00106
Thiamine hydrochloride	4	0.0119
i-Inositol	7.2	0.04
Inorganic Salts:		
Calcium Chloride ($CaCl_2$-$2H_2O$)	200	1.8
Ferric Nitrate ($Fe(NO_3)_3$-$9H_2O$)	0.1	0.000248
Magnesium Sulfate ($MgSO_4$-$7H_2O$)	97.67	0.813
Potassium Chloride (KCl)	400	5.33
Sodium Bicarbonate ($NaHCO_3$)	3700	44.05
Sodium Chloride (NaCl)	6400	110.34
Sodium Phosphate monobasic (NaH_2PO_4-$2H_2O$)	125	0.906
Other Components:		
D-Glucose (Dextrose)	4500	25

DMEM/F12 1:1 – Dulbecco's Modified Eagle Medium (SHSY-5Y)

Components	Concentration (mg/L)	Molarity (mM)
Amino Acids:		
Glycine	18.75	0.25
L-Alanine	4.45	0.05
L-Alanyl-L-Glutamine	542	2.5
L-Arginine hydrochloride	147.5	0.699
L-Asparagine-H_2O	7.5	0.05
L-Aspartic acid	6.65	0.05
L-Cysteine hydrochloride-H_2O	17.56	0.0998
L-Cystine 2HCl	31.29	0.1
L-Glutamic Acid	7.35	0.05
L-Histidine hydrochloride-H_2O	31.48	0.15
L-Isoleucine	54.47	0.416
L-Leucine	59.05	0.451
L-Lysine hydrochloride	91.25	0.499
L-Methionine	17.24	0.116
L-Phenylalanine	35.48	0.215
L-Proline	17.25	0.15
L-Serine	26.25	0.25
L-Threonine	53.45	0.449
L-Tryptophan	9.02	0.0442
L-Tyrosine disodium salt dihydrate	55.79	0.214
L-Valine	25.85	0.221
Vitamins:		
Biotin	0.0035	0.0000143
Choline chloride	8.98	0.0641
D-Calcium pantothenate	2.24	0.0047
Folic Acid	2.65	0.00601
Niacinamide	2.02	0.0166
Pyridoxine hydrochloride	2	0.00971
Riboflavin	0.219	0.000582
Thiamine hydrochloride	2.17	0.00644
Vitamin B12	0.68	0.000502
i-Inositol	12.6	0.07

Continued

Components	Concentration (mg/L)	Molarity (mM)
Inorganic Salts:		
Calcium Chloride ($CaCl_2$) (anhydrous)	116.6	1.05
Cupric sulfate ($CuSO_4$-$5H_2O$)	0.0013	0.0000052
Ferric Nitrate ($Fe(NO_3)_3$-$9H_2O$)	0.05	0.000124
Ferric sulfate ($FeSO_4$-$7H_2O$)	0.417	0.0015
Magnesium Chloride ($MgCl_2$-$6H_2O$)	61	0.3
Magnesium Sulfate ($MgSO_4$-$7H_2O$)	100	0.407
Potassium Chloride (KCl)	311.8	4.16
Sodium Bicarbonate ($NaHCO_3$)	1200	14.29
Sodium Chloride (NaCl)	6995.5	120.61
Sodium Phosphate dibasic (Na_2HPO_4-$7H_2O$)	134	0.5
Sodium Phosphate monobasic (NaH_2PO_4-H_2O)	62.5	0.453
Zinc sulfate ($ZnSO_4$-$7H_2O$)	0.432	0.0015
Other Components:		
D-Glucose (Dextrose)	3151	17.51
Hypoxanthine Na	2.39	0.015
Linoleic Acid	0.042	0.00015
Lipoic Acid	0.105	0.00051
Phenol Red	8.1	0.0215
Putrescine 2HCl	0.081	0.000503
Sodium Pyruvate	55	0.5
Thymidine	0.365	0.00151

Leibovitz's L15 Medium (SW480)

Components	Concentration (mg/L)	Molarity (mM)
Amino Acids:		
Glycine	200	2.67
L-Alanine	225	2.53
L-Arginine	500	2.87
L-Asparagine	250	1.89
L-Cysteine	120	0.992
L-Glutamine	300	2.05
L-Histidine	250	1.61
L-Isoleucine	250	1.91
L-Leucine	125	0.954
L-Lysine	75	0.514
L-Methionine	75	0.503
L-Phenylalanine	125	0.758
L-Serine	200	1.9
L-Threonine	300	2.52
L-Tryptophan	20	0.098
L-Tyrosine	300	1.66
L-Valine	100	0.855
Vitamins:		
Choline chloride	1	0.00714
D-Calcium pantothenate	1	0.0021
Folic Acid	1	0.00227
Niacinamide	1	0.0082
Pyridoxine hydrochloride	1	0.00485
Riboflavin 5'-phosphate Na	0.1	0.000209
Thiamine monophosphate	1	0.00226
i-Inositol	2	0.0111
Inorganic Salts:		
Calcium Chloride ($CaCl_2$) (anhydrous)	140	1.26
Magnesium Chloride (anhydrous)	93.7	0.986
Magnesium Sulfate ($MgSO_4$) (anhydrous)	97.67	0.814
Potassium Chloride (KCl)	400	5.33
Potassium Phosphate monobasic (KH_2PO4)	60	0.441
Sodium Chloride (NaCl)	8000	137.93
Sodium Phosphate dibasic (Na_2HPO_4) anhydrous	190	1.34
Other Components:		
D+ Galactose	900	5
Phenol Red	10	0.0266
Sodium Pyruvate	550	5

MEM – Minimum Essential Medium (MCF-7)

Components	Concentration (mg/L)	Molarity (mM)
Amino Acids:		
L-Arginine hydrochloride	126	0.597
L-Cystine	24	0.1
L-Glutamine	292	2
L-Histidine hydrochloride-H_2O	42	0.2
L-Isoleucine	52	0.397
L-Leucine	52	0.397
L-Lysine hydrochloride	73	0.399
L-Methionine	15	0.101
L-Phenylalanine	32	0.194
L-Threonine	48	0.403
L-Tryptophan	10	0.049
L-Tyrosine	36	0.199
L-Valine	46	0.393
Vitamins:		
Choline chloride	1	0.00714
D-Calcium pantothenate	1	0.0021
Folic Acid	1	0.00227
Niacinamide	1	0.0082
Pyridoxal hydrochloride	1	0.0049
Riboflavin	0.1	0.000266
Thiamine hydrochloride	1	0.00297
i-Inositol	2	0.0111
Inorganic Salts:		
Calcium Chloride ($CaCl_2$-$2H_2O$)	264	1.8
Magnesium Sulfate ($MgSO_4$-$7H_2O$)	200	0.813
Potassium Chloride (KCl)	400	5.33
Sodium Bicarbonate ($NaHCO_3$)	2200	26.19
Sodium Chloride (NaCl)	6800	117.24
Sodium Phosphate monobasic (NaH_2PO_4-$2H_2O$)	158	1.01
Other Components:		
D-Glucose (Dextrose)	1000	5.56
Phenol Red	10	0.0266

Appendix C: **Methylation standard curves for pyrosequencing**

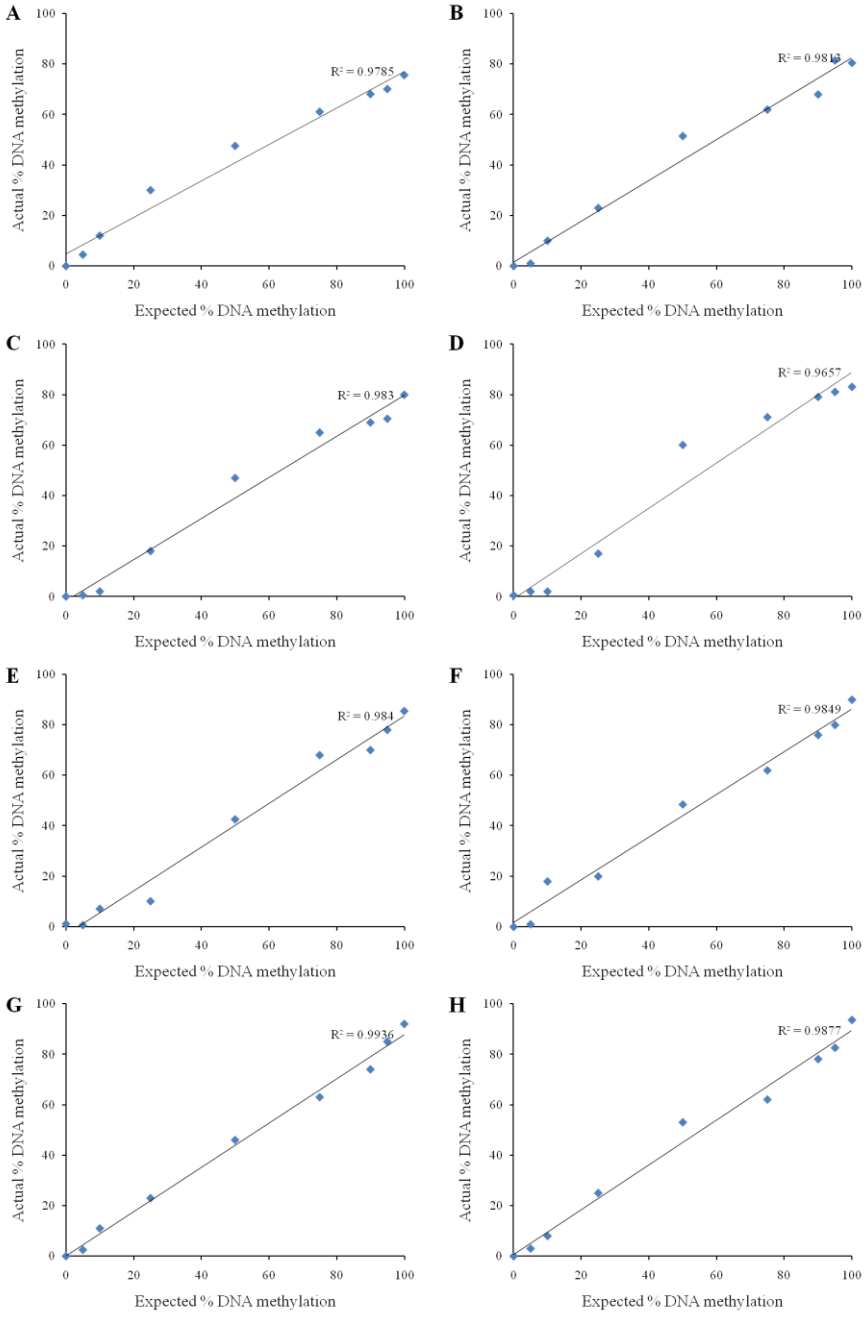

Figure C.1. Standard curves generated for the CDC7 PCR product to confirm linear amplification of the methylated and unmethylated DNA. *Linear amplification of methylated and unmethylated DNA for CpG sites at positions -58, -51, -49, -43, -27, -10, -7 and -4 bp relative to the start of transcription of the CDC7 sequence are shown in A – H respectively and R^2 values are indicated.*

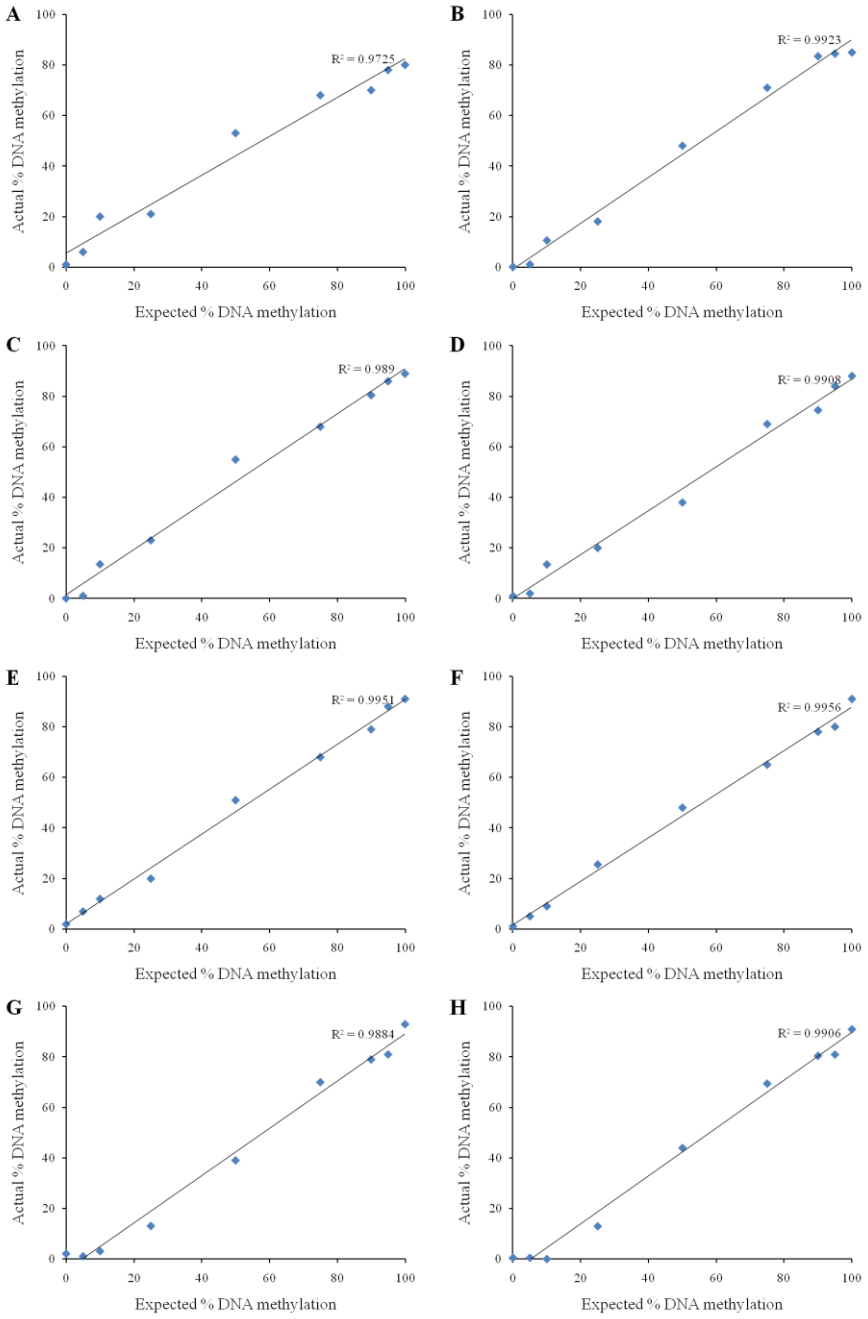

Figure C.2. Standard curves generated for the EIF5 PCR product to confirm linear amplification of the methylated and unmethylated DNA. *Linear amplification of methylated and unmethylated DNA for CpG sites at positions -60, -58, -48, -41, -38, -32, -21 and -17 bp relative to the start of transcription of the EIF5 sequence are shown in A – H respectively and R^2 values are indicated.*

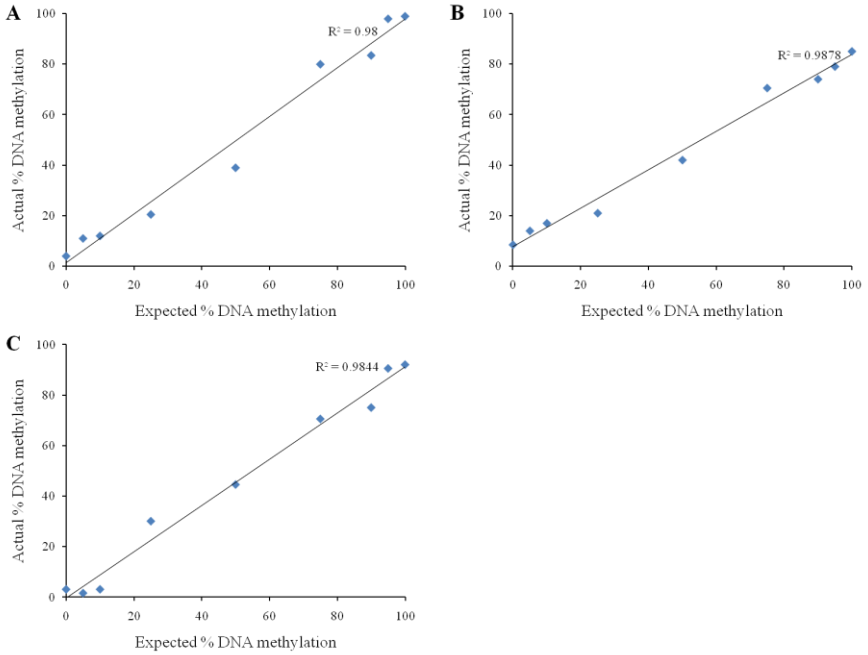

Figure C.3. Standard curves generated for the IRX3 PCR product to confirm linear amplification of the methylated and unmethylated DNA. *Linear amplification of methylated and unmethylated DNA for CpG sites at positions -64, -19 and -16 bp relative to the start of transcription of the IRX3 sequence are shown in A – C respectively and R^2 values are indicated.*

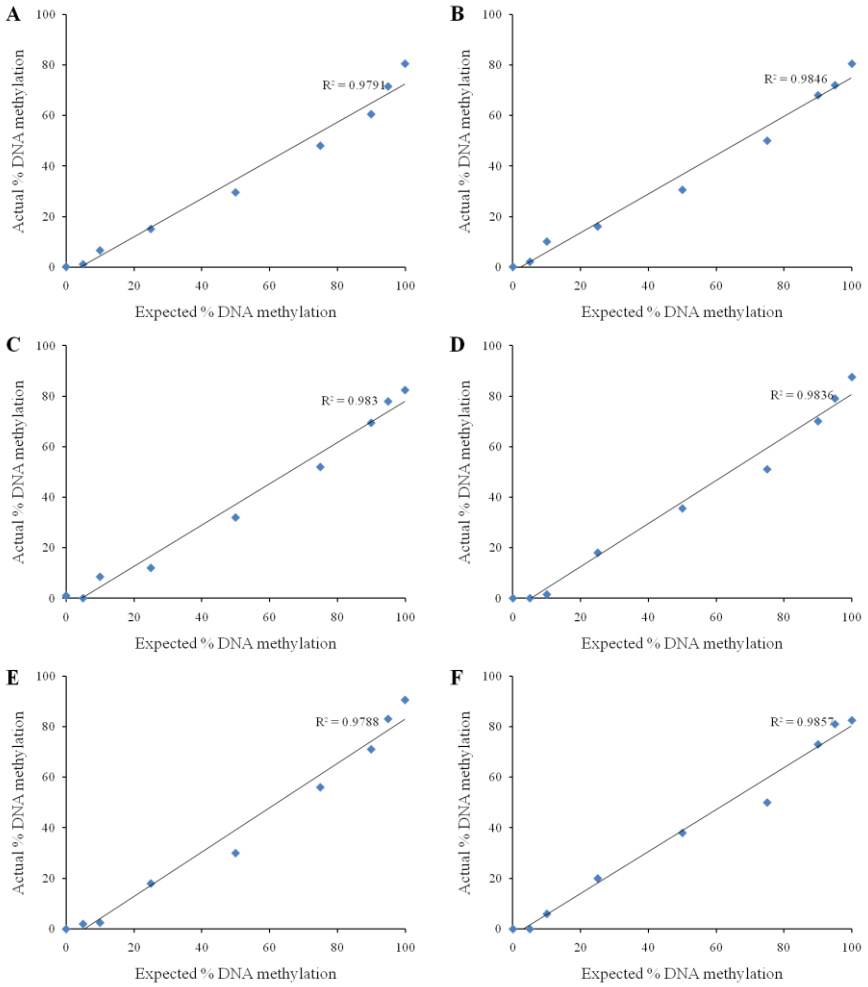

Figure C.4. Standard curves generated for the KLF3 PCR product to confirm linear amplification of the methylated and unmethylated DNA. *Linear amplification of methylated and unmethylated DNA for CpG sites at positions -69, -60, -56, -52, -50 and -47 bp relative to the start of transcription of the KLF3 sequence are shown in A – F respectively and R^2 values are indicated.*

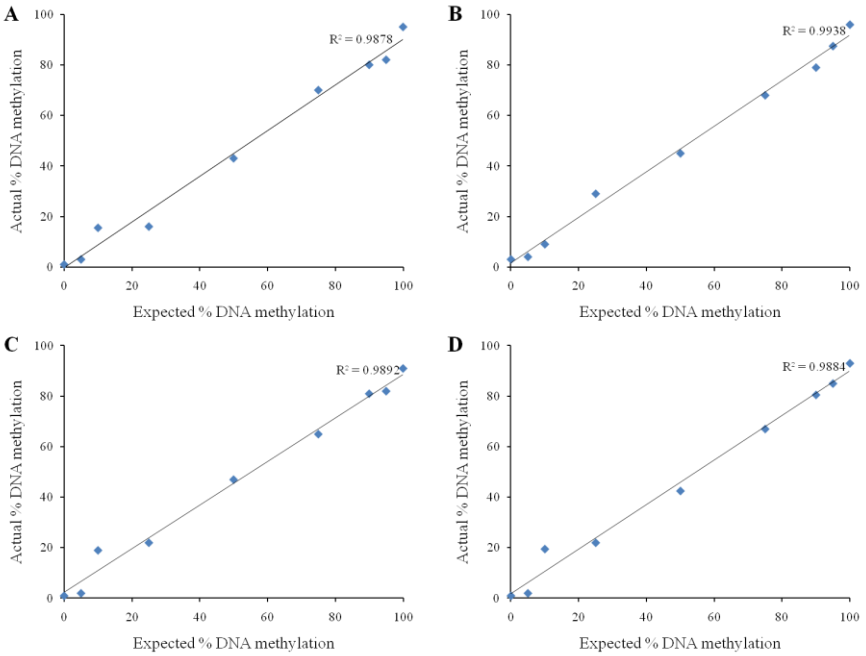

Figure C.5. Standard curves generated for LINE-1 PCR product to confirm linear amplification of methylated and unmethylated DNA. *Linear amplification of methylated and unmethylated DNA for CpG sites at positions 232, 252, 256 and 270 bp into the LINE-1 sequence are shown in A – D respectively and R^2 values are indicated.*

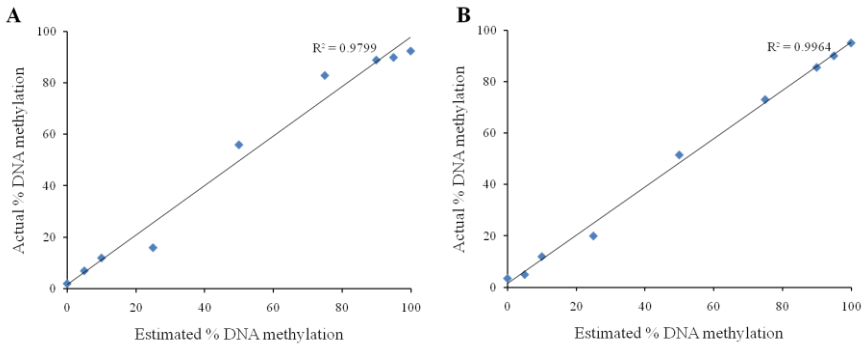

Figure C.6. Standard curves generated for the PCYT1A PCR product to confirm linear amplification of the methylated and unmethylated DNA. *Linear amplification of methylated and unmethylated DNA for CpG sites at positions -88 and -21 bp relative to the start of transcription of the PCYT1A sequence are shown in A and B respectively and R^2 values are indicated.*

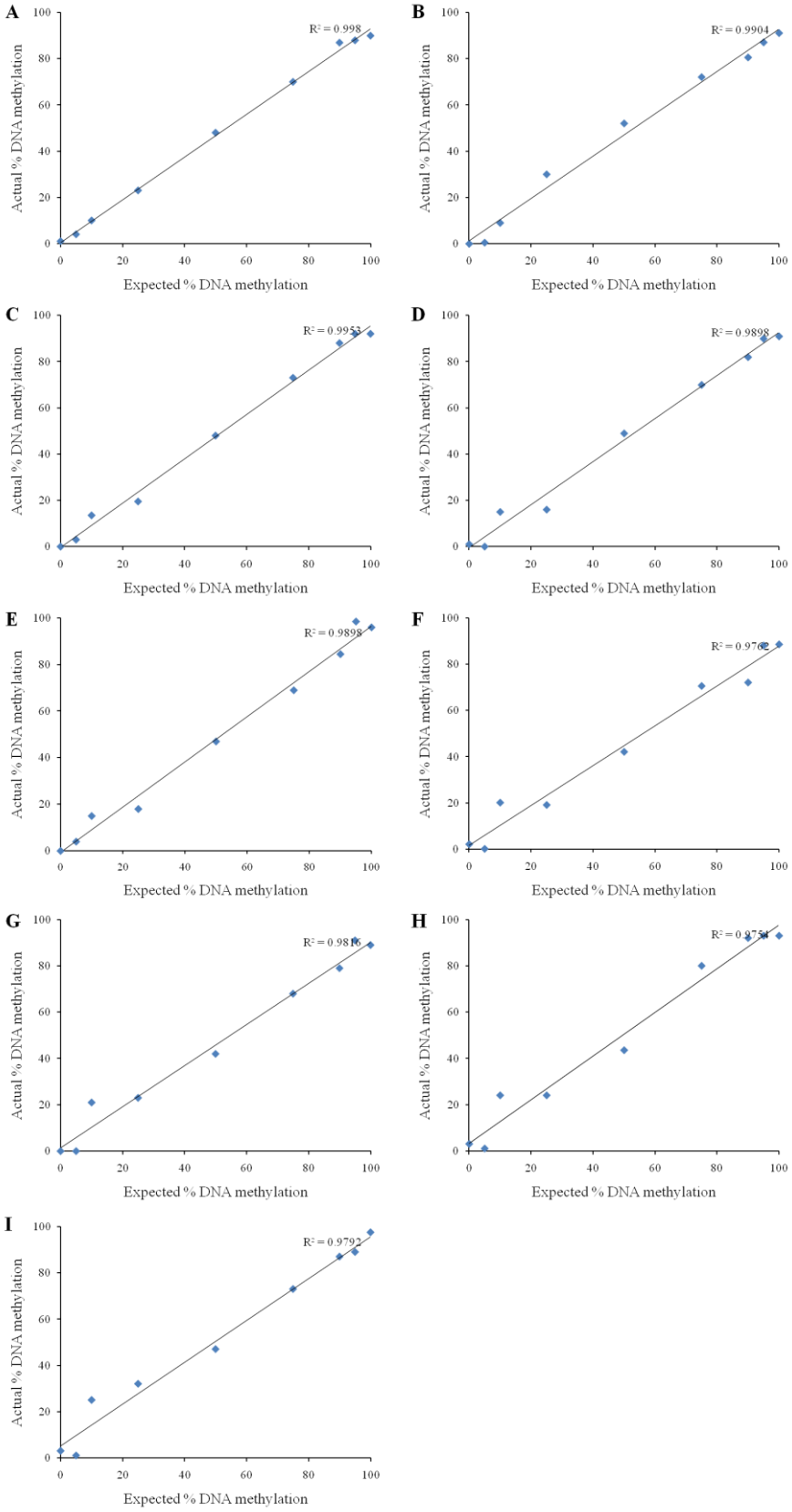

Figure C.7. Standard curves generated for the PTPRG PCR product to confirm linear amplification of the methylated and unmethylated DNA. *Linear amplification of methylated and unmethylated DNA for CpG sites at positions -72, -66, -64, -62, -51, -47, -39, -35 and -32 bp relative to the start of transcription of the PTPRG sequence are shown in A – I respectively and R^2 values are indicated.*

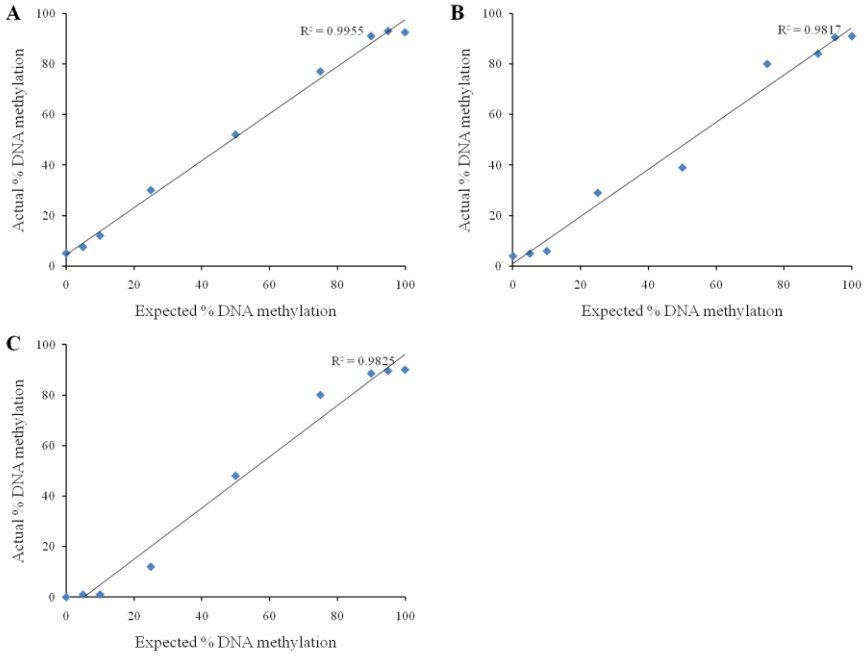

Figure C.8. Standard curves generated for the SLC39A4 PCR product to confirm linear amplification of the methylated and unmethylated DNA. *Linear amplification of methylated and unmethylated DNA for CpG sites at positions -91, -81 and -61 bp relative to the start of transcription of the SLC39A4 sequence are shown in A – C respectively and R^2 values are indicated.*

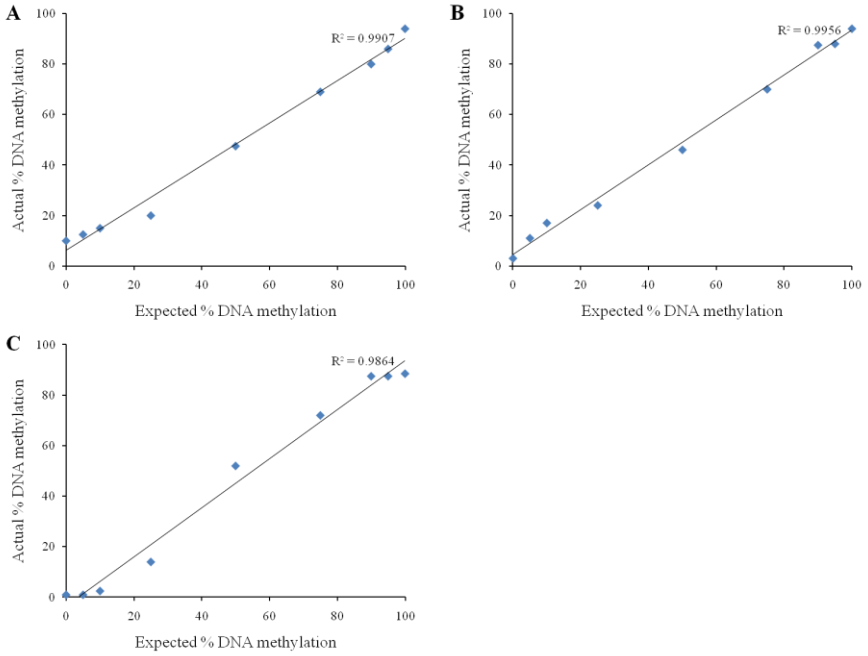

Figure C.9. Standard curves generated for the TBX3 PCR product to confirm linear amplification of the methylated and unmethylated DNA. *Linear amplification of methylated and unmethylated DNA for CpG sites at positions -137, -125 and -105 bp relative to the start of transcription of the TBX3 sequence are shown in A – C respectively and R^2 values are indicated.*

Appendix D: Amplification and Standard Curves for qPCR

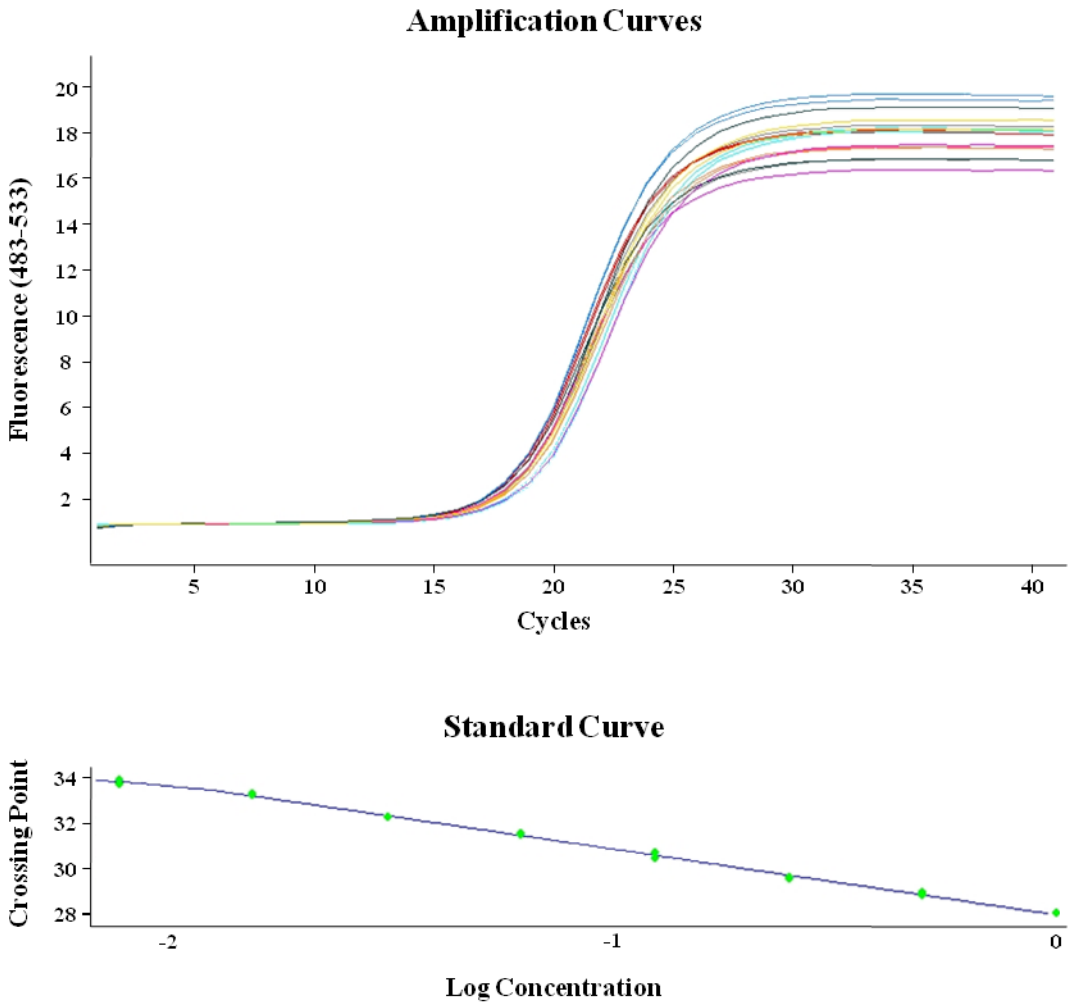

Figure D.1. RT-qPCR amplification (A) and standard (B) curves using primers for β ACTIN on reverse-transcribed Caco-2 cell RNA. *A – Typical amplification curves generated using primers for β ACTIN. Fluorescence intensity generated by amplification of cDNA of unknown concentration was measured and plotted against PCR cycle number to determine the threshold crossing point (C_T values). Each sample was measured in duplicate. B – Typical standard curve generated for β ACTIN. The mean log concentration of each cDNA sample within a two-fold dilution series was plotted against the C_T value. The standard curve was then used to calculate the relative levels of β ACTIN in each unknown sample.*

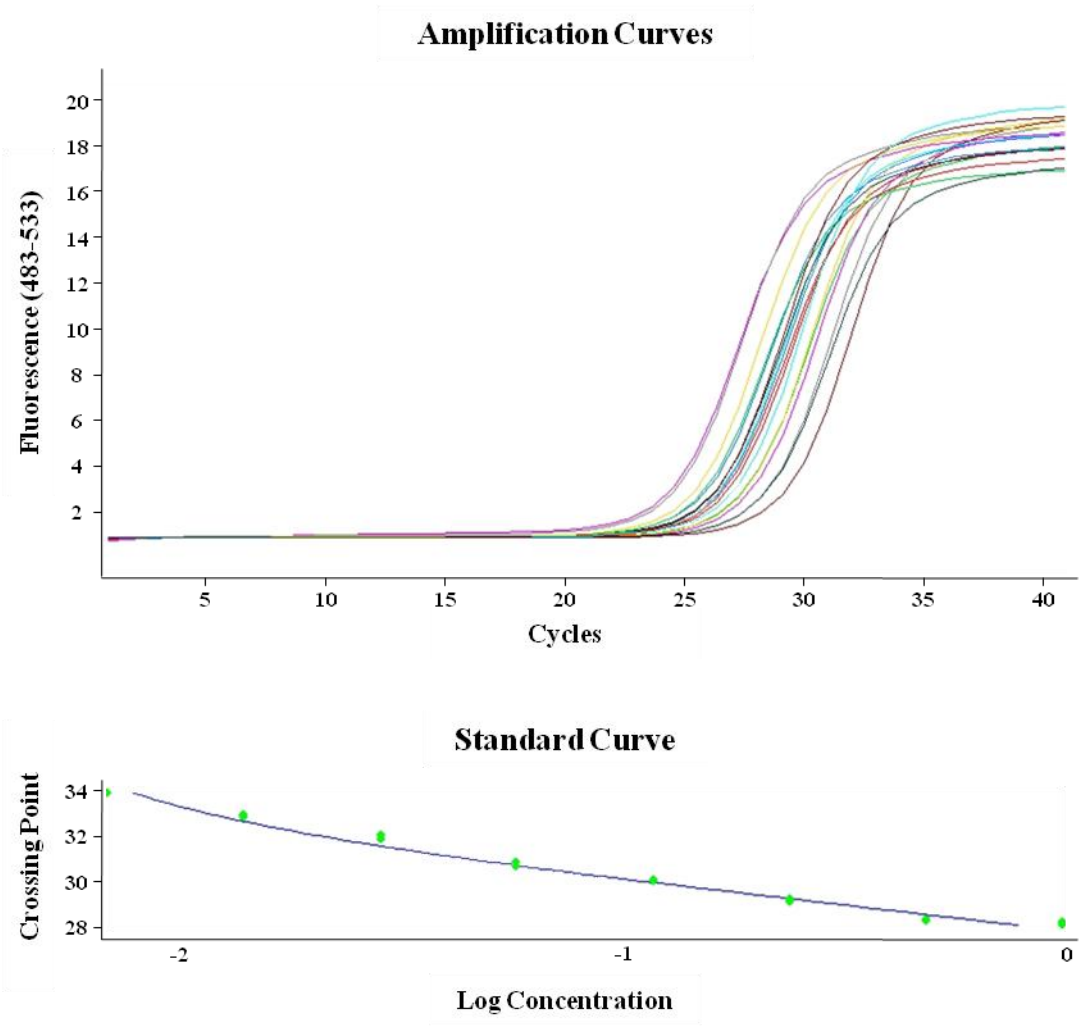

Figure D.2. RT-qPCR amplification (A) and standard (B) curves using primers for CDC7 on reverse-transcribed Caco-2 cell RNA. *A – Typical amplification curves generated using primers for CDC7. Fluorescence intensity generated by amplification of cDNA of unknown concentration was measured and plotted against PCR cycle number to determine the threshold crossing point (C_T values). Each sample was measured in duplicate. B – Typical standard curve generated for CDC7. The mean log concentration of each cDNA sample within a two-fold dilution series was plotted against the C_T value. The standard curve was then used to calculate the relative levels of CDC7 in each unknown sample.*

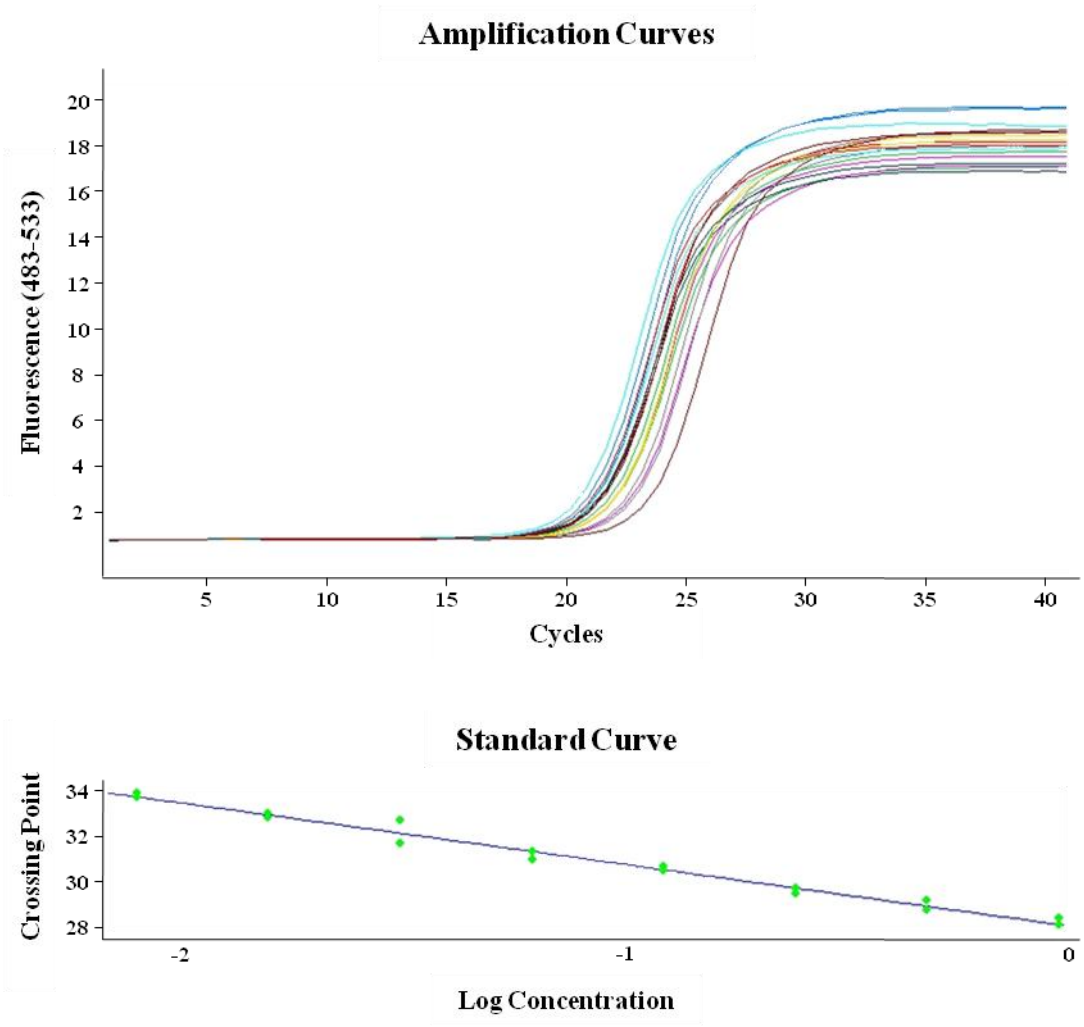

Figure D.3. RT-qPCR amplification (A) and standard (B) curves using primers for EIF5 on reverse-transcribed Caco-2 cell RNA. *A – Typical amplification curves generated using primers for EIF5. Fluorescence intensity generated by amplification of cDNA of unknown concentration was measured and plotted against PCR cycle number to determine the threshold crossing point (C_T values). Each sample was measured in duplicate. B – Typical standard curve generated for EIF5. The mean log concentration of each cDNA sample within a two-fold dilution series was plotted against the C_T value. The standard curve was then used to calculate the relative levels of EIF5 in each unknown sample.*

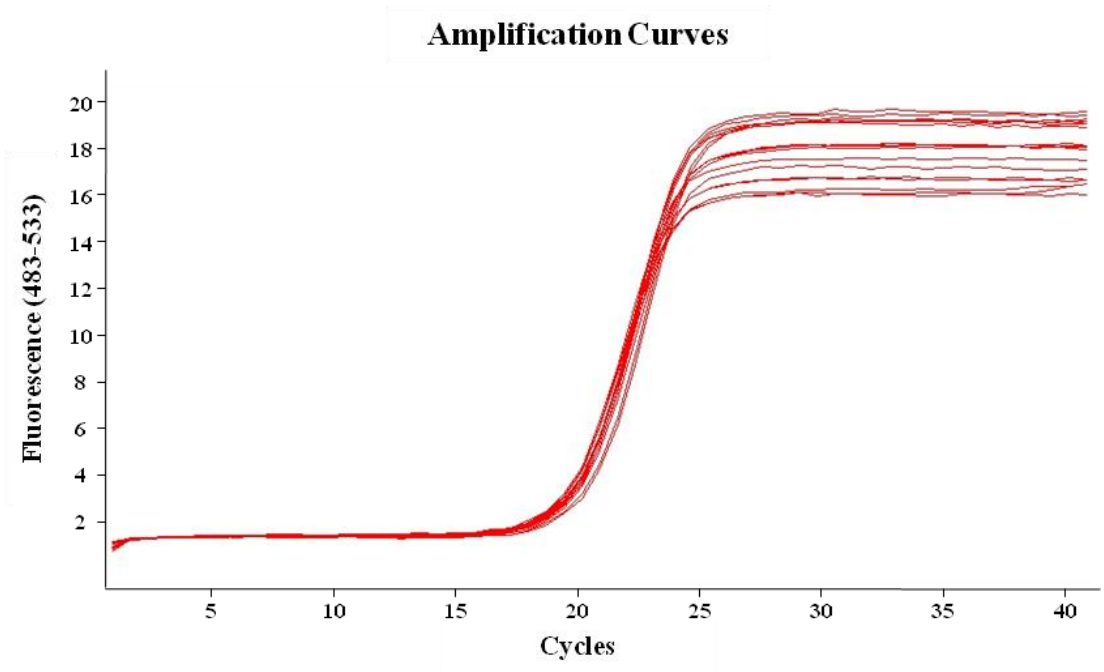

Figure D.4. qPCR amplification curve using primers for H19 on Caco-2 cell DNA. *A – Typical amplification curves generated using primers for H19. Fluorescence intensity generated by amplification of DNA of unknown concentration was measured and plotted against PCR cycle number to determine the threshold crossing point (C_T values). Each sample was measured in duplicate.*

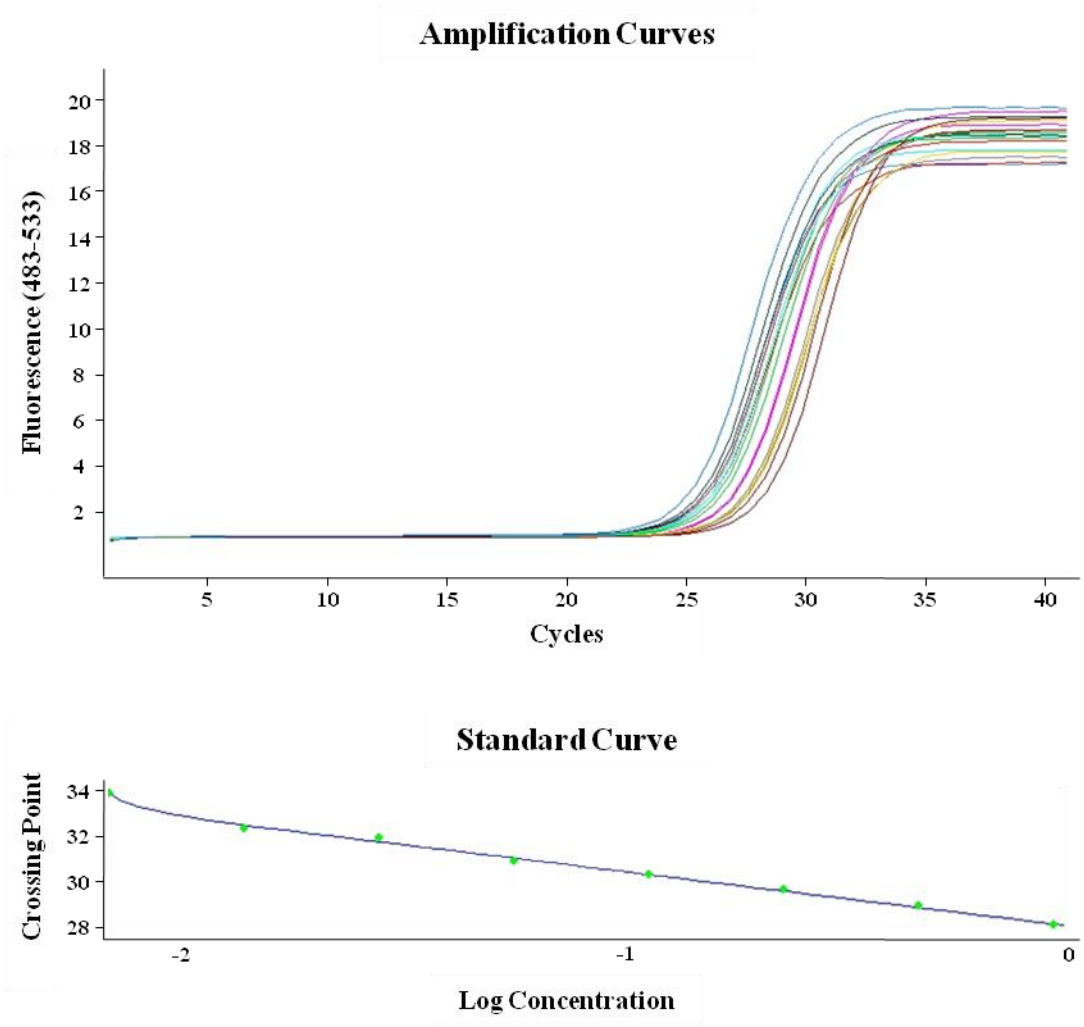

Figure D.5. RT-qPCR amplification (A) and standard (B) curves using primers for IRX3 on reverse-transcribed Caco-2 cell RNA. *A – Typical amplification curves generated using primers for IRX3. Fluorescence intensity generated by amplification of cDNA of unknown concentration was measured and plotted against PCR cycle number to determine the threshold crossing point (C_T values). Each sample was measured in duplicate. B – Typical standard curve generated for IRX3. The mean log concentration of each cDNA sample within a two-fold dilution series was plotted against the C_T value. The standard curve was then used to calculate the relative levels of IRX3 in each unknown sample.*

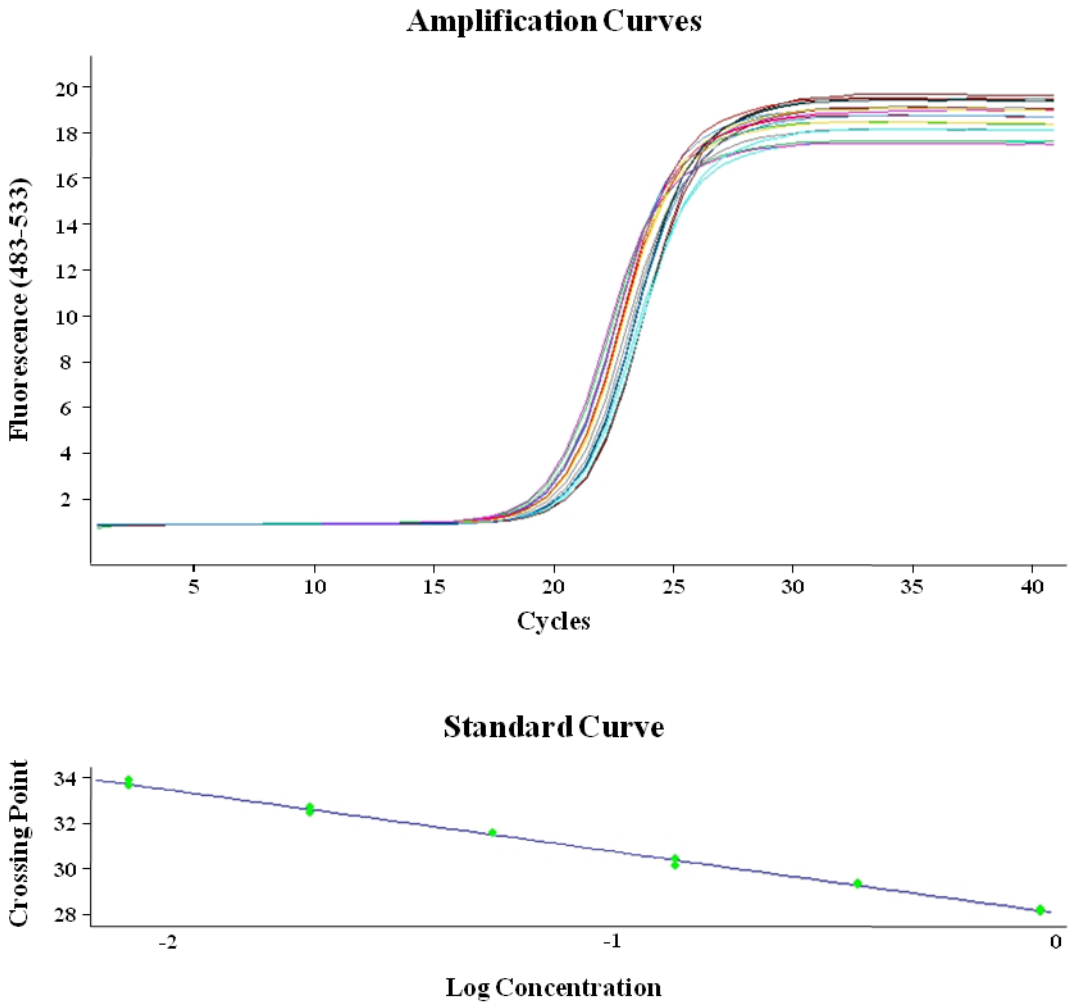

Figure D.6. RT-qPCR amplification (A) and standard (B) curves using primers for KLF3 on reverse-transcribed Caco-2 cell RNA. *A – Typical amplification curves generated using primers for KLF3. Fluorescence intensity generated by amplification of cDNA of unknown concentration was measured and plotted against PCR cycle number to determine the threshold crossing point (C_T values). Each sample was measured in duplicate. B – Typical standard curve generated for KLF3. The mean log concentration of each cDNA sample within a two-fold dilution series was plotted against the C_T value. The standard curve was then used to calculate the relative levels of KLF3 in each unknown sample.*

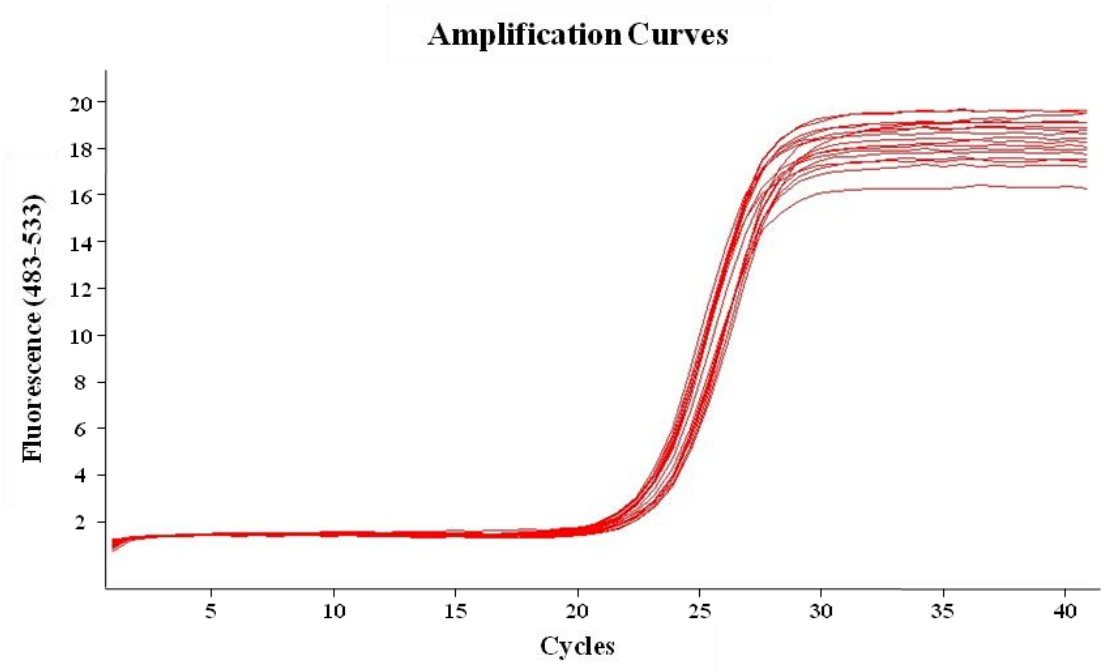

Figure D.7. qPCR amplification curve using primers for L1.2 on Caco-2 cell DNA. *A – Typical amplification curves generated using primers for L1.2. Fluorescence intensity generated by amplification of DNA of unknown concentration was measured and plotted against PCR cycle number to determine the threshold crossing point (C_T values). Each sample was measured in duplicate.*

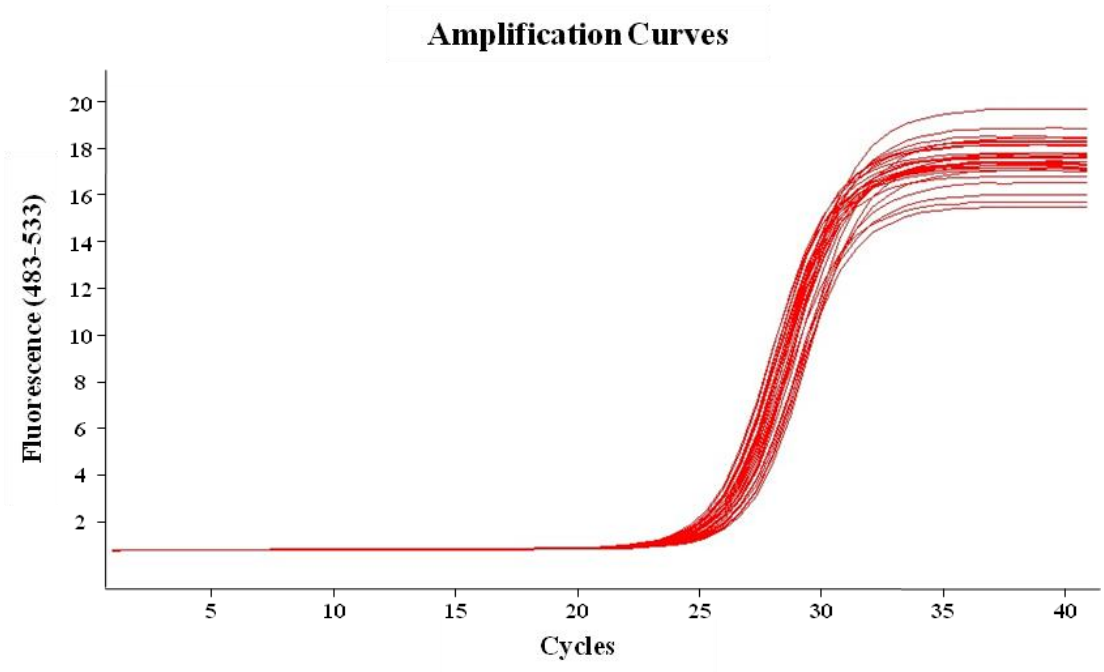

Figure D.8. qPCR amplification curve using primers for the Lambda Phage 'methylated' fragment spiked into Caco-2 cell DNA. *A – Typical amplification curves generated using primers for methylated Lambda Phage. Fluorescence intensity generated by amplification of DNA of unknown concentration was measured and plotted against PCR cycle number to determine the threshold crossing point (C_T values). Each sample was measured in duplicate.*

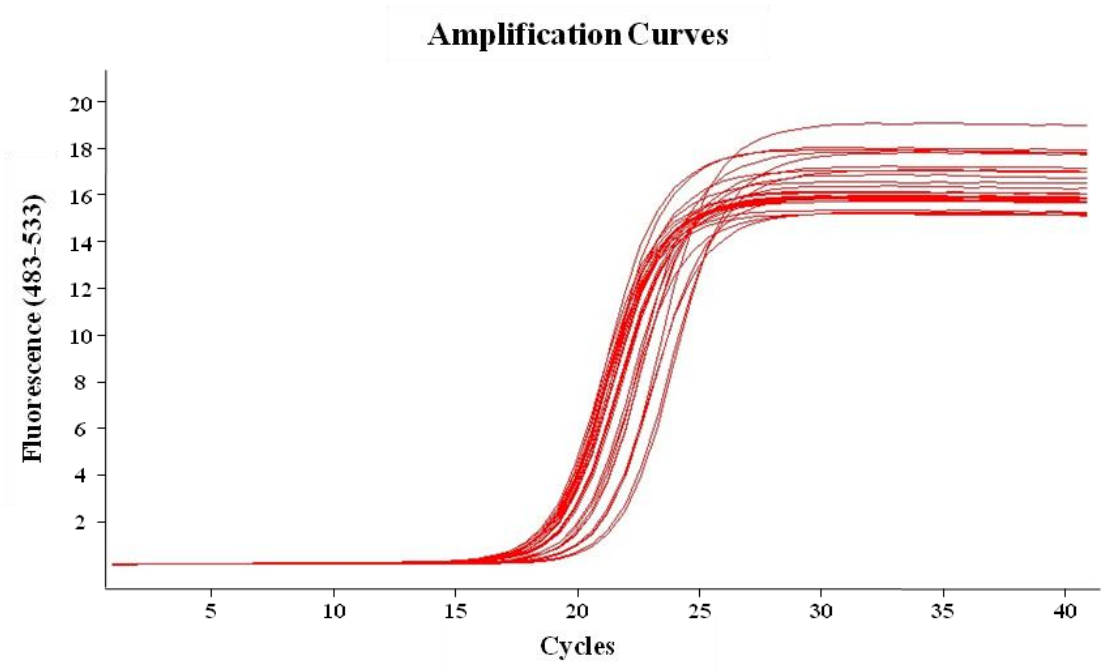

Figure D.9. qPCR amplification curve using primers for the Lambda Phage 'unmethylated' fragment spiked into Caco-2 cell DNA. *A – Typical amplification curves generated using primers for unmethylated Lambda Phage. Fluorescence intensity generated by amplification of DNA of unknown concentration was measured and plotted against PCR cycle number to determine the threshold crossing point (C_T values). Each sample was measured in duplicate.*

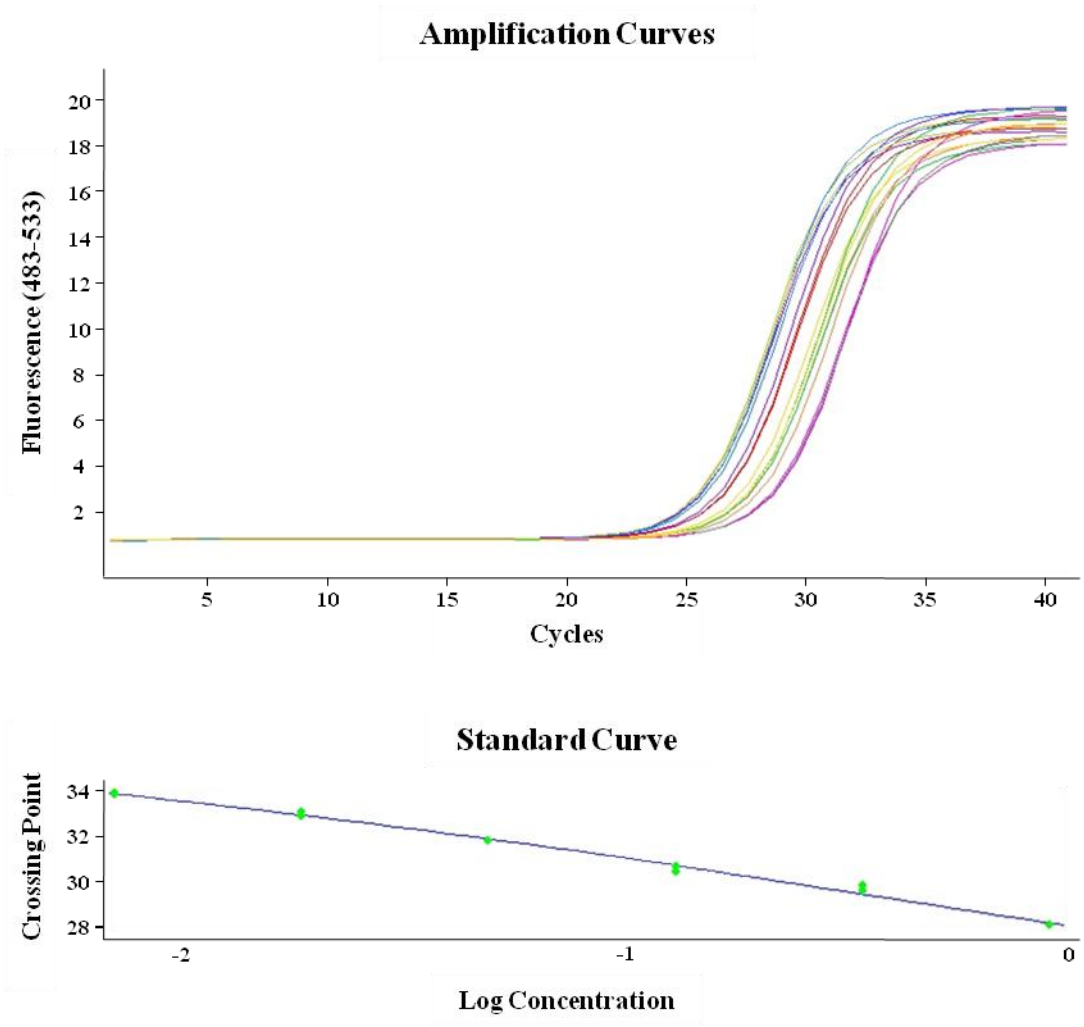

Figure D.10. RT-qPCR amplification (A) and standard (B) curves using primers for PCYT1A on reverse-transcribed Caco-2 cell RNA. *A – Typical amplification curves generated using primers for PCYT1A. Fluorescence intensity generated by amplification of cDNA of unknown concentration was measured and plotted against PCR cycle number to determine the threshold crossing point (C_T values). Each sample was measured in duplicate. B – Typical standard curve generated for PCYT1A. The mean log concentration of each cDNA sample within a two-fold dilution series was plotted against the C_T value. The standard curve was then used to calculate the relative levels of PCYT1A in each unknown sample.*

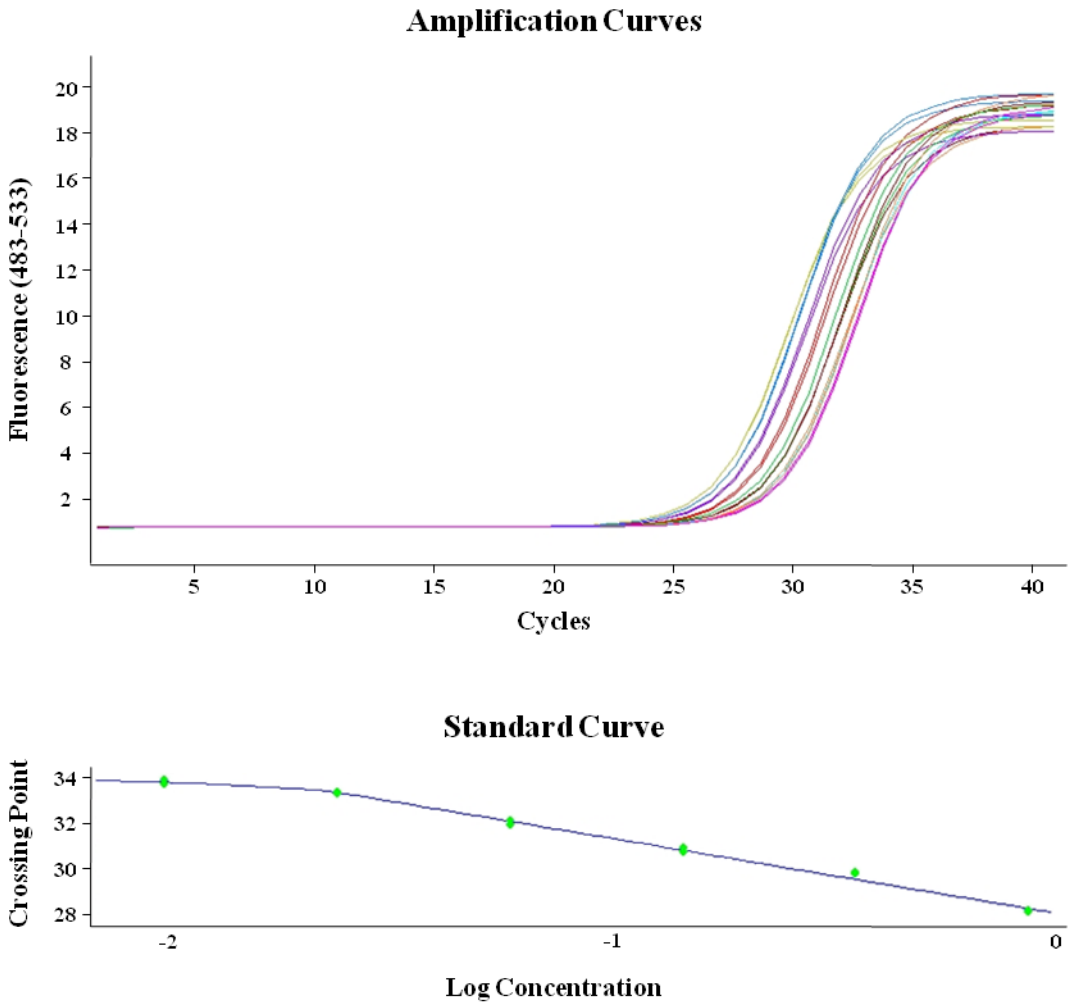

Figure D.11. RT-qPCR amplification (A) and standard (B) curves using primers for PTPRG on reverse-transcribed Caco-2 cell RNA. *A – Typical amplification curves generated using primers for PTPRG. Fluorescence intensity generated by amplification of cDNA of unknown concentration was measured and plotted against PCR cycle number to determine the threshold crossing point (C_T values). Each sample was measured in duplicate. B – Typical standard curve generated for PTPRG. The mean log concentration of each cDNA sample within a two-fold dilution series was plotted against the C_T value. The standard curve was then used to calculate the relative levels of PTPRG in each unknown sample.*

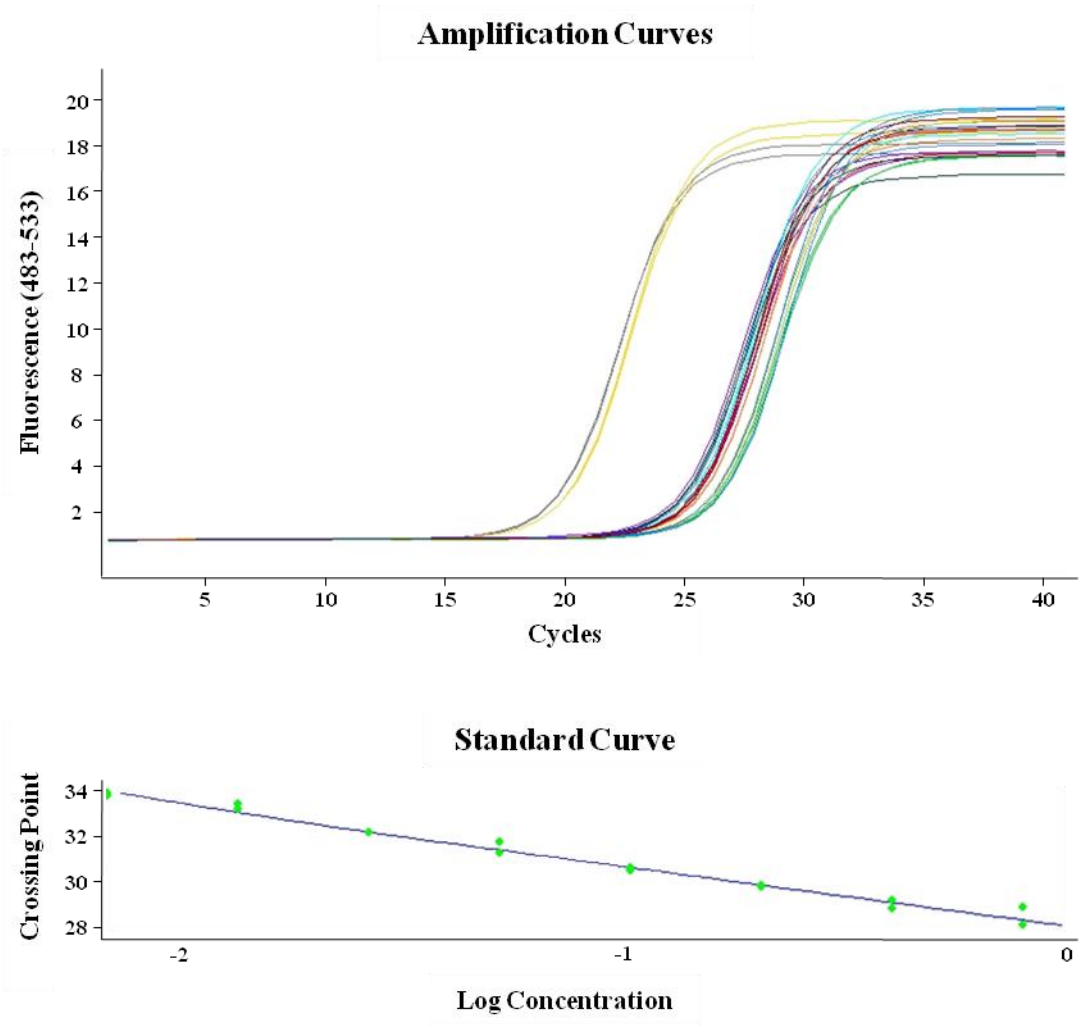

Figure D.12. RT-qPCR amplification (A) and standard (B) using primers for SIRT1 on reverse-transcribed Caco-2 cell RNA. *A – Typical amplification curves generated using primers for SIRT1. Fluorescence intensity generated by amplification of cDNA of unknown concentration was measured and plotted against PCR cycle number to determine the threshold crossing point (C_T values). Each sample was measured in duplicate. B – Typical standard curve generated for SIRT1. The mean log concentration of each cDNA sample within a two-fold dilution series was plotted against the C_T value. The standard curve was then used to calculate the relative levels of SIRT1 in each unknown sample.*

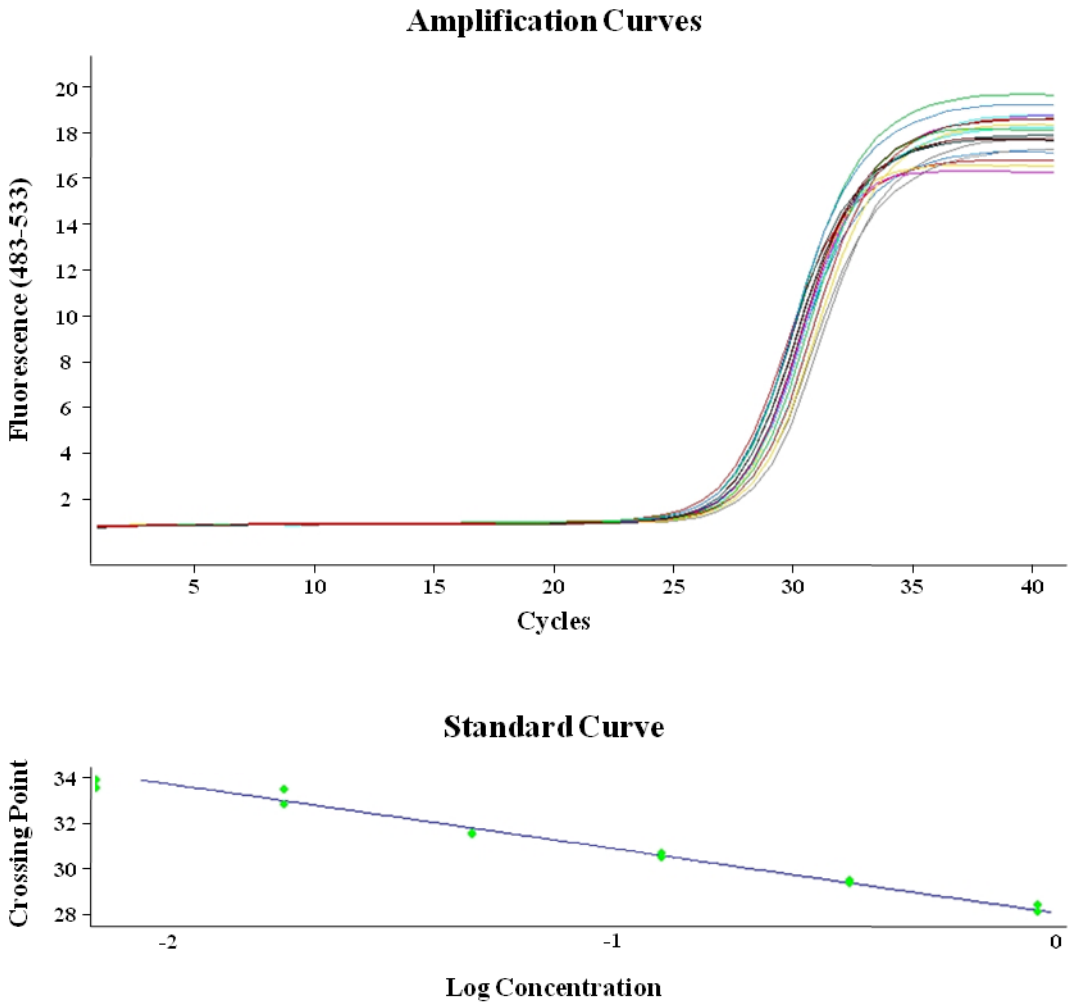

Figure D.13. RT-qPCR amplification (A) and standard (B) curves using primers for SLC39A4 on reverse-transcribed Caco-2 cell RNA. *A – Typical amplification curves generated using primers for SLC39A4. Fluorescence intensity generated by amplification of cDNA of unknown concentration was measured and plotted against PCR cycle number to determine the threshold crossing point (C_T values). Each sample was measured in duplicate. B – Typical standard curve generated for SLC39A4. The mean log concentration of each cDNA sample within a two-fold dilution series was plotted against the C_T value. The standard curve was then used to calculate the relative levels of SLC39A4 in each unknown sample.*

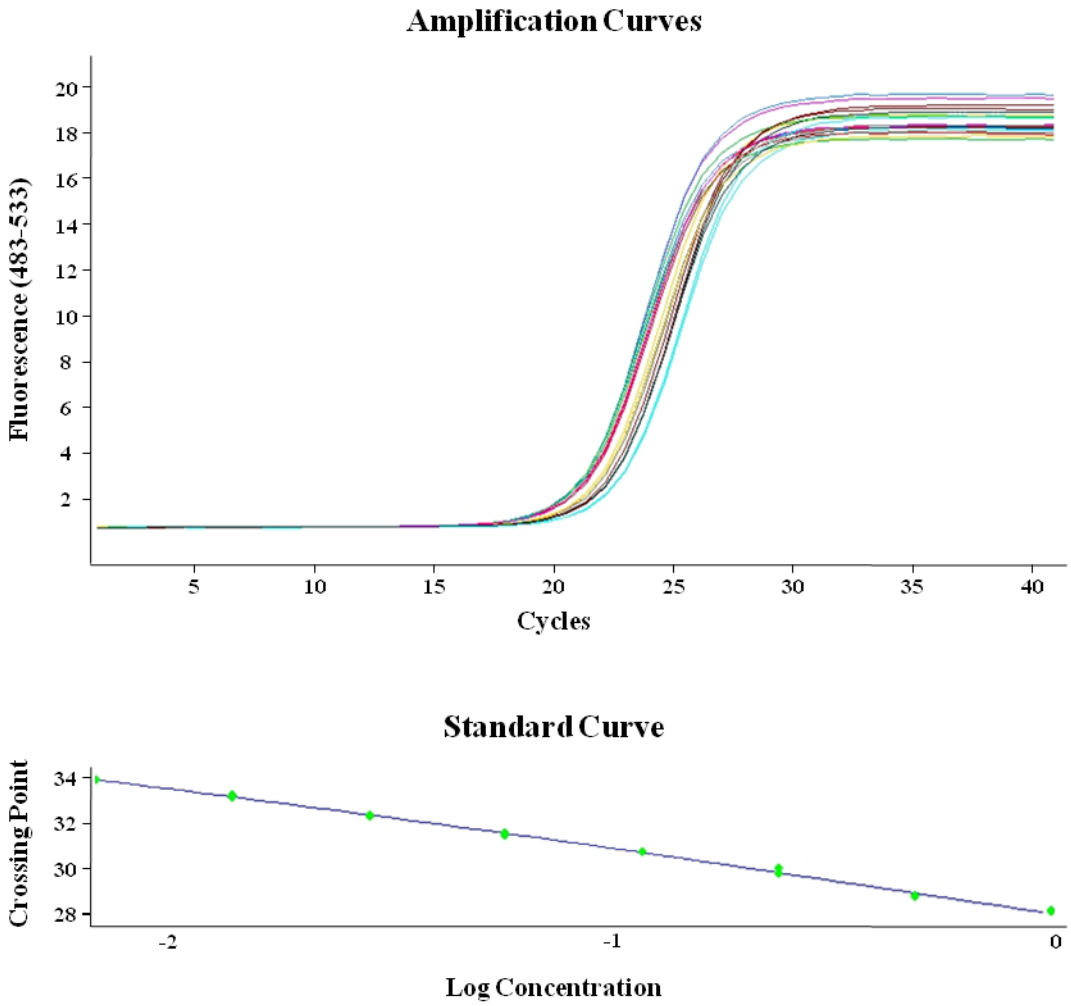

Figure D.14. RT-qPCR amplification (A) and standard (B) curves using primers for TBX3 on reverse-transcribed Caco-2 cell RNA. *A – Typical amplification curves generated using primers for TBX3. Fluorescence intensity generated by amplification of cDNA of unknown concentration was measured and plotted against PCR cycle number to determine the threshold crossing point (C_T values). Each sample was measured in duplicate. B – Typical standard curve generated for TBX3. The mean log concentration of each cDNA sample within a two-fold dilution series was plotted against the C_T value. The standard curve was then used to calculate the relative levels of TBX3 in each unknown sample.*

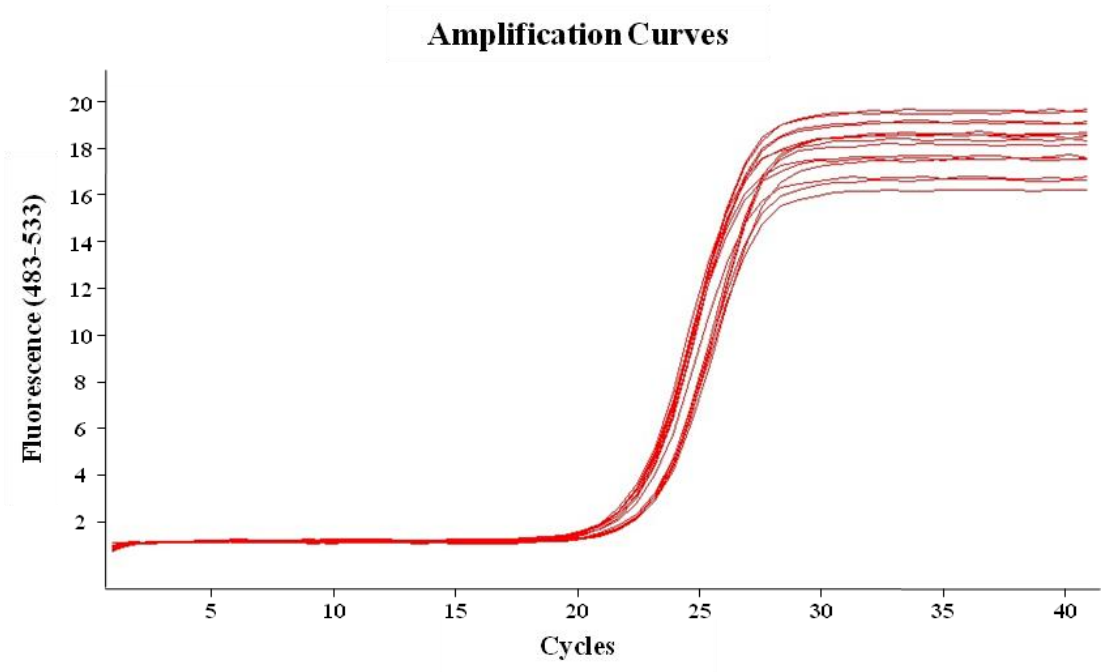

Figure D.15. qPCR amplification curve using primers for UBE2B in Caco-2 cell DNA. *A – Typical amplification curves generated using primers for UBE2B. Fluorescence intensity generated by amplification of DNA of unknown concentration was measured and plotted against PCR cycle number to determine the threshold crossing point (C_T values). Each sample was measured in duplicate.*

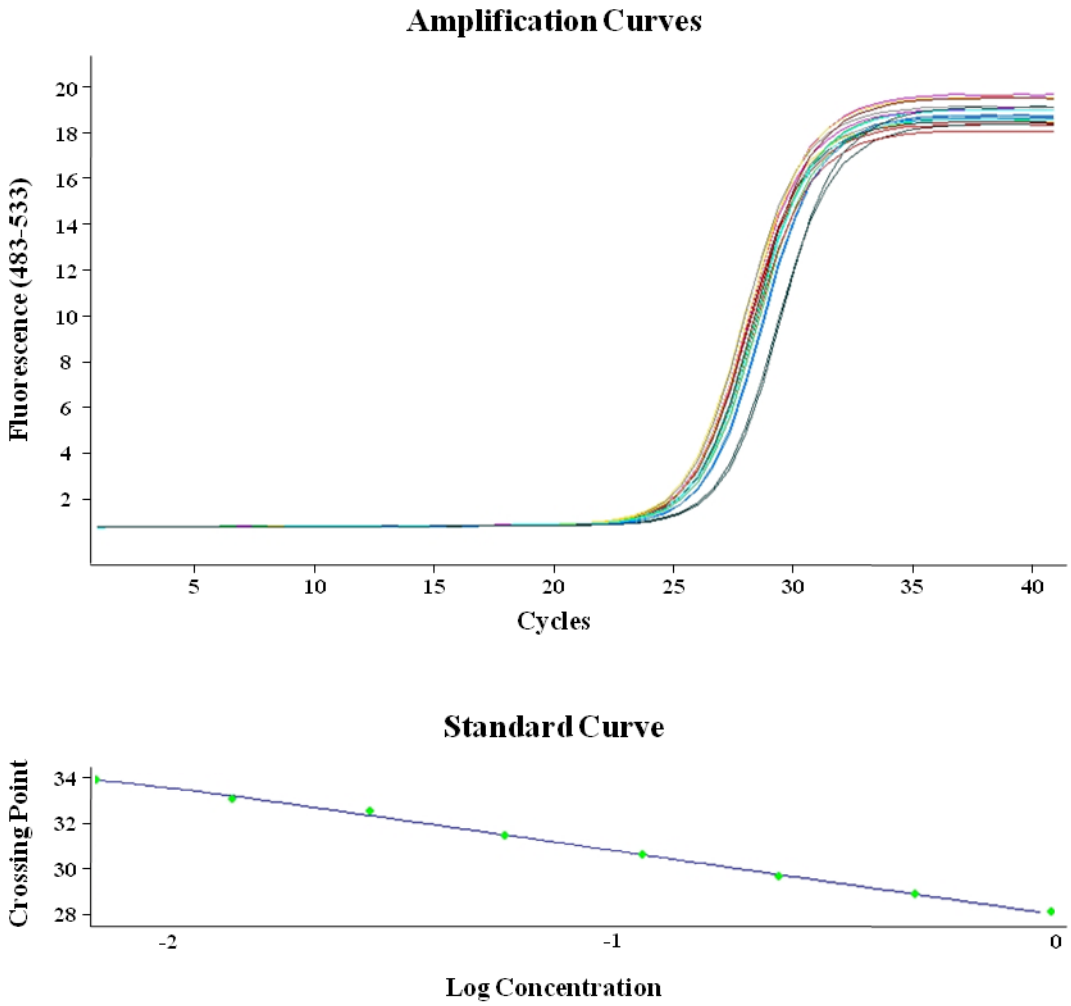

Figure D.16. RT-qPCR amplification (A) and standard (B) curves using primers for WNT11 on reverse-transcribed Caco-2 cell RNA. *A – Typical amplification curves generated using primers for WNT11 (accession number: NM_004626.2). Fluorescence intensity generated by amplification of cDNA of unknown concentration was measured and plotted against PCR cycle number to determine the threshold crossing point (C_T values). Each sample was measured in duplicate. B – Typical standard curve generated for WNT11. The mean log concentration of each cDNA sample within a two-fold dilution series was plotted against the C_T value. The standard curve was then used to calculate the relative levels of WNT11 in each unknown sample.*

Appendix E: Gene identifiers

(See CD insert)

I. from published sources

II. for genes whose methylation changed with SIRT1 manipulation

III. for genes whose expression changed with SIRT1 knockdown

IV. for genes whose methylation and expression changed with SIRT1 manipulation

Locations of the above gene lists are denoted on the spreadsheet tabs.

Appendix F: Related Publications

Papers published:

Ford D, **Ions LJ**, Alatawi F and Wakeling LA. The potential role of epigenetic responses to diet in ageing. Proceedings of the Nutrition Society 2011. 70: 374-384.

Ions LJ, Wakeling LA and Ford D. Can soyabean isoflavones mimic the effects of energy restriction on healthy ageing? Nutrition Bulletin 2009. 34: 303-308.

Wakeling LA, **Ions LJ** and Ford D. Could Sirt1-mediated epigenetic effects contribute to the longevity response to dietary restriction and be mimicked by other dietary interventions? Age 2009. 31: 327-341.